THE CONCEPTUAL DESIGN OF A TILT-DUCT VTOL UAV

A THESIS SUBMITTED TO
THE GRADUATE SCHOOL OF NATURAL AND APPLIED SCIENCES
OF
THE MIDDLE EAST TECHNICAL UNIVERSITY

BY

ÖZLEM ARMUTCUOĞLU

IN PARTIAL FULFILLMENT OF THE REQUIREMENTS FOR THE
DEGREE OF

MASTER OF SCIENCE

IN

THE DEPARTMENT OF AERONAUTICAL ENGINEERING

DECEMBER 2000

Approval of the Graduate School of Natural and Applied Sciences.

Prof. Dr. Tayfur ÖZTÜRK

Director

I certify that this thesis satisfies all the requirements as a thesis for the degree of Master of Science.

Prof. Dr. Nafiz ALEMDAROĞLU

Head of Department

This is to certify that we have read this thesis and that in our opinion it is fully adequate, in scope and quality, as a thesis for the degree of Master of Science.

Assoc. Prof. Dr. Mehmet Ş. KAVSAOĞLU

Supervisor

Examining Committee Members

Prof. Dr. Cahit ÇIRAY

Prof. Dr. İ. Sinan AKMANDOR

Assoc. Prof. Dr. Mehmet Ş. KAVSAOĞLU

Assoc. Prof. Dr. Ozan TEKINALP

Dr. Volkan NALBANTOĞLU

ABSTRACT

THE CONCEPTUAL DESIGN OF A TILT-DUCT VTOL UAV

ARMUTCUOĞLU, Özlem
M.S., Department of Aeronautical Engineering

Supervisor : Assoc. Prof. Dr. KAVSAOĞLU, Mehmet Ş.
December 2000, 272 pages

In this thesis, the conceptual design of a newly developed 'Tilt-Duct' VTOL UAV is presented. Besides a Visual Basic 5.0 ™ computer program is introduced which is developed by the author to enable Aspect Ratio optimization of UAVs and numerous types of aircraft.

First, the conceptual design process is presented. This process begins with a broad literature survey, continues with Airfoil and Geometry Selection, Initial Sizing, Stability and Control, etc. and ends with an approximate cost analysis of the designed UAV.

The design and control analysis of the newly developed 'Tilt-Duct VTOL UAV' is a co-work of a research group from Middle East Technical University, where the author is an active member. The design UAV combines the vertical takeoff capability of a helicopter and the forward flight performance of a conventional aircraft. It has two ducts located at the wing tips. Inside the ducts, there exists piston propeller engines with two propellers. It is basically designed for civil purposes, such as aerial surveys for agriculture, traffic monitoring and pollution control; meteorological data collection; pipeline survey; early forest fire detection; etc.

In the final chapter of this thesis, the Aspect Ratio Optimization computer program which is built by use of Visual Basic 5.0™ programming language is introduced. This

program has the characteristics of being web-interactive, user-friendly, and having an easy-to-use visual interface.

Keywords : VTOL, UAV, Tilt-Duct, Conceptual Design, Design Optimization, Computer Program- Visual Basic 5.0 ™.

ÖZ

AÇI VERİLEBİLİR KANAL-İÇİ-PERVANE / MOTOR SİSTEMLİ BİR İNSANSIZ HAVA ARACININ (İHA) KAVRAMSAL TASARIMI

ARMUTCUOĞLU, Özlem
Yüksek Lisans, Havacılık Mühendisliği Bölümü

Tez Yöneticisi : Doç. Dr. Mehmet Ş. KAVSAOĞLU
Aralık 2000, 272 sayfa

Bu tezde, Açı Verilebilir Kanal-İçi-Pervane Sistemli bir İnsansız Hava Aracı'nın tasarım süreci sunulmaktadır. Bunun yanısıra, yazarın Visual Basic 5.0™ programlama dilinde uçağın cephe oranını optimize etmek amacıyla gelistirdiği, çeşitli uçak ve insansız hava araçlarına uygulanabilen, bir bilgisayar programı tanıtılmaktadır.

Öncelikle, kavramsal tasarım süreci açıklanmıştır. Bu süreç, geniş bir kaynak araştırmasıyle baslayıp; Airfoil ve Geometri Seçimi, Ön Boyutlama, Kararlılık ve Kontrol, vb., gibi başlıklarla devam etmektedir. Bu sürecin son bölümünde uçağın yaklaşık bir maaliyet fiyatı hesaplanmaktadır.

'Açı Verilebilir Kanal-İçi-Pervane Sistemli İnsansız Hava Aracı'nın tasarımı ve kontrol analizleri yazarın da aktif bir üyesi olduğu, Orta Doğu Teknik Üniversitesi'nden bir araştırma grubunun ortak bir çalışmasıdır. Tasarım konusu olan insansız hava aracı, bir helikopterin dikine kalkış kapasitesiyle, geleneksel bir uçağın ileri uçuş performansını birleştirir. Uçak, gövdenin her iki yanında, kanatların ucunda yer alan kanallara sahiptir. Bu kanalların içinde iki pervane kanatlı, piston-pervane motorları bulunur. Uçak temel olarak, tarımsal hava gözlemleri, trafik gözlemi, hava kirliliği tesbiti, meteoroloji kaynaklı veri toplanması, petrol boru hattı gözetimi, orman yangını erken tesbiti, gibi sivil amaçlı kullanımlara yönelik tasarlanmıştır.

Tezin son bölümünde cephe oranı optimizasyonu için geliştirilmiş olan bilgisayar programı tanıtılmaktadır. Bu programda Visual Basic 5.0 programa dili kullanılmıştır. Program web-uyumlu ve kullanıcı dostu olmak, kullanımı kolay bir görsel yapıya sahip olmak gibi özellikleri bünyesinde barındırmaktadır.

Anahtar Kelimeler : Dikine Kalkış / İniş, İnsansız Hava Aracı, Açı Verilebilir Kanal-içi-Pervane/Motor Sistemi, Kavramsal Tasarım, Tasarım Optimizasyonu, Bilgisayar Programı – Visual Basic 5.0™.

To my family for their endless love and patience and to my friends for their irreplaceable moral support...

Aileme, sonsuz sevgi ve sabırları için, ve arkadaşlarıma, yeri doldurulamaz moral destekleri için....

ACKNOWLEDGMENTS

First of all, I would like to indicate that, I am grateful to my supervisor Assoc. Prof. Dr. Mehmet Ş. KAVSAOĞLU for his precious suggestions, encouragement and care during all the stages of this thesis.

I would also like to thank to the rest of the core members of Tilt-Duct VTOL UAV project, i.e. Prof. Ersin TULUNAY, Assoc. Prof. Dr. Ozan TEKİNALP and MS student Mr. Aycan OKAN, for their valuable contributions during the regular meetings. I also would indicate my special thanks to the rest of faculty members at Aeronautical Engineering Department for their moral support and encouragement during this study.

During my hard days, when I had to work until very late hours at night (I remember I had left the department by 05:00 a.m.!), my parents and my brother never left me alone in the huge (and lonely at that hours) department building. It was very precious for me, to feel their support and love and the warm environment of home that they bring together, especially while having such hard times.

My friends Nazmiye Açıkgöz and Cengizhan Bahar deserves special thanks for their useful comments on my thesis, cheering me up at very hard times and above all, being my best friends. I would also like to thank Aycan Okan, a precious friend, always tried to help me as much as he can, whenever I needed.

Finally, I would like to thank the Department of Aeronautical Engineering for having provided me the opportunity of graduate study with all technical equipment, together with a graduate assistantship.

TABLE OF CONTENTS

LIST OF TABLES

TABLE

LIST OF FIGURES

FIGURE

LIST OF SYMBOLS

REGULAR SYMBOLS

Symbol	Definition
A	Aspect ratio
A_{eff}	Effective aspect ratio due to endplate effect, etc.
A_h	Horizontal tail aspect ratio.
b	Wing Span
b_h	Horizontal tail span.
b_v	Vertical tail span.
$\bar{c}$	Mean geometric chord
C_{bhp}	Specific fuel consumption
C_D	Aircraft drag coefficient
$C_{D_{fus}}$	Fuselage drag coefficient.
$C_{D_{gear}}$	Landing gear drag coefficient.
$C_{D_{misc}}$	Miscellaneous drag coefficient.
C_{D_n}	Nacelle drag coefficient.
C_{D_q}	Drag due to pitch rate derivative
C_{D_u}	Drag coefficient due to speed
C_{D_w}	Wing drag coefficient.

C_{D_0}	Total airplane drag coefficient ($\alpha = i_h = \delta_e = 0$)
$C_{D_{0_{fus}}}$	Fuselage zero-lift drag coefficient.
$C_{D_{0_w}}$	Wing zero-lift drag coefficient.
C_{D_α}	Total airplane drag change due to angle of attack derivative
$C_{D_{\dot{\alpha}}}$	Drag due to rate of angle of attack derivative
$C_{D_{\delta_e}}$	Total airplane drag change due to elevator, $\alpha = 0°$
C_f	Flat-plate skin-friction drag coefficient
C_{f_e}	Equivalent skin friction coefficient
$\bar{c}_{HT}$	Horizontal tail mean chord.
C_{HT}	Horizontal tail volume coefficient
C_L	Aircraft lift coefficient
C_{L_1}	Aircraft steady-state lift coefficient
$C_{L_{i_h}}$	Change in total airplane lift for unit stabilizer angle
$C_{L_{max}}$	Maximum lift coefficient
$C_{L_{max_w}}$	The wing maximum lift coefficient
C_{l_p}	The rolling moment due to roll rate derivative
C_{L_q}	Lift due to pitch rate derivative
C_{l_r}	The rolling moment due to yaw rate derivative
C_{L_u}	Lift coefficient due to speed
C_{L_w}	Wing lift coefficient
C_{L_0}	Total airplane lift coefficient ($\alpha = i_h = \delta_e = 0$)
$C_{L_{0_h}}$	Horizontal tail lift coefficient for zero angle of attack

$C_{L_{0_{wf}}}$	Wing-fuselage lift coefficient for zero angle of attack
C_{L_α}	Total airplane lift curve slope (rad^{-1})
$C_{L_{\dot{\alpha}}}$	Lift due to rate of angle of attack derivative (rad^{-1})
$C_{\ell_{\alpha_v}}$	The average wing airfoil lift curve slope (rad^{-1})
$C_{L_{\alpha_h}}$	Horizontal tail lift curve slope (rad^{-1})
$C_{L_{\delta_e}}$	Change in total airplane lift for unit elevator angle (rad^{-1})
C_{ℓ_β}	The rolling moment due to sideslip derivative (rad^{-1})
$C_{\ell_{\dot{\beta}}}$	The rolling moment due to rate of sideslip derivative (rad^{-1})
C_m	Aircraft pitching moment coefficient
$C_{m_{ac_{wf}}}$	Pitching moment coefficient of wing-fuselage at aerodynamic center
C_{m_q}	Pitching moment due to pitch rate derivative
C_{m_o}	Total airplane pitching moment coefficient ($\alpha = i_h = \delta_e = 0$)
$C_{m_{of}}$	Fuselage pitching moment for zero angle of attack
$C_{m_{o_h}}$	Horizontal tail pitching moment for zero angle of attack
$C_{m_{o_w}}$	Wing pitching moment for zero angle of attack
$C_{m_{o_{wf}}}$	Wing-fuselage pitching moment for zero angle of attack
C_{m_1}	Steady state pitching moment
C_{m_α}	Total airplane pitching moment coefficient derivative wrt. angle of attack slope (rad^{-1})
$C_{m_{\dot{\alpha}}}$	Pitching moment due to rate of angle of attack derivative (rad^{-1})

$C_{m_{\delta_e}}$	Change in total airplane pitching moment for unit elevator angle (rad^{-1})
C_{n_p}	The yawing moment due to roll rate derivative
C_{n_β}	The yawing moment due to sideslip derivative (rad^{-1})
$C_{n_{\dot{\beta}}}$	The yawing moment due to rate of sideslip derivative (rad^{-1})
$c_{r_{HT}}$	Horizontal tail chord length at root section (ft)
$c_{r_{VT}}$	Vertical tail chord length at root section (ft)
C_T	Thrust coefficient
$c_{t_{HT}}$	Horizontal tail chord length at tip section (ft)
$c_{t_{VT}}$	Vertical tail chord length at tip section (ft)
c_{t_w}	Wing chord length at tip section (ft)
$\bar{c}_v$	Vertical tail mean chord (ft)
C_{VT}	Vertical tail volume coefficient
$\bar{c}_w$	Wing mean chord (ft)
d	Diameter (ft)
d_f	Equivalent fuselage diameter (ft)
D_p	Propeller diameter (ft)
e	Oswald span efficiency factor
E	Endurance (hr)
f	Parasite area of the aircraft (ft^2)
F	Fuselage lift factor
FF	Component form factor
g	Acceleration of gravity (ft/s^2)
G	Climb Gradient (ft/s)
h	Altitude (ft)

hp/W	Horsepower-to-Weight ratio (*hp/lb*)
k	Skin roughness value (*ft*)
K	Drag-due-to-Lift Factor
K_f	Empirical pitching moment factor
K_{vs}	Variable Sweep Constant, (= 1.00 if fixed sweep)
L/D	Lift to Drag ratio
L_{HT}	Longitudinal distance between aerodynamic center of horizontal tail and center of gravity.
L_{VT}	Longitudinal distance between aerodynamic center of vertical tail and center of gravity.
M	Airplane aerodynamic pitching moment, Mach number
n	Aircraft load factor, engine rpm (*rpm*)
N_{gear}	Gear load factor
p	Perturbed roll rate (*rad/s*)
P	Perimeter (*ft*), Power (*hp, W*)
P_{io}	Induced static power (*hp, W*)
q	Dynamic pressure ($slug/ft.s^2$), Perturbed pitch rate (*rad/s*)
Q	Interference factor
R	Aircraft Range (*nmi*)
Re	Reynolds number
S	Wing planform area (ft^2), shock-absorber stroke (*in*)
S_a	Obstacle-clearance distance in Landing (*ft*)
$S_{exposed}$	True-view exposed planform area (ft^2)
S_{f_s}	Fuselage side surface area (ft^2)
$S_{landing}$	Total Landing distance (ft)
S_h	Horizontal tail area (ft^2)
S_{gear}	Reference landing gear area (ft^2)

S_T	Tire stroke (in)
S_v	Vertical tail area (ft^2)
S_{wet}	Wetted surface area (ft^2)
$S_{wet_{a/c}}$	Wetted surface area of the aircraft (ft^2)
T	Thrust force (lb, N)
T_c	Thrust coefficient
t/c	Thickness ratio
u	Perturbed forward velocity (ft/sec)
V	Aircraft velocity (ft/sec)
V_{max}	Maximum cruise velocity (ft/sec)
V_S	Stall speed (ft/sec)
s_L	The stall speed for landing configuration (ft/sec)
s_{TO}	Stall speed at takeoff configuration (ft/sec)
Vol	Volume (ft^3)
W/S	Wing Loading (lb/ft^2)
W_e	Empty Weight (lb)
W_f	Fuel Weight (lb)
W_0	Aircraft Takeoff Gross Weight (lb)
W_{str}	Structural Weight (lb)
W_p	Payload Weight (lb)
X	Longitudinal Distance Measured from Aircraft Nose (ft)
$\overline{X}$	X, non-dimensionalized with mac (X/mac)
$\bar{x}_{ac}$	The location of the aircraft aerodynamic center in fractions of the mean geometric center.
$\overline{X}_{acw}$	Wing Aerodynamic Center Location
$\bar{X}_{ac_h}$	Horizontal Tail Aerodynamic Center Location

$\bar{X}_{ac_{wf}}$	Wing-fuselage aerodynamic center location
$\bar{X}_{cg}$	Aircraft center of gravity location
$\overline{X}_{m\,lg}$	Main Landing Gear Location
$\overline{X}_{np}$	Aircraft Neutral Point Location
$\overline{X}_{p}$	Main Engines Thrust Line Location
$\overline{X}_{ref}$	Position of reference point
Y	Lateral Distance Measured from Aircraft Longitudinal Centerline (ft)
$\overline{Y}$	Y, nondimensionalized with mac (Y/mac)
Z	Vertical distance wrt. reference axis; i.e. fuselage baseline (ft)
$\overline{Z}$	Z, nondimensionalized with mac (Z/mac)
$\overline{Z}_t$	Vertical distance from Thrust Line to Moment Reference Point

GREEK SYMBOLS

α	Angle of attack *(deg, rad)*
$\dot{\alpha}$	Angle of attack rate *(rad/s)*
$\alpha_{C_{L_{max}}}$	Angle of attack for maximum lift coefficient *(deg, rad)*
α_{oL}	Angle of attack at zero-lift *(deg, rad)*
β	Sideslip angle, Propeller blade angle *(deg, rad)*
$\dot{\beta}$	Sideslip angle rate *(rad/s)*
δ	Deflection angle of aileron, rudder or elevator *(deg, rad)*
δ_a	Aileron deflection angle *(deg, rad)*
δ_e	Elevator deflection angle *(deg, rad)*

δ_r	Rudder deflection angle (*deg, rad*)
ε	Downwash angle (*deg, rad*)
η	Shock-absorbing efficiency
η_h	Dynamic pressure ratio of the horizontal tail
η_i	Ideal efficiency
η_p	Propeller efficiency
λ	Taper ($= c_t / c_r$)
$\Lambda_{c/4}$	Wing quarter chord sweep angle (*deg, rad*)
$\Lambda_{l.e.}$	Leading edge sweep angle (*deg, rad*)
Λ_{max}	Wing sweep angle at the chord-wise location of maximum airfoil thickness (*deg, rad*)
Γ	The wing geometric dihedral angle (*deg, rad*)
ν	Kinematic Viscosity (ft^2/s)
ρ	Air density (sl/ft^3)
Ψ	Over turn angle (*deg*)
$\frac{d\varepsilon}{d\alpha}$	Rate of change in downwash angle due to angle of attack
ΔC_ℓ	Incremental airfoil lift coefficient due to flaps.
ΔC_{L_h}	Incremental tail lift coefficient to trim
Δx_i	Length of the i^{th} fuselage part
$\Delta\alpha_{C_{L_{max}}}$	Incremental aircraft angle of attack for maximum lift

SUBSCRIPTS

a	Aileron, aft
ac	Aerodynamic center

b.e.	Best endurance
b.r.	Best range
c	Component
calculated	The calculated value of a parameter that is a result of an iterative solution.
cruise	Valid for cruise segment
cw	Crosswind
e	Elevator
eng	Engine
f	Forward
fus	Fuselage
guessed	The guessed value of a parameter in order to use in an iterative solution.
h, ht	Horizontal tail
i	i^{th} item, particle, component
lg	Landing gear
ℓ	Airfoil lift
M	(at a given) Mach number
max	Maximum
misc	Miscellaneous
mc	At maximum celing
mlg	Main landing gear
n	Nacelle
nlg	Nose landing gear
r	rudder *or* root
SL	at Sea level
T	Thrust or power effect, tire
TO	Takeoff

v or *vt*	Vertical tail
w	Wing
wb	Wing-body
wf	wing-fuselage
o	Trim condition
1	Steady state

ACRONYMS & ABBREVIATIONS

AAA	The software Advanced Aircraft Analysis
A/c	Aircraft
AOA	Angle of attack
cg, CG	Center of gravity
Eqn.	Equation
FAR	Federal Aviation Regulation
mac	Mean aerodynamic chord
mgc	Mean geometric chord
o.t.a	Over turn angle
rpm	Revolution per minute
SHP	Shaft horsepower
SM	Static Margin ($\overline{X}_{np} - \overline{X}_{cg}$)
STOL	Short Takeoff / Landing
UAV	Unmanned Air Vehicle
VB 5.0	Visual Basic 5.0™ programming language.
vs.	Versus

VTOL	Vertical Takeoff / Landing
wrt.	With respect to
@	at

CHAPTER 1

INTRODUCTION

1.1 The Conceptual Design of theTilt-Duct VTOL UAV

Conceptual design is a very changeable process. New ideas and problems are very likely to emerge as further detailed calculations are performed on a design. As new decisions are made and relevant modifications are required, these should be reflected to the current design which should be redrawn accordingly, Fig. 1.1.

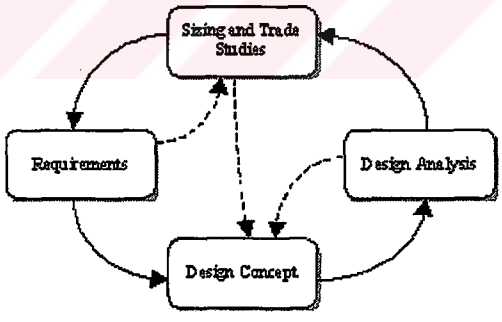

Figure 1. 1 Iterative Design Process. [1]

This thesis aims to illustrate the conceptual design process of the Tilt-Duct VTOL UAV, which combines the vertical flight capability of a helicopter and the superior forward flight performance of an airplane. Here, the abbreviation VTOL stands for Vertical Takeoff and Landing, and UAV stands for Unmanned/Uninhabited Air Vehicle. In Figure 1.2, top view of the design UAV in hover mode is presented.

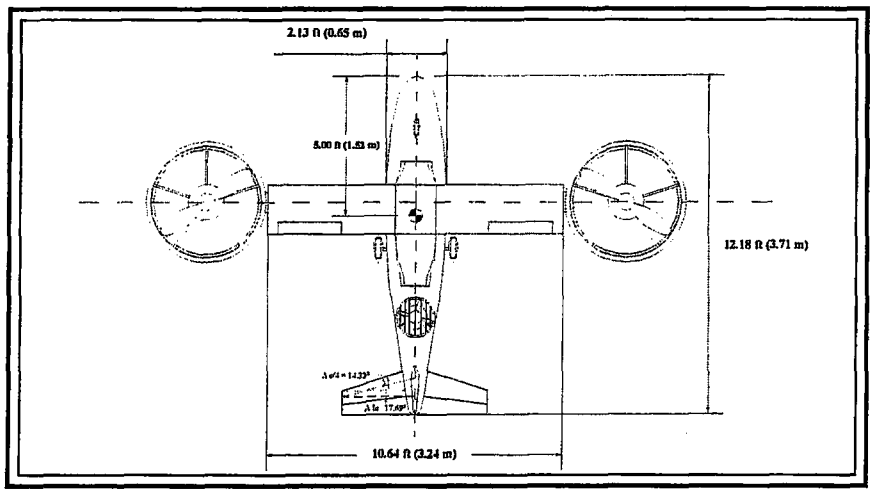

Figure 1. 2 Top view of Tilt-Duct VTOL UAV in hover mode.

The Tilt-Duct VTOL UAV achieves the vertical take off capability by tilting the propeller-ducts mechanisms, which are located at the tips of the wing, on each side of the fuselage. The two main engines are of Limbach L-275 E type, 24 hp, piston propellers. There is another engine and propeller mechanism which is located in the aft fuselage, see Figure 1.2. While the main engines provide thrust, the aft engine is used to control pitch by controlling throttle in hover and transition modes. It also contributes to lift. The aft engine is of Limbach L-90 E, 4 hp, type piston propeller. Additional pitch control of the UAV, as well as yaw control, is realized through exit guide vanes located at the exit of the aft engine. Roll control is achieved by differential thrust realized at the main engines.

The Tilt-Duct VTOL UAV has a maximum gross weight of 226 lb. It weighs 151.5 pounds empty and measures slightly more than 12 feet in length. The distance from the ground to the top of the vertical tail is 4.68 feet, and the span of its non-swept, non-tapered wing is 10.64 feet. It features two two-bladed propellers, each measuring 4.34 feet in diameter. It can reach a maximum cruising speed of 173 knots and a range of 558 nmi with 30 lb of payload. If the payload amount is reduced, the UAV achieves larger ranges, e.g. with a 22.05 lb of payload it covers a range of 702 nmi.

1.2 The Mission Profile

The Tilt-Duct VTOL UAV has a design mission profile as illustrated in Figure 1.3. The mission segments are defined in the figure.

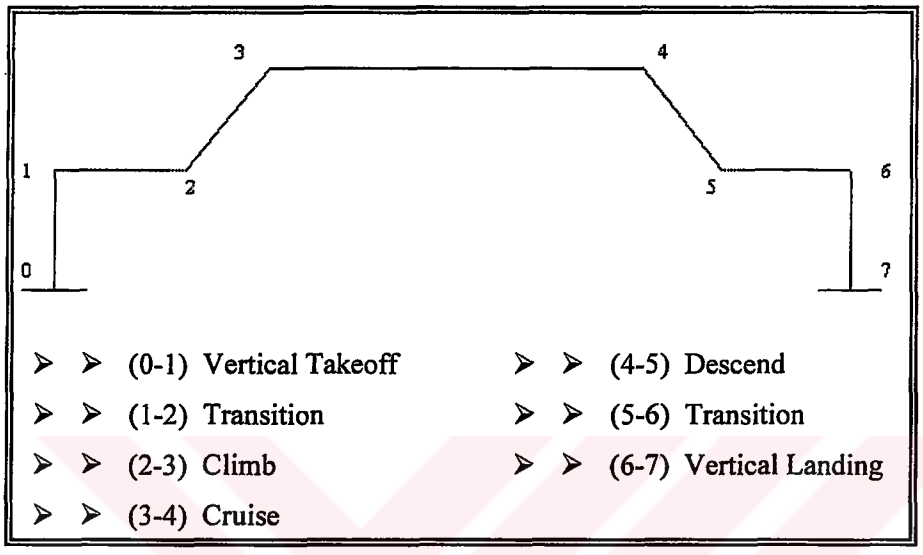

Figure 1. 3 The design mission profile, cruise, of the Tilt-Duct VTOL UAV.

The following set of requirements were taken into account in this conceptual design process.

- h_{cruise} : 2000 m = 6562 ft
- $W_{payload}$: 10 kg = 22.05 lb
- V_{stall} : 50 knots @ 1000 m altitude.
- Crew : None

1.3 About the Tilt-Duct VTOL UAV Research Group

This study is a part of an research activity being carried out in the research group, with members from the Department of Aeronautical Engineering and the Department of Electrical and Electronics Engineering, Middle East Technical University. The group decided to work on UAVs due to the challenging issues and considerable interest on UAVs in our country. The core of the team consists of three faculty members and two

research assistants. The project had started in 1998. The main purpose of the group is to develop an autonomously controlled VTOL UAV which can takeoff and land vertically as helicopter and convert to a propeller driven airplane in forward flight mode by tilting its ducted propellers forward. In this way, the aircraft would not need a runway for takeoff or landing besides it could reach higher speeds than a conventional helicopter in forward flight.

The members of the research group are :

Prof. Dr. Ersin Tulunay (EE), *Project Director*

Assoc. Prof. Dr. Mehmet Ş. Kavsaoğlu (AEE), *Supervisor*

Assoc. Prof. Dr. Ozan Tekinalp (AEE), *Supervisor*

Graduate Research Assistant Özlem Armutcuoğlu (AEE), *Researcher*

Graduate Research Assistant Aycan Okan (AEE), *Researcher*

The abbreviations EE stands for, Electrical and Electronic Engineering Department and AEE stands for, Aeronautical Engineering Department. Both departments belong to Middle East Technical University.

CHAPTER 2

LITERATURE SURVEY

2.1 Introduction

This chapter illustrates the literature survey performed prior to the conceptual design of the 'Tilt-Duct VTOL UAV.' As a competitor, unfortunately, there is only one VTOL UAV data in hand, which is the Eagle Eye, a tiltrotor unmanned air vehicle belonging to the Boeing Company. These data on this UAV will be examined as a part of this chapter. Then, a brief history of the VTOL aircraft will be given, and the best known VTOL aircraft configurations up to today, will be explored.

2.2 VTOL UAVs

In this age of acronyms, the term VTOL stands for vertical takeoff and landing, and UAV stands for unmanned (uninhabited) air vehicle. Although similar in many respects to conventional aircraft design, VTOL concept presents many key differences and challenges.

It is quite self-evident that vertical takeoff and landing capability brings many operational benefits to an aircraft. While the conventional transportation depends on airports and long paved runways, VTOL can be performed in a quite compact area. It should be also taken into account how rare airports exist where it is wished to go and how crowded they usually are, causing delays in the air and on the ground.

Today, UAV's have increasing importance and interest in the commercial market. Their applications are being discovered in civilian uses; such as aerial surveys for agriculture, traffic monitoring and pollution control; meteorological data collection; pipeline survey; early forest fire detection; etc. On the other hand, they continue to be very important for the military, especially for reconnaissance missions. Additionally, they are supposed to be much cheaper than traditional reconnaissance aircraft.

In this respect, two VTOL UAV configurations will be examined as follows. One is the Tilt-Duct VTOL UAV for which this thesis represents the conceptual design process. The other one is the Bell Eagle Eye, the tiltrotor UAV, which is the one and only recognized VTOL UAV in the market, today.

2.2.1 The Tilt-Duct VTOL UAV

The Tilt-Duct UAV, shown in Figure 2.1, can take off and land as a helicopter and, can convert to a propeller driven airplane when airborne. When the nacelles are in vertical position, it operates as a helicopter. There are two main engines and propellers in ducts located at the tips of the wing. Another engine and propeller mechanism is integrated to the fuselage at the aft. This aft engine is used to control pitch by controlling throttle in hover and transition modes. It also contributes to lift. Additional pitch control as well as yaw control is realized through exit guide vanes located at the exit of the aft engine. Roll control is achieved by differential thrust realized at the main engines.

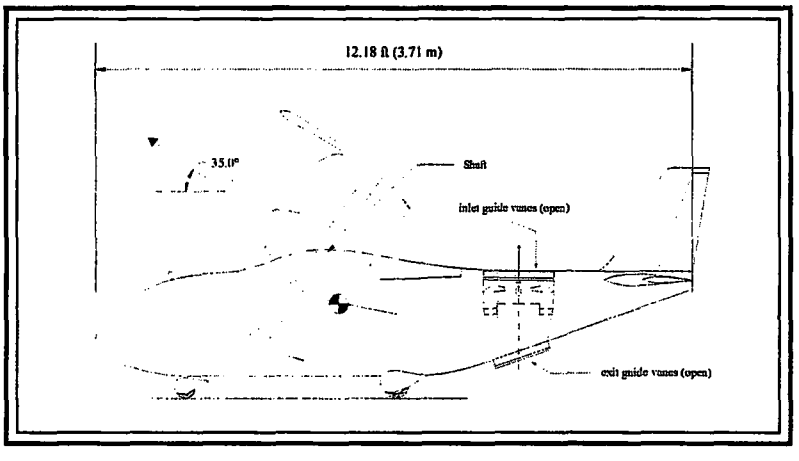

Figure 2. 1 Side view of Tilt-Duct VTOL UAV in transition mode, e.g. tilt angle = 35°.

When the ducts/propellers become horizontal, the aircraft operates as a conventional propeller driven airplane. The wings provide necessary lift. Conventional, rudder, aileron, elevator control surfaces are used. All of the guide vanes (i.e., inlet and exit) are closed during forward flight. Aft section engine is used only to obtain electricity in this mode and disconnected from the aft propeller through and electromagnetic clutch.

Tilt-duct concept has some basic differences than the *tilt-rotor* concept; such that the propellers are located in the ducts attached to the tip of the wings. This brings an advantage of 'end-plate' effect. Another difference is that, the propellers require no hinge or swash-plate design and manufacturing. During transitional flight, asymmetric disc loading may be produced due to the forward speed of the aircraft. This problem may be solved by employing a cyclic pitch mechanism. However, such a mechanism will not be employed for this design UAV. Such details require too much expertise which conflicts with one of the main objectives of this design, 'cheap and easy manufacturing.' Hence, application of a ducted propeller may help to eliminate this asymmetric loading. This will also help to suppress the vibrational effects on shaft due the asymmetric loading on propellers.

i. The Advantages of Using Ducts

In Figure 2.1, the engines and propellers are shown to be located in ducts. This approach is preferred for the design UAV in reference of the following issues,

i. By this way, the wings will have no interference with the downwash of propellers. In V-22 Osprey, which is a tiltrotor multimission aircraft, the downwash air flow of the strong Allison T406 engines apply very high pressure on the wings, perpendicularly. For this purpose, especially during vertical takeoff, transition and landing, in order to minimize the surface area subjected to the high pressure, the flaps are pushed full down. The interesting point is that, during takeoff, this is a quite unusual case for the conventional aircraft.

   In the case of Tilt-Duct UAV, this brings an advantage of minimizing the need of complicated flapping mechanisms. This will consequently reduce the overall cost of the UAV and ease the manufacturing process.

ii. The ducts will act like an 'endplate'. By this way, the effective aspect ratio of the wing will be higher than the design aspect ratio. Let's comment on this subject.

An obvious way to prevent the induced drag is to use an endplate, i.e. a vertical plate at the wing tip. Induced drag is caused by the higher-pressure air at the bottom of the wing escaping around the wing tip to the top of the wing. This air escaping around the wing tip lowers the pressure difference between the upper and lower surfaces. This reduces the lift near the tip. A wing with higher aspect ratio will have the tips farther apart than a lower aspect ratio wing which has the same surface area. Therefore, the amount of the wing affected by the tip vortex is less for a wing having a higher aspect ratio. Besides, the strength of the tip vortex is reduced.

iii. The Tilt-Duct VTOL UAV does not use rotors, i.e. no hinge or swash-plate design. Just the regular propellers that can be found in the market. This will also ease the manufacturing process and reduces the requirement of too much expertise.

iv. Locating ducts at the wing tips, the pressure and load distribution will be more uniform from the roots to the tips. It is a common fact that the maximum amount of load is applied to the roots of the wings. The pressure distribution shows a decay from maximum to minimum, starting from the root to the tip of the wing. By applying load to the wing tips, i.e. installing ducts, a more uniform pressure/load distribution will be obtained.

v. Depending on the duct's shape, i.e. proportion of the inlet and exit areas, probably the thrust output will be increased. In hover flight, this may cause an increase in power-to-thrust ratio up to an amount of 41%.

vi. It will produce less noise. This may be an advantage, especially in the reconnaissance purposed flights.

ii. The Disadvantages of Using Ducts

The approach of using ducts will also have some disadvantages. These may be listed as follows,

i. The ducts will create drag themselves. Although they create endplate effect, and reduce the strength of tip vortex, i.e. induced drag, they themselves create drag due to their own wetted area. This drag force will also apply pressure to the roots of the wings due to the long moment arm.

ii. They will increase the structural weight of the UAV.

iii. It will be somewhat difficult to handle the horizontally opposed piston engines at low velocities. The horizontally opposed engines vibrates at low speeds. In the case of the Tilt-Duct VTOL UAV, the engines are located at the centerline of the ducts by means of five airfoil profiled sticks-clip combination. For this purpose, the reaction of the duct-engine combination should be tested for vibration durability at low speeds.

This conceptual design study of the 'Tilt-Duct' VTOL UAV is basically purposed for civilian uses. It is a part of a research activity being carried out in Middle East Technical University. Since, will be manufactured in a university type environment, it is aimed to be cheap and easy to manufacture. Hence, the structural complexity is minimized whereas possible. Some of the properties of Tilt-Duct VTOL UAV are listed in Table 2.1.

2.2.2 The Bell Eagle Eye

The Bell Eagle Eye is a tiltrotor UAV capable of taking off and landing like a helicopter and fly with the high speed and range of a traditional fixed wing aircraft. It is, unfortunately, the one and the only VTOL UAV that can be found in the market. Generally, VTOL UAVs are of helicopter type, which are out of scope of this literature survey.

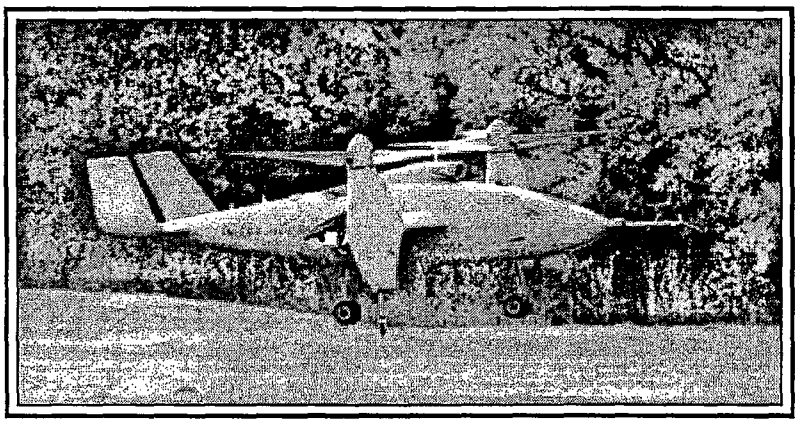

Figure 2. 2 The Bell Eagle Eye, a tiltrotor VTOL UAV. [15]

The TiltRotor Eagle Eye UAV was designed to meet the criteria of the Naval Services of the US for a tactical VTOL UAV that can operate safely and effectively from small ships and confined areas to provide real-time data in support of Reconnaissance, Surveillance, Targeting and Acquisition (RSTA) related missions. These criteria were as follows:

- It must be easy to launch, recover and maintain in a variety of sea conditions.

- The aircraft's cruise performance must be robust enough to get a 200 pound payload to a target area 110 nautical miles away against a 25 knot head wind.

- It must have 3-4 hours endurance on station to both cover large search areas and to avoid interference with other shipboard operations.

- It must be able to survive against a sophisticated array of air defense missiles and guns, electronic warfare systems and armed fixed and rotary wing aircraft.

- It must be affordable both in terms of initial purchase and life cycle operational costs.

The Eagle Eye was one of three VTOL UAVs selected for the U.S. Navy's VTOL UAV demonstration program, flying 55.5 hrs in 43 flights at Yuma, AZ, USA (Mar-May 98). In transition to airplane mode, the counter-rotating proprotors mounted on each wing tip nacelle are rotated 90 ° forward, thus converting the VTOL UAV into a highly efficient turboprop airplane. It uses a government inventory, heavy fuel gas turbine engine where heavy fuel is required on board ship for safe operation. [15], [21] & [22]

Because of its dual requirements to both hover and to fly as a conventional aircraft, the Eagle Eye required a very complex structural arrangement. Its gas turbine engine (an Allison C20) is mounted in the center fuselage and is attached to a combining transmission. Drive shafts from the combining transmission pass through the center of the wing and connect to transmissions at each wingtip. The wingtips house the transmission as well as the actuator used to tilt the wingtip transmission and rotor assemblies.

The cantilever wing box experiences very diverse structural loads during hover and conventional forward flight. An additional challenge was to make the wingbox a fuel

tank (wet wing), while preserving the dry integrity of the transmission drive shaft conduits.

The composite sandwich fuselage featured three removable sections; the nose, center section and tail. This was done to allow for a reduction in overall length during transport and storage. The nose section was mounted on hinges to allow easy access to the avionics and other mission equipment. The center section incorporated the wingbox, fuel tanks engine and landing gear. Access to the center section is through the removal of the entire top section of the fuselage. The removable tail was attached with a simple lightweight screw row. The tail contains numerous antenna and actuators for the pitch control surfaces. All of the hard points and mounts were installed by the Scaled Composites company and all the system components including engine, transmissions, oil coolers, avionics, flight control systems, flaps, and control surfaces were mounted and checked for clearance, interference and fit in the fuselage structure before the vehicles were delivered to Bell. The company, Scaled Composites also manufactured and integrated all the landing gear components for both vehicles.

About the Naval environmental conditions, another important area is the Electro-Magnetic Interference (EMI). The Eagle Eye meets the Navy's 200 volt per meter capability by the use of a conductive carbon/epoxy skin, in conjunction with that provided by equipment installation techniques and shielded filter line wiring where required.

For the dynamic naval situations, two alternative cruise speeds are considered, 75 knots and 165 knots. The Eagle Eye, returns in two hours for another mission with a 165 knots of cruise speed. Conversely, the 75 knot cruise alternative returns to the ship more than eight hours later (assuming it has enough fuel to complete the mission) because of the wind and ship speed. [15]

The Naval Service requires payload carrying of at least 150-200 lb, e.g. payloads, required for mine detection, ECM and targeting missions. The Eagle Eye can carry 300 lb of mission payload and remain airborne for more than five hours.

Its flight controls are all electric. This is a lightweight approach which eliminates the opportunity for chafing and leaking hydraulic lines and cylinders. The Eagle Eye is also designed to be easily washed and drain holes are provided to prevent collection of fluids.

Some of the properties of the Bell Eagle Eye tiltrotor UAV are listed in Table 2.1.

Table 2. 1 Some performance characteristics of two VTOL UAVs.

AIRCRAFT	***Tilt-Duct VTOL UAV***	**Bell Eagle Eye**
COUNTRY	TURKEY	USA
Type	Tilt-duct VTOL UAV	Tiltrotor UAV
Payload Weight (lb)	22.05	100 - 300
Empty Weight (lb)	151.5	-
Max. Gross Weight (lb)	226.6	1960
Power Plant	2 * 24 hp Limbach L 275E	1*Allison C20
Wing Span (ft)	10.64	15.2
Airfoil type	Eppler E 583 & E 527	-
Fuselage Length (ft)	12.2	17.9
Height (ft)	4.68	-
Cruise Speed (km/h)	164.5	0-370
Operation Altitude (ft)	> 20,000	20,000
Endurance (hr)	8.8	8 / 5 (with 300 lb payload)
Range (km)	1300	-
Guidance / Tracking	GPS auto. flight control	GPS, encrypted digital link, dual redundant flight control / navigation
Launch / Recovery	automatic VTOL	automatic VTOL
Payload / sensors	TV camera	FLIR, day/night EO/IR
Use(s)	reconnaissance, surveillance, civil, target acquisition	Surveillance, reconnaissance, target acquisition

2.3 VTOL Aircraft

Since 1930s, numerous VTOL aircraft configurations were built and flown with varying degrees of success and which proved that there were many promising approaches to VTOL. These efforts covered many concepts from propeller driven tail sitters through tilting rotors, tilting wings, deflected slipstream, lift fans and jet lift types. The main points, in these design attempts were to combine the vertical flight capability of the helicopter with the superior forward flight performance of the fixed-wing airplane. As a matter of fact, there happened many unsuccessful attempts. While many flew, technical shortcomings, and lack of performance or finance prohibited further development.

In the followings, a concise chronological history of these aircraft is presented.

2.3.1 The Transcendental 1-G

This is known as the first tiltrotor VTOL aircraft. In the 1940s, *The Transcendental Aircraft Co.* designed and built the Model 1-G. this single place, research aircraft, shown in Figure 2.3, has a gross weight of 1750 lb and two, 17-ft diameter, tilting rotors. It experienced dynamic problems with coupling between the wing and rotors and crashed in 1951. It was rebuilt and flew again in 1956.

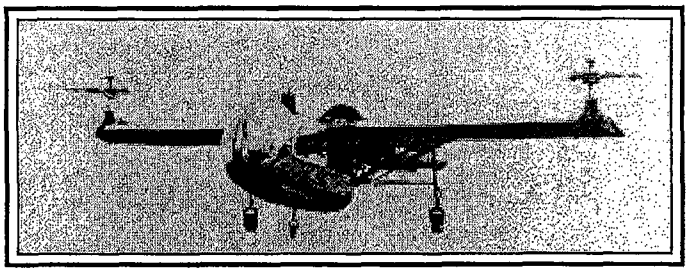

Figure 2. 3 The Transcendental 1-G, the first tilt-rotor VTOL aircraft. [5]

2.3.2 The Bell XV-3

In 1950s, a "convertiplane" competition for an observation and reconnaissance V/STOL airplane was held. 19 designs were submitted by 17 companies. Only two of these were selected for prototype development, the McDonnel XV-1 and the Bell XV-3. The XV-1 was a compound airplane having a wing, rotor and propeller. The rotor was

driven by tip-burning jets. It made its first transition from vertical to horizontal flight on April 29, 1955, but the program was eventually canceled because of excessive noise and some aerodynamic problems. [5]

The XV-3, a tilt rotor configuration, shown in Figure 2.4, built by the *Bell Helicopter Co.*, first flew on August 23, 1955. The principle employed was that of the tilt rotor with twin engines located at the extremities of a conventional wing. During takeoff, the rotors were positioned with axes such that the aircraft operated as a conventional helicopter, even if a twin rotor helicopter. As the aircraft transitioned into the cruise, the rotor tilted forward until eventually both rotors acted as conventional propellers or airscrews pulling the aircraft forward in the normal way. For landing, the situation was reversed with the rotors being tilted aft until the aircraft was flying in the helicopter mode once again. [5] & [6].

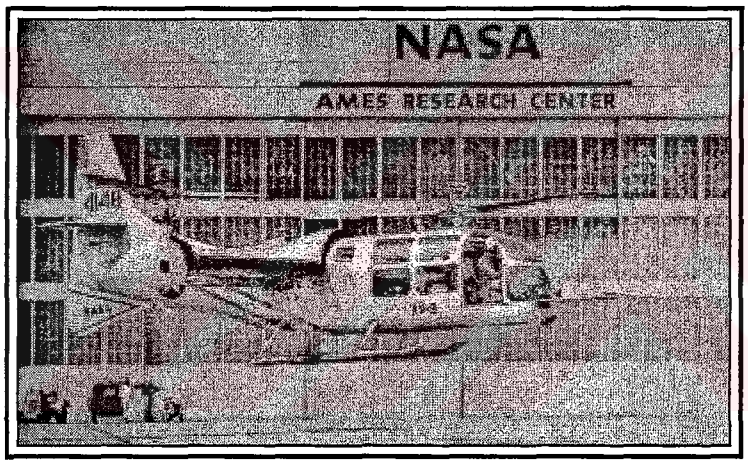

Figure 2. 4 The Bell XV-3 tilt rotor VTOL aircraft. [7]

The XV-3 was powered by a single 450 hp, R-985 Pratt & Whitney piston engine which transmitted power to the rotors via a complex mechanical arrangement. It had a design gross weight of 4,700 lb. Originally it was equipped with 3-bladed rotors, an aeroelastic problem required a switch to a 2-bladed system. The XV-3 attained a maximum speed of 115 knots in level airplane mode and a speed of 155 knots in a dive. The optimal airplane mode rotor speed was found to be 324 rpm, and the helicopter mode rotor speed, 532 rpm. Its pylon-rotor-wing instability caused it to go unstable inside the NASA Ames 40 ft × 80 ft wind tunnel and it was severely damaged. It did show that tiltrotor flight was possible, but there were 6 major problems with the XV-3 : 1) large variations in the power required during approaches to hover, 2) a significant nose down pitching moment during transition, 3) lateral instability when hovering In

Ground Effect (IGE), 4) lightly damped dynamic stability, 5) low control response, and 6) unsatisfactory control harmony. [11]

In 1956, the aircraft suffered a serious crash which halted the development. It appears that the fundamental problem was a lack of structural rigidity due to rotor pylon coupling which led to a catastrophic failure whilst in the hover. [6]

Nevertheless, the Bell XV-3 flew and demonstrated the concept of the tilt rotor with the transition to and from the contrasting conventional and helicopter modes of flight.

2.3.3 The Doak VZ-4

The Doak VZ-4, shown in Figure 2.5, was first tested in February 1958. It was utilizing tilting, ducted propellers mounted on each wing tip to achieve VTOL performance. After flying successfully, the design was purchased by the Douglas Aircraft Co., but after losing to the Bell XV-15 in the tri-service competition, it was never developed further. [5]

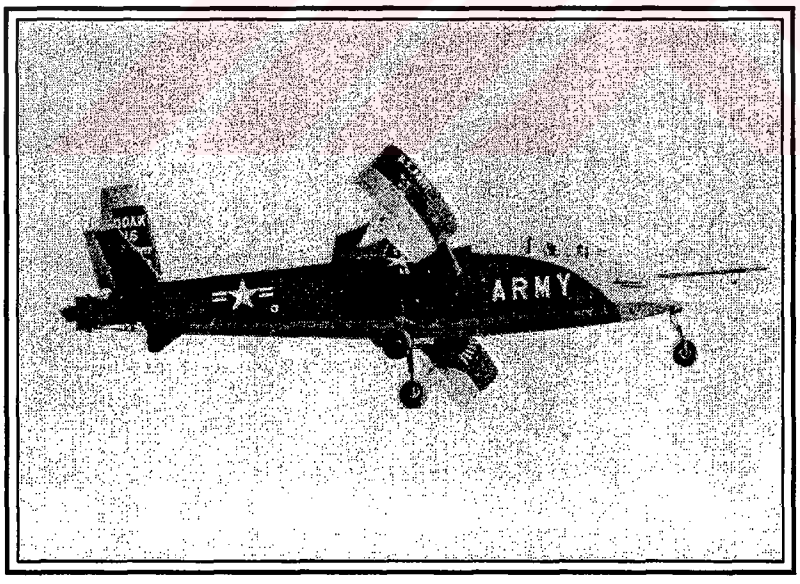

Figure 2. 5 The Doak 16-Army VZ-4 DA, a tilting duct VTOL aircraft in mid-conversion. [16]

The highly loaded ducted rotors on the wing-tips supported the aircraft in hovering, and rotate forward to produce forward thrust in cruising flight. There were conventional airplane controls for that condition. In hovering, yaw and pitch were controlled by

deflection of the jet exhaust at the tail, while the roll control was achieved by differential thrust between the two rotors.

The handling qualities in hovering were almost identical to that of the high disc-loading helicopter. The angular damping was low, but easily augmented, and the velocity stability was unfavorably high. But given enough artificial damping and control power, helicopter type properties were obtainable. Lag in vertical control would be serious for this aircraft, where the vertical damping was probably light. [16]

2.3.4 The Curtiss-Wright X-100

In 1960s, The Curtiss-Wright X-100, tilt-propeller VTOL aircraft was tested by NASA. Figure 2.6 illustrates this aircraft. In hovering, the two propellers support the aircraft directly, with control in yaw and pitch were achieved by jet deflection at the tail. The roll control was achieved by differential pitch between the two propellers. In forward flight, conventional ailerons, elevators and rudder were utilized.

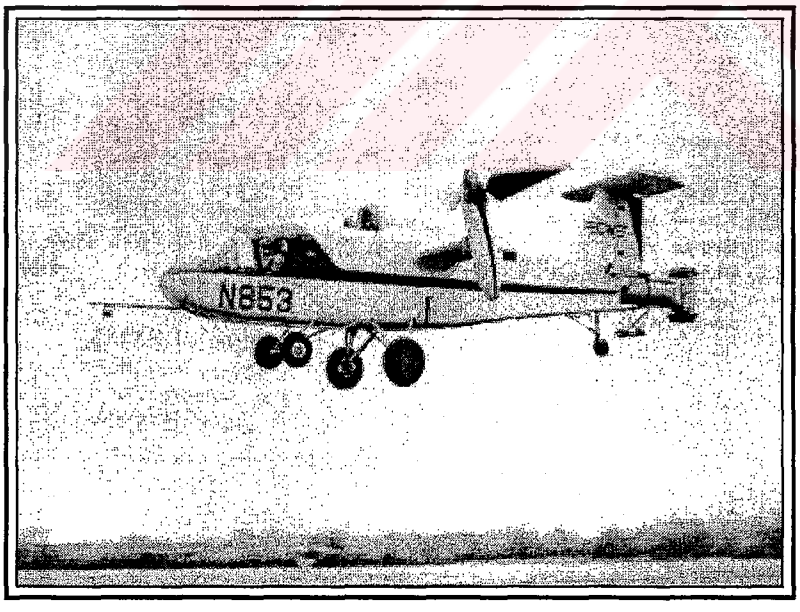

Figure 2. 6 The Curtiss-Wright X-100, a tilt-propeller VTOL aircraft. [16]

A basic design factor of X-100 was the use of propeller radial force to help provide lift during transition and allow the and allow the wing area to be sized by cruise flight requirements instead of transition. X-100 was flown to a speed of 152 knots, with the

propeller producing 1100 lb of lift due to radial force. The propeller shaft angle of attack was 25 degrees. [9]

The hovering characteristics of the X-100 were those of a high disc-loading helicopter. The angular damping was too low and velocity stability was probably undesirably high. The angular damping is something that can be augmented, but like other types, the velocity stability is something hard to defeat. [16]

The X-100 experienced especially severe disturbances when approaching to the ground in hovering and low speed flight. There was a pronounced ground effect on thrust (for a given power),

Which would normally be an advantage for vertical stability and power to hover. It was found, however, that the changes in bank or pitch attitude, or small translation velocity, would cause the ground effect to disappear and result in rapid settling of the aircraft. This characteristic, coupled with the yaw and roll disturbances, made for rather unpredictable behavior and favorable handling qualities at low speed near the ground.

In the intermediate speed range, with partial tilt, the aircraft apparently performed more smoothly than the other designs where wing stall was more of a problem. The wing of the X-100 was quite small, so that the separation effects were not strongly felt. The propellers were of very high solidity, and were capable of generating very high "normal" force, which actually provided most of the lift in forward flight. [16]

2.3.5 Ling-Temco-Vought XC-142A

In the early 1960s, the US Tri-Service Competition resulted in three aircraft being built and flown. These are the XC-142A, X-19 and X-22A. This section will focus on XC-142A.

The XC-142A, a four-engine, tilt-wing transport, shown in Figures 2.7 and 2.8, monitored by the Navy, was built by a consortium of *Hiller*, *Vought*, and *Ryan*.

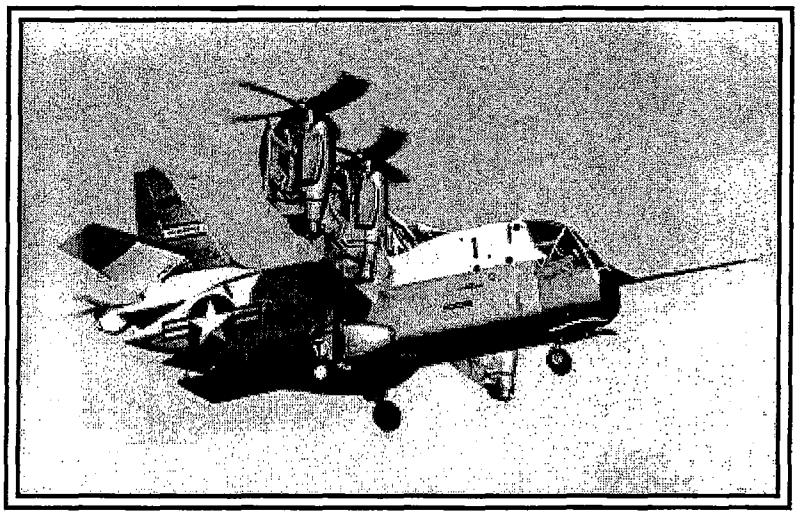

Figure 2. 7 XC-142A in hover flight mode. [8]

Although a tilt-wing aircraft seems at a first glance to be an aerodynamic anomaly, it is in fact in many ways more sound than the tilt-prop and tilt-rotor, since the propeller/rotor slipstream needn't battle with the flat side of the wing during hover and transition.

The XC-142A was a conventionally configured aircraft with four engines driving four propellers through gear boxes and interconnect shafting, see Figure 2.8. These were all mounted on a single tilting wing. A horizontal tail rotor for longitudinal control was located aft of the fuselage and was driven by shafting connecting to the engine interconnect shaft, located in the wing. Figure 2.8 illustrates the drive management of XC-142A.

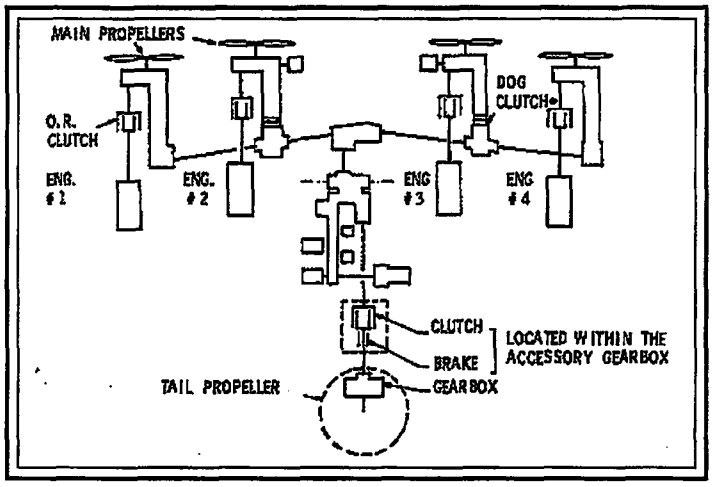

Figure 2. 8 XC-142A drive system. [9]

This cargo-assault aircraft had a gross weight of 38,000 lb and was primarily designed for sea level operation with a 200 nmi radius of action at a cruising speed of 250 knots. The three view geometry of this aircraft is given in Figure 2.9.

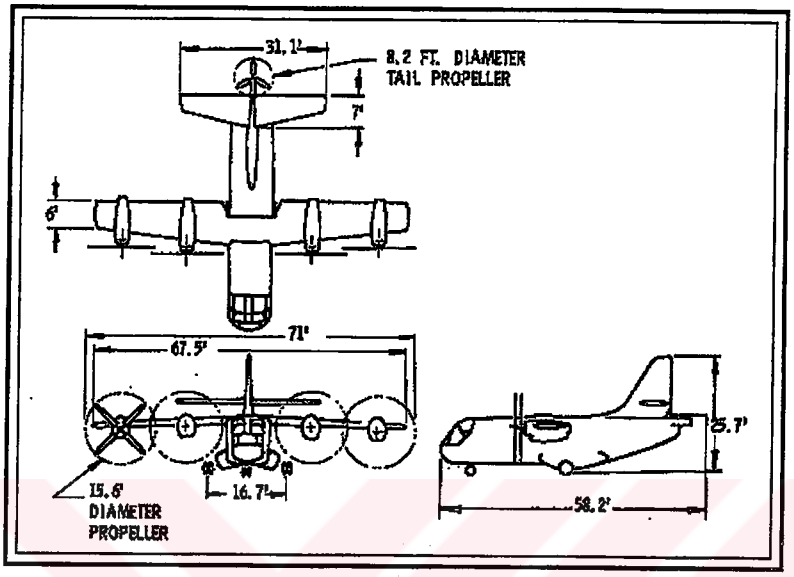

Figure 2. 9 Three views of XC-142A. [9]

For XC-142A, a thrust-to-weight ratio (T/W) of minimum 1.17 was required in order to achieve the VTOL missions, so that the landing gear sink rate limit of 12 ft/s would not exceed upon loss of engine. In addition to these thrust allowances, the XC-142A expended 6.7% of its power to the drive of the tail rotor. Because of the pitching moment characteristics in transition, the tail rotor was not used to produce lift in hover.

In Ref. [9], an accident summary for the XC-142A is presented with the factors caused the failure. Since, very useful information are presented in this respect and in order to form an example and give an idea about the failures and their resulting damages in this kind of VTOL aircraft, this accident summary will be included here, as follows.

The program of XC-142A involved five separate aircraft with flight testing starting in October 1964. 420 hours of testing were accomplished during the tri-service program. This program was completed in late 1967. During this time, four of the aircraft were lost due to accident. Upon completion of the tri-service program, the remaining aircraft was tested at NASA Langley for approximately two years and then was retired to the Air Force Museum in 1970. [8] & [9]

The aircraft accidents resulting in the loss of the aircraft or severe damage are presented as follows:

Aircraft #2 – On 19 October 1965, this aircraft experienced a ground loop on landing which caused extensive damage to the wing and propellers. The hydraulic system had a fatigue failure which caused the left outboard propeller actuator to fail during the flare-out and landing. This caused an asymmetrical thrust and a ground loop to the left.

Aircraft #3 – On 4 January 1966, this aircraft made a hard landing in the vertical mode. The aircraft sustained major damage to the fuselage. The cause of this accident was the pilot's failure to select the proper propeller speed for vertical mode flight. The pilot procedures were revised subsequently to assure the proper propeller speeds would be selected. The wing of this machine was later mated with the fuselage of the aircraft # 2 for further flight testing.

Aircraft #4 – On 27 January 1966, there was a turbine failure in the number #1 engine caused by the failure of the overriding clutch to engage. This caused extensive damage to the wing, the outboard aileron, the number #2 nacelle, the aft engine shroud and the fuselage. This aircraft was repaired, used by NASA for flight research, and is now the one in the Air Force Museum.

Aircraft #5 – On 28 December 1966, this aircraft was taxied into a hangar door causing major damage to the fuselage nose, the wing, the wing hinge and the propellers. The accident was caused by the pilot failing to actuate the hydraulic system; therefore the pilot had no brakes or nose wheel steering available.

Aircraft #1 – On 10 May 1967, the failure of the spring capsule in the tail rotor pitch control system gave full pitch to the tail rotor, as the aircraft approached to the hover configuration. It nosed over at about 200 ft altitude and crashed in an inverted altitude killing the pilots. This is the only accident during the tri-service program that could be directly attributable to the V/STOL configuration.

Aircraft #1 – On 9 October 1967, this aircraft experienced a hard landing due to a high sink rate at low forward speed. The pilot reduced power while attempting to go into a hover configuration causing a high rate of descent which could not be stopped prior to ground impact. The hard landing broke the fuselage and the wing. The aircraft was considered beyond repair. [9]

2.3.6 Bell X-22A

Another aircraft in the Tri-Service competition was the Bell X-22A. This airplane, supported in part by the US Navy and US Air Force, employed four ducted rotors mounted at the tips of tandem wings, shown in Figure 2.10.

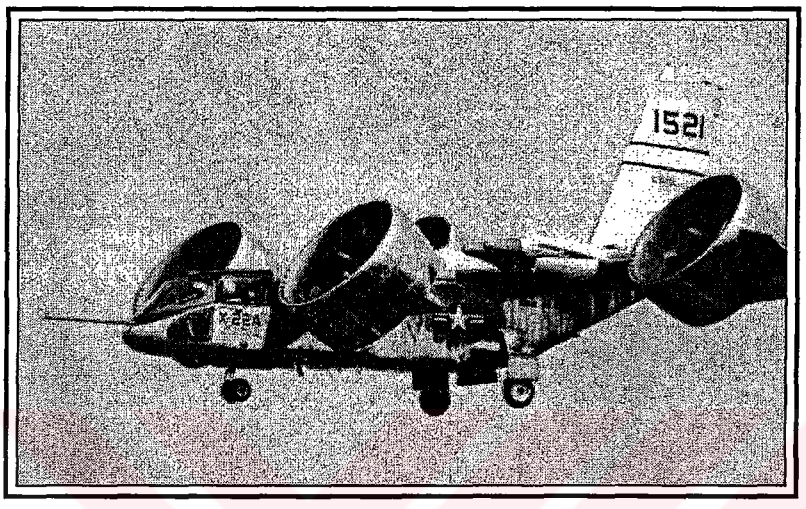

Figure 2. 10 The Bell X-22A. [7]

The X-22A was designed as a light transport of 14,830 lb gross weight, but was to be used as a flight control research vehicle, and therefore incorporated a variable stability system.

The aircraft was based on the use of tilting shrouded propellers, two located near the front of the fuselage and two aft. The forward shrouds are close to the fuselage while those at the rear are mounted at the ends of a short span, non-tilting wing with short tip panels extending beyond the outboard shroud walls. A three view sketch of X-22A is shown in Figure 2.11. Since the shrouds act as ring wings in forward flight, the system can be considered as a tandem wing arrangement. All four shrouded propellers are identical, except for direction of rotation.

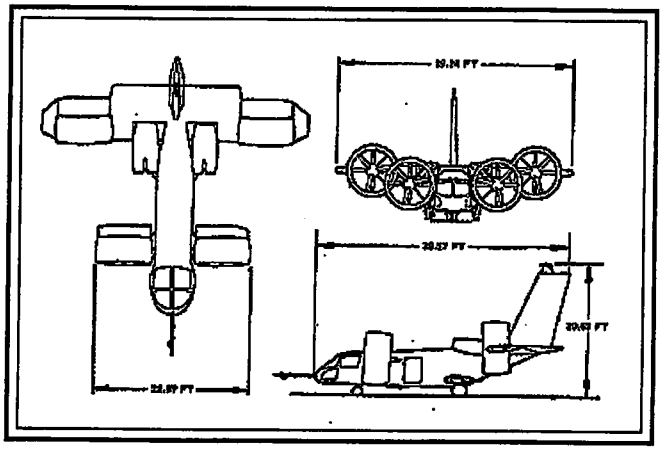

Figure 2. 11 Three view of Bell X-22A. [9]

Inside the shroud are center body containing the propeller gear box, a horizontal wing-like stator which houses the transverse drive shaft, and a vertical stator or strut to provide additional spacing between shroud and center body. Four engines are used to provide power and these are located at the rear wing leading edge and adjacent to the fuselage. Transmission shafting and gearing are arranged as shown in Figure 2.12.

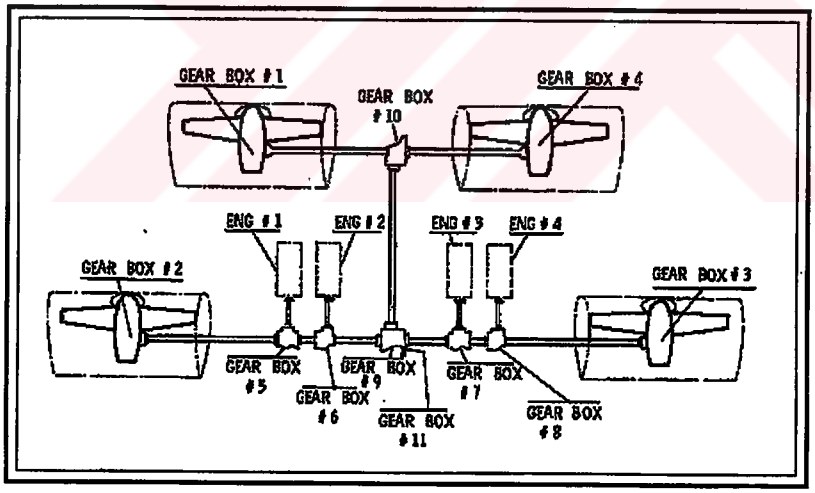

Figure 2. 12 The Bell X-22A drive system. [9]

The X-22A has a large vertical tail mounted above the fuselage. Since, this aircraft was to be used for flight control research, it was provided with large amounts of engine power and control power for use in hover flight and low speed flight. Hover on three engines at design gross weight is also possible.

The X-22A was designed to have a thrust-to-weight ratio (T/W) of 1.04 after the loss of one engine in hover. This produced a T/W of approximately 1.35 with all four engines

operating. In the case of X-22A, this extremely high T/W was primarily provided to aid in the aircraft's basic research mission as a variable stability and control vehicle.

In terms of flight control, the X-22A was found to behave well in hover and low speed flight, but this should not be surprising considering the high control power and effective SAS (Stability Augmentation System) system incorporated into the machine. Hovering in ground effect did produce random accelerations about all-axes, but caused no difficulties.

Referring to Ref. [9], the accident summary of the Bell X-22A will be given as follows.

The flight test program of X-22A began in March 1966. This program involved two aircraft and the tests began with aircraft #1. However after 15 flights for a total flight time of slightly over 3 hours, the machine suffered severe damage while making an emergency landing following sequential failure of the dualized hydraulic system. The aircraft was not repaired. The second aircraft, however, went on being used as a part of the tri-service V/STOL research program until late 1970s. hence, it served to establish V/STOL handling qualities design criteria.

Let's focus on the accident that the aircraft #1 experienced in 1966. This accident was caused by improper manufacture of hydraulic lines which led to their failure in fatigue during flight. The X-22A was having a dual hydraulic control system, whose purpose was to provide redundancy to handle a malfunction or failure. However, in this case, both sets of hydraulic lines had the same manufacturing defect. Failure of one line was followed by failure of the second line after about one minute. The first failure occurred approximately 5 miles from the airfield and triggered a warning light, whereupon the pilots headed for the runway at about 2000 ft altitude. When they were still approximately 3.5 miles from the runway and at about 1000 ft altitude, the second hydraulic failure occurred. Since the pilot still had control, he attempted to make an emergency landing in the shortest possible time in an attempt to save the aircraft. However, upon making a hard landing, the fuselage was broken in half. Hence, having a dual hydraulic system does not bring a complete safety to the aircraft, since there is always a possibility to have both systems failing simultaneously which is generally assumed to be something extremely remote. [9]

2.3.7 The Ryan XV-5

The Ryan XV-5, shown in Figure 2.13, was a unique configuration referred to as a "fan in wing." Two large fans, covering much of the planform, were mounted in the wing on each side of the aircraft. These fans were driven by turbine blades mounted directly to a ring around the fan blade tips.

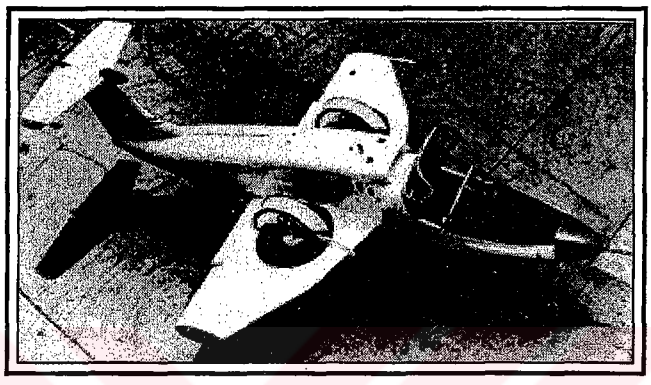

Figure 2. 13 The Ryan XV-5, a fan-in-wing VTOL aircraft. [5]

For vertical takeoff, panels on the wing surface were opened and the engine exhaust was diverted to drive the tip turbines. After transitioning to forward flight, the panels were closed to form a solid wing surface and the engine exhaust was directed rearward.

The XV-5 first went into transition from vertical flight and back on November 5, 1964. It made approximately 100 flights, a total of 42 hours and reached up to speeds of 450 mph. Unfortunately, the XV-5 suffered two crashes that resulted in the program being canceled. Neither of the crashes were related with the VTOL system. With the lower disk loading of the fan, as compared to a lift engine, the fan-in-wing configuration would appear to offer, for the same cruise performance, a better hover performance than a deflected jet VTOL system. But, however, the program was terminated following these two crashes. [5]

2.3.8 The Bell XV-15

The development of the XV-15 Tiltrotor research aircraft, shown in Figure 2.14, was initiated in 1973 with joint Army/NASA funding as a "proof of concept", or "technology demonstrator" program, with two aircraft being built by Bell Helicopter Textron (BHT) in 1977.

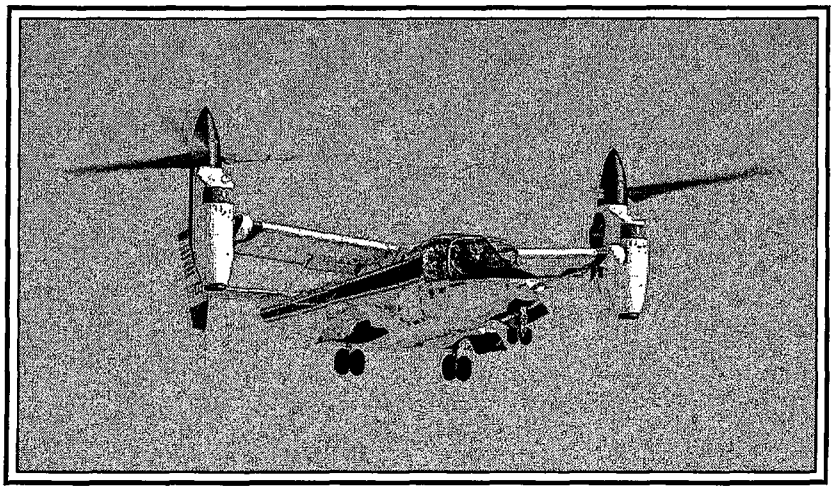

Figure 2. 14 The Bell XV-15, a tiltrotor VTOL aircraft. [10]

The XV-15 program objected to fix the major problems (see Section 2.3.2, *The Bell XV-3*) of the XV-3 tiltrotor aircraft. The first three major problems of the XV-3 were the characteristics of a VTOL aircraft which occurs by the combination of laterally separated rotors, wing and horizontal stabilizer. These problems were corrected in the XV-15 with a better control system. The last 3 major problems were unique to the XV-3 and were corrected in the XV-15 by increasing the tail volume to offset the rotor destabilization effects, by adding a rotor hub spring to increase the rotor control effectiveness, and by including the Force Feel System (FFS) which improved the control harmony. In the event of complete power failure, the rotors could windmill in airplane mode and autorotate in helicopter mode. [11]

The XV-15 is powered by twin Lycoming T-53 turboshaft engines that are connected by a cross-shaft and drive three-bladed, 25 ft diameter metal rotors (the size extensively tested in a wind tunnel) having highly twisted blades which twist 45 degrees from root to tip. They are gimbal mounted to the hub and have an elastrometric spring for control augmentation. The engines and main transmissions are located in wing-tip nacelles to minimize the operational loads on the cross-shaft system and, with the rotors, tilt as a single unit. The nacelles can tilt from 0° to 95°. [10] & [11]

The XV-15 has a gross weight of 13,000 lb, and a maximum gross weight of 15,000 lb. It weighs 9,076 pounds empty and measured slightly more than 46 feet in length. The distance from the ground to the top of the tail was nearly 13 feet, and the span of its forward-swept wings was about 32 feet. As mentioned before, It featured two three-bladed rotors, each measuring 25 feet in diameter. [10], [11] & [12]

The aircraft began its contractor flight tests at NASA Ames on April 23, 1979, after completing the wind-tunnel testing in the Ames Center in a 40-by-80-foot wind tunnel. Bell Army, and U.S. Marine pilots flew it on 140 separate missions over the following year before turning the aircraft over to Ames. The research flights continued until April 1994. The successful flight research with the XV-15, spearheaded by the team at Ames, led to the military V-22 Osprey and to the possibility of using tilt-rotor aircraft as a solution to the problem of crowded airports and highways. [12]

2.3.9 The Bell-Boeing V-22 Osprey

In 1985, the program for V-22 Osprey, got fully under way with US Navy and US Marine sponsorship. Besides, the V-22 Osprey, shown in Figure 2.15, is the first aircraft designed from the ground up to meet the needs of all four US armed services. It was developed/built by the joint Bell/Boeing Vertol team. [6] & [13]

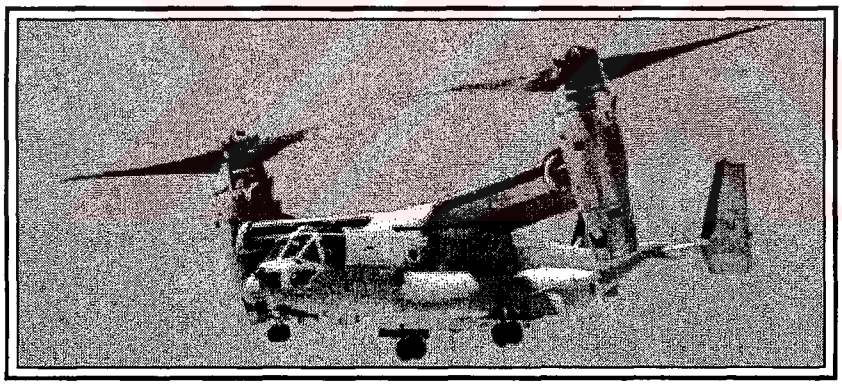

Figure 2. 15 The Bell-Boeing V-22 Osprey, a tiltrotor VTOL multimission aircraft. [13]

The V-22 Osprey is a tiltrotor multimission VTOL aircraft. A four-view picture is illustrated in Figure 2.16. The aircraft is powered by two 6000 shp Allison T-406-AD-400 turbine engines each of which is contained within the tilting nacelles. Each engine/nacelle combination weighs about 5000 lb which is almost the same as the total weight of the original Bell XV-3. The V-22 Osprey has a maximum gross weight of 47,500 lb for the VTOL mission, 55,000 lb for the STOL mission and 60,500 lb for the self-deploy mission. It weighs 33,140 lb pounds empty and measures slightly more than 57 feet in length. The distance from the ground to the top of the tail is nearly 18 feet, and it measures about 84 ft from one rotor tip to the other, including the wing span. It

features two three-bladed rotors, each measuring 38 feet in diameter and made of graphite/fiberglass. [6] & [13]

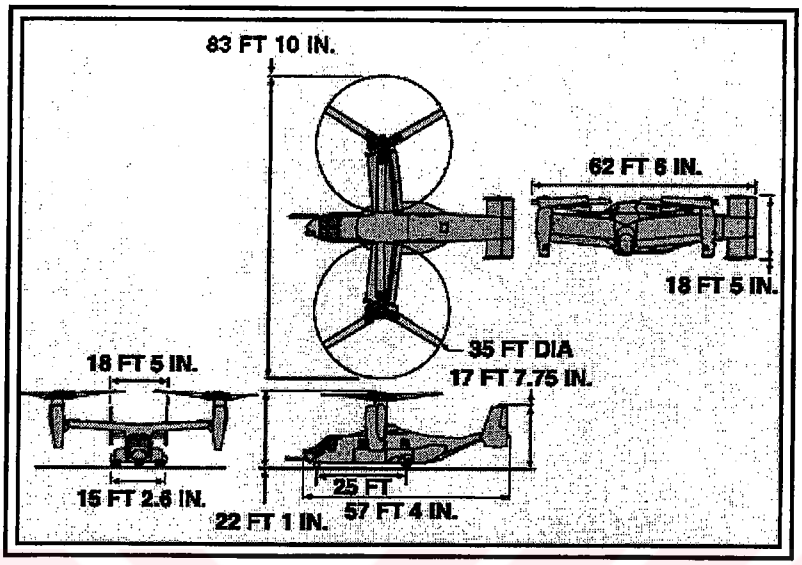

Figure 2. 16 Four-view sketch of the V-22 Osprey. [13]

Each engine of V-22 Osprey drives a prop rotor gearbox located in the nacelles from which each rotor is driven in the opposing direction to the other, thereby counterbalancing torque effects, see Figure 2.17.

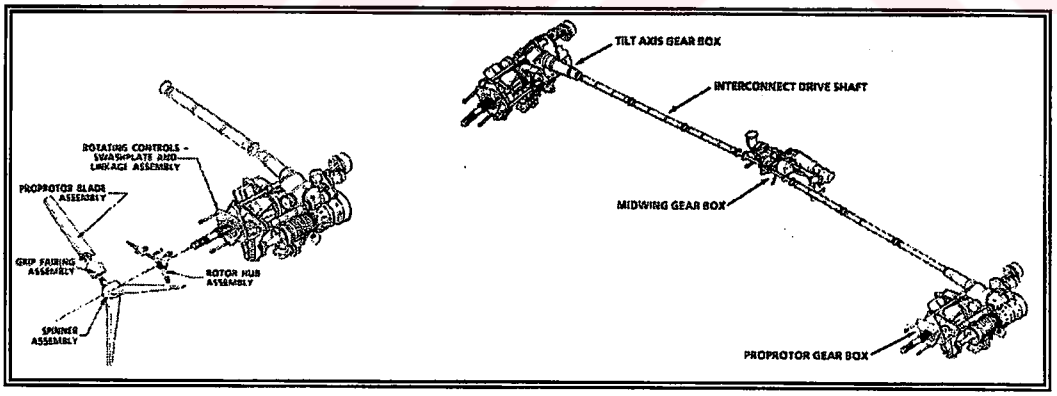

Figure 2. 17 The V-22 Osprey drive system (Bell-Boeing V-22 Tiltrotor Team). [6]

Each prop rotor gearbox also drives through a tilt axis gearbox and mechanical linkage running through the wing to a mid-wing gearbox which effectively interconnects the two systems and also acts as the main aircraft accessory gearbox driving the constant frequency ac generators (two per aircraft, each rated at 40 kVA) and variable ac

generators (two per aircraft, each rated at 50/80 kVA) and 5000 psi hydraulic system pumps. [6]

The flight control system of V-22 Osprey effectively controls two different modes of flight and the transition between them. Figure 2.18 and 2.19 shows two different flight modes for the V-22 in the helicopter and airplane modes. In the helicopter/VTOL mode, cyclic and collective pitch are used as for a conventional helicopter except that differential cyclic pitch provides aircraft roll and differential cyclic pitch provides aircraft yaw. In the airplane mode of flight, pitch, roll and yaw are provided by elevators., flaperons and rudders respectively. At an appropriate point in the nacelle tilt operation, the vertical flight control functions are "washed out" and the aircraft established in the aeroplane mode. The flight control computations are provided by a triple-redundant all developed by General Electric. For further information on the digital fly-by-wire system, see Ref. [14], [6] & [13]

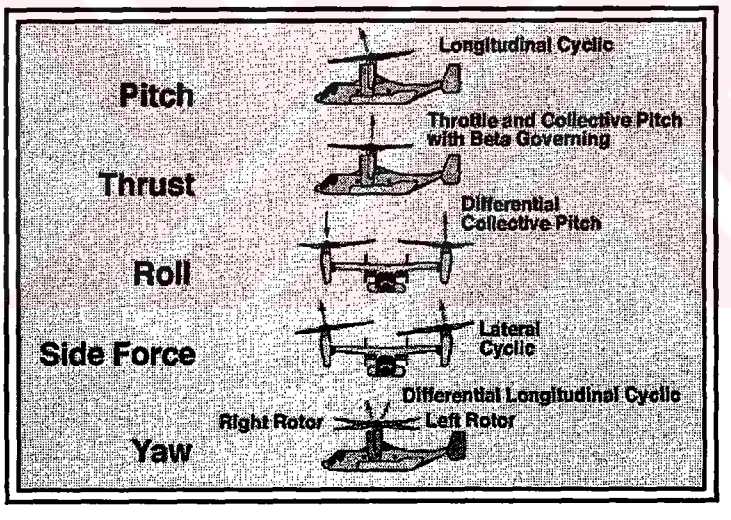

Figure 2. 18 The Bell-Boeing V-22 Osprey control characteristics, i.e. helicopter mode. [13]

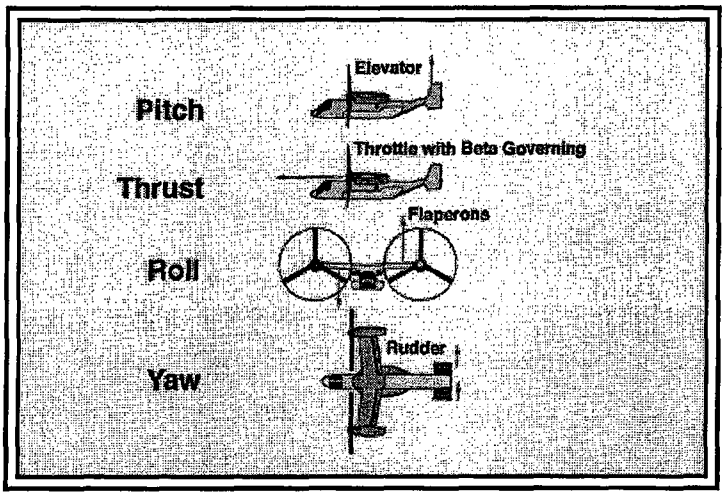

Figure 2. 19 The Bell-Boeing V-22 Osprey control characteristics, i.e. airplane mode. [13]

A further interesting and probably unique feature of the V-22 Osprey is the rotor and wing stowage facility. In Figure 2.16, the view in the most right shows the stowed configuration of the aircraft. In order to achieve this configuration, first the rotor blades are folded inboard to align with the wing. Then, the nacelles are tilted forward to place the rotor blades parallel with the wing leading edges. Finally, the whole wing is rotated 90 degrees clockwise to be positioned along the top of the fuselage. [14], [6] & [13]

2.3.10 The Bell/Augusta 609

The Bell/Agusta 609, shown in Figure 2.20, is a civil tiltrotor aircraft designed primarily for executive transportation, natural resource exploration, emergency medical evacuation, governmental support roles and disaster relief.

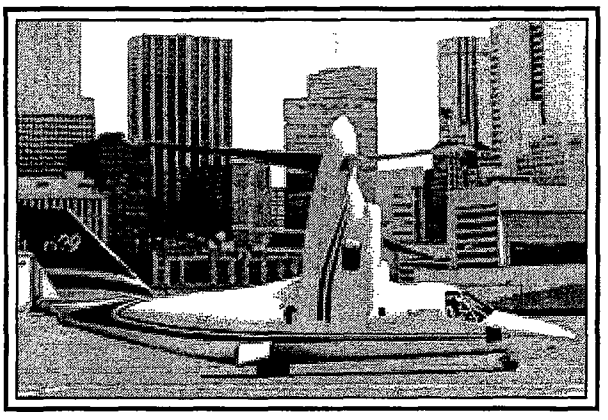

Figure 2. 20 The Bell/Augusta 609, a tiltrotor VTOL commercial aircraft. [15]

A three-view picture of the Bell/Augusta 609 is illustrated in Figure 2.21. The aircraft is powered by two 1850 shp Pratt & Whitney PT-6 series turboshaft engines each of which is contained within the tilting nacelles. The Bell/Augusta 609 has a maximum gross weight of 16,000 lb. It weighs 10,500 lb pounds empty and measures about 44 feet in length. The distance from the ground to the top of the tail is nearly 15 feet, and it measures about 60 ft from one rotor tip to the other, including the wing span. It features two three-bladed rotors, each measuring 26 feet in diameter and made of graphite/fiberglass. [15]

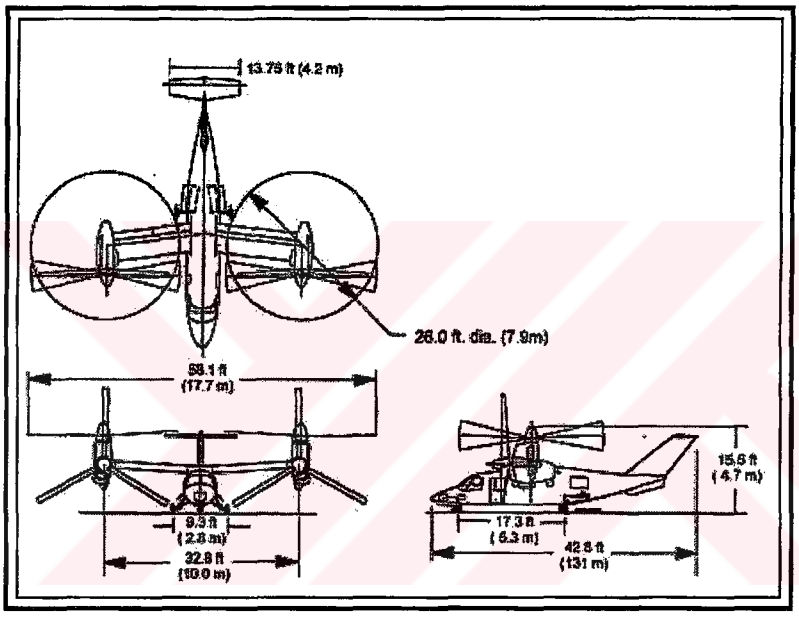

Figure 2. 21 Three-views of the Bell/Augusta 609 civil tiltrotor VTOL aircraft. [15]

The Bell/Augusta 609 can reach to cruise speeds up to 275 knots and at ranges up to 750 nautical miles. It has an operational ceiling of 25,000 ft. [15]

2.3.11 Tabulated Characteristics of VTOL Aircraft

In Table 2.2, six of the ten VTOL aircraft introduced in this section will be tabulated according to some specific characteristics. It should be noted that, the table will be limited by the amount of available information on the related aircraft.

Table 2. 2 Tabulated characteristics of the six VTOL aircraft introduced above. The aircraft with insufficient data are not included in this table.

AIRCRAFT	*Bell/Augusta 609*	*Bell/Boeing V22-Osprey*	*Bell XV-15*	*Bell X-22A*	*Ling-Temco-Vought XC-142A*	*Bell XV-3*
COUNTRY	USA	USA	USA	USA	USA	USA
Type	Civil Tiltrotor VTOL	Tiltrotor VTOL multimission	Tiltrotor VTOL multimission	Tilt-shrouded propellers VTOL	Tilt-wing VTOL	Tiltrotor VTOL
Payload Weight (lb)	< 5500	20,000	-	-	-	-
Empty Weight (lb)	10,500	33,140	9,076	11,150	25,550	-
Max. Gross Weight (lb)	16,000	47,500	15,000	14,830 (VTOL) 18,420 (STOL)	37,500 (VTOL) 43,700 (STOL)	4,700
Power Plant	2* 1850 shp P&W PT-6 Turboshaft	2*6000 shp Allison T406-AD-400	-	4*T58-GE-8	4*T-64-GE-1	1*450 hp R-985 Pratt & Whitney
Wing Span (ft)	33	46	32	22	67.5	-
Airfoil type	-	-	-	-	-	-
Fuselage Length (ft)	44	57.33	46	39.57	58.2	-
Height (ft)	15	17.65	13	20.69	25.7	-

Cruise Speed (km/h)	509 (max)	185 - 509	-	342.62	463	287
Operation Height (ft)	25,000	26,000 (max)	-	-	-	-
Endurance (hr)		-	-	-	-	-
Range (km)	1390	2224	-	-	-	-
Guidance / Tracking	-	Tacan, VOR/ILS, AHRS	-	-	-	-
Launch / Recovery	VTOL / wheeled take-off and landing	VTOL / wheeled take-off and landing	VTOL	V/STOL	V/STOL	VTOL
Payload / sensors	-	-	-	-	-	-
Use(s)	6-9 Passenger transport	multimission	multimission	Flight control research	Assault-transport	-

2.4 Conclusion

This chapter illustrated the literature survey performed for the case of VTOL aircraft/UAVs configurations. For this purpose, one tiltrotor VTOL UAV, the Bell Eagle Eye, and eight VTOL aircraft which are of tiltrotor, tiltwing, and tilt-shrouded-propellers types are examined in a chronological order. The properties of these aircraft are presented in Table 2.1 and 2.2 within this chapter.

As a part of this chapter, as available, the accident summary of the VTOL aircraft of concern is examined. This is found quite useful in terms of giving an idea about the failures a VTOL aircraft may experience during a test flight, and what failure causes what kind of damage to which structural part of the aircraft.

The next chapter will illustrate the First Guess Sizing for the Tilt-Duct VTOL UAV. Some initial calculations will be performed on the basic characteristics of the aircraft. This will also form the initial step of the conceptual design process which is the scope of this thesis.

CHAPTER 3

FIRST GUESS SIZING

3.1 Introduction

In this level of the design procedure, initial estimates for the takeoff weight, fuel and empty weights are performed for the design Tilt-Duct VTOL UAV. The requirements and the mission profile of the aircraft will be reminded to the reader as a part of this section. During the calculations, it is assumed that no payload drop or combat exists. At the end of this chapter, trade-off studies on payload weight, range and cruise velocity are carried out and the results are tabulated.

It should be noted that, unless otherwise is stated, all the equations used in this chapter are taken from Ref. [1].

3.1.1 Requirements

As mentioned before, the following requirements were set for the design VTOL UAV. The aircraft is thought to carry just a TV camera as payload, so the payload weight is kept small approximately at about 10 kg (22.05 lb). The cruise height is set to be 2000 m (6562 ft). This value is predicted assuming that the UAV will fly approximately 1,100 m above the city of Ankara.

- h_{cruise} : 2000 m = 6562 ft
- $W_{payload}$: 10 kg = 22.05 lb
- V_{stall} : 50 knots @ 1000 m. altitude.
- Crew : None (→ since, UAV)
- V_{cruise} : ≥ 85.5 knots
- Range : > 1000 km

3.1.2 Mission Profile

The mission profile of the Tilt-Duct VTOL UAV is given in Figure 3.1.

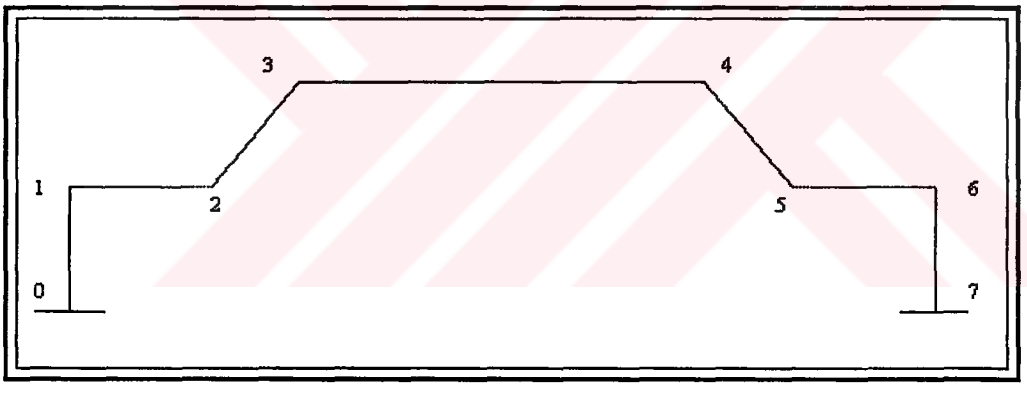

Figure 3. 1 The mission profile of the Tilt-Duct VTOL UAV.

The flight segments shown in Figure 3.1 are defined as the following:

3.2 Takeoff Weight Estimation

Takeoff weight of the design UAV is one of the most important parameters that will be estimated as a part of this chapter. This will be an initial estimation, but will give an idea about the approximate weight of the design UAV. For this purpose, the methods given in Ref. [1] will be utilized. Eqn. (3.1) gives the takeoff weight of a conventional aircraft. It should be noted that, in the case of the design UAV, there will be no crew.

$$_{o} = \frac{W_{crew} + W_{payload}}{1 - (W_f / W_o) - (W_e / W_o)} \qquad (3.1)$$

In the following, the methods that will be used to evaluate the fractions in Eqn. (3.1) will be introduced.

i. Estimation of Empty Weight Fraction vs. W_o

An simple method is introduced in Ref. [1], in order to obtain a relation between the aircraft empty and takeoff weights. Eqn. (3.2) gives this relation.

$$\frac{W_e}{W_o} = \mathrm{A} W_o^{c} \mathrm{K}_{us} \qquad (3.2)$$

where, From Table 3.1 of Ref.[1], for *Homebuilt*-composite a/c:

$A = 0.99,\ c = -0.09$

$K_{us} = 1.00$, for *fixed sweep*

Then Eqn. (3.2) becomes,

$$\boxed{\frac{W_e}{W_o} = 0.99 W_o^{-0.09}}$$

ii. Estimation of Fuel Weight Fraction vs. W_o

In order to obtain a relation between the aircraft fuel and takeoff weights, the method defined in Ref. [1] will be utilized. Eqn. (3.3) gives this relation.

$$\frac{W_f}{W_o} = 1.06\left(1 - \frac{W_x}{W_o}\right) \qquad (3.3)$$

where,

$$\frac{W_x}{W_o} = \frac{W_1}{W_o}\frac{W_2}{W_1}\frac{W_3}{W_2}\frac{W_4}{W_3}\frac{W_5}{W_4}\frac{W_6}{W_5}\frac{W_7}{W_6} = \frac{W_7}{W_o}$$

In determining the segment weight fractions, an important point is that the design UAV flies at an altitude of 2000 m. Therefore, it obviously takes less time and less fuel to climb at the cruising altitude. The *segment weight fractions* are set as follows:

[VTO (0-1) + Transition (1-2)] : $\frac{W_1}{W_o}\frac{W_2}{W_1} = 0.96$

[Climb (2-3)] : $\frac{W_3}{W_2} = 0.99$

[Descend (4-5)] : $\frac{W_5}{W_4} \cong 1$

[Transition (5-6) + VL (6-7)] : $\frac{W_6}{W_5}\frac{W_7}{W_6} = 0.97$

iii. Weight Fraction of Cruise (3-4) Segment

The cruise segment weight fraction will be evaluated by use of the Breguet's Range Equation, which is given in Eqn. (3.4).

"Breguet's Range equation" : $$\frac{W_i}{W_{i-1}} = \exp\left(-\frac{RC}{V(L/D)}\right) \qquad (3.4)$$

where,

$$\left.\frac{L}{D}\right)_{cruise} = \left.\frac{L}{D}\right)_{\max} \qquad \text{(for propeller aircraft, in cruise mode)} \qquad (3.5)$$

$$C = C_{bhp}\frac{V}{550\eta_p} \qquad \text{(specific fuel consumption)} \qquad (3.6)$$

where, from Figure 3.6 of Ref. [1] (for fixed-gear prop a/c) : $\left.\frac{L}{D}\right)_{\max} \cong 10$

From Table 3.4 of Ref. [1] For piston-prop (fixed pitch)-*cruise*: $C_{bhp} = 0.4,\ \eta_p = 0.8$

Then, Eqn. (3.6) gives the specific fuel consumption as the following.

$$C = (0.4)\frac{(124.2)}{550(0.8)}\frac{1}{(3600)} = 3.136\times10^{-5}\ \text{1/s}$$

Assuming a range of 1500 km, the corresponding aircraft takeoff weight is evaluated as follows.

The cruise segment weight fraction from Eqn. (3.4) :

$$\frac{W_4}{W_3} = \exp\left(-\frac{(5{,}000{,}000)(3.136\times10^{-5})}{(124.2)(10)}\right) = 0.8814$$

The overall weight fraction :

$$\frac{W_7}{W_o} = (0.96)(0.99)(0.8814)(0.99)(0.97) = 0.8044$$

The fuel weight fraction from Eqn. (3.3):

$$\frac{W_f}{W_o} = 1.06(1 - 0.8044) = 0.2073$$

Then, from Eqn. (3.1) :

$$_o = \frac{W_{crew} + W_{payload}}{1 - (W_f / W_o) - (W_e / W_o)} = \frac{0 + 22.05}{1 - 0.2073 - 0.99W_o^{-0.09}} = \frac{22.05}{0.793 - 0.99W_o^{-0.09}}$$

This requires an iterative solution procedure which finally yields:

$$\Rightarrow W_o = 139.4lb$$

$$\Rightarrow W_e = 0.99W_o^{0.91} = 0.99(139.4)^{0.09} = 88.49lb$$

$$\Rightarrow W_f = (0.2073)W_o = (0.2073)(139.4) = 28.898lb$$

3.3 Trade-Off Studies

In this section, range and payload trade-off calculations will be performed. That is, with different amounts of range and payload requirements, the takeoff, empty and fuel weights of the design UAV will be calculated.

3.3.1 Payload Trade Studies

In this section, with different payloads, i.e. 30 kg (66.15 lb) and 20 kg (44.1 lb), the calculations for the takeoff weight of the design UAV will be repeated. First the aircraft empty, fuel and takeoff weights will be calculated for the case of a 30 kg (66.15 lb) of payload.

i. $W_p = 30kg = 66.15lb$:

The result will directly obtained from Eqn. (3.1), since no other parameters are changed.

$$_o = \frac{66.15}{1 - 0.2073 - 0.99W_o^{-0.09}} = \frac{66.15}{0.793 - 0.99W_o^{-0.09}}$$

The iterative solution procedure which yields the following results.

$$\Rightarrow W_o = 323.4lb$$

$$\Rightarrow W_e = 0.99W_o^{0.91} = 0.99(323.4)^{0.91} = 190.33lb$$

$$\Rightarrow W_f = (0.2073)W_o = (0.2073)(323.4) = 67.04lb$$

ii. $W_p = 20kg = 44.1lb$:

Following the same procedure, by use of Eqn. (3.1),

$$_o = \frac{44.1}{1 - 0.2073 - 0.99W_o^{-0.09}} = \frac{44.1}{0.793 - 0.99W_o^{-0.09}}$$

The iterative solution procedure which yields the following results.

$$\Rightarrow W_o = 235.3lb$$

$$\Rightarrow W_e = 0.99W_o^{0.91} = 0.99(235.3)^{0.91} = 142.5lb$$

$$\Rightarrow W_f = (0.2073)W_o = (0.2073)(235.3) = 48.78lb$$

3.3.2 Range Trade Studies

In this section, with different range values, i.e. 1200 km (3,940,000 ft) and 1800 km (5,906,000 ft), the calculations for the takeoff weight of the design UAV will be repeated. First the aircraft empty, fuel and takeoff weights will be calculated for the case of a 1200 km (3,940,000 ft) of range.

i. **Range = 1200 km = 3,940,000 ft**

A change in range affects the cruise segment weight fraction, which was defined by Eqn. (3.3). Then,

$$\frac{W_3}{W_2} = \exp\left(-\frac{RC}{V(L/D)}\right) = \exp\left(-\frac{3.94\times10^6(3.136\times10^{-5})}{124.2(10)}\right) = 0.905$$

Then, following the same procedures,

$$\frac{W_x}{W_o} = (0.96)(0.99)(0.905)(0.99)(0.97) = 0.826$$

$$\frac{W_f}{W_o} = 1.06(1-0.826) = 0.1844$$

Finally, from Eqn. (3.1),

$$_o = \frac{22.05}{1-0.1844-0.99W_o^{-0.09}} = \frac{22.05}{0.8156-0.99W_o^{-0.09}}$$

The iterative solution procedure which yields the following results.

$$\Rightarrow W_o = 126lb$$

$$\Rightarrow W_e = 0.99W_o^{0.91} = 0.99(126)^{0.91} = 80.72lb$$

$$\Rightarrow W_f = (0.1844)W_o = (0.1844)(126) = 23.23lb$$

ii. **Range = 1800 km = 5,906,000 ft**

Following the same procedure, from Eqn. (3.3),

$$\frac{W_3}{W_2} = \exp\left(-\frac{RC}{V(L/D)}\right) = \exp\left(-\frac{5.906\times10^6(3.136\times10^{-5})}{124.2(10)}\right) = 0.861$$

Then,

$$\frac{W_x}{W_o} = (0.96)(0.99)(0.861)(0.99)(0.97) = 0.786$$

$$\frac{W_f}{W_o} = 1.06(1-0.786) = 0.227$$

Finally, from Eqn. (3.1),

$$_o = \frac{22.05}{1-0.227-0.99W_o^{-0.09}} = \frac{22.05}{0.773-0.99W_o^{-0.09}}$$

The iterative solution procedure which yields the following results.

$$\Rightarrow W_o = 153.4lb$$

$$\Rightarrow W_e = 0.99W_o^{0.91} = 0.99(153.4)^{0.91} = 96.55lb$$

$$\Rightarrow W_f = (0.227)W_o = (0.227)(153.4) = 34.82lb$$

3.4 Results Of Chapter 3

In this section, the results obtained as a part of this chapter, First Guess Sizing, are presented in the form of charts and tables.

3.4.1 Charts

In Figure 3.2, the results of the payload trade studies are presented. The figure involves the plots of the design UAV's takeoff, empty and fuel weights vs. the three different payload weights; i.e. 22.05 lb, 44.1 lb and 66.15 lb.

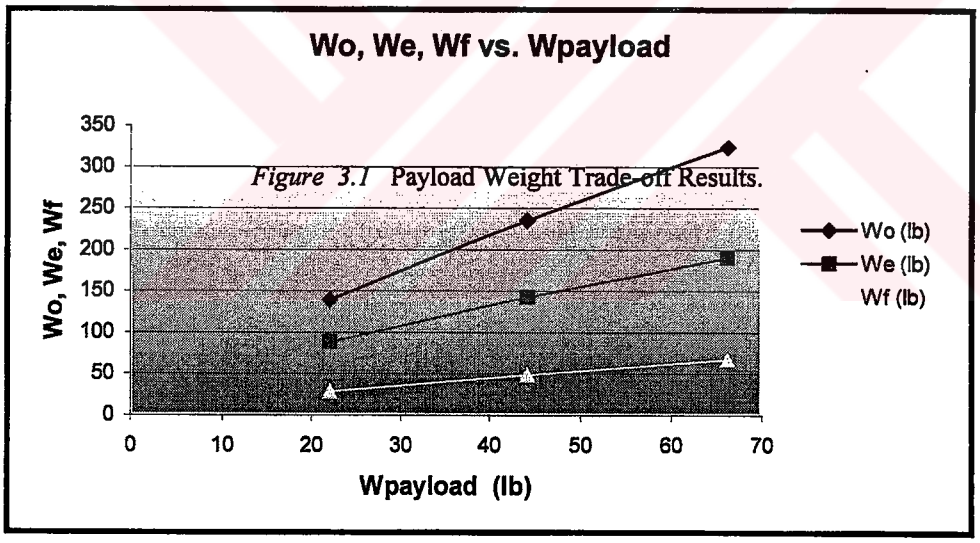

Figure 3.1 Payload Weight Trade-off Results.

Figure 3. 2 The results of payload trade studies.

In Figure 3.3, the results of the range trade studies are presented. The figure involves the plots of the design UAV's takeoff, empty and fuel weights vs. the three different ranges; i.e. 1200 km, 1500 km and 1800 km.

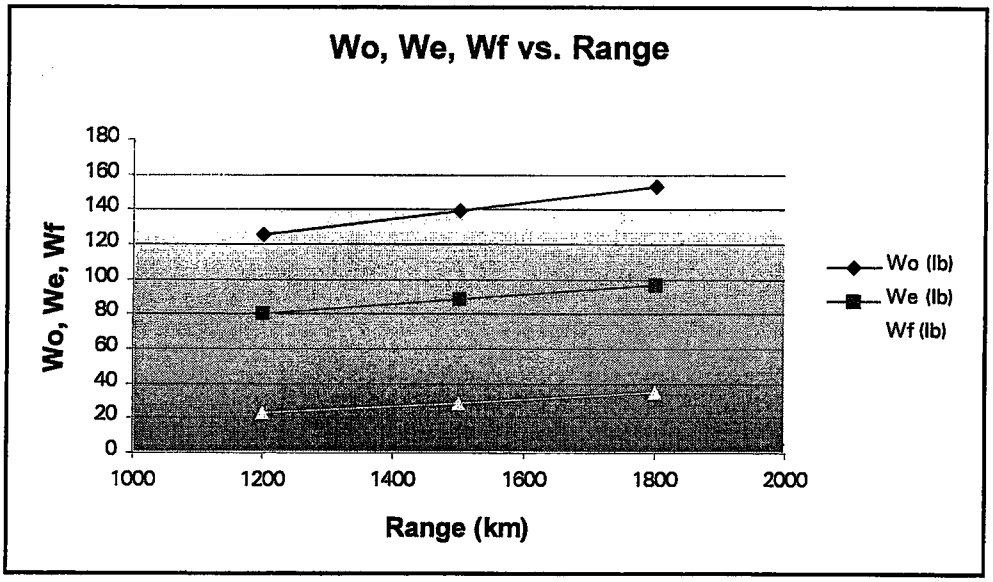

Figure 3. 3 The results of range trade studies.

3.4.2 Tabulated Results

Table 3.1 and 3.2 present the list of results calculated as the result of the range and payload trade studies, respectively.

Table 3. 1 The results of Range Trade Studies (V_{cruise} = 124.2 ft/s, $W_{payload}$ = 10 kg).

Range (km)	1200	1520	1800
Wo (lb)	126	139.4	153.4
We (lb)	80.72	88.49	96.55
Wf (lb)	25.63	28.898	34.82

Table 3. 2 The results of Payload Weight Trade Studies (V_{cruise} = 124.2 ft/s, Range = 1520 km)

Wpayload (lb)	**22.05**	**44.1**	**66.15**
Wo (lb)	139.4	253.3	323.4
We (lb)	88.49	142.5	190.33
Wf (lb)	28.898	48.78	67.04

3.5 Conclusion

The results reveal the fact that, as the required payload weight or the desired range values are increased, the take-off, empty and fuel weights of the a/c increases correspondingly, in a linear manner. This means more material, more fuel and thus more money. Next chapter will illustrate the Airfoil and Geometry Selection.

CHAPTER 4

AIRFOIL and GEOMETRY SELECTION

4.1 Introduction

Before starting the design layout, a number of parameters should be selected for the mission UAV. In this chapter, the airfoil, wing and tail geometry will be selected, which will yield us a starting point for the further calculations.

4.2 Airfoil Selection For The Wing

4.2.1 Required Characteristics of the Airfoil

- For subsonic a/c, the wing should be selected as thick as possible, since it can be manufactured with less material, thus lighter and saves cost. Besides it yields additional volume to store the fuel. But, on the other hand, it should be noted that any increment in thickness must be paid for by a drag penalty due to the shorter laminar flow over the airfoil. Thin airfoil is better for reducing drag. As *t/c* increases, $C_{d_{subsonic}}$ increases and so do the drag.

- After $C_{L_{max}}$, sharp changes are not preferable. For better stall characteristics, gradual loss of lift, small changes in pitching moment are desirable.

- *t/c* directly affects drag, maximum lift, stall characteristics and structural weight. Since, the structural weight of the aircraft is inversely proportional with the thickness ratio, as *t/c* increases structural weight decreases. On the other hand, as *t/c* increases, separation increases, hence the drag increases. At this point it should be noted that the design mission a/c is a small one, thus reducing drag becomes more important than the structural weight.

- *t/c* affects the nose shape. For example, for a wing of fairly high aspect ratio and moderate sweep, a larger nose radius provides a higher stall angle and a greater $C_{L_{max}}$.
- Attached flow over the airfoil is desirable. Low bubble formation and longer laminar flow region are also desirable, see Figure 4.1.

Note that the Reynold's number corresponding to cruise conditions is determined by use of the chord length found in the previous chapter.

$$\mathrm{Re} = \frac{V_{cr.}c}{\nu} = \frac{(1.775)(124.22)}{0.1846\times10^{-3}} \cong 1.1\times10^{6}$$

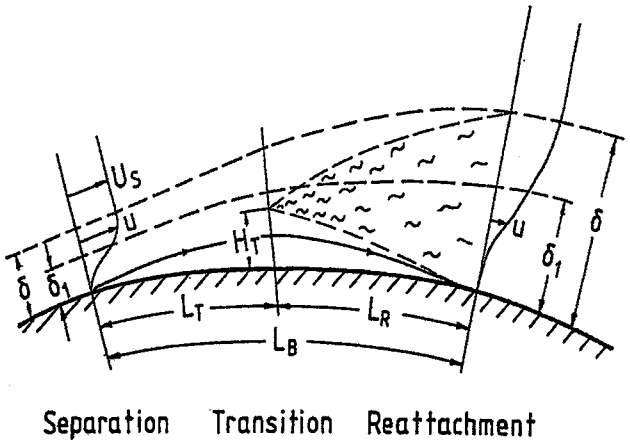

Figure 4. 1 Sketch of the laminar separation bubble [17].

4.2.2 Discussion and Selection of the Airfoil

In this section, the airfoil selection criteria will be discussed. For this purpose, three Eppler airfoils, i.e. E 582, E 583 and E 585, selected as candidates from Ref. [17]. Eppler airfoils are selected because they are known to yield a good performance in low-speed laminar flows. In the following, the properties of these airfoils will be discussed and one of them will be selected.

i. All have similar Re number range. They all show better laminar flow and low bubble formation well above Re = 7×10^5. Since the design mission a/c is a low subsonic one, i.e. Re $\approx 1.3\times10^6$, this Re range is satisfactory.

ii. The thickness ratios are 14.75%, 14.63% and 16.5% for E 582, E 585 and E 583 respectively. Since the design a/c will include some subsystems inside the wing, the higher t/c ratio is preferable. Note that, the increased thickness must be paid by a drag penalty due to shorter laminar flow.

iii. In comparison with airfoils E 582 and E 585, E 583 has a higher amount of pressure recovery on both sides.

iv. Cm(α) characteristics are also better for E 583 since, it is more positive than the other two.

∴ **E 583** – Eppler (Ref. [17]) airfoil profile is chosen as the wing airfoil, see Figures 4.2 and 4.3.

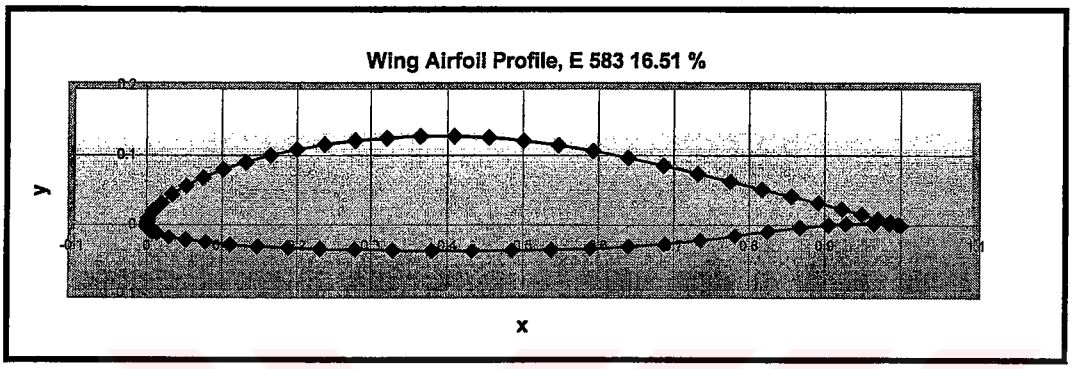

Figure 4. 2 Profile of the selected airfoil, Eppler-E583 with 16.51% t/c.

4.2.3 Some performance parameters of Eppler E 583 Airfoil Profile

As can be seen from the graphs separation bubble warning is only given for $\mathrm{Re} = 7\times10^5$. Since the design a/c has a Re number of 1.2×10^6, it will not have such kind of problems as can be seen in the Figure 4.3.

$C_{d\,min} \cong 0.0053$ $\quad C_l)_{C_{d\,\min}} \cong 0.28$ $\quad \alpha_{C_{d\,\min}} \cong -3°$

$C_{\ell\max} \cong 1.45$ $\quad \alpha)_{Cl\,\max} \cong 11°$

$$\left.\frac{L}{D}\right)_{\max} \cong \frac{1.19}{0.0095} \cong 125$$

Max *t/c* occurs at *0.38 c* of the E583 wing profile, see Figure 4.2.

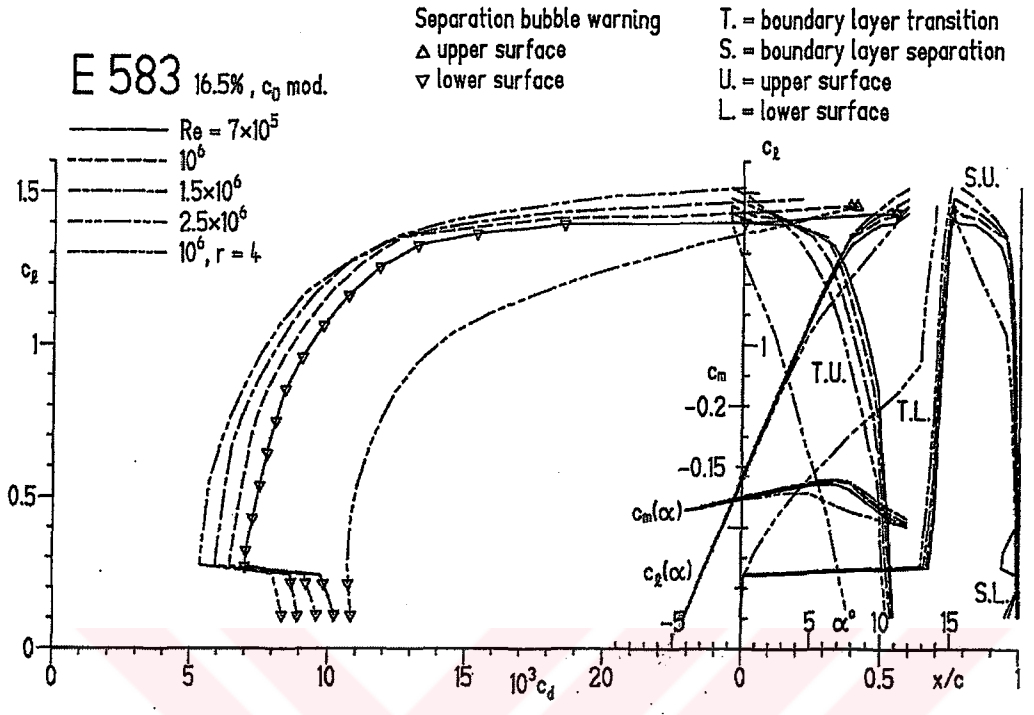

Figure 4. 3 Various plots indicating the E 583 airfoil performance. [17]

Here, in order not to be close to the stall value, $C_l)_{\frac{L}{D})_{max}}$ and $\alpha)_{\frac{L}{D})_{max}}$ values will be set as follows instead of the graph read values: 1.19 and 6.5° respectively.

$$C_l)_{\frac{L}{D})_{max}} \cong 1.0 \qquad \alpha)_{\frac{L}{D})_{max}} \cong 4.0°$$

$$C_{l\alpha} \cong \frac{0.43}{4°(\pi/180°)} = 6.16\ rad^{-1} \qquad \alpha_{o_w} \cong -5.5°$$

4.3 Wing Geometry Selection

4.3.1 Wing Aspect Ratio

It should be stated that the design UAV has ducts at the wing tips. One of the contributions of this design feature is its 'endplate effect', i.e. helps to block the higher-pressure air on the bottom of the wing to escape around the tip to the top of the wing. This makes an effective increase of about %20 in wing aspect ratio. This contribution is taken into account during the selection of the aspect ratio. [1]

Before making a proper selection, we have to note that, as the aspect ratio increases, lift will increase and drag will decrease, but the wing stalls later as the aspect ratio decreases. Besides, as the aspect ratio increases, the wing will be heavier which means more cost. Under the light of the latter notes and in terms of the control characteristics, a reasonable selection of Aspect ratio will be **6.0** for the time being.

4.3.2 Wing Sweep Angle, Taper Ratio & Twist

- *Wing sweep* improves stability and has a natural dihedral effect. At supersonic speeds, the lift loss associated with the supersonic flow can be reduced by sweeping the wing aft of the Mach cone angle. But, since our mission a/c is a subsonic one, no sweep at the leading edges is required.

  No sweep is preferred at the moment. This will also help to achieve one of the basic design objectives, *easy production,* in this design concept.

- *Taper* affects the distribution of lift along the span of the wing. As proven by the Prandtl wing theory early in this century, minimum drag due to lift or "induced" drag is achieved when the lift is distributed in an elliptical fashion. At this point, the contribution of the engine + propeller + duct combination, located at the tip of the wings of this design UAV, should be taken into account. Being located at the tip of

the wings, they will simulate an 'endplate effect' and help to achieve a uniform lift distribution along the span of the wing. This advantage reduces the need of taper in the wings. Besides, an elliptical planform is known to be difficult and expensive to build. Where as an untapered ($\lambda = 1$) rectangle wing is the easiest type to build where this advantage is paid by 7% more drag than that of an elliptical wing of the same aspect ratio.

Untapered wing ($\lambda = 1$) configuration is preferred at the moment. This will also help to achieve one of the basic design objectives, *easy production,* in this design concept.

- *Wing twist* prevents tip stall and revises the lift distribution to approximate an elliptic form. The design UAV will not be affected by the tip vortices due to the 'endplate effect' of the ducts located at the wing tips.

  Hence, taking into account the easy production goal and the latter notes **no twist** is selected at this stage.

4.3.3 Wing Incidence

Wing incidence is used to minimize drag at some operating conditions, usually the cruise. It is generally applied such that when the angle is at correct angle of attack for the selected design condition, the fuselage is at the angle of minimum drag.

Considering the value of $\alpha\left(\frac{L}{D}\right)_{max} \cong 4.0°$ given in section 4.2.2, the wing incidence is set to **3°** for the time being (the typical value of a homebuilt a/c is given as 2° in Ref. [2].)

4.3.4 Wing Vertical Location

- With a high wing, propellers, as in the case of our design UAV, will have sufficient ground clearance. Since, this is a VTOL UAV, the ducts located at the wing tips should be able to rotate without the possibility of any hazardous ground touch.

In the case of the design UAV, the landing gear are located under the fuselage. In this respect, the high wing configuration will also reduce the need of any excessive landing gear length. Hence the weight of landing gear will be reduced. Besides, the high wing configuration places the engines and the propellers away from flying rocks and debris as well.

- As a disadvantage, the high wing configuration brings increased fuselage weight due to strengthening to support the landing-gear loads.

High wing configuration is preferred for the design VTOL UAV.

4.3.5 Wing Dihedral

Wing dihedral is the angle of the wing with respect to the horizontal when seen from the front. Dihedral tends to roll the a/c whenever it is banked.

In the high wing configuration, the air will be pushed over the top of the fuselage which will push up the forward wing, thus provides an increased dihedral effect. It reduces the need of a dihedral for the design UAV, which has a high wing configuration. It should also be stated that, in the case of an excess of effective dihedral produces 'dutch roll' which is a repeated side-to-side motion involving yaw and roll.

No dihedral is selected for the design UAV. This will also help to achieve one of the basic design objectives, *easy production,* in this design concept.

4.3.6 Wing Tips

The escape of the higher-pressure air, at the bottom of the wing by turning around the wing tip to the top produces the induced drag for an aircraft. However, in the case of this design UAV, the ducts at the wing tips will act as an endplate and will not permit the air escape to the top of the wing, together with reducing the tip vortices.

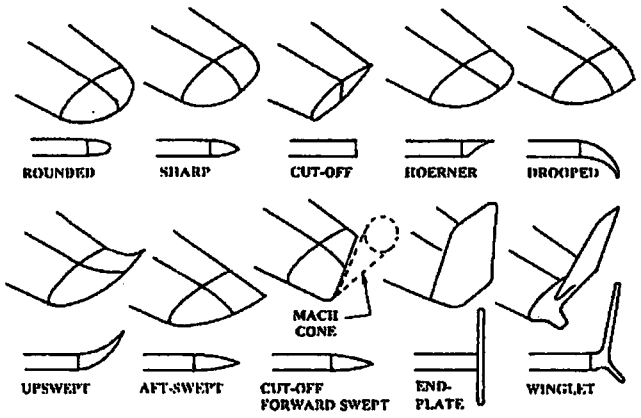

Figure 4. 4 Wing tip types. [1]

'Cut-off' type of wing tip is selected in order to facilitate the operation of the tilt mechanism, see Figure 4.4.

4.4 Tail Arrangement

4.4.1 Type of Tail

Not to increase the structural weight and to prevent any pitch up risk, ***'the conventional type of tail'*** is selected which provides adequate stability and control at the lightest weight, see Figure 4.5.

For spin recovery, the horizontal tail will be arranged such that at least one third of the rudder should be out of the wake that horizontal tail produces at high angle of attacks.

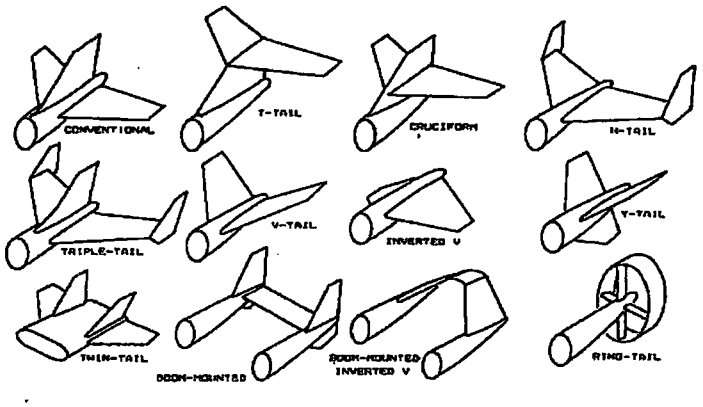

Figure 4. 5 Aft tail types. [1]

4.4.2 Tail Geometry

At this stage, we can decide the tail aspect ratio, taper ratio and the horizontal wing airfoil by fixing it thinner than the wing airfoil, hence it will be stalled at a higher angle of attack than the wing. Eppler E521 (Ref. [17]) is the airfoil selected for the tail configuration, see Figures 4.6 and 4.7.

Leading edge sweep of the horizontal tail is generally set 5° more than the wing sweep. Our selection will be **17°**. This provides the tail to be stalled after the wing.

Vertical tail sweep is chosen as **30°**, which is based on the typical values available in Table 4.3 of Ref.[1].

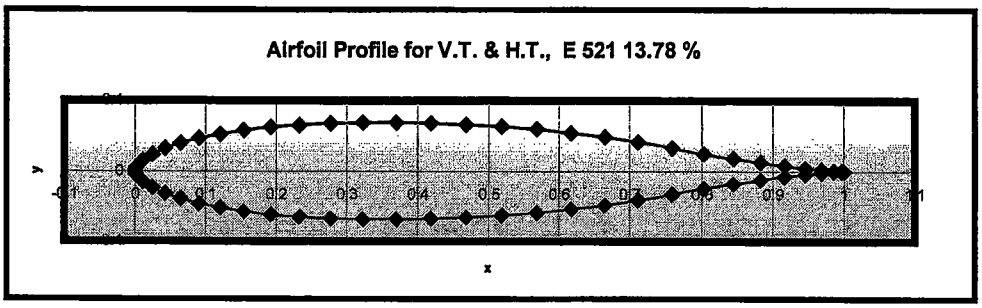

Figure 4. 6 Airfoil profile selected for the horizontal and vertical tails, *E 521* with *t/c* 13.78%.

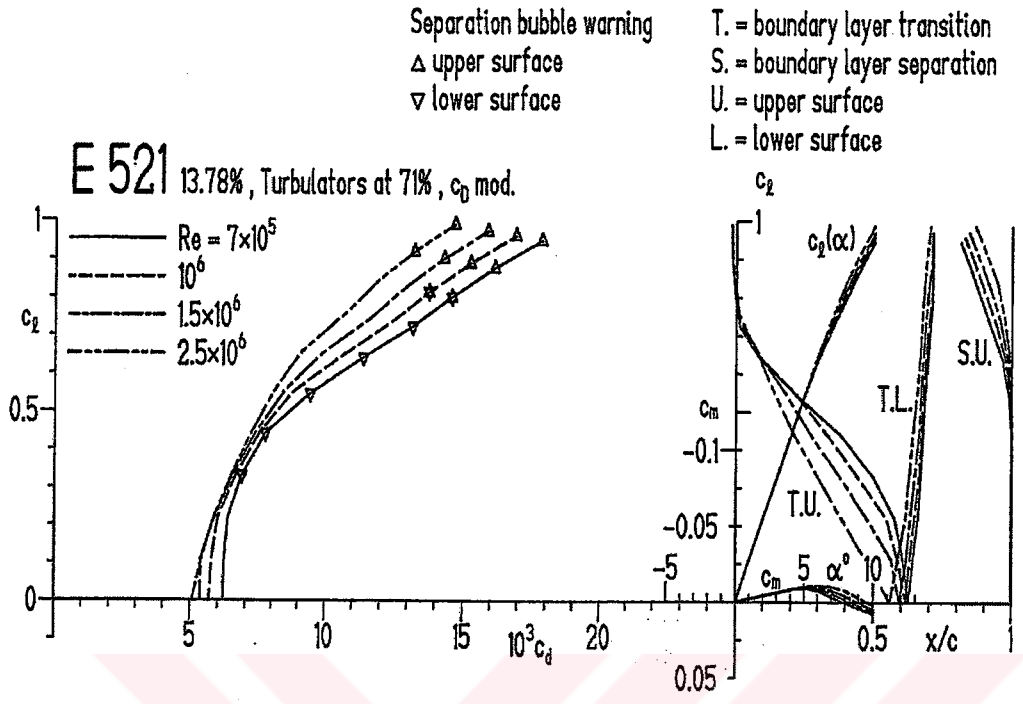

Figure 4. 7 Various plots indicating the E 521 airfoil performance. [17]

4.4.3 Some performance parameters of E 521

As can be seen from Figure 4.7, separation bubble warning is only given for $\mathrm{Re} = 7\times10^5$. Since the design a/c has a Re number of 1.1×10^6, it will not have such kind of problems.

$C_{d\,min} \cong 0.0058$ $\qquad$ $C_{l\max} \cong 1.0$

$\alpha)_{Cl\max} \cong 10°$ $\qquad$ $\left.\frac{L}{D}\right)_{\max} \cong \frac{0.55}{0.0088} \cong 62.5$

Max *t/c* occurs at ~ *0.30 c* of the E521 wing profile, see Fig 4.6.

$C_l)_{\left(\frac{L}{D}\right)_{max}} \cong 0.55$ $\alpha)_{\left(\frac{L}{D}\right)_{max}} \cong 5.2°$

$C_{l\alpha} \cong \frac{0.5}{4.5°(\pi/180°)} = 6.366$ $\alpha_{ow} \cong 0°$

4.5 Results of Chapter 4

Table 4. 1 The geometry parameters for the wing, horizontal tail and vertical tail of Chapter 4.

	Wing	**Horizontal Tail**	**Vertical Tail**
A	6	4	1.6
λ	1	0.5	0.5
Sweep ($\Lambda_{l.e.}$)	0°	17°	30°
Airfoil Type[4]	E-583	E-521	E-521
Airfoil t/c	%16.5	%13.78	%13.78
Dihedral	None	None	None
Twist	None	None	None
Incidence	3°	None	None
Type	High Wing	Conventional	Conventional
Tips	Sharp	Hoerner	Sharp

4.6 Conclusion

In this chapter, the airfoil, wing and tail geometries are selected by taking into account the design criteria, the typical and statistical values available in the references and the results of the competitor survey. These selections may be changed in the proceeding chapters in the case of any necessity.

CHAPTER 5

HORSEPOWER to WEIGHT RATIO and WING LOADING SELECTION

5.1 Introduction

In this chapter, it is aimed to select the horsepower to weight ratio and the wing loading settings for the mission UAV. These estimations are crucial before beginning to the initial design layout.

As the hp/W and W/S are selected, some corresponding a/c performance parameters will be calculated depending on these values.

Unless otherwise is stated, all the formulations used in this chapter are taken from Ref. [1].

5.2 Horsepower-to-Weight Ratio Selection

Power loading is the equivalent parameter of thrust to weight ratio, which is defined for jet a/c, and it is very crucial in the name of the a/c performance. If the hp/W is high, then the

a/c will accelerate more quickly, climb more rapidly, reach a higher max. velocity and achieve higher turn rates. But, a higher hp/W means a larger engine, which consumes more fuel. Hence, the cost will increase.

The competitors survey yields hp/W ratios for Bell V-22 Osprey as 0.252 and for Bell/Augusta 609 as 0.231.

The procedure followed in this section begins with the selection of the engine as in the first step. The a/c performance parameters will depend on the properties of this engine. For this purpose, a market search was performed. The required properties of the main engines were to be piston-prop, small, efficient, cheap and reliable. Hence, *Limbach L-275-E, 24 hp, 7300 rpm*, piston-propeller engine is selected to be the main engine type, see Figure 5.1 and Table 5.1.

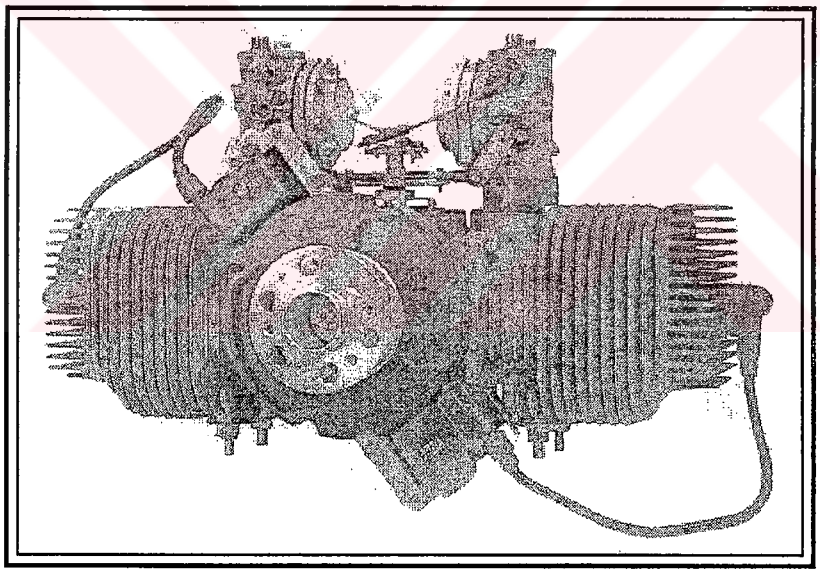

Figure 5. 1 Limbach L 275E two-stroke for microlight aircraft and RPV applications, rated at 18 kW (24 hp) [5].

Table 5. 1 The characteristics of the selected engine, Limbach L-275E. [18]

Properties	Limbach L-275E
Type	two cylinder, horizontally opposed, two-stroke, air-cooled piston engine

Cylinders	cast aluminum alloy with Nicasil Liner, bore 66 mm, stroke 40 mm, 274 cc
Induction	two all-attitude-diaphragm carburetors
Fuel	90 octane, mixed 25:1 with two stroke oil
Ignition	12 V Bosch transistored, one Bosch WK 175T6 plug per cylinder
Accessories	Leistritz type turbo silencer (muffler)
Weight (with silencer)	16.54 lb (7.5 kg)
Performance Rating	24 hp (18 kW) @ 7300 rpm
Length	8.9 in (22.6 cm)
Width	15.35 in (39.0 cm)
Height	7.36 in (18.7 cm)

This procedure, selecting the engine first, is a different application than the standard procedures. This procedure is followed in order not to have any difficulty in finding the required engine in the market. The thrust achieved by the propellers is found by use of the methods defined in Ref. [5], see Chapter 8. These methods give the thrust produced as 142 lb (630 N) of thrust per engine and 3.94 ft (1.2m) of propeller diameter.

Having selected the main engines first, the maximum takeoff weight can be calculated by using an adequate safety factor in order to guarantee the VTOL performance of the design UAV. By taking into account that the engine will not run in an ideal state and it is necessary to obtain a thrust greater than the max. take-off weight during the VTOL mission, a safety factor of **1.25** is selected. Then,

$$W_{o_{max}} = \frac{142 \times 2}{1.25} = 226.6lb$$

$$\left.\frac{hp}{W}\right)_{TO} = \left(\frac{24 \times 2}{226.6}\right) = 0.212$$

∴ The horse power-to-weight ratio will be set to **0.212** hp/lb.

➢ hp/W = **0.212** hp/lb

5.3 Wing Loading Selection

W/S is a very important parameter that affects the aircraft stall speed, climb rate, take-off and landing distance, turn performance; determines the design lift coefficient and drag.

W/S has significant effects on the TO gross weight. If W/S is low, then the wing will be larger, which will increase the performance but this time the empty weight and drag will increase. Table 5.5 of Ref. [1] yields a typical value of **W/S ≈ 11** lb/ft^2, for a homebuilt a/c.

The requirement for the wing loading selection depends on the stall characteristics of the a/c. In this case,

$V_{stall} \cong 50\ knots\ @\ 3281ft\ altitude$

Then,

$V_{Stall} = 50 knots = 84.45 ft/s$

$\rho_{stall} = 0.00216 sl/ft^3$ (at h =1000 m = 3280 ft)

$$\frac{W}{S} = \frac{1}{2}\rho . V_{stall}^2 C_{L_{max}} \qquad (5.1)$$

From Figure 5.3 of Ref. [1] : $C_{L_{MAX}} \cong 1.5$ (**unflapped**)

$$\Rightarrow \quad \frac{W}{S} = \frac{1}{2}(0.00216)(84.45)^2(1.5) = 11.6$$

$\therefore$ The wing loading will be set to **12** lb/ft^2.

➢ $\boxed{W/S)_{TO} = 12 \text{ lb/ft}^2}$

5.4 Estimation of Related Performance Parameters

In the previous sections, the horsepower-to weight ratio and wing loading selections for the design Tilt-Duct VTOL UAV are performed. These are two important parameters that predicts the main performance characteristics of an aircraft. In this section, some performance parameters of the design UAV will be evaluated depending on the previous selections performed in this chapter.

5.4.1 Stall Speed (3281 ft, standard day)

Since, it comes from the requirements, no calculations are performed for this case.

➢ $\boxed{V_{stall} \cong 50 \text{ knots } @ \text{ 3281 ft altitude}}$

5.4.2 Stall Speed (sea level, standard day, takeoff/landing)

$$V_{stall} = \sqrt{\frac{2(W/S)_{TO}}{\rho_{S/L} C_{L\max_{TO}}}} = \sqrt{\frac{2(12)}{0.00238(1.305)}} 87.9 ft/s = 52.05 knots$$

5.4.3 Cruise Speed

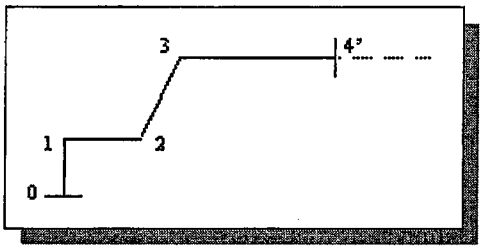

Figure 5.2 Related flight mission segments

$$Avg\ \left(\frac{W_{cruise}}{W_{TO}}\right)=\frac{W_{4'}}{W_0}=\frac{W_{4'}}{W_3}\frac{W_3}{W_2}\frac{W_2}{W_0}=(0.94)(0.99)(0.96)=0.8934$$

$$\left(\frac{W}{S}\right)_{cruise}=\left(\frac{W}{S}\right)_{TO}\left(\frac{W_{cruise}}{W_{TO}}\right)=(12)(0.8934)=10.72$$

$$\left(\frac{W}{S}\right)_{cruise}=q\sqrt{\pi.A_{eff}eC_{D_o}}=\frac{1}{2}\rho.V_{cruise}^2\sqrt{\pi.A_{eff}eC_{D_o}} \qquad (5.2)$$

where :

$C_{D_o}=0.041$

$A_{eff} \cong (1.2)\,A = (1.2)\times 6 = 7.2$

The A_{eff}, *effective aspect ratio,* is determined by multiplying A, the geometric aspect ratio, by a factor of *1.2*. Here, the basic logic is that the 3-D effects due to tip vortices at the wing are eliminated by use of ducts just at the tip of the wings, creating an *endplate* effect.

Please note that, after all, in all the calculations of a/c performance parameters, except the geometry sizing sections, A_{eff} will be used instead of the parameter A.

From Table A.2-1 of Ref. [1] : $\rho_{cruise} \cong 0.1953\times10^{-2}$ *sl/ft*^{3} @ *2000 m. altitude*

$$_{cruise} = \sqrt{\frac{2(W/S)}{\rho_{cruise}\sqrt{\pi.AeC_{D_o}}}} = \sqrt{\frac{2(10.72)}{(0.1953\times10^{-2})\sqrt{\pi.(7.2)(0.833)(0.041)}}} = 111.76ft/s$$

But, since the design UAV is of a VTOL type the selected engines are powerful than required. Then, the cruise velocity will be set to a higher value in order to increase the competitiveness in the market as the follows,

➢ $V_{cruise} = 124.2$ ft/s @ $h_{cruise} = 2000$ m

5.4.4 Cruise Mach Number

From Table A.2-1 of Ref. [1] : a = 1101 ft/s, at cruise altitude

$$M_{cruise} = \frac{V_{cruise}}{a_{cruise}} = \frac{124.2}{1101} = 0.113$$

➢ $M_{cruise} = 0.113$

5.4.5 L/D)$_{max}$

$$C_{L_{min}} = \sqrt{\frac{C_{D_o}}{K}} \qquad (5.3)$$

where:

$$K = \frac{1}{\pi eA} \qquad (5.4)$$

An average *Equivalent Skin Friction Coefficient* (C_f) is assumed for this UAV, i.e. 0.005 within range of 0.002-0.008 given in Ref. [2].

From Ref. [2], Part I, Section 3.4.1, p. 118-127,

$$\log_{10} S_{wet_{a/c}} = c + d \log_{10} W_o \qquad (5.5)$$

$$\log_{10} f = a + b \log_{10} S_{wet_{a/c}} \qquad (5.6)$$

where, c, d are "Regression Coefficients" used to estimate Wetted Area of the aircraft from Take-off Weight and a, b are "Regression Coefficients" used to estimate Parasite Area from the Wetted Area of the aircraft.

$$C_{Do} = \frac{f}{S_{wing}} \qquad (5.7)$$

By use of Equations (5.5), (5.6) & (5.7),

$$\Rightarrow \quad \log_{10} S_{wet_{a/c}} = 0.8635 + (0.5632)\log_{10}(226.57) = 2.1899$$

$$\boxed{S_{wet_{a/c}} = 154.864 ft^2}$$

$$\Rightarrow \quad \log_{10} f = -2.301 + \log_{10}(154.864) = -0.1111$$

$$\boxed{f = 0.7743}$$

$$\therefore \quad C_{Do} = \frac{0.7743}{18.88} = 0.041$$

➢ $\boxed{C_{Do} = 0.041}$

Then,

$$D_{\min} = qS(C_{D_o} + C_{D_o}) = qSC_D \Rightarrow C_D = 2C_{D_o} = 0.082$$

$$e = 1.78\left(1 - 0.045A^{0.68}\right) - 0.64 \qquad (\textit{for Straight-Wing Aircraft.})$$

$$\Rightarrow \quad e = 1.78\left(1 - 0.045(7.2)^{0.68}\right) - 0.64 = 0.8334$$

➢ $\boxed{e = 0.833}$

By use of Equations (5.3) and (5.4),

$$C_{L_{\min}} = \sqrt{\frac{0.041}{0.0531}} = 0.879$$

$$K = \frac{1}{\pi(0.833)(7.2)} = 0.0531$$

$$\Rightarrow \quad \left.\frac{L}{D}\right)_{\max} = \left.\frac{C_L}{C_D}\right)_{\substack{Best\\Range}} = \frac{0.879}{0.082} = 10.72$$

or,

$$\left.\frac{L}{D}\right)_{\max} = \frac{1}{2\sqrt{C_{D0}K}} = \frac{1}{2\sqrt{(0.041)(0.0531)}} = 10.72$$

➢ $\boxed{L/D)_{\max} = 10.72}$

5.4.6 hp_{cruise} / hp_{TO}

For a piston-powered, propeller driven aircraft, the power available varies with the density of the air provided to the intake manifold. If the engine is not supercharged, the power falls of with increasing altitude according to density ratio, σ. Since, this is an exceptional case, i.e. the aircraft is of VTOL type, it requires more *hp* for takeoff and landing than that of a conventional aircraft. Hence, a lower hp ratio should be set for cruise.

$$\left(\frac{hp}{W}\right)_{TO} = \left(\frac{V_{cruise}}{550\eta_p}\right)\left(\frac{1}{L/D)_{cruise}}\right)\left(\frac{W_{cruise}}{W_{TO}}\right)\left(\frac{hp_{TO}}{hp_{cruise}}\right) \qquad (5.8)$$

In Eqn. (5.8), we have to take into account that the propulsive efficiency, η_p, will be very low during cruise since the engine will not operate at a high rating, as in takeoff. Also, please note that, the following *hp* ratio is calculated for the beginning of cruise.

Then, by recalling Eqn. (3.5), (5.8) and the parameters evaluated in the previous sections in this Chapter,

$$0.212 = \left(\frac{124.2}{550(0.6)}\right)\left(\frac{1}{10.72}\right)(0.9504)\left(\frac{hp_{TO}}{hp_{cruise}}\right)$$

$$\left(\frac{hp_{cruise}}{hp_{TO}}\right) = 0.157$$

In the condition that the maximum available *hp* decreases with the altitude,

$$\Rightarrow \frac{hp)_{\max,6562\,ft}}{hp)_{\max,S/L}} \approx \frac{\rho_{6562\,ft}}{\rho_{S/L}} \quad \Rightarrow hp)_{\max,6562\,ft} = \frac{1.953\times10^{-3}}{2.377\times10^{-3}}(0.212) = 0.174$$

$$\Rightarrow \frac{hp)_{\max,6562\,ft}}{hp)_{\max,S/L}} = 0.82$$

$$\Rightarrow \left[hp)_{cruise} / hp)_{\max} \right]_{@6562\,ft} = 0.191$$

This value can be set to **0.3** at the moment, in order to take into account any need of performance increments, such as increasing the velocity during cruise.

5.4.7 Takeoff Ground Roll (Far 23, sea level, standard day)

For a propeller aircraft,

$$TOP = \frac{(W/S)}{\sigma C_{L_{TO}} (hp/W)} = \frac{12}{(1)(1.08)(0.212)} = 52.41$$

where,

$$C_{L_{TO}} \cong C_{L\max_{TO}} / 1.1^2 = 1.305/1.21 = 1.08$$

Here, C_{LTO} (takeoff lift coefficient) is the actual lift coefficient at takeoff, not the maximum lift coefficient at takeoff conditions used for stall calculation. Usually, the aircraft takes off at about 1.1 times the stall speed, so the takeoff lift coefficient becomes the maximum takeoff lift coefficient divided by 1.21 (square of 1.1), see Ref. [1].

Then, from Figure 5.4 of Ref. [1],

➢ *Takeoff Ground Roll* ≈ 250 ft = 76.2 m

➢ Takeoff Distance to clear a 50 ft obstacle ≈ 500 ft = 152.4 m

5.4.8 Landing Field Length (sea level, standard day)

$$S_{Landing} = 80\left(\frac{W}{S}\right)\left(\frac{1}{\sigma C_{L\max}}\right) + S_a \qquad (5.9)$$

where, in Ref. [1], the following values are given for the constant parameter, S_a,

S_a = 1000 ft (airliner type, 3-deg glideslope)
= 600 ft (general aviation-type power-off approach)
= 450 ft (STOL, 7-deg glideslope)

$$\left(\frac{W}{S}\right)_{Landing} = 12(0.99)(0.96)(0.88) = 10.04$$

Since the design aircraft is a VTOL-UAV, it is required to reduce the value given for STOL aircraft above. Hence, for the time being, it will be taken as 350 ft approximately for S_a. Then, from Equation (5.9),

$$\Rightarrow \quad S_{Landing} = 80(10.04)\left(\frac{1}{(1)(1.305)}\right) + 350 = 615.5 + 350 = 965.5\,ft = 294m$$

➢ Landing Field Length ≈ 965.5 ft ≈ 294 m

5.4.9 Endurance

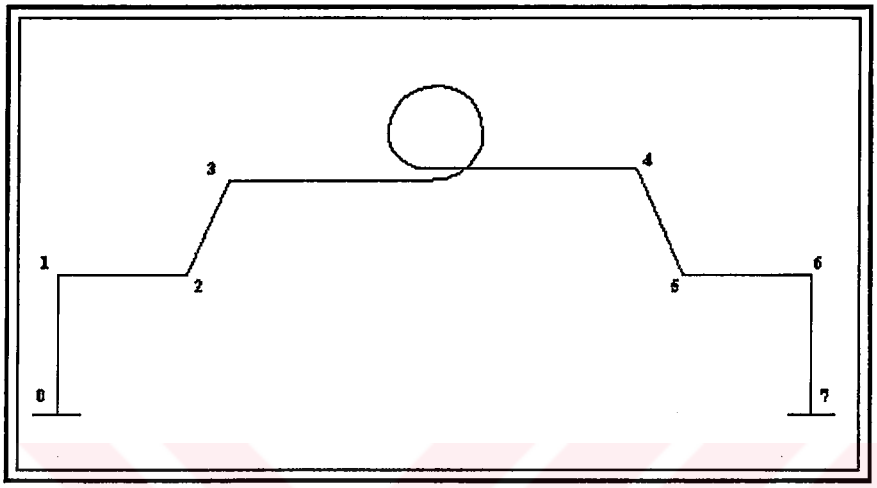

Figure 5.3 Mission profile with loiter in segment (3-4).

$$\frac{W_i}{W_{i-1}} = \exp\left(-\frac{EV_{loiter}C_{bhp}}{550\eta_p (L/D)_{loiter}}\right) \qquad (5.10)$$

For prop a/c,

$$\left.\frac{L}{D}\right)_{loiter} = 0.866\left.\frac{L}{D}\right)_{\max} = 9.29$$

$$_{loiter} = \frac{1}{\sqrt[4]{3}}\sqrt{\frac{\rho_{cruise}}{\rho_{loiter}}}V_{cruise} \qquad (5.11)$$

Loiter mission will be assumed to take place at the cruising altitude, see Figure 5.3. Then from Equation (5.11),

$$_{loiter} = \frac{1}{\sqrt[4]{3}}(124.2) = 94.372 ft/s$$

Then, Equation (5.10) becomes,

$$\Rightarrow \frac{W_4}{W_3} = \exp\left(-\frac{E(94.372)(0.5)}{550(0.7)(9.29)}\right)$$

Here, an iterative solution process is required. By trial and error, the endurance is evaluated which matches with the mission aircraft takeoff weight. For example, with a fuel amount of *45 lb*, and a payload weight of *30 lb*, the aircraft has an endurance of approximately *8.8 hr*, see Table 5.3 for Trade-off results.. The evaluation procedure used, is given below,

$$\frac{W_f}{W_o} = \frac{45}{226.6} = 0.199$$

Then,

$$\Rightarrow \frac{W_7}{W_o} = 0.8126 = (0.99)(0.96)\frac{W_4}{W_3}(0.97)(0.99)$$

$$\Rightarrow \frac{W_4}{W_3} = 0.8904$$

Then by use of Eqn. (5.10),

➢ E ≅ 8.8 hr

5.4.10 Loiter Speed for Best Endurance (6562 ft, standard day)

In the case that an aircraft is to be optimized for loiter, the wing loading should be selected to provide a high *L/D*. For propeller aircraft, loiter is optimized when the induced drag is three times the parasite drag, which yields Eqn. (5.12).

$$\left(\frac{W}{S}\right)_{loiter} = q\sqrt{3\pi A e C_{Do}} \qquad (5.12)$$

$$\left.\frac{W}{S}\right)_{loiter} = \frac{W_o}{S}\frac{W_{loiter}}{W_o} \cong (12)(0.89) = 10.68 \ \textbf{lb/ft}^2$$

Then, from Eqn. (5.12),

$$\Rightarrow \quad q = 7.015 lb/ft^2 = \frac{1}{2}\rho V_{loiter}^{\ 2}$$

$$\Rightarrow \qquad \boxed{V_{loiter} = 84.76 ft/s = 50.2 knots}$$

5.4.11 Instantaneous Turn Rate

In the case of the instantaneous turn, the aircraft is allowed to slow down during the turn. Therefore, the load factor n will be limited only by the maximum lift coefficient or structural strength of the aircraft.

$$\dot{\Psi} = \frac{g\sqrt{n^2 - 1}}{V} \quad \text{(rad/s)} \qquad (5.13)$$

$$n = \frac{qC_L}{W/S} \qquad (5.14)$$

$$C_{L_{Max}} = 0.9 C_{l_{Max}} \cos\Lambda_{c/4}$$

$$\Rightarrow C_{L_{Max}} = 0.9(1.45)(\cos 0°) = 1.305$$

➢ $\boxed{C_{Lmax} = 1.305}$

Since, required conditions are cruise conditions,

$$\Rightarrow \left(\frac{W}{S}\right)_{\substack{ins\tan t.\\ turn}} = \left(\frac{W}{S}\right)_{cruise} = 10.72$$

where, $\rho_{cruise} \cong 0.1953 \times 10^{-2}$ *sl/ft*^{3} @ *2000 m. altitude*

$$\Rightarrow n = \frac{1}{2}\frac{(0.1953\times10^{-2})(124.2)^2(1.305)}{10.72} = 1.834$$

$$\Rightarrow \dot{\Psi} = \frac{32.2\sqrt{1.834^2 - 1}}{124.2} = 0.398 \quad rad/s = 22.83 \quad \text{deg./sec}$$

➢ inst. turn rate = 0.398 rad/s

5.4.12 Climb Gradient & Rate of Climb at the Beginning of Climb (sea level, M=0.1)

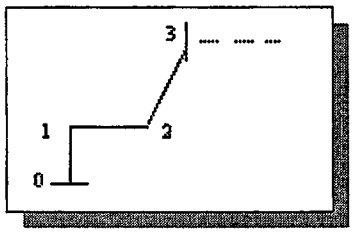

Figure 5.4 Related mission segments

The beginning of the climb corresponds to location 2 in Figure 5.4. Then,

$$\Rightarrow \left(\frac{W}{S}\right)_2 = \left(\frac{W}{S}\right)_{TO}\left(\frac{W_2}{W_0}\right) = 12(0.96) = 11.52$$

$$\left(\frac{T}{W}\right)_2 = \left(\frac{550\eta_p}{V_2}\right)\left(\frac{hp}{W}\right)_{TO} \qquad (5.15)$$

where,

$$\left(\frac{hp}{W}\right)_2 \cong \left(\frac{hp}{W}\right)_{TO}$$

From Table A.2-1 of Ref. [1] : $V_2 = M.a_{S/L} = (0.1)(1116.4) = 111.64\,ft/s$

$$\Rightarrow \left(\frac{T}{W}\right)_2 = \left(\frac{550(0.8)}{111.64}\right)(0.212) = 0.835$$

$$\left(\frac{D}{W}\right) = \frac{qC_{D_o}}{W/S} + \frac{W}{S}\frac{1}{q\pi.Ae} \qquad (5.16)$$

where,

$$q_2 = \frac{1}{2}\rho_{S/L}V_2^2$$

Then, from Eqn. (5.16),

$$\Rightarrow \left(\frac{D}{W}\right)_2 = \frac{1}{2}\frac{(0.00238)(111.64)^2(0.041)}{11.52} + (11.52)\frac{2}{(0.00238)(111.64)^2\pi.(7.2)(0.833)} = 0.0940$$

$$\frac{D}{W} = \frac{T}{W} - G \Rightarrow G = \frac{T}{W} - \frac{D}{W} = \frac{x_{vertical}}{x_{horizontal}} = \frac{V_V.t}{V_H.t} = \frac{V_V}{V_H} \qquad (5.17)$$

$$\Rightarrow G_2 = 0.835 - 0.0940 = 0.741$$

From Eqn. (5.17),

$$\Rightarrow \frac{V_V}{V_H} = 0.741 \quad \Rightarrow \quad V_H = 1.349.V_V$$

where,

$$\Rightarrow V_2 = \sqrt{V_V^2 + V_H^2} = \sqrt{V_V^2 + (1.349V_V)^2} = 111.64 \Rightarrow V_V = 66.48\,ft/s = 3989\,ft/\min$$

➢ Rate of Climb at the beginning of climb = **3989** ft/min

5.4.13 Climb Gradient & Rate of Climb At the End of Climb (cruising altitude & speed)

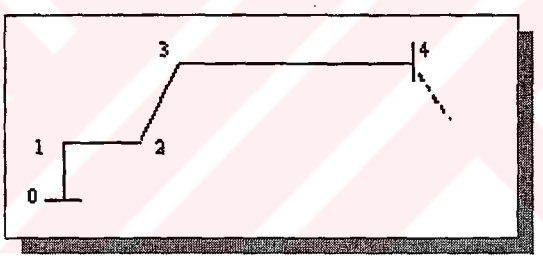

Figure 5.5 Related mission segments.

At the end of the climb, the a/c will be at station 3, see Figure5.5. Then,

$$\Rightarrow \left(\frac{W}{S}\right)_3 = \left(\frac{W}{S}\right)_{TO}\left(\frac{W_3}{W_2}\right)\left(\frac{W_2}{W_0}\right) = (12)(0.99)(0.96) = 11.405$$

$$\left(\frac{T}{W}\right)_3 = \left(\frac{550\eta_p}{V_{cruise}}\right)\left(\frac{hp}{W}\right)_{cruise} \qquad (5.18)$$

where,

$$\left(\frac{hp}{W}\right)_{cruise} \cong 0.3\left(\frac{hp}{W}\right)_{TO} = (0.3)(0.212) = 0.0636$$

Then, from Equation (5.18),

$$\left(\frac{T}{W}\right)_3 = \left(\frac{550(0.8)}{111.76}\right)(0.0636) = 0.25$$

Similar to Equation (5.16),

$$\left(\frac{D}{W}\right) = \frac{qC_{D_o}}{W/S} + \frac{W}{S}\frac{1}{q\pi.Ae}$$

where,

$$q_3 = \frac{1}{2}\rho_{cruise}V^2_{cruise}$$

$$\Rightarrow \left(\frac{D}{W}\right)_3 = \frac{1}{2}\frac{(1.953\times10^{-3})(124.2)^2(0.041)}{11.405} + (11.405)\frac{2}{(1.953\times10^{-3})(124.2)^2\pi.(7.2)(0.833)} = 0.0943$$

Then, from Equation (5.17),

$$G_3 = 0.25 - 0.0943 = 0.1557 = \frac{V_V}{V_H}$$

$$\Rightarrow \frac{V_V}{V_H} = 0.1557 \quad \Rightarrow \quad V_H = 6.423V_V$$

where,

$$V_{cr} = \sqrt{V_V^2 + V_H^2} = \sqrt{V_V^2 + (6.423V_V)^2} = 124.2$$

$$\Rightarrow V_V = 19.11 ft/s = 1146.5 ft/\min$$

➢ Rate of Climb at the end of climb = 1146 ft/min

5.4.14 Maximum Ceiling

The maximum ceiling that the design UAV will possess is determined according to the following procedure. These calculations mainly depend on the methods described in Ref. [1].

$$\left(\frac{W}{S}\right)_{cruise} = q_{design}.C_L)_{design} = 10.72 lb/ft^2$$

where,

$$C_L)_{design} = (\pi Ae C_{Do})^{1/2} = 1.295$$

In order to calculate the maximum ceiling, the following formulation can be used,

$$\frac{W}{S} = \frac{[T/W - G] \pm \sqrt{[T/W - G]^2 - (4C_{Do}/\pi Ae)}}{2/q\pi Ae} \qquad (5.19)$$

Equation (5.19) can be used to calculate the maximum ceiling. The climb gradient *G* can be set to *zero* in order to represent level flight at the desired altitude. Then setting G as zero, Equation (5.19) becomes,

$$\frac{W}{S} = \frac{(T/W)_{cruise} \pm \sqrt{(T/W)^2_{cruise} - (4C_{Do}/\pi Ae)}}{2/q\pi Ae} \qquad (5.20)$$

where,

$$V_{mc} = (2q_{design}/\rho_{mc}) = 4.069/\sqrt{\rho_{mc}}$$

$$\left(\frac{hp}{W}\right)_{mc} = \left(\frac{hp}{W}\right)_{TO}\left(\frac{W_{TO}}{W_{cruise}}\right)\left(\frac{hp_{cruise}}{hp_{TO}}\right) = (0.212)(0893)^{-1}(\rho_{mc}/0.0023769)0.6 = 59.93\rho_{mc}$$

A factor of 0.6 is added into the above calculation, since the design is of a VTOL type and will use much lower of the power during cruise than in the case of a regular a/c.

$$\left(\frac{T}{W}\right)_{mc} = \left(\frac{550\eta_p}{V_{mc}}\right)\left(\frac{hp}{W}\right)_{mc} = 6480(\rho_{mc})^{3/2}$$

By substituting these values into Equation (5.20),

$$\Rightarrow \quad 10.72 = \left[6{,}480(\rho_{mc})^{3/2} \pm \sqrt{41.99\times10^{6}(\rho_{mc})^{3} - 8.704\times10^{-3}}\right](77.987)$$

By trial and error method, the following results are evaluated,

$$\Rightarrow \quad \rho_{mc} = 0.62\times10^{-3}\, sl/ft^{3}$$

$$\Rightarrow \quad h_{mc} = 38.871 ft = 11{,}847 m$$

➢ **Maximum Ceiling = 38,871 ft = 11,847 m**

5.5 Summary of Results of Chapter 5

Table 5.2 The list of parameters evaluated in Ch5.

Quantity	**Ch5 Results**
$hp/W)_{TO}$	0.212 hp/lb
$W/S)_{TO}$	12 lb/ft^2
V_{stall} @ 3281 ft	50 knots (84.45 ft/s)
V_{cruise} @ 6562 ft	124.2 ft/s
M_{cruise}	0.113
$L/D)_{max}$	10.72
C_{Do}	0.041
e (Oswald Efficiency Factor)	0.833
$hp)_{cruise} / hp)_{TO}$	0.3
Takeoff Ground Roll	250 ft (76.2 m)
Takeoff Distance to clear 50 ft obstacle	500 ft (152.4 m)
Landing Field Length	965.5 ft (294 m)
Endurance	8.8 hr ($W_f = 45$ lb, $W_p = 30$ lb)
V_{loiter}	50.2 knots (84.76 ft/s)
C_{Lmax}	1.305
Instantaneous Turn Rate	0.398 rad/s
Rate of Climb (at the beginning of Climb)	3989 ft/sec
Rate of Climb (at the end of Climb)	1146 ft/sec
Max. Ceiling	38,871 ft (11,847 m)

Table 5.3 Trade-Off Study Results for Endurance of the UAV.

W_o (lb)	W_f (lb)	W_p (lb)	E (Endurance) (hr)
226.6	35	40	5.01
226.6	45	30	8.8
226.6	55	20	12.78

5.6 Conclusion

This chapter represented the initial estimation of the wing loading and the power loading for the design UAV. It is followed by the estimations of some performance parameters depending on these values, such as stall speed, C_{Do}, takeoff / landing distances, maximum ceiling, etc.

Instantaneous turn rate is high. This result depends on the powerful engines selected to add the vertical flight capability to the UAV. Besides, for the calculations of takeoff and landing distances, please note that the equations available for this purpose are the ones improved for the conventional type of aircraft. In the case of a UAV, some modifications are required in these equations, especially in the constant terms that are directly added to the final distance. In the relevant sections, some approximate modifications are done for this purpose. In order to obtain more accurate results, performing flight tests on a scaled model or a prototype is highly recommended.

CHAPTER 6

INITIAL SIZING

6.1 Introduction

Aircraft sizing is the process of determining the takeoff gross weight, fuel weight, empty weight, etc. required for an aircraft concept to perform the design mission. This chapter will represent this work. Besides these evaluations, "geometry sizing" will be performed to estimate the a/c's geometric properties such as, wing and tail surface areas, spans, chords, etc. Initial geometric estimations for control surfaces will be performed in the last section of this chapter.

6.2 The Engine Selection

As stated in the previous chapters, this conceptual design procedure is based on the engine selection at the first place. What performed from then on, served to evaluate what can be achieved with that engine, with that much of thrust, etc.

Recall from Chapter 5 that *Limbach L-275 E* was the engine type selected for this design (see Figure 5.1 and Table 5.1). It is a product of *Limbach Flugmotoren GmbH, Germany,* which is a respectable company manufacturing four and two-stroke piston engines for very light aeroplanes, powered gliders and UAV's.

L-275E is a model generally preferred for low cost propulsion of RPV's and microlight's. It is also suitable for UAV applications.

Additional to the main engines located at the tips of the wing, a smaller engine, Limbach L-90E, and propeller mechanism is integrated in the aft fuselage. This aft engine is used to control pitch by controlling throttle in hover and transition modes. It also contributes to lift. For the properties of the aft engine, see Table 6.1 and Figure 6.1.

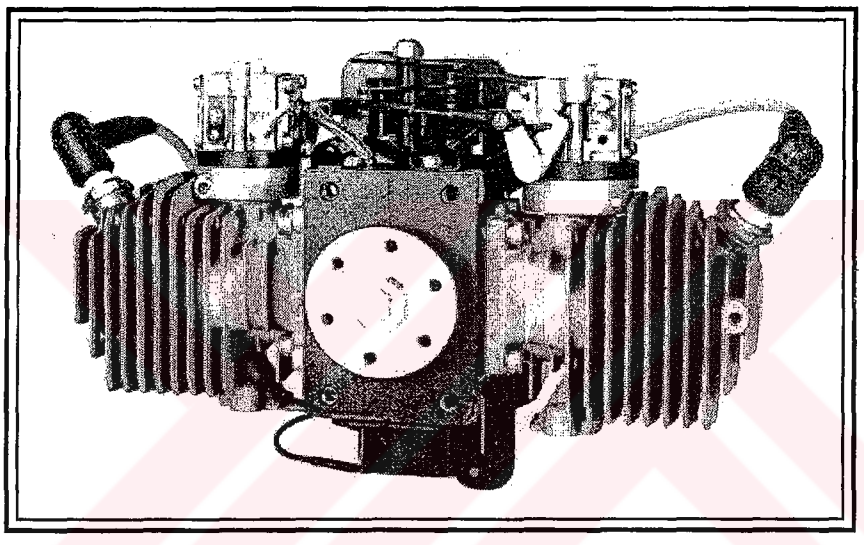

Figure 6. 1 Limbach L 90 E [6].

Table 6. 1 The characteristics of the aft engine, Limbach L 90 E [6].

Properties	Limbach L 90 E
Type	two cylinder, horizontally opposed, two-stroke, air-cooled piston engine
Cylinders	casted aluminum alloy with Nicasil Liner, bore 1.654 in, stroke 1.221 in, 5.248 in^3
Fuel	96 RON, mixed 25:1 with two stroke oil
Ignition	BOSH – solid state magneto ignition. Bosh WSR 6 F plugs per cylinder.
Weight	8.82 lb (4.0 kg)
Performance Rating	4.0 hp (2.9 kW) @ 7000 rpm

Length	5.51 in (14.0 cm)
Width	10.63 in (27.0 cm)
Height	5.276 in (13.4 cm)

6.3 Selection of Cruise Velocity

In this section, the cruise velocity of the design Tilt-Duct VTOL UAV will be predicted. For this purpose, mainly the methods presented in Ref. [1] is used.

6.3.1 Best Range Cruise Velocity

Eqn. (6.1), will be used in order to evaluate the best range cruise velocity,

$$V_{b.r.} = \sqrt{\frac{2W}{\rho S}}\sqrt{\frac{K}{C_{Do}}} \qquad (6.1)$$

where, W/S corresponds to the one at the beginning of cruise segment.

Since, no special mission is dedicated to the design UAV at the moment, the cruise segment will be assumed to take place at an altitude of 6562 ft, i.e. 2000 m. Then, setting h = 6562 ft = 2000 m., $V_{b.r.}$ becomes,

$$V_{b.r.} = \sqrt{\frac{2(10.72)}{0.001953}}\sqrt{\frac{1}{(0.041)\pi(0.833)(7.2)}} = 111.76 ft/s = 66.17 knots$$

This means that, if the design UAV flies at this much of velocity during cruise, it will achieve the maximum amount of range.

Then, the required *hp/W* ratio corresponding to this velocity will be evaluated by means of Eqn. (6.2),

$$\frac{hp}{W} = \frac{1}{(L/D)_{max}}\frac{V}{550\eta_p} \qquad (6.2)$$

$$\frac{hp}{W} = \frac{1}{10.72}\frac{111.76}{550(0.8)} = 0.0237 hp/lb$$

This available power at this altitude can be evaluated as follows,

$$\frac{hp/W)_{max@6562ft}}{hp/W)_{max@S/L}} = \frac{\rho_{6562ft}}{\rho_{S/L}} \Rightarrow \frac{hp}{W}\Big)_{max@6562ft} = \frac{1.953\times10^{-3}}{0.00238}(0.212) = 0.174$$

Then, the ratio of the hp used for cruise to the maximum available hp at this altitude becomes,

$$\left[\frac{hp}{W}\Big)_{cruise} \Big/ \frac{hp}{W}\Big)_{max}\right]_{6562ft} = \frac{0.0237}{0.174} = 13.62\%$$

6.3.2 Best Endurance Velocity

In this section, the cruise velocity will be evaluated which yields the best endurance for the design aircraft. For this purpose, Eqn. (6.3) will be used which is obtained from Eqn. (5.10), by taking the derivative of Endurance with respect to velocity and equating it to zero. Then,

$$_{b.e.} = \sqrt{\frac{2W}{\rho S}}\sqrt{\frac{K}{3C_{Do}}} \qquad (6.3)$$

Then, inserting the related variables for cruise in Eqn. (6.3), the corresponding best endurance velocity turns out to be,

$$_{b.e.} = \sqrt{\frac{2(10.72)}{0.001953}}\sqrt{\frac{1}{3(0.041)\pi(0.833)(7.2)}} = 84.92 ft/s = 50.3 knots$$

6.3.3 Maximum Cruise Velocity

In order to obtain a relation that gives the maximum cruise velocity that this design UAV could reach, first of all, Eqn. 6.4 and 6.5 are introduced. Then, by the help of these equations a relation will be obtained which enables to find out the maximum cruise velocity.

$$\frac{T}{W}=\left(\frac{550\eta_P}{V}\right)\left(\frac{hp}{W}\right) \qquad (6.4)$$

$$\left.\frac{T}{W}\right)_{cruise}=\frac{1}{L/D)_{cruise}} \qquad (6.5)$$

Then, from Eqn.s 6.1, 6.4, 6.5 and recalling Eqn. 3.4,

$$\left.\frac{qC_{D_0}}{W/S)_{cr}}+\frac{W}{S}\right)_{cr}\frac{K}{q}=\left(\frac{550\eta_p}{V_{max}}\right)\left(\frac{hp}{W}\right)_{max} \qquad (6.6)$$

Then, from Eqn. 6.6,

$$\Rightarrow \frac{1}{2}\frac{(0.001953)V^{2}_{max}(0.041)}{10.72}+(10.72)\frac{2}{(0.001953)V^{2}_{max}\pi(0.833)7.2}$$
$$=\left(\frac{550(0.8)}{V_{max}}\right)(0.212)$$

$$\Rightarrow \quad _{max}=\frac{92.28}{\left(3.73\times10^{-6}V^{2}_{max}+\frac{582.63}{V^{2}_{max}}\right)}$$

This requires an iterative solution technique, which finally gives,

➢ $$\boxed{_{max}=290ft/s=172.25knts=318.13km/hr}$$

This result shows that the design UAV has a capacity of this much of cruise velocity with full throttle setting. The large amount of difference in between Best Range and Maximum

velocities is due the fact that since, this UAV is of VTOL type, the engines are selected to be quite powerful in order to achieve this mission. But, during cruise, since, the UAV will behave like a conventional twin-prop aircraft, only a small portion of the full throttle setting will be sufficient.

In fact, the velocity settings depends on the mission requirements and the pilot's preferences. If the mission is not an emergency and there is lot's of way to go, then the pilot may use the Best Range velocity. If this is an emergency case, the engines of this UAV are quite powerful enough to support very high velocities.

Some of the main objectives of the design UAV are to achieve the VTOL mission and be faster than a helicopter when the propellers are tilted forward. For this purpose, the cruise speed will be set to a higher value, i.e. **150 ft/s**, but this is still closer to the Best Range velocity.

Table 6. 2 Results of Section 6.3.

Variable	ft/s	knots	km/hr	-
V_{Max}	290	172.25	318.13	-
$V_{Best\ Range}$	113.9	67.43	124.94	-
V_{cruise}	150	88.8	164.54	-
M_{cruise}	-	-	-	0.136

6.4 Fixed Engine Sizing

In this section, the corresponding range will be estimated by use of the predetermined take-off weight. Here, it will be calculated by more accurate methods than used in Chapter 3. Since, there is no payload drop for the design mission , some equations used in Chapter 3 will still be valid, such as Eqn. 3.1 and 3.3. But, for simplicity, Eqn. 3.1 will be simplified to Eqn. 6.7, removing the crew weight from the fraction.

$$_o = \frac{W_{payload}}{1-(W_f/W_o)-(W_e/W_o)} \qquad (6.7)$$

In order to evaluate the aircraft's empty weight fraction, a more precise method will be utilized as given in Eqn. 6.7.

$$\frac{W_e}{W_o} = a + bW_o^{C_1} A^{C_2} \left(\frac{hp}{W}\right)_{TO}^{C_3} \left(\frac{W}{S}\right)_{TO}^{C_4} V_{\max}^{C_5} \qquad (6.8)$$

where, for homebult-composite → a = 0.0 , b = 0.59 , C_1 = -0.1 , C_2 = 0.05 , C_3 = 0.1 ,

C_4 = -0.05 , C_5 = 0.17

$$_{\max} = V_{cruise}(mph) = 150(0.6818) = 102.27mph$$

Then, from Eqn. 6.8,

$$\frac{W_e}{W_o} = 0.0 + (0.59)W_o^{-0.1}(7.2)^{0.05}(0.212)^{0.1}(12)^{-0.05}(102.27)^{0.17}$$

$$\frac{W_e}{W_o} = 1.081(W_o)^{-0.1}$$

In order to include the third (aft) engine in the empty weight, the coefficient *1.08* will be modified to be *1.15*.

➢ $$\boxed{\frac{W_e}{W_o} = 1.15(W_o)^{-0.1}}$$

6.4.1 Range Estimation

From here on, an "iterative" technique will be used to evaluate the range. The procedure starts with a guessed range value. Then, the takeoff weight that will be evaluated with this guessed range will be the $W_{0,\ calculated}$. Then, this $W_{0,\ calculated}$ will be compared with $W_{0,\ design}$ at each iterative leg. The solution reaches the target when $W_{0,\ calculated} \cong W_{0,\ design}$.

Please note that, the following range calculations are valid for the cruise segment, i.e. (3-4).

6.4.1.a $R_{guessed} = 1500$ km $= 4.921\times10^6$ ft @ $h = 6562$ ft & $W_p = 22.5$ lb

The trade off studies will use the cruise segment properties, so before performing the trade off studies, the following variables will be evaluated at cruise altitude.

Wing Loading at cruise becomes,

$$\left.\frac{W}{S}\right)_{cruise} = \left.\frac{W}{S}\right)_{TO} \frac{W_4}{W_3}\frac{W_3}{W_2}\frac{W_1}{W_0} = (12)(0.94)(0.99)(0.96) = 10.72$$

Dynamic pressure at cruise altitude is evaluated as follows,

$$q_{6562ft} = \frac{1}{2}\rho V^2 = \frac{1}{2}(1.953\times10^{-3})(150)^2 = 21.97$$

Lift to Drag ratio at cruise will be evaluated by use of the following relation, i.e. Eqn. 6.9,

$$\frac{L}{D} = \frac{1}{\dfrac{qC_{D_0}}{(W/S)} + (W/S)\dfrac{1}{q\pi eA}} \qquad (6.9)$$

Then, from Eqn. 6.9,

$$\left.\frac{L}{D}\right)_{cruise} = \frac{1}{\frac{(21.97)(0.041)}{10.72} + (10.72)\frac{1}{(21.97)\pi.(7.2)(0.833)}} = 9.097$$

Now, based on this new L/D for cruise and the range assumed, the cruise segment weight fraction can be evaluated by use of Eqn. 3.5,

$$\frac{W_4}{W_3} = \exp\left[-\frac{(4.921\times10^6)(0.5)}{550(0.8)(9.097)(3600)}\right] = 0.843$$

Then, Eqn. 3.3 becomes,

$$\frac{W_f}{W_o} = 1.06\left(1-\frac{W_7}{W_o}\right) = 1.06(1-0.769) = 0.245$$

where ,

$$\frac{W_7}{W_o} = \frac{W_7}{W_5}\frac{W_5}{W_4}\frac{W_4}{W_3}\frac{W_3}{W_2}\frac{W_2}{W_0} = (0.96)(0.99)(0.843)(0.99)(0.97) = 0.769$$

Finally, by use of Eqn. 6.7,

$$_o = \frac{22.05}{1-0.245-1.15W_o^{-0.1})} = \frac{22.05}{0.755-1.15W_o^{-0.1}}$$

Then, the last equation yields W_o by iteration as the following,

➢ $W_{0,\ calculated} = 242\ lb$

The same iterative technique is used, for several range values, see Table 6.3. Finally, it is concluded that this Tilt-Duct VTOL UAV has a range of **756 nmi** (1400 km) with this amount of fuel and payload.

Table 6. 3 Range trade studies.

Range	810 nmi (1500 km)	756 nmi (1400 km)	702 nmi (1300 km)
W_o	242	226.6	216
W_p	22.05	22.05	22.05
W_e	161.8	151.5	144.4
W_f	59.3	53.02	33.48
$W_f + W_p$	81.3	75.1	55.55

6.4.1.b Payload Trade-off's

Here, the trade-offs will be performed considering the total sum of payload and fuel weights is constant.

➢ **For $W_p = 40$ lb & $W_f = 35.1$ lb**

Here, the trade off studies will be performed with different amounts of payload weight, but keeping the total amount of fuel and payload as constant. Hence, again the cruise segment weight fraction will change but, this time the range will be the unknown variable. But, before starting the trade off studies, some fractions should be calculated.

Fuel weight fraction,

$$\frac{W_f}{W_0} = \frac{35.1}{226.6} = 0.155$$

Fraction of UAV's landing weight to the total takeoff weight,

$$\frac{W_7}{W_0} = 1 - \frac{W_f/W_0}{1.06} = 1 - \frac{0.155}{1.06} = 0.854$$

$$\left.\frac{W_4}{W_3}\right)_{new} = \frac{W_4/W_3)_{old}}{W_7/W_0)_{old}} \times \left.\frac{W_7}{W_0}\right)_{new} \Rightarrow \left.\frac{W_4}{W_3}\right)_{new} = (0.854)\frac{0.853}{0.779} = 0.935$$

Here, the "old" subscript is used in order to represent the value that corresponds to the case which is showed with shaded pattern in Table 6.3. Then, the weight fraction for the cruise segment becomes,

$$\frac{W_4}{W_3} = \exp\left[-\frac{R(0.5)}{550(0.8)(9.097)(3600)}\right] = 0.935$$

This equation yields the following range value for this amount of payload and fuel weights.

➢ **Range = 319 nmi = 590.34 km**

The same procedure is used, for several payload and fuel weight combinations, but having constant the summation of two, see Table 6.4. It is obvious that as the payload is reduced and the fuel amount is increased, the UAV gains range in significant amounts.

Table 6. 4 Payload Trade-off results for range.

Range	**319 nmi (590 km)**	**558 nmi (1033 km)**	**702 nmi (1300 km)**
W_o	226.6	226.6	226.6
W_p	40	30	22.05
W_e	151.5	151.5	151.5
W_f	35.1	45.1	53.02
$W_f + W_p$	75.1	75.1	75.1

6.5 Geometry Sizing

In this section, basic geometric properties of wing, tails and control surfaces will be performed. The emerging geometrical shapes will be presented in figures at the end of each related subsection.

6.5.1 Wing Sizing

The actual wing area can be found as,

$$S_w = S_{ref} = \frac{W_o}{(W/S)_o} = \frac{226.6}{12} = 18.88 ft^2 = 1.754 m^2$$

➢ $S_w = 18.88 \text{ ft}^2 = 1.754 \text{ m}^2$

Then, the wing span is calculated as,

$$b_{wing} = \sqrt{A_w S_w} = \sqrt{6(18.88)} = 10.64 ft = 3.243 m$$

Since it is an untapered wing, root, tip and the mean aerodynamic chords turn out to be the same,

$$S_w = b_w \times c_w \Rightarrow c_{tip} = c_{root} = (18.88) / (10.64) = 1.77 ft = c_w$$

➢ $c_w = \bar{c}_w = 1.77 \text{ ft} = 0.541 \text{ m}$

The final geometry of the main wing is presented in Figure 6.2 as below,

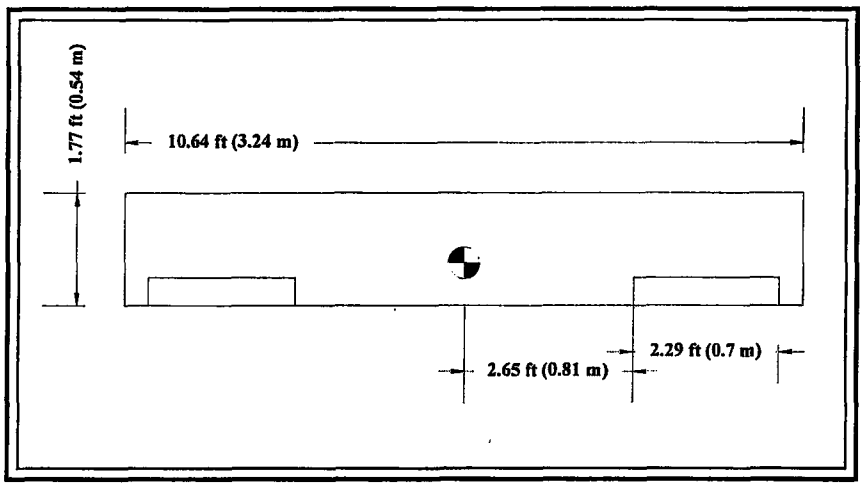

Figure 6. 2 The top view of the main wing. The shaded areas represent the ailerons.

6.5.2 Fuselage Sizing

The fuselage length is determined by use of Table 6.3 given in Ref. [1],

$$L_{fus} = aW_o^C$$

where, a = 3.50 & C = 0.23 for homebuilt / composite aircraft. This is taken because, this type of the aircraft can give the nearest results for this design UAV, out of the other aircraft types.

$$L_{fu} = 3.50(226.6)^{0.23} = 12.18ft = 3.713m$$

➢ L_{fus} = 12.18 ft = 3.713 m

An FFR (Fuselage Fine Ratio) of **5.70** is suitable in terms of drag minimization. Then, the corresponding fuselage diameter becomes,

$$D_f = \frac{L_f}{FFR} = \frac{12.18}{5.70} = 2.133ft = 0.65m$$

➢ $D_{fus} = 2.13 \text{ ft} = 0.65 \text{ m}$

6.5.3 Tail Geometry Sizing

In this subsection, basic geometry of the horizontal and vertical tails will be predicted.

6.5.3.1 Horizontal Tail

The area of the horizontal tail will be evaluated as follows,

$$S_{HT} = c_{HT} \bar{C}_W S_W / L_{HT} \qquad (6.10)$$

For an a/c with the engines on the wings, the tail arm L is given about 50-55% of the fuselage length in Ref. [1]. Since the tail was selected to be of *conventional type,* $L_{HT} \approx 52\%$ of fuselage length is assumed, by considering the horizontal tail to be closer to the a/c center-line than the vertical tale. Then,

$$L_{HT} = L_{fu}(0.52) = (12.18)(0.52) = 6.33ft$$

From Table 6.4 of Ref. [1], tail volume coefficient for Twin turboprop a/c is $C_{HT} = 0.90$. This type of aircraft is chosen since the design UAV is of a twin-piston prop type. Besides, the homebuilt type does not give enough tail surface area in order to satisfy the control requirements of this Tilt-Duct VTOL UAV.

Average of the competitors survey results, selecting the aircraft having newest technology, i.e. V22 Osprey, Bell 609 Tiltrotor, is as follows (see Table 2.2).

$$C_{HT} = \frac{1.136 + 1.44}{2} = 1.288$$

The competitors average result yields better control characteristics for the design UAV. Hence this value will be used in the geometry sizing of the tails. Finally, from Eqn. 6.9,

$$S_{HT} = C_{HT}\,\bar{c}_W\,S_W / L_{HT} = \frac{(1.288)(1.77)(18.88)}{0.52(12.18)} = 6.796ft^2 = 0.631m^2$$

$$b_{HT} = \sqrt{A_{HT}S_{HT}} = \sqrt{4(6.796)} = 5.214ft = 1.589m$$

$$c_{r_{HT}} = \frac{2S_{HT}}{[b_{HT}(1+\lambda_{HT})]} = \frac{2(6.796)}{[5.214(1.5)]} = 1.738ft = 0.53m$$

$$c_{t_{HT}} = \lambda C_{r_{HT}} = 0.5(1.738) = 0.869ft = 0.265m$$

The final geometry of the horizontal tail is presented in Figure 6.3 as below,

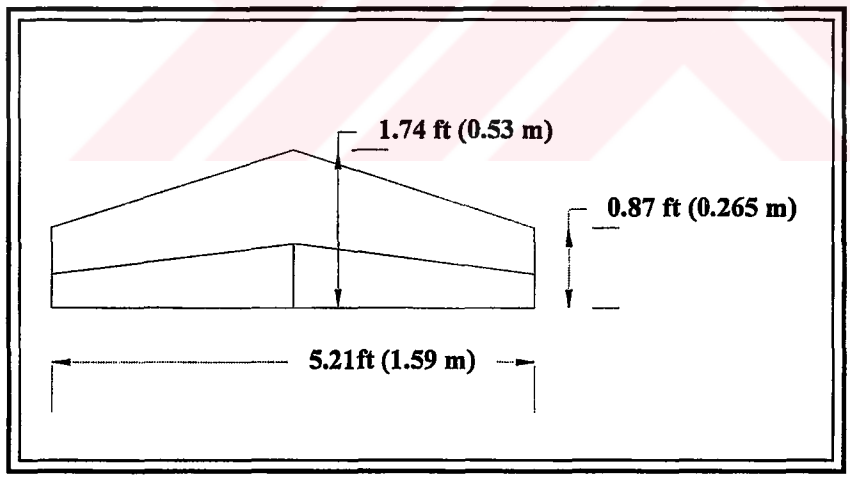

Figure 6. 3 The top view of horizontal tail. The shaded areas represent the elevators.

6.5.3.2 Vertical Tail

The area of the vertical tail will be evaluated as follows,

$$S_{VT} = C_{VT}\, b_W S_W / L_{VT} \qquad (6.11)$$

$L_{VT} \approx 54\%$ of fuselage length will be assumed, by considering the horizontal tail to be closer to the a/c center-line than the vertical tale. Then,

$$L_{VT} = L_f (0.54) = (12.18)(0.54) = 6.577ft$$

From Table 6.4 of Ref. [1], tail volume coefficient for Twin-Turboprop a/c is given as: $C_{VT} = 0.08$. Average of the competitors survey results yields,

$$C_{VT} = \frac{0.176 + 0.26}{2} = 0.218$$

This average result does not suit to the design UAV. It yields a quite large area which is not compatible with Tilt-Duct VTOL UAV's sizes. Therefore, a C_{HT} of **0.09** is selected for this conceptual design process. Then from Eqn. 6.11,

$$S_{VT} = C_{VT}\, b_W S_W / L_{VT} = \frac{(0.09)(10.64)(18.88)}{0.54(12.18)} = 2.749ft^2 = 0.255m^2$$

$$b_{VT} = \sqrt{A_{VT} S_{VT}} = \sqrt{1.6(2.749)} = 2.1ft = 0.64m$$

$$c_{rVT} = \frac{2S_{VT}}{[b_{VT}(1+\lambda_{VT})]} = \frac{2(2.749)}{[2.1(1.5)]} = 1.745ft = 0.531m$$

$$C_{tVT} = \lambda C_{rVT} = 0.5(1.745) = 0.873ft = 0.266m$$

The final geometry of the vertical tail is presented in Figure 6.4 as below,

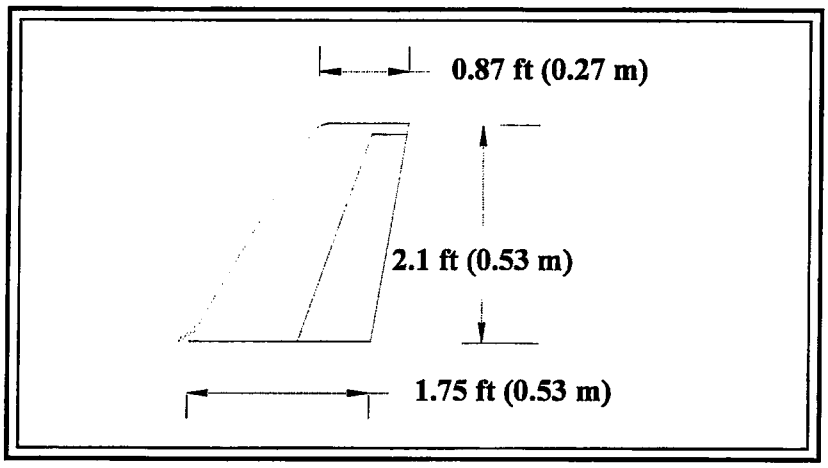

Figure 6. 4 The side view of the vertical tail. The shaded area represents the rudder.

6.5.4 Sizing of Control Surfaces

Final sizing of the control surfaces, ailerons(roll), elevator(pitch), rudder(yaw) will be performed in the proceeding chapters.

Elevators and rudders generally begin at the side of the fuselage and extend to the tip of the tail or to about 90% of the tail span.

To obtain a constant percent chord, the control surfaces are generally tapered by the same amount with the wing or tail surface. This also allows the spars to be straight tapered rather than curved.

Ailerons and flaps are generally 15-25% of the wing chord, while rudders and elevators are typically about 25-50% of the tail chord.

Now, in the light of these information, initial sizing of control surfaces will be done as follows.

6.5.4.1 Ailerons

The ailerons will be taken to extend from 50% to about 93% of the wing span and 25% of the wing chord. Then,

$b_a = 0.43(b_w) = 0.43(10.64) = 4.575\,ft = 1.394\,m$

$c_a = 0.25(c_w) = 0.25(1.77) = 0.442\,ft = 0.135\,m$

Since the wing is untapered,

$S_a = b_a \times c_a = (4.575) \times (0.442) = 2.022\,ft^2 = 0.188\,m^2$

$$\frac{S_a}{S_w} = \frac{2.022}{18.88} = 0.107 = 10.7\%$$

The geometry of ailerons is represented in Figure 6.2.

6.5.4.2 Elevators

Elevators are taken to begin from the root of the horizontal tail and extend all over the span with *40 %* of the horizontal tail chord. Then,

$b_e = b_{HT} = 5.214\,ft = 1.589\,m$

$(c_r)_e = 0.40\,(c_r)_{HT} = 0.40\,(1.738) = 0.695\,ft = 0.212\,m$

$(c_t)_e = 0.40(c_{tip})_{HT} = 0.40\,(0.542) = 0.348\,ft = 0.106\,m$

$$S_e = \frac{(c_r + c_t)_e b_e}{2} = \frac{(0.695 + 0.348)(5.214)}{2} = 2.72ft^2 = 0.253m^2$$

$$\frac{S_e}{S_{HT}} = \frac{2.72}{6.796} = 0.40 = 40\%$$

The geometry of elevators is represented in Figure 6.3.

6.5.4.3 Rudder

Rudder is taken to begin from the root of the vertical tail and extend to *95%* of the tail span with *40 %* of the vertical tail chord. Then,

$b_r = 0.95\,(b_{VT}) = 0.95\,(2.1) = 1.995\,ft = 0.608m$

$(c_r)_r = 0.40\ (c_r)_{VT} = 0.40\ (1.745) = 0.698\,ft = 0.213\ m$

$(c_t)_r = 0.40\ (c_t)_{VT} = 0.40\ (0.873) = 0.349\,ft = 0.106\ m$

$$S_r = \frac{(c_r + c_t)_r b_r}{2} = \frac{(0.698 + 0.349)(2.1)}{2} = 1.1 ft^2 = 0.102 m^2$$

$$\frac{S_r}{S_{VT}} = \frac{1.1}{2.749} = 0.40 = 40\%$$

The geometry of the rudder is represented in Figure 6.4.

6.6 Results of Chapter 6

Table 6. 5 Summary of Results for Geometry Sizing of Wing, Fuselage and Tails.

Structural Part(s)	Quantity	Ch 6 Results
Wing	S_w	18.88 ft^2 (1.754 m^2)
	b_w	10.64 ft (3.24 m)
	c_w	1.77 ft (0.541 m)
Fuselage	L_{fus}	12.18 ft (3.71 m)
	D_{fus}	2.13 ft (0.65 m)
Horizontal Tail	L_{HT}	6.33 ft (1.93 m)
	C_{HT}	1.29
	S_{HT}	6.8 ft^2 (0.63 m^2)
	b_{HT}	5.21 ft (1.59 m)
	c_r	1.74 ft (0.53 m)
	c_t	0.87 ft (0.26 m)
Vertical tail	L_{VT}	6.58 ft (2.00 m)
	C_{VT}	0.09
	S_{VT}	2.75 ft^2 (0.25 m^2)
	b_{VT}	2.1 ft (0.53 m)
	c_r	1.75 ft (0.53 m)
	c_t	0.87 ft (0.27 m)

Table 6. 6 Summary of Results for Geometry Sizing of Control Surfaces.

Control Surface	Quantity	Ch 6 Results
ailerons	S_a	2.02 ft^2 (0.19 m^2)
	b_a	4.57 ft (1.394 m)
	c_a	0.44 ft (0.13 m)
	S_a / S_w	10.7 %
elevators	S_e	2.72 ft^2 (0.25 m^2)
	b_e	5.21 ft (1.59 m)
	c_r	0.69 ft (0.21 m)
	c_t	0.35 ft (0.11 m)
	S_e / S_{HT}	40 %
rudder	S_r	1.10 ft^2 (0.10 m^2)
	b_r	2.00 ft (0.61 m)
	c_r	0.70 ft (0.21 m)
	c_t	0.35 ft (0.11 m)
	S_r / S_{HT}	40 %

6.7 Conclusion

In this chapter, based on the selected engine, some of the performance characteristics of the Tilt-Duct VTOL UAV are predicted. For example, the best range and maximum cruise velocities are evaluated at the first place. It was seen that there is a quite big difference between the both. This depends on the powerful engines of the design UAV. Since, they are selected to achieve the VTOL mission, the UAV is capable to gain high velocities. Then, aircraft range is evaluated together with some payload trade-off's. It is followed by the geometry sizing where the wing, horizontal and vertical tail areas, spans, tip and root chords, etc. are evaluated. The control surface sizing is performed at a primary level.

CHAPTER 7

CONFIGURATION LAYOUT

7.1 Introduction

This chapter will illustrate the configuration layout of the design UAV, including the initial estimates for the aircraft c.g. location. Many geometric properties, e.g. aircraft, fuselage wetted areas, fuselage volume, etc. are determined. All the drawings included in this chapter are performed via *AutoCAD R14*. The design UAV will almost have its geometrical shape by the end of this chapter.

7.2 Fuselage Lofting

In the development of the fuselage, since no cockpit is of concern, it is aimed to have a cylindrical shape as much as possible. This will allow to obtain empty space in the fuselage as much as possible and also enhance the easy production goal.

Aft upsweep of the fuselage, by use of the angle property in AutoCAD R14, see Figure 7.1,

Fuselage aft upsweep angle = **19.76 °**

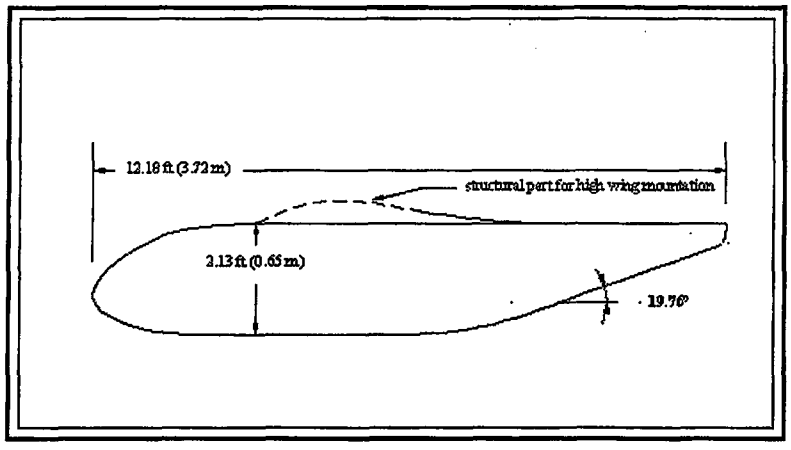

Figure 7. 1 The fuselage side view of the Tilt-Duct VTOL UAV.

7.3 Wing and Tails Configuration

The wings are located by use of the tail moment arms selected in Chapter 6. First, the vertical tail is located on the fuselage according to the 54% of the fuselage length, measured from the location point of the wing c/4 line. Then the others are mounted.

In this process, it is aimed to have the aircraft c.g. located behind the thrust line of the main engines. More accurate calculations will be done in the further chapters, especially after performing the weight and balance calculations.

7.4 Mean Aerodynamic Chord and Its Location On The Wing And Tails

$$\bar{c} = (2/3)C_{root}(1+\lambda+\lambda^2)/(1+\lambda) \qquad (7.1)$$

From the geometry given in Figure 4.17 of Ref. [1], the following equation is derived in order to evaluate the location of mean aerodynamic chord along the span,

$$\frac{\bar{y}}{b/2-\bar{y}} = \frac{C_{tip}+0.5C_{root}}{C_{root}+0.5.C_{tip}} \qquad (7.2)$$

7.4.1 Wing

Since, in this design, the main wings are untapered and unswept, the tip, root and the mean aerodynamic chords are the same. Then from Eqn.s (7.1) and (7.2),

$$\bar{c}_w = c_w = 1.77ft = 0.54m$$

$$\bar{y}_w = b/4 = 2.66ft = 0.811m$$

Wing mean aerodynamic chord and its location is shown in Figure 7.2.

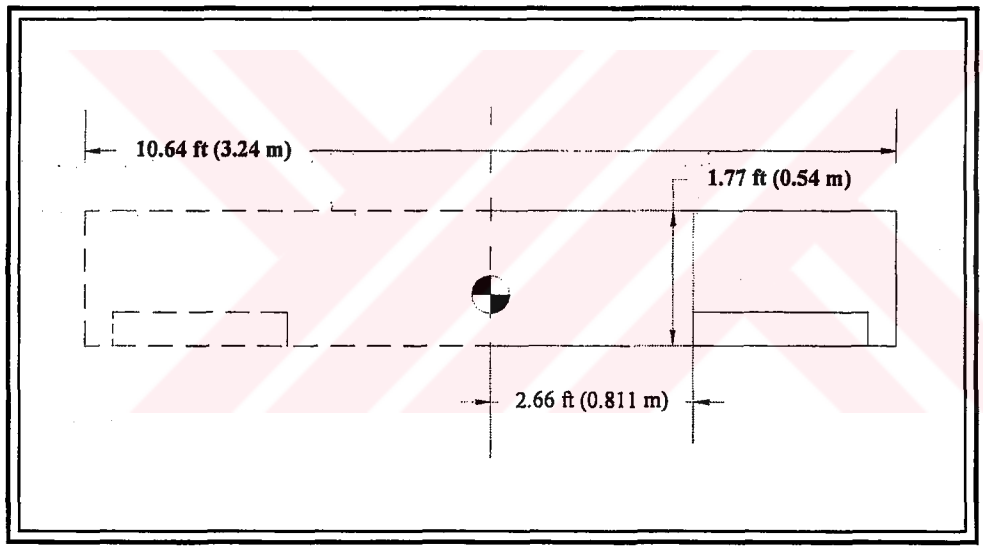

Figure 7. 2 Mean aerodynamic chord and its location on the wing.

7.4.2 Vertical tail

The same procedure by using Eqn.s (7.1) and (7.2),

$$\bar{c}_{VT} = 1.357ft = 0.414m$$

$$\bar{y}_{VT} = 0.933ft = 0.284m$$

Vertical tail mean aerodynamic chord and its location is shown in Figure 7.3.

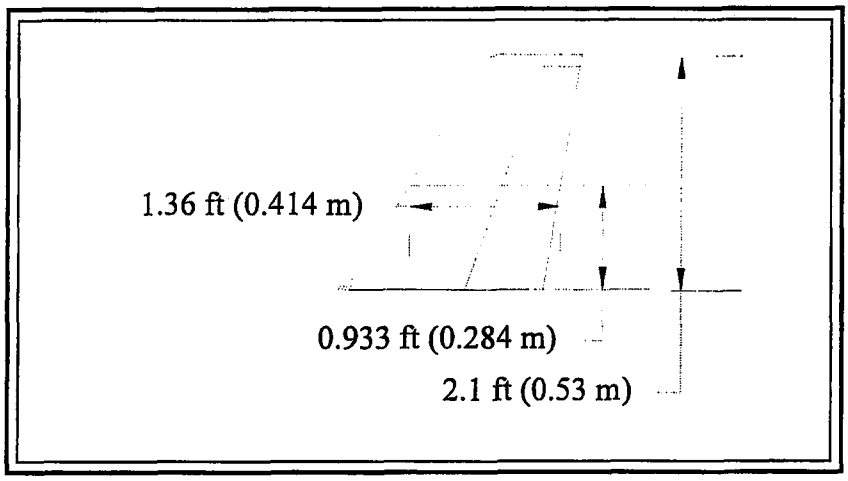

Figure 7. 3 Mean aerodynamic chord and its location on the vertical tail.

7.4.3 Horizontal Tail

$\bar{c}_{HT} = 1.351ft = 0.411m$

$\bar{y}_{HT} = 1.159ft = 0.353m$

Horizontal tail mean aerodynamic chord and its location is shown in Figure 7.4.

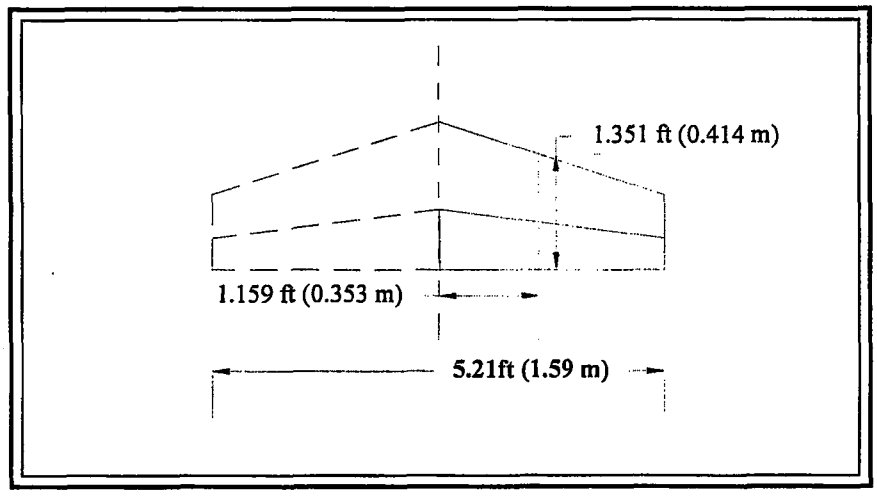

Figure 7. 4 Mean aerodynamic chord and its location on the horizontal tail.

7.5 Wetted Area And Volume Determination

7.5.1 Wetted Area Estimation

A/c wetted area (S_{wet}), the total exposed surface area, can be visualized as the area of the external parts of the a/c that would get wet if it were dipped into water. It directly affects the frictional drag, thus it should be minimized as much as possible, i.e by tight internal packaging and a low fineness ratio. The necessary area calculations will be performed by use of the "Area" command of AutoCAD R14. It yields the following results:

In Forward Flight Mode, the total aircarft,

$S_{exposed} = 30.29\,ft^2 = 2.814\,m^2$ *(side)*

$S_{exposed} = 58.897\,ft^2 = 5.471\,m^2$ *(top)*

In Hover Mode, ,

$S_{exposed} = 30.4628\,ft^2 = 2.830\,m^2$ *(side)*

$S_{exposed} = 59.685\,ft^2 = 5.544\,m^2$ *(top)*

Fuselage,

Top : $S_{exposed} = 19.291\,ft^2 = 1.792\,m^2$

Side : $S_{exposed} = 21.169\,ft^2 = 1.966\,m^2$

Wing,

$S_{exposed,w} = 18.88\,ft^2$

Horizontal Tail,

$S_{exposed,HT} = 6.796\,ft^2$

Vertical Tail,

$S_{exposed,VT} = 2.75\,ft^2$

Since, there is no dihedral and exposed areas are the same with the true views, the remaining exposed areas will be taken equal to the pre-determined real areas, as shown above.

In order to evaluate the exposed areas of the nacelles, i.e. top and side, the "area" command of Autocad program is used. The results are as follows,

$$S_{exposed_n} = 14.757\,ft^2 = 1.371\,m^2 \qquad (side)$$

$$S_{exposed_n} = \pi\left(r_o^2 - r_{\min}^2\right) + S_{engine_{top}} + S_{propellers_{top}} + 5\left(S_{engine\_holder_{top}}\right) \qquad (top) \qquad (7.3)$$

$$= 3.5714 + 2.3788 + 5(0.0945)$$
$$= 6.423ft^2 = 0.597m^2$$

There are 5 sticks in the nacelle that hold the engine and propellers. So, the number "5" in Eqn. (7.3) represents that.

As calculated in section 5.4.5, the aircraft wetted area was,

➢ $\boxed{S_{wet_{a/c}} = 154.864ft^2 = 14.39m^2}$

For *fuselage* of a typical a/c,

$$S_{wet_{fus}} \cong 3.4\left(\frac{19.291 + 21.169}{2}\right) \cong 68.782ft^2 \cong 6.389m^2$$

For wing and tails with *t/c > 0.05*;

$$S_{wet} = S_{exposed}[1.977 + 0.52(t/c)] \qquad (7.4)$$

Since, the t/c for the wing and the tails are 0.165 and 0.1378 respectively, Eqn. (7.4) is used to obtain the corresponding wetted areas. Then for,

wing,

$$S_{wet})_w = (18.88)[1.977 + 0.52(0.165)] = 39.945 ft^2 = 3.618 m^2$$

horizontal tail,

$$S_{wet})_{HT} = (6.796)[1.977 + 0.52(0.1378)] = 13.921 ft^2 = 1.293 m^2$$

vertical tail,

$$S_{wet})_{VT} = (2.749)[1.977 + 0.52(0.1378)] = 5.631 ft^2 = 0.523 m^2$$

nacelles,

$$S_{wet})_n \approx 2\pi(r_o + r_i)h = 2\pi(2.17 + 2.05)(3.29) = 87.234 ft^2 = 8.104 m^2$$

7.5.2 Volume Determination

The volume of the wing will be evaluated by use of the wing airfoil surface area and wing span. In order to evaluate the airfoil, i.e. E 582, surface area, the "area" command of Autocad program is used. The results are as follows,

$$S_\ell = 0.2436 ft^2 = 2.263 \times 10^{-2} m^2$$

$$P_\ell = 3.69 ft = 1.125 m$$

Then, the following simple relation can be utilized in order to evaluate the total wing volume,

$$ol_w = S_\ell b_w = 0.2436(10.64) = 2.592 ft^3 = 7.339 \times 10^{-2} m^3$$

For the nacelles, the volume will be evaluated by approximating the shape to a cylinder having the same outer diameter and height of the nacelle. Then,

$$ol_n \approx \pi r^2 h = (14.793)(3.29) = 48.67 ft^3 = 1.378 m^3$$

By use of the method explained in Ref. [1], the fuselage volume is evaluated as,

$$ol_{fus} \cong 3.4 \frac{(A_{top})(A_{side})}{4L_f} \cong 3.4 \frac{(19.291)(21.169)}{4(12.18)} \cong 28.499 ft^3 \cong 2.647 m^3$$

7.6 Results of Chapter 7

Tabe 7. 1 Table of Results for Chapter 7.

Property	Wing	Horizontal Tail	Vertical Tail	Fuselage	Nacelles	Total a/c
$\bar{c}$	1.77 ft (0.54 m)	1.35 ft (0.41 m)	1.36 ft (0.41 m)	-	-	-
$\bar{y}$	2.66 ft (0.81 m)	1.16 ft (0.35 m^2)	0.93 ft (0.28 m^2)	-	-	-
$S_{exposed}$ (Top)	-	-	-	19.29 ft^2 (1.79 m^2)	6.42 ft^2 (0.60 m^2)	59.68 ft^2 (5.54 m^2) ***(hover)*** 58.90 ft^2 (5.47 m^2) ***(forward)***
$S_{exposed}$ (Side)	-	-	-	21.17 ft^2 (1.97 m^2)	14.76 ft^2 (1.37 m^2)	30.46 ft^2 (2.83 m^2) ***(hover)*** 30.29 ft^2 (2.81 m^2) ***(forward)***
$S_{exposed}$	18.88 ft^2 (1.75 m^2)	6.80 ft^2 (0.63 m^2)	2.75 ft^2 (0.25 m^2)	-	-	-
S_{wet}	39.94 ft^2 (3.62 m^2)	13.92 ft^2 (1.29 m^2)	5.63 ft^2 (0.52 m^2)	68.78 ft^2 (6.39 m^2)	87.23 ft^2 (8.10 m^2)	154.86 ft^2 (14.39 m^2)
Volume	2.59 ft^3 (0.07m^3)	-	-	28.50 ft^3 (2.65 m^3)	48.67 ft^3 (1.38 m^3)	-
Fuselage Aft Sweep	-	-	-	19.76°	-	-
Fuselage Fineness R.	-	-	-	5.718	-	-

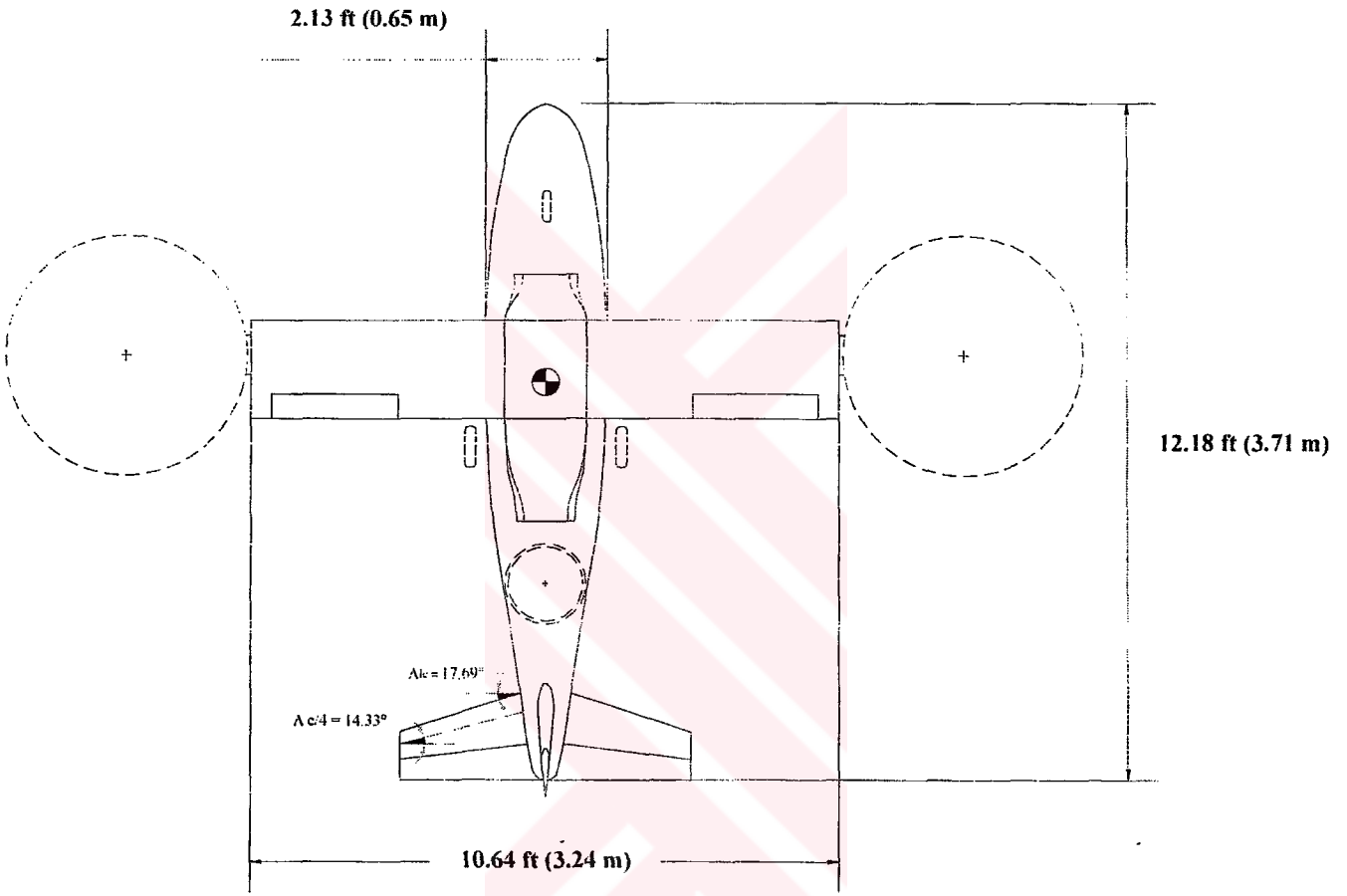

Figure 7. 5 Top view of Tilt-Duct VTOL UAV in hover mode (without landing gears and propulsion system installed).

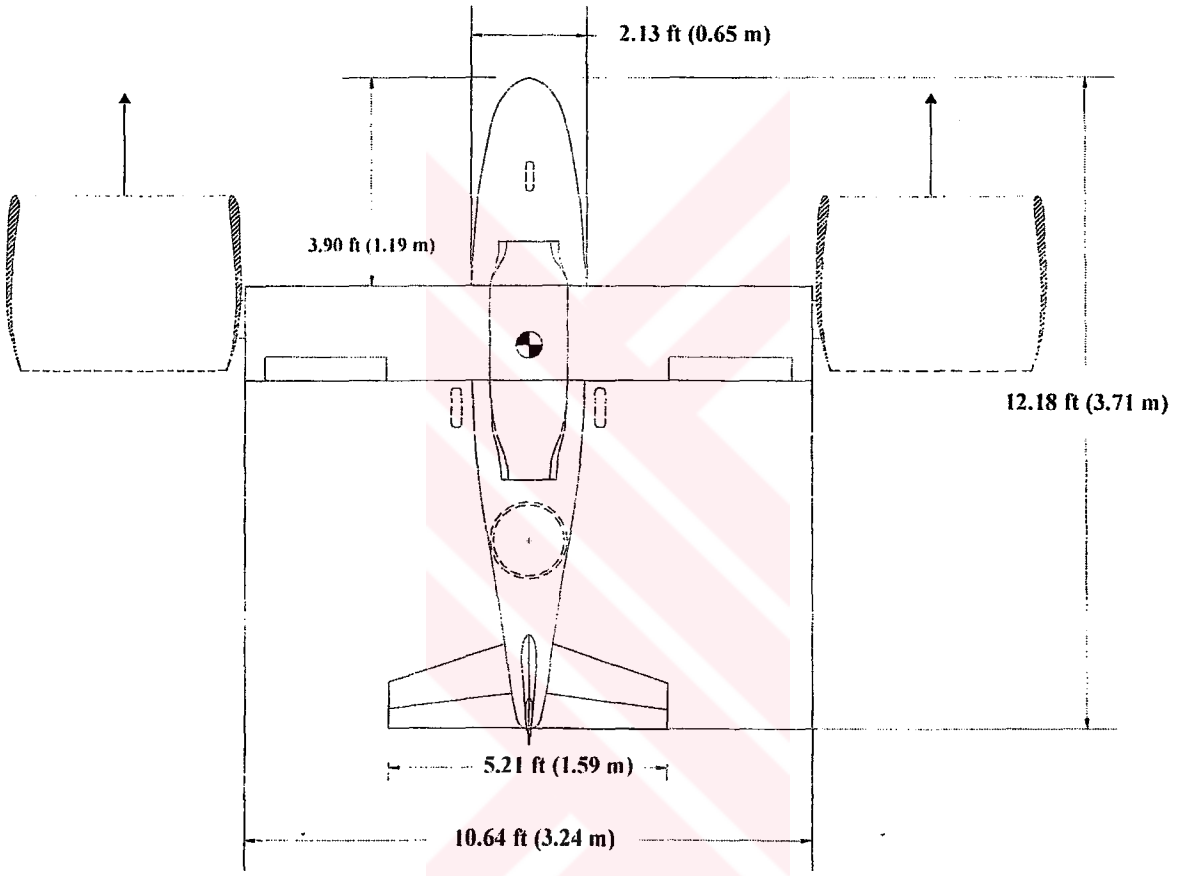

Figure 7. 6 Top view of Tilt-Duct VTOL UAV in forward flight mode (without landing gears and propulsion system installed).

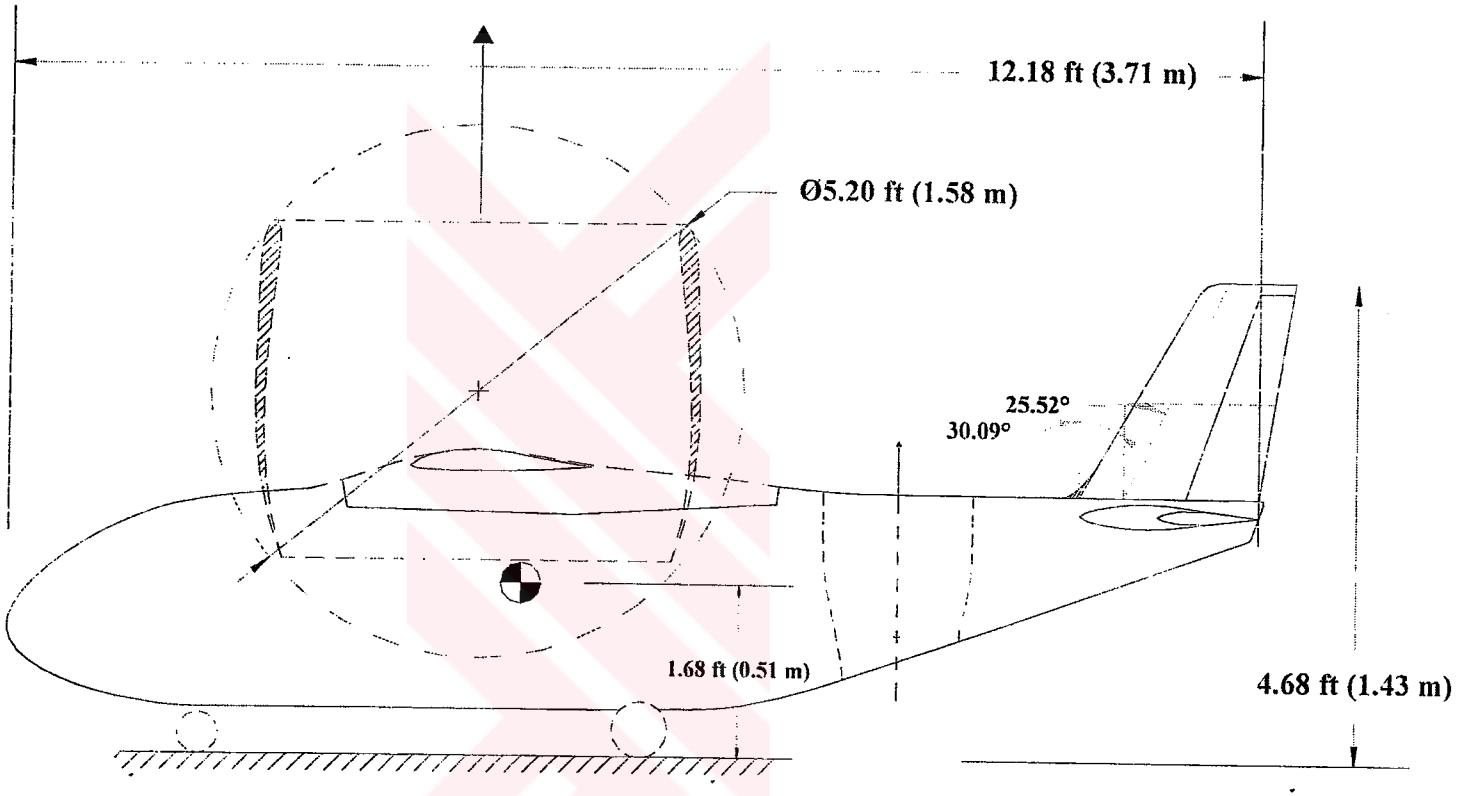

Figure 7. 7 Side view of Tilt-Duct VTOL UAV in hover mode (without landing gears and propulsion system installed).

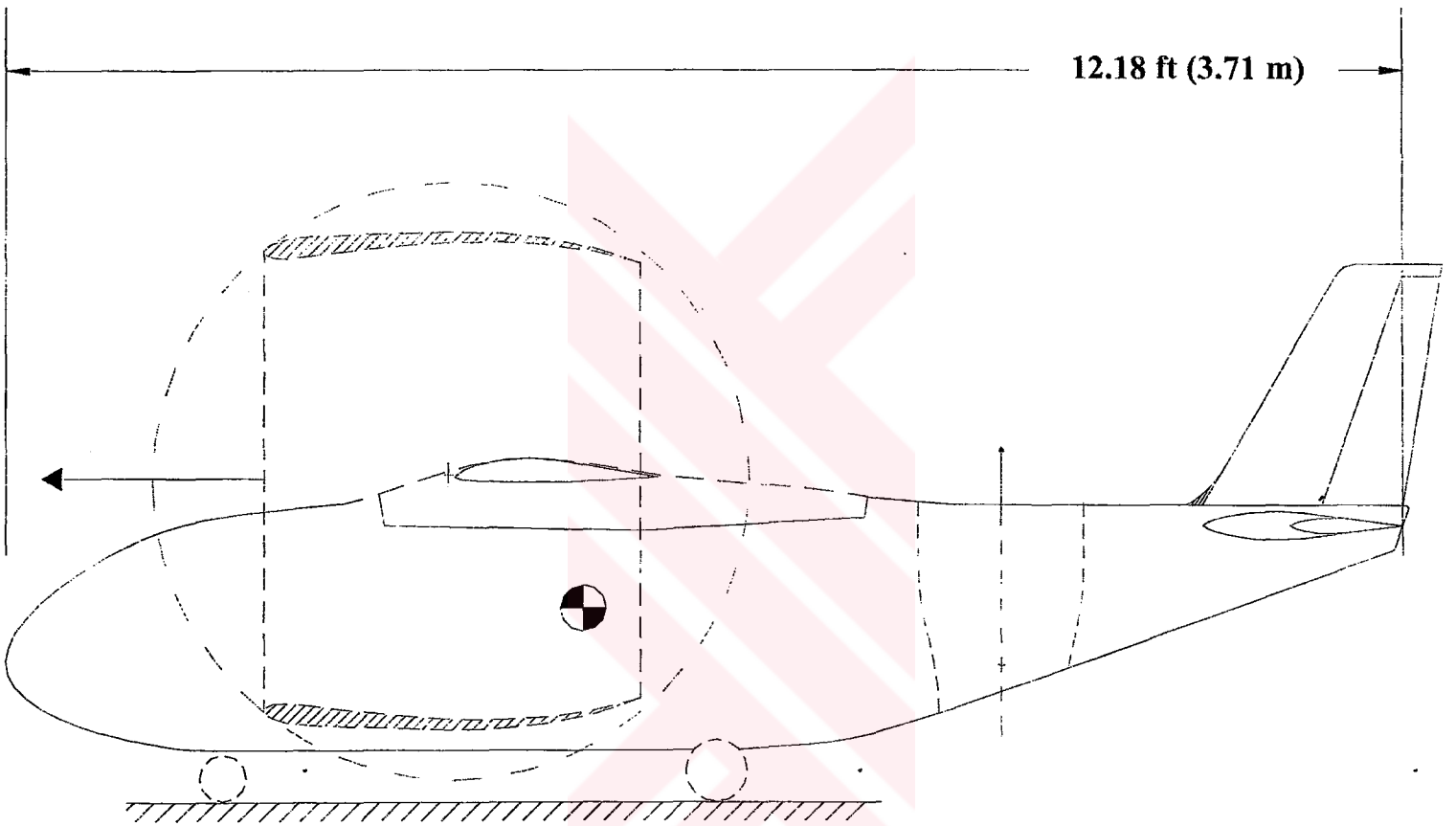

Figure 7. 8 Side view of Tilt-Duct VTOL UAV in forward flight mode (without landing gears and propulsion system installed).

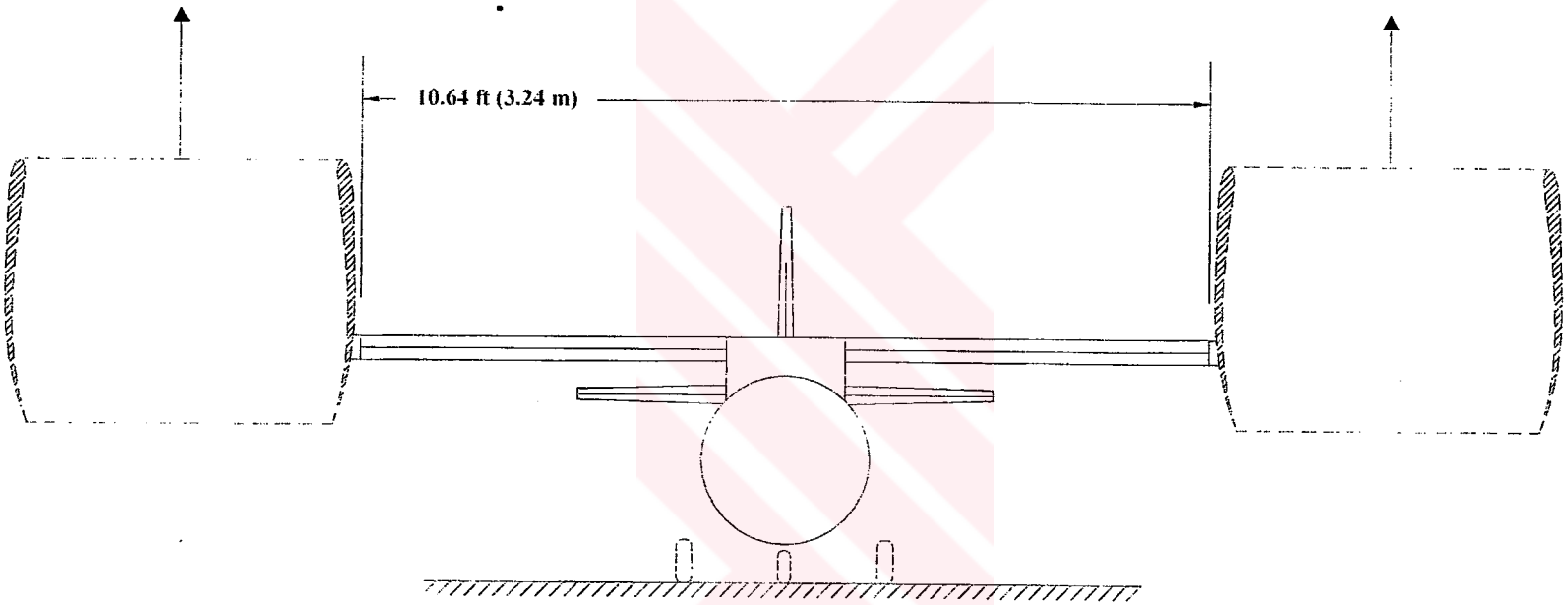

Figure 7. 9 Front view of Tilt-Duct VTOL UAV in hover mode (without landing gears and propulsion system installed).

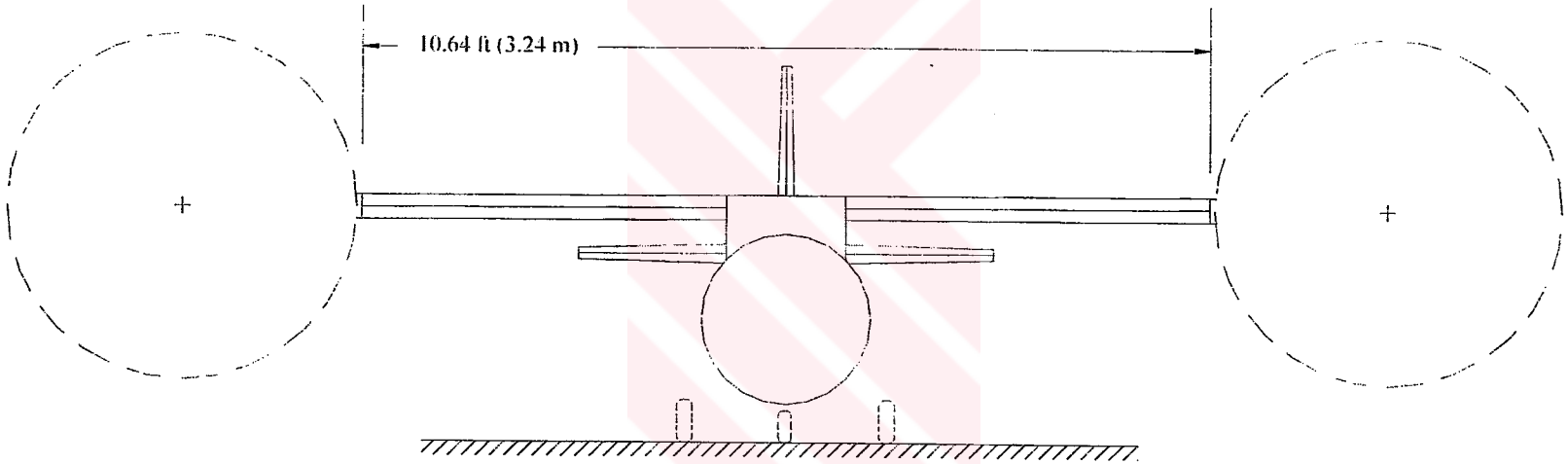

Figure 7. 10 Front view of Tilt-Duct VTOL UAV in forward flight mode (without landing gears and propulsion system installed).

7.7 CONCLUSION

In this chapter, the configuration layout properties of the wing, tails, fuselage and the whole UAV are evaluated. For this purpose, mean aerodynamic chords and their locations on the wing and tails are shown in Figures, i.e. Figures 7.2, 7.3 and 7.4, as soon as they are calculated. The exposed and wetted areas and the volumes (where necessary) of wings, tails, fuselage, nacelles and the total UAV are also predicted in this sense and tabulated in Table 7.1. Landing gears and propulsion related parameters are left for the two proceeding chapters, i.e. Chapter 8 and 9.

CHAPTER 8

PROPULSION and FUEL SYSTEM INTEGRATION

8.1 Introduction

In this study, size, location and the properties of the propeller will be determined. The required engine size will be calculated by the statistical methods, then will be compared with the size of the selected engine. The engines will be installed next, the fuel system will be designed and the wing fuel tank volume will be calculated and checked if there is enough volume for the required amount of fuel. Besides, possible spaces for fuel will be predicted in the fuselage. The final view of the a/c configuration will be shown in the corresponding figures by the end of this chapter.

8.2 Propulsion System Design and Installation

Let's recall that, *Limbach L-275E,* was the model selected as the main engines, see Figure 5.1 and Table 5.1, and *Limbach L-90 E* was the model selected as the aft engine, see Figure 6.1 and Table 6.1.

From now on, the propulsion system design and installation will be performed according to the properties of these selected engines.

8.2.1 Propeller Sizing and Selection

In this conceptual design concept, the main engines will have two propellers, while the aft engine has four. In the process of determining the diameter of the propellers, it should be noted that, the larger the propeller, the more efficient the propeller will be. But, the limitation comes from the tip speed which must be smaller than sonic speed. For this purpose Eqn. (8.1) will be utilized. By the way, in Eqn. (8.1), the factor of 60 is used in order to convert the tip static velocity to the unit of 'ft/s'.

$$(V_{tip})_{static} = \pi n D_p / 60 \qquad (8.1)$$

The tip of the propeller follows a helical path through the air. Tip speed is the vector sum of the rotational speed, see Eqn. (8.1), and the aircraft's forward speed as defined in Eqn. (8.2).

$$(V_{tip})_{helical} = \sqrt{V_{tip}^2 + V_{a/c}^2} \qquad (8.2)$$

For a metal propeller, the helical tip speed should not exceed 950 fps. If noise is of concern, the upper limit for both metal and wooden propellers should be ~ 700 fps during take-off. But here, a UAV is of concern, hence, the noise criteria will not be taken into account. Then,

Let, $(V_{tip})_{helical} \cong 900$ ft/s

$V_{a\,c} = V_{cruise} = 150$ ft/s

Then, from Eqn. (8.2),

$$900 = \sqrt{(V_{tip})_{static}^{\ 2} + (150)^2} \Rightarrow (V_{tip})_{static} = 887.41 ft/s$$

Then, from Eqn. (8.1),

$$887.41 = \pi(3392)D_p / 60$$

$$D_p \approx 4.99ft = 1.52m$$

Here, it is assumed that the a/c uses 46 % of the engine rpm during cruise; i.e. 3392 of 7300 rpm.

These thrust outputs of the selected engines will be evaluated through the theoretical methods given in Ref. [5] as follows.

The *maximum* static thrust that one might expect from a propeller can be calculated by solving Eqn. (8.3) for T.

$$T = P_{io}^{2/3}(2\rho A)^{1/3} \qquad (8.3)$$

where,

P_{io} = Static induced power (W, hp)
A = Propeller disc area (m^2, ft^2)

Then,

$$T = (17{,}900)^{2/3}\left[2(1.226)\pi(.625)^2\right]^{1/3} = 987.9N$$

This value of T represents an upper limit that is not attainable in practice, since the momentum theory neglects profile drag of the propeller blades. Also, additional induced losses occur near the tips of the blades.

In forward flight, an ideal efficiency, η_i, can be defined as the ratio of the useful power to the total power given by Eqn. (8.3).

$$\eta_i = \frac{2}{1+\sqrt{1+T_c}} \qquad (8.4)$$

where T_c is a thrust coefficient defined by,

$$T_c = \frac{T}{qA} \qquad (8.5)$$

For the case of Tilt-Duct VTOL UAV, Equations (8.5) and (8.4) becomes, respectively,

$$T_c = \frac{987.9}{\frac{1}{2}(1.226)(45)^2 \pi (.625)^2} = 0.648$$

$$\eta_i = \frac{2}{1+\sqrt{1+0.648}} = 0.876$$

It should be noted that, as with the static thrust, η_i, given by the momentum theory is optimistic and represents an upper limit that is really not attainable. As an example, Cherokee 180 has a T_c of 0.224 and a η_i of 0.95. But, the actual propeller efficiency is more like 0.83. Hence, it is obvious that things will turn out to be similar for the case of the design UAV. Following a similar procedure, the actual thrust of Tilt-Duct VTOL UAV will be around 0.75. Adding a safety factor of 10%, the thrust output will be around 640 N. Adding such a safety factor is vital, in order to take into account any additional, unexpected losses. Since, the design UAV is of VTOL type, any unexpected induction in thrust output will endanger the VTOL mission.

➢ $T_{per\ engine} = 640\ N = 143.9\ lb$

Then, the total thrust will become,

➢ $T_{total} = 1280\ N = 287.8\ lb$

This calculation procedure was also presented in Chapter 6.

Now, propeller sizing will be done according to the method given Ref. [5]. First, the advance ratio and the speed power coefficient will be evaluated by use of Equation (8.6) and (8.7), respectively. Then, by use of several figures given in Ref. [5], the optimum propeller diameter, D_p, the blade angle, β, the thrust and power coefficients, C_T, C_p, will be approximately estimated. Then,

$$J = \frac{V}{nD_p} \tag{8.6}$$

where,

J: Advance ratio

n: revolutions per second (rps)

D_p: Propeller diameter (ft, m)

The speed power coefficient, C_s, is defined by,

$$C_s = \left(\frac{\rho V^5}{Pn^2} \right)^{1/5} \tag{8.7}$$

Considering the selection of a propeller to absorb 75% of the maximum power of 24 hp (17,900 W) at 3392 rpm at standard sea level conditions, Eqn. (8.5) gives a C_s as the following,

$$C_s = \left(\frac{1.226(45)^5}{13{,}425(56.53)^2} \right)^{1/5} = 1.394$$

From the maximum efficiency line in Figure 6.24 of Ref. [5], a J of 0.80 and a β of 20° are obtained. These values in turn lead to a C_T value of approximately 0.06. Then from the obtained data, and Eqn. (8.7), the optimum propeller diameter turns out to be,

$$J = \frac{45}{56.33(D_p)} = 0.80 \Rightarrow D_p = 0.995m = 3.26ft$$

Figures 6.16, 6.19, and 6.24 are used for determination of C_T, η and J. Consequently, the properties evaluated at this stage are,

$J = 0.80$

$\beta = 20°$

$C_T = 0.06$

$\eta = 0.87$

$D_p = 0.995$ m

It should be noted that the figures available for the above estimations were given for a three-bladed propeller. These figures were the only ones that the author could utilize. Hence, they are approximate. Taking into account that a two-bladed propeller should have a higher diameter in order to produce the same thrust with a three-bladed propeller, the propeller diameter of the design UAV will be obviously larger than 0.995 m. Here, it should be reminded that at the beginning of this section the propeller diameter was found out to be 1.52 m according to the approximate methods given in Ref. [1]. Hence, the design UAV will have a propeller diameter in between these two values. Here, it is selected as follows.

➢ $D_p = 3.94$ m = 1.2 m

8.2.2 Propeller Location

Basically, two types of propeller locations are available : *tractor* and *pusher*.

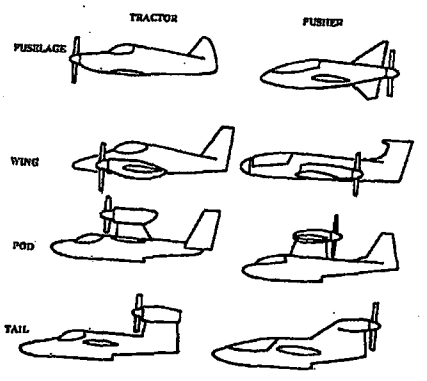

Figure 8. 1 Propulsion location matrix.

Tractor location puts the engine up front which shortens the a/c fore body, allows a smaller tail area and improved stability characteristics. It is also preferable, since it places the propeller in the undisturbed air and providing a ready source of cooling air.

On the other hand, with a tractor propeller, the a/c flies in the turbulence of the propeller wake, which increases the friction drag.

Pusher location has many disadvantages in many points of views, such that the propeller may be damaged by the rocks thrown up by the wheels. Also, due to the engine exhaust exposed on the propeller and the difficulty of cooling the engine, a pusher location for a piston-propeller engine can create problems.

This design will use the '**tractor**' location.

8.2.3 Engine Size Estimations

By use of Table 10.4, i.e. piston and turboprop statistical models, of Ref. [1], a statistical engine size estimation will be performed as follows,

$$X = a(bhp)^b \qquad (lb. \text{ or } in) \qquad (8.8)$$

For 'piston- horizontally opposed' engines, the variables, a and b become,

Weight $\rightarrow$ $a = 5.47$, $b = 0.780$

Length $\rightarrow$ $a = 3.86$, $b = 0.424$

Per engine the output power will be 24 *hp*. Then, by use of Eqn. (8.8),

$$_{eng} = 5.47(24)^{0.780} \cong 65.25lb = 29.59kg$$

$$L_{eng} = 3.86(24)^{0.424} \cong 14.85in = 0.377m$$

At this stage, in order to make a comparison of the statistical data and the actual data of the selected main engine, L 275 E, and the results obtained by statistical methods of Ref. [1] will be tabulated in Table 8.1.

Table 8. 1 Comparison of the statistical and actual engine data.

Property	*Statistical*	*Actual*
Weight	65.25 lb (25.29 kg)	16.54 lb (7.5 kg)
Length	14.85 in (37.7 cm)	8.9 in (22.6 cm)
Width	-	15.35 in (39.0 cm)
Height	-	7.36 in (18.7 cm)

As a consequence, it is observed that the selected engine is obviously smaller in all dimensions than the statistically estimated engine. In this case, it should be noted that, the statistically determined values are quite generalized. Producing a new piston-prop engine requires a very high cost and consumes a huge amount of time, the selected engine is the best choice to go on with the calculations.

8.2.4 Engine Installation

When the installation of a propeller engine is of concern, the thrust output of a propeller depends on the shape and size of airplane components behind or ahead of it.

Wing mounting of the engines reduces the wing structural weight through a span loading effect, and reduces the friction drag by removing the fuselage from the wake of the propeller.

On the other hand, wing mounting of the engines introduces engine- out controllability problems which can cause an increase in the size of the rudder and vertical tail.

As a consequence, 'Wing mounted' configuration is selected. The engines will be located on both sides of the wing in a fan, symmetrically. This is done in order to protect the propellers against the side and bottom winds. Having the engine center lines in front of the c.g. was another point of concern, in the name of stability control of the a/c.

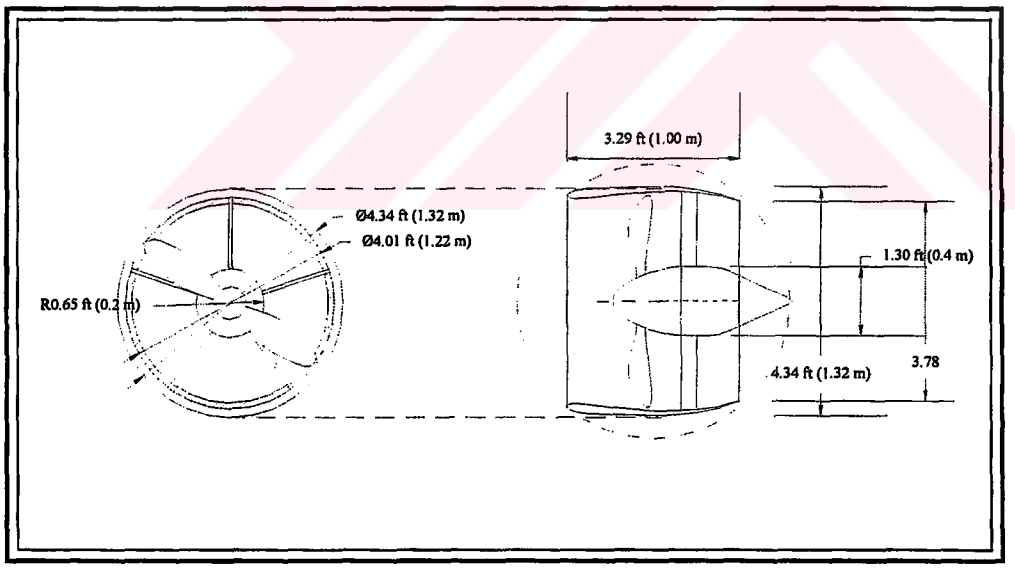

Figure 8. 2 Front and side views of the engine-propeller-duct combination.

8.2.5 The Advantages of Using Ducts

In Figure 8.2, the engines and propellers are shown to be located in ducts. This approach is preferred for the design UAV in reference of the following issues,

i. By this way, the wings will have no interference with the downwash of propellers. In V-22 Osprey, which is a tiltrotor multimission aircraft, the downwash air flow of the strong Allison T406 engines apply very high pressure on the wings, perpendicularly. For this purpose, especially during vertical takeoff, transition and landing, in order to minimize the surface area subjected to the high pressure, the flaps are pushed full down. The interesting point is that, during takeoff, this is a quite unusual case for the conventional aircraft.

   In the case of Tilt-Duct UAV, this brings an advantage of minimizing the need of complicated flapping mechanisms. This will consequently reduce the overall cost of the UAV and ease the manufacturing process.

ii. The ducts will act like an 'endplate'. By this way, the effective aspect ratio of the wing will be higher than the design aspect ratio. Let's comment on this subject.

   An obvious way to prevent the induced drag is to use an endplate, i.e. a vertical plate at the wing tip. Induced drag is caused by the higher-pressure air at the bottom of the wing escaping around the wing tip to the top of the wing. This air escaping around the wing tip lowers the pressure difference between the upper and lower surfaces. This reduces the lift near the tip. A wing with higher aspect ratio will have the tips farther apart than a lower aspect ratio wing which has the same surface area. Therefore, the amount of the wing affected by the tip vortex is less for a wing having a higher aspect ratio. Besides, the strength of the tip vortex is reduced.

iii. The Tilt-Duct VTOL UAV does not use rotors, i.e. no hinge or swash-plate design. Just the regular propellers that can be found in the market. This will also ease the manufacturing process and reduces the requirement of too much expertise.

iv. Locating ducts at the wing tips, the pressure and load distribution will be more uniform from the roots to the tips. It is a common fact that the maximum amount of load is applied to the roots of the wings. The pressure distribution shows a decay from maximum to minimum, starting from the root to the tip of the wing. By applying load to the wing tips, i.e. installing ducts, a more uniform pressure/load distribution will be obtained.

v. Depending on the duct's shape, i.e. proportion of the inlet and exit areas, probably the thrust output will be increased. In hover flight, this may cause an increase in power-to-thrust ratio up to an amount of 41%. [7]

vi. It will produce less noise. This may be an advantage, especially in the reconnaissance purposed flights.

8.2.6 The Disadvantages of Using Ducts

The approach of using ducts will also have some disadvantages. These may be listed as follows,

i. The ducts will create drag themselves. Although they create endplate effect, and reduce the strength of tip vortex, i.e. induced drag, they themselves create drag due to their own wetted area. This drag force will also apply pressure to the roots of the wings due to the long moment arm.

ii. They will increase the structural weight of the UAV.

iii. It will be somewhat difficult to handle the horizontally opposed piston engines at low velocities. The horizontally opposed engines vibrates at low speeds. In the case of the Tilt-Duct VTOL UAV, the engines are located at the centerline of the ducts by means of five airfoil profiled sticks-clip combination. For this purpose, the reaction of the duct-engine combination should be tested for vibration durability at low speeds.

8.3 Fuel System Design

An a/c fuel system includes the fuel tanks, fuel lines, fuel pumps, vents and fuel management controls. But the fuel tanks are the components that affect the overall a/c layout.

In our mission a/c *integral* type of fuel tanks will be used. The main idea of the integral fuel tanks is the use of the cavities within the airframe structure by sealing it to prevent any leaks and to form an appropriate fuel tank.

The available wing fuel tank volume will be calculated according to the method presented in Ref. [2], Volume II, pg. 153, as follows,

$$_{WF} = 0.54\left(S^2/b\right)(t/c)_r \left\{\left(1+\lambda_w\ \tau_w^{1/2}+\lambda_w^2\tau_w\right)/(1+\lambda_w)^2\right\} \qquad (8.9)$$

where, since, the same airfoil is used at both tip and the root,

$\tau_w = (t/c)_t/(t/c)_r = 1$

$\lambda_w = 1$

$S_w = 18.88\ ft^2$

$b_w = 10.64\,ft$

$(t/c)_t = (t/c)_r = 0.165$

It should be noted that, the accuracy of Eqn. (8.9) is given about 10%. Then,

$$_{WF} = 0.54\left(18.88^2/10.64\right)(0.165)\left\{(1+1+1)/(1+1)^2\right\}$$

$$\cong 2.239ft^3 = 63.4cm^3 \cong 16.75gallons$$

From Table 10.5 of Ref. [1], Military specific density for aviation gasoline is taken as 6 lb / gal.

Then the weight of the fuel amount that the available wing fuel tank is capable to carry is,

$$_F = V_F.\rho_F = (16.75)(6) = 100.5lb.$$

This amount of fuel is about 2.5 times the required amount as previously calculated. For the fuel system components' installation the cavities within the wing box and the fuselage will be used.

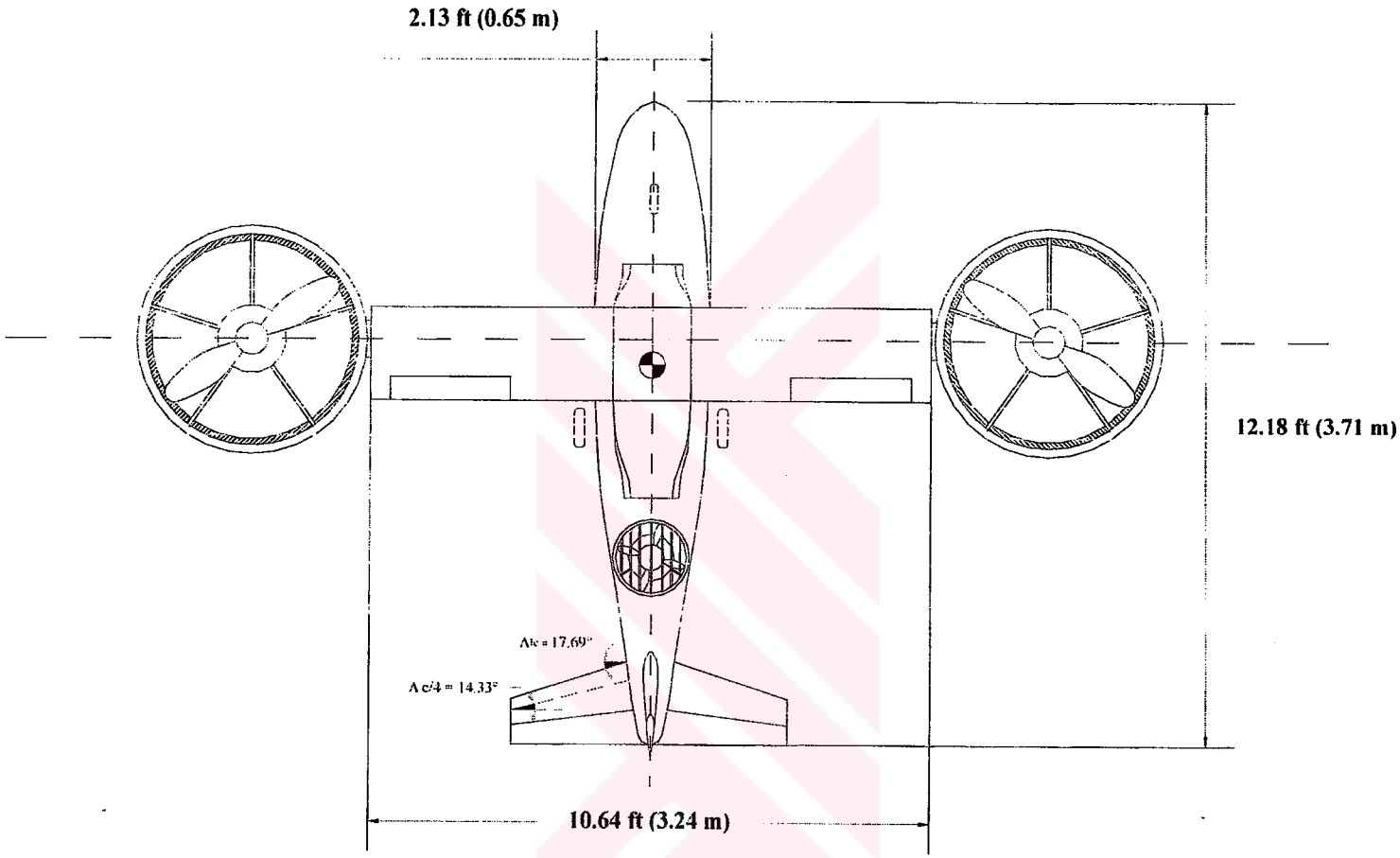

Figure 8. 3 Top view of Tilt-Duct VTOL UAV in hover mode (without landing gears installed).

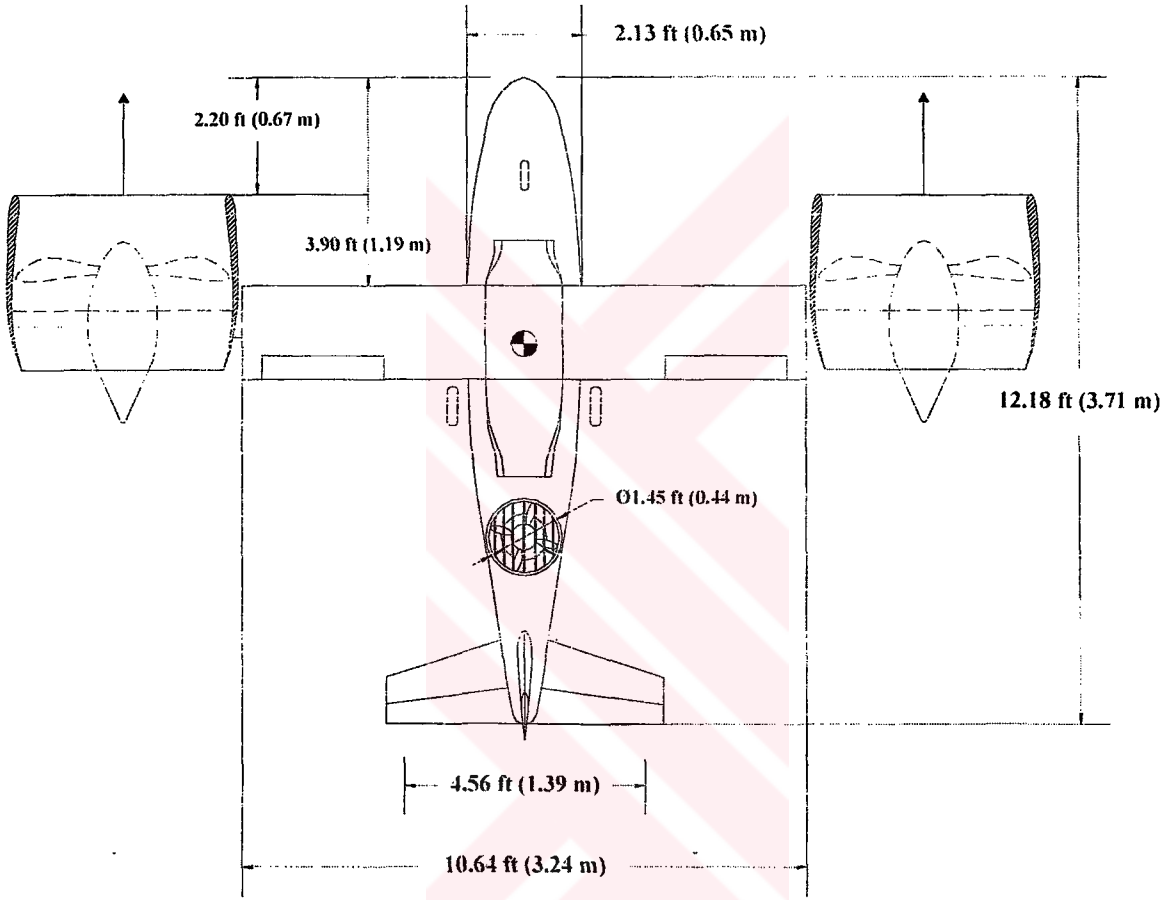

Figure 8. 4 Top view of Tilt-Duct VTOL UAV in forward flight mode (without landing gears installed).

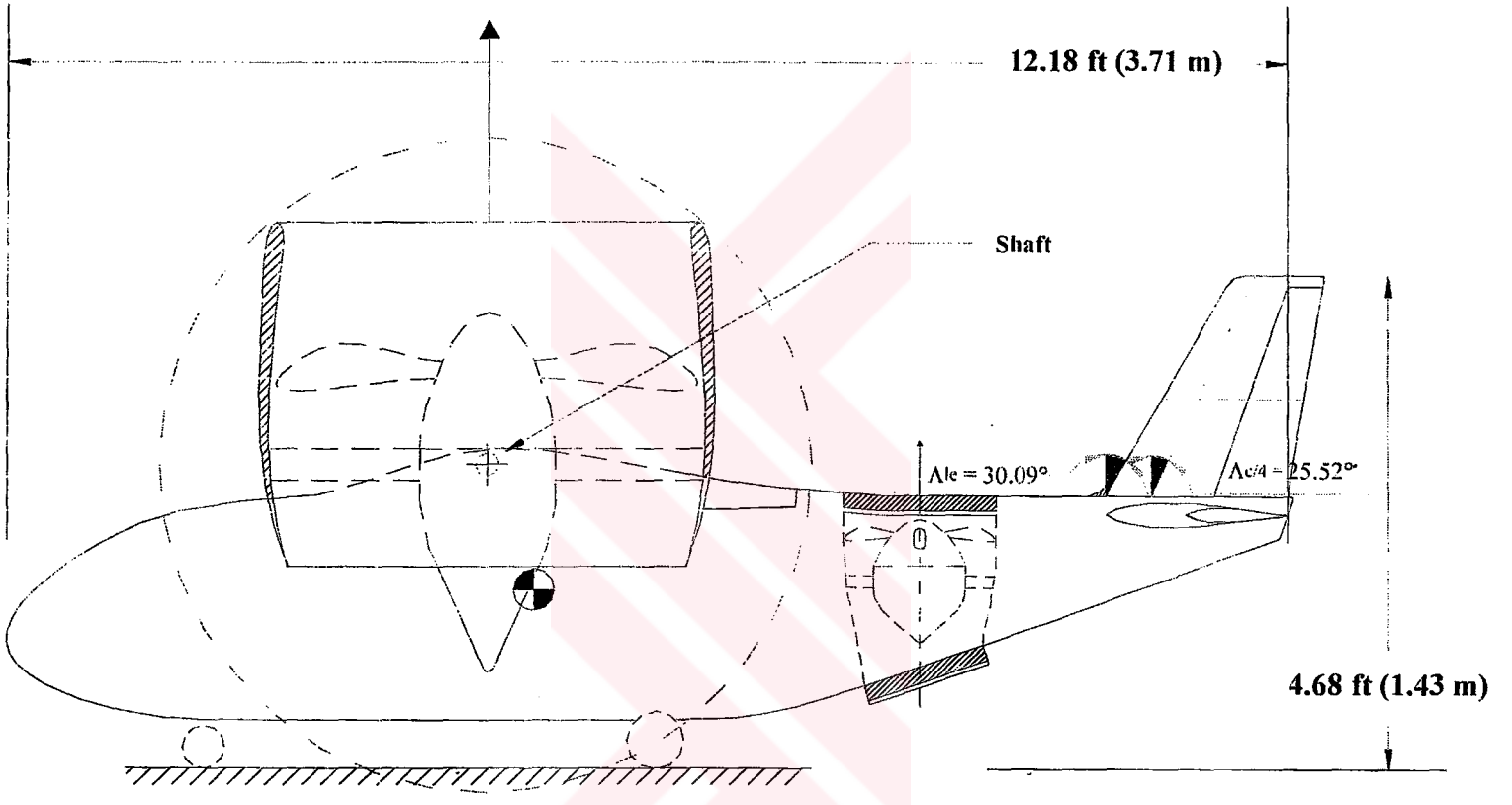

Figure 8. 5 Side view of Tilt-Duct VTOL UAV in hover mode (without landing gears installed).

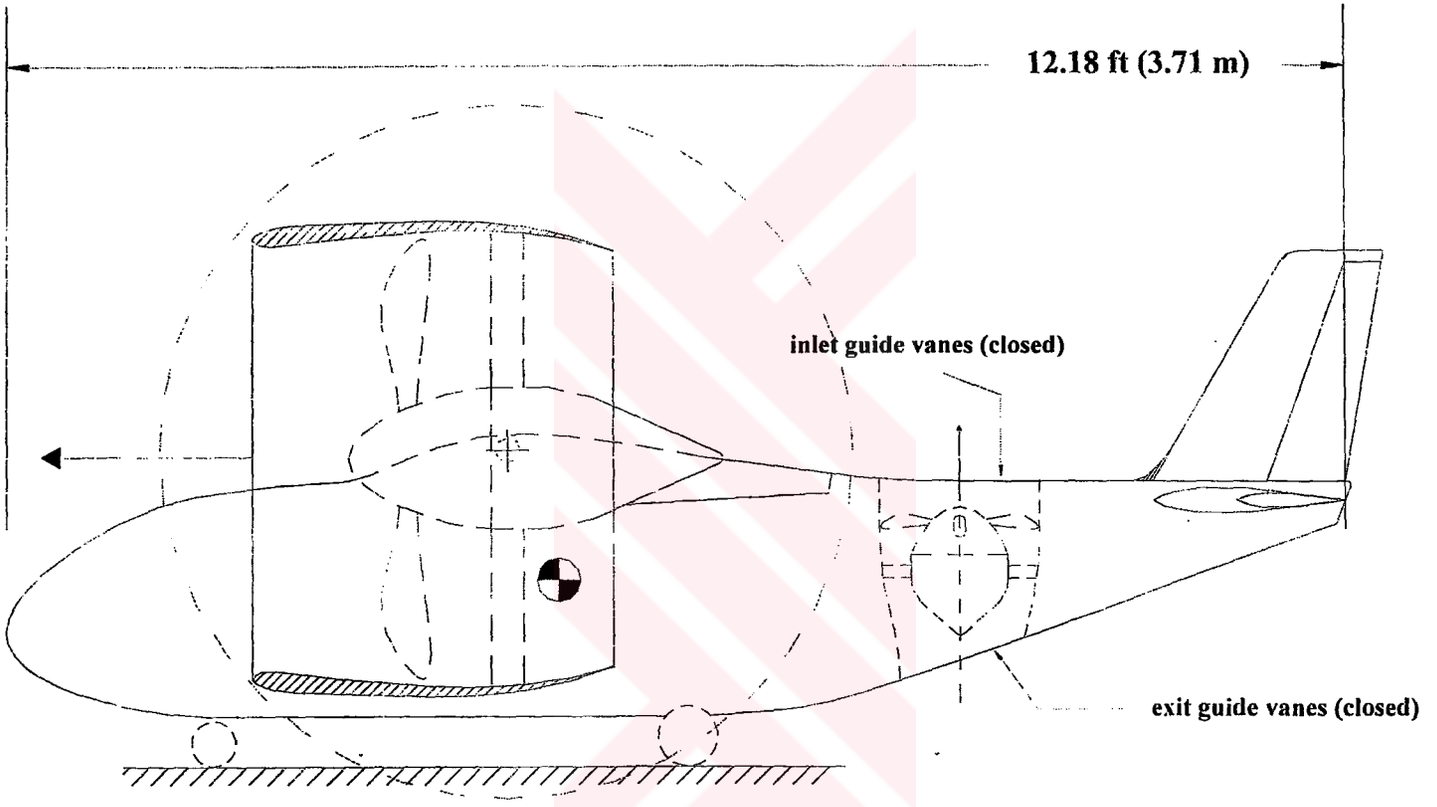

Figure 8. 6 Side view of Tilt-Duct VTOL UAV in forward flight mode (without landing gears installed).

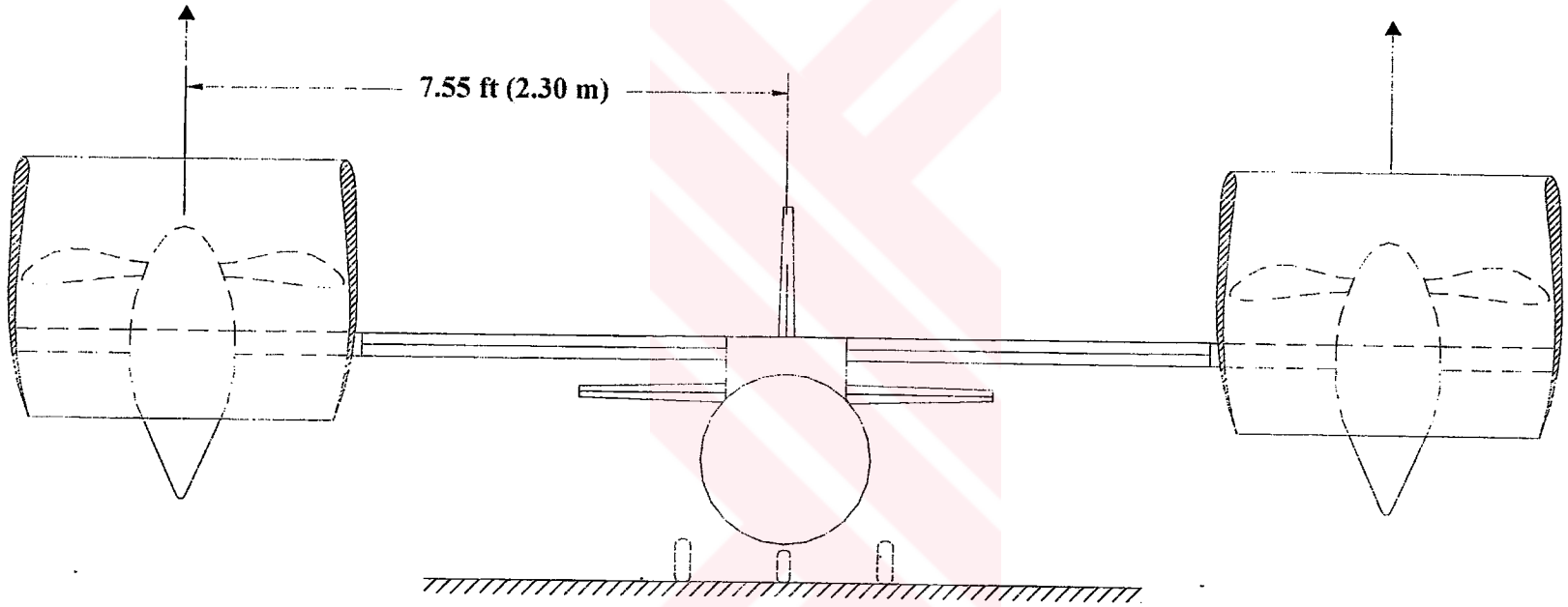

Figure 8. 7 Forward view of Tilt-Duct VTOL UAV in hover mode (without landing gears installed).

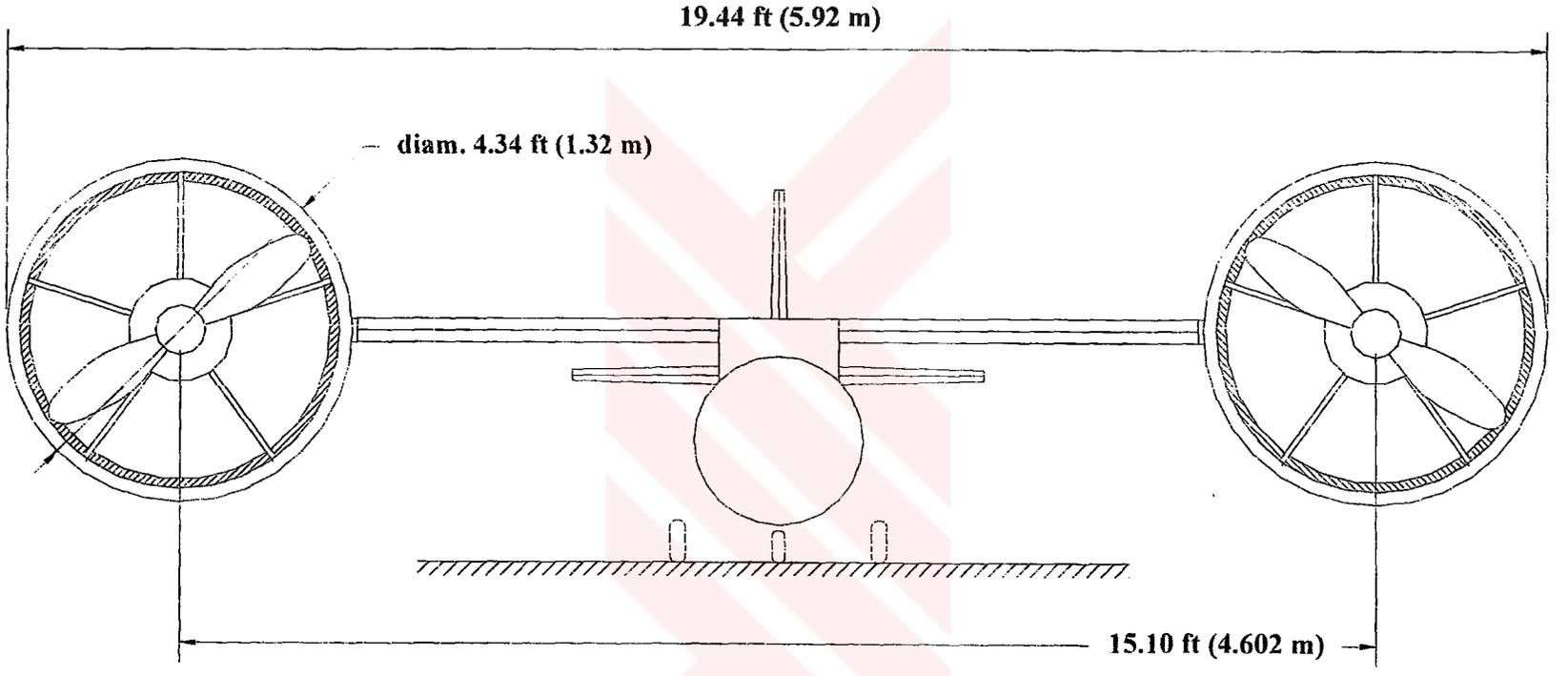

Figure 8. 8 Front view of Tilt-Duct VTOL UAV in forward flight mode (without landing gears installed).

8.4 Conclusion

This chapter represents the calculations based on the propulsion system configuration. For this purpose, propeller sizing and installation, engine installation are some section headings performed within this chapter.

During the engine sizing process, statistical methods for the engine size estimations yielded larger dimensions than those of the selected engine. But, since the relevant equations are very generalized ones and since it is a highly expensive and time consuming business to produce a new turboprop engine which suits the estimated dimensions, the selected engine will be preferred.

The wing fuel tank volume is calculated and found to be highly sufficient to carry the required amount of fuel. But, it has to be taken into account that, the fuel may also be carried in the fuselage. This is will create more space for the shaft mechanism and connection systems between the main engines. And, since there is only one TV camera as a payload, there will be enough empty space in the fuselage, in order to locate a fuel tank in it. Thus, no modification in the fuselage layout is needed in order to create additional volume for fuel. For the other fuel system components, the available cavities in wing-box and the interior fuselage will be used.

CHAPTER 9

LANDING GEAR and SUBSYSTEMS

9.1 Introduction

This chapter illustrates the design and installation process of landing gear of the design VTOL UAV. The tire, shock absorber selections, stroke determinations, oleo sizing, castoring wheel geometry design are some of the headings that are performed in this concept.

In selection of the landing gear, first it is decided whether to have a retractable or non-retractable landing gear and then discussed. Lastly, the discussions on the selections of a/c subsystems are given. The designs performed are given in the relevant figures.

9.2 Tire Sizing

In this sub section, the selection of the tires for the landing gears are done. For this purpose, many characteristics of the design UAV are taken into account in order to predict the requirements needed for the selection of the tires.

9.2.1 Landing Gear Functions

The basic functions of landing gears can be summarized as follows,

i. To absorb landing and take off shocks.

ii. To provide ability for taxi, take-off ground roll, landing ground roll and steering.

iii. To provide braking capability.

iv. To protect the base of the a/c from crashes, absorb and transmit landing loads to the airframe.

v. To allow for a/c towing.

9.2.2 Maximum Tire Loads

For the Tilt-Duct VTOL UAV, 'non-retractable tricycle gear configuration' will be used. For this type of gear configuration, generally 90% of the a/c weight is carried by the main wheels, while 10% of it is carried by the nose wheels. Nose wheels can be assumed to be about 60-100% of the main tires. In the following calculations *one* nose and *two* main tires will be used.

The distance between the two landing gears, *B*, can be determined due to desired margin between the aft and forward cg locations, see Figure 9.1,

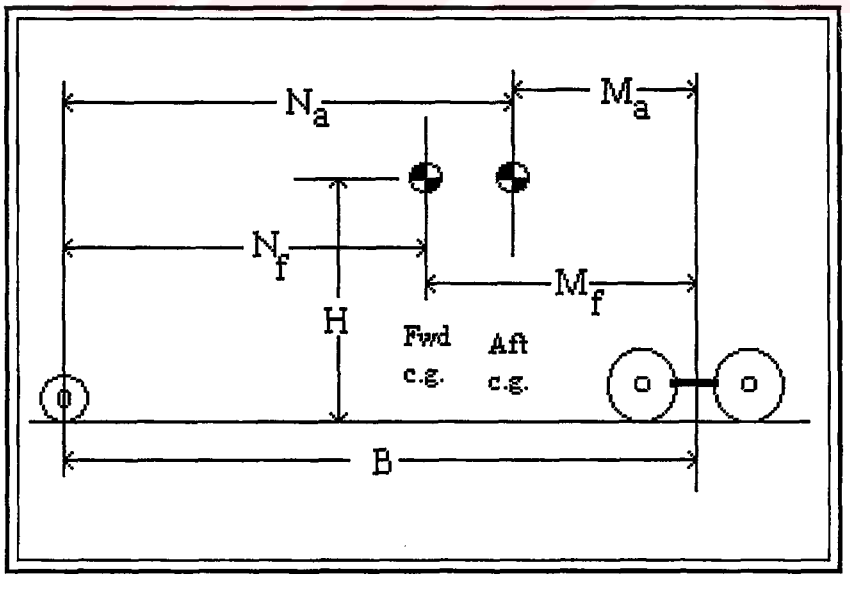

Figure 9. 1 Wheel – load geometry for tricycle gear configuration. [1]

Here, M_a stands for the most aft location of the aircraft c.g., and M_f stands for the most forward location of the aircraft c.g..

i. Let, $M_a - M_f = 0.1\ \bar{c}$

where, the recommended values for the following ratios are given as follows in Ref. [1],

$Ma / B \approx 0.09$, $Mf / B \approx 0.17$

$\Rightarrow\ M_a - M_f = (0.17-0.09)B = 0.08B = 0.1\ \bar{c}$

$$\Rightarrow\ B = \frac{0.1(1.77)}{0.08} = 2.2125ft$$

ii. Let, $M_a - M_f = 0.15\ \bar{c}$

$\Rightarrow\ M_a - M_f = (0.17-0.09)B = 0.08B = 0.15\ \bar{c}$

$$\Rightarrow\ B = \frac{0.15(1.77)}{0.08} = 3.319ft$$

iii. Let, $M_a - M_f = 0.2\ \bar{c}$

$\Rightarrow\ M_a - M_f = (0.17-0.09)B = 0.08B = 0.2\ \bar{c}$

$$\Rightarrow\ B = \frac{0.2(1.77)}{0.08} = 4.425ft$$

B will be set to 4.3 ft. according to the competitor survey. Based on the location of the nose gear, the values of N_a, N_f, and correspondingly M_a, M_f change. For the case of the design VTOL UAV, the nose and main landing gears are located as shown in Figure 9.2.

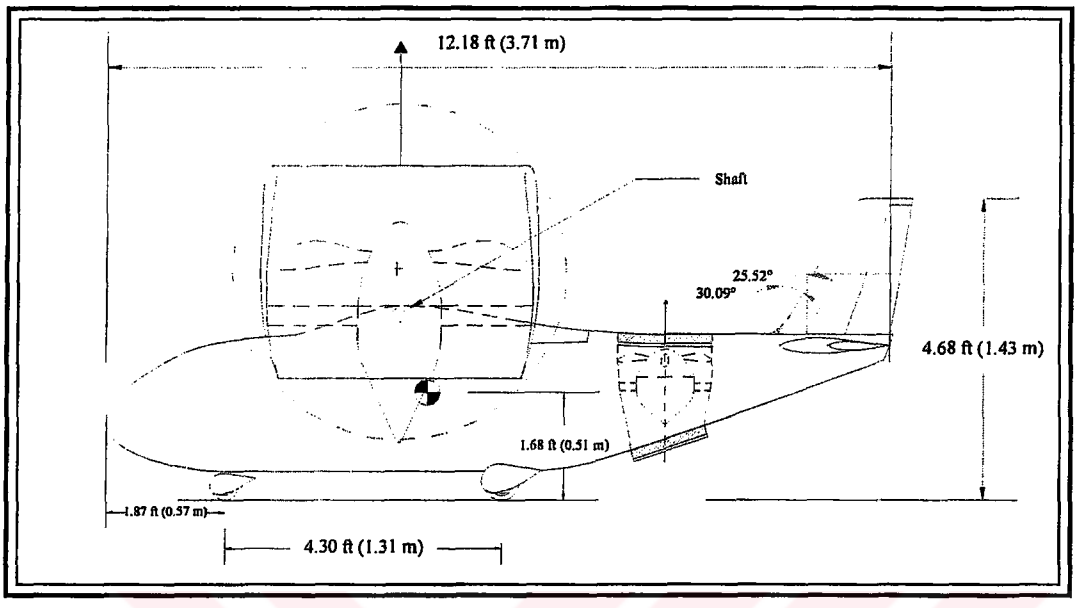

Figure 9. 2 The side view of the Tilt-Duct VTOL UAV with landing gears installed.

Then, the corresponding margin becomes,

$\Rightarrow$ $M_a - M_f = (0.30\text{-}0.20)B = 0.10B = 0.10(4.3) = 0.430 = 0.243\ \bar{c}$

$\Rightarrow$ $\boxed{M_a = 0.2B = 0.86ft}$

$\Rightarrow$ $\boxed{M_f = 0.30B = 1.29ft}$

$\Rightarrow$ $\boxed{N_a = 3.44ft}$

$\Rightarrow$ $\boxed{N_f = 3.01ft}$

The following values are found to be convenient to use in the further calculations,

➢

$$B = 4.3\,ft$$
$$X_{cg} = 5.00\,ft$$

Since, the location of the landing gears are predicted, some related properties will be evaluated by use of Figure 9.3.

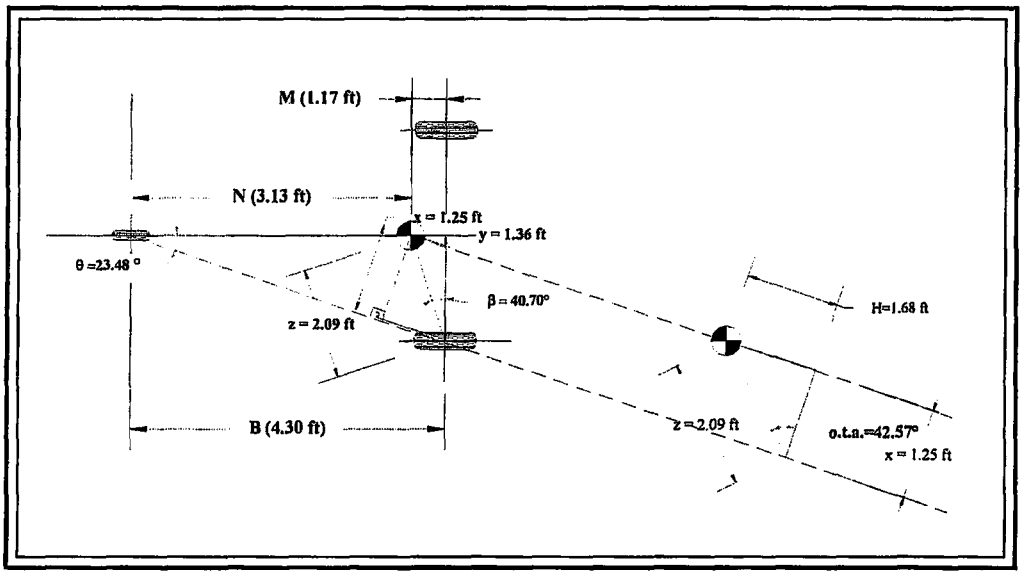

Figure 9. 3 Tricycle landing gear geometry.

$$o.t.a = \tan^{-1}\left(\frac{1.68}{1.25}\right) = 53.35°$$

Since, 53.35° is smaller than 63°, i.e. limit for the over turn angle, this can be considered as an acceptable value.

Now, the loads that the tires of the design UAV will carry, will be calculated. In order to satisfy FAR 25 provisions, 7%, and for later growth of a/c design 25% are added to all tire loads. Then,

$(\text{Max. Static Load})_{main} = W.\ N_a / B = (1.32)(226.6)(0.91) = 271.72\ lb$

$(\text{Max. Static Load})_{nose} = W.\ M_f / B = (1.32)(226.6)(0.17) = 50.76\ lb$

$(\text{Min. Static Load})_{nose} = W.\ M_a / B = (1.32)\ (226.6)(0.09) = 26.83\ lb$

$$(\text{Dynamic Breaking Load})_{nose} = (1.32)\frac{10HW}{gB} = (1.32)\frac{10(1.64)(226.6)}{32.2(4.3)} = 26.84lb$$

9.2.3 Landing Gear Arrangement

Before proceeding in this sub-section, it is convenient to recall that the relevant design a/c is a VTOL one. But, here the design procedure will be carried out for the case that the a/c will be able to take-off as an ordinary a/c as far as a suitable runway is available.

For a tricycle landing gear , the landing gear must be set so that the tail does not hit the ground during landing. This corresponds to the *'tip back angle'*. To prevent the a/c from tipping back on its tail, the angle between the vertical of the main wheel and c.g. should be greater than the tip back angle, or $> 15°$.

The *'over turn angle'* determines the a/c's tendency to overturn when taxied around a sharp corner. This corresponds to the angle between the static ground line and the line attaches the main wheel to c.g. For most ac, this angle should not exceed 63°. In the case of the design VTOL UAV, it is found as 53.35° in section 9.2.2.

A *'strut travel angle'* of about 7 deg. is desirable for a smooth ride out. It enables the tire to move upwards and backwards when a large bump is encountered.

The location of the c.g. is taken as .Then, $M_{c.g.} = 1.17$ ft. Then the corresponding tip back angle is,

$$t.b.a. = \tan^{-1}\left(\frac{M_{c.g.}}{H}\right) = \tan^{-1}\left(\frac{1.17}{1.68}\right) = 34.8° > 15°$$

The wheel diameter according to the braking requirements will be calculated as follows. Since, the brakes should absorb the kinetic energy of the a/c at touchdown, the following equation will be used for this purpose,

$$KE_{\substack{braking \\ per wheel}} = \frac{1}{2}\frac{W_{landing}}{g.N_w}V_{stall}^2 \qquad (9.1)$$

To allow an emergency landing shortly after take-off, $W_{landing}$ will be approximated as 90% of the take-off weight.

$$KE_{\substack{braking \\ perwheel}} = \frac{1}{2}\frac{(0.9)(226.6)}{(32.2)(2)}(84.45)^2 = 1.129 \times 10^4 ft.lb/\sec.$$

9.2.4 Main and Nose Wheel Selections

Tires should be selected such that the smallest area carries the maximum loads and a smooth surface contour in order to reduce the surface drag for the case of non-retractable landing gears.

A tire supports a load almost entirely by its internal pressure. Operating a tire at a lower internal pressure will increase the tire life, but this will yield greater drag, greater weight and wheel-well diameter.

Type I Wheels : Smooth contour. Designed for non-retractable landing gears, see Figure 9.4. [2]

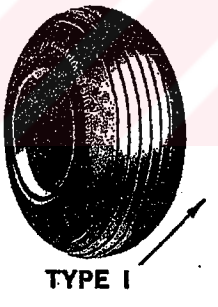

Figure 9. 4 Type I, smooth contour airplane tire. [2]

The main tires will be selected according to the load corresponds to each main wheel, which is max. static load per wheel, as calculated below,

$$Load\ per\ each\ main\ wheel = \frac{271.72}{2} = 135.86lb$$

The nose wheel characteristics will be selected according to the total dynamic nose wheel load (static + dynamic) divided by 1.4 for *Type I* tires:

$$Total\ Dynamic\ Nosewheel\ Load = \frac{50.76 + 23.83}{1.4} = 53.28lb$$

The corresponding selected tires are : *8×3.00-2.88, TT, Type I* as nose tire and *10×4.09-3.19, TT, Type I* as main tires, see Table 9.1.

The footprint area and inflation pressure calculations for the selected tires will be done according to the methods given in Ref. [1], see Figure 9.5.

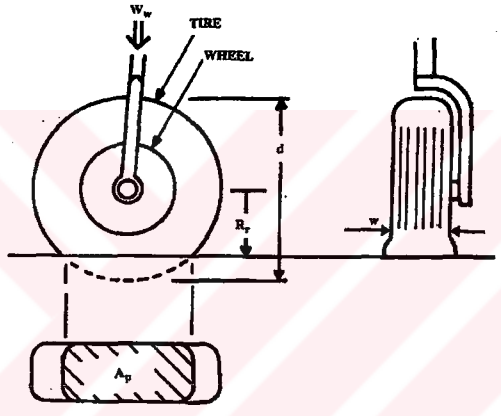

Figure 9. 5 Tire contact area. [1]

Main wheel :

$$A_p = 2.3\sqrt{w\ d}\left(\frac{d}{2} + R_r\right) = 2.3\sqrt{(4.09)(10)}\left(\frac{10}{2} + 3.25\right) = 121.35in^2 = 0.864ft^2$$

Nose wheel :

$$A_p = 2.3\sqrt{w\ d}\left(\frac{d}{2} + R_r\right) = 2.3\sqrt{(3.0)(8.0)}\left(\frac{8.0}{2} + 2.85\right) = 77.18in^2 = 0.536ft^2$$

where,

A_p : Foot print area, i.e. the contact area of the tire with the pavement.

9.3 Shock Absorber Selection

9.3.1 Shock Absorber Type

The landing gear should be able to absorb the shock of a bad landing and yield a smooth ride during taxiing (for the forward flight mode). To provide this, a proper type of shock absorber should be used, recalling that the tires themselves also provide some shock absorbing ability by deflecting when a bumb occurs.

Many general aviation a/c use solid spring gear, but since it is heavy and causes the a/c tend to bounce a lot, in order to eliminate the possibility of the propeller hit the ground, it will not be the choice for the being, see Figure 9.6.

Figure 9. 6 Solid spring type of gear/shock arrangement. [1]

The *'oleopneumatic* or *oleo'* type of shock struts selected, for both the main and nose gears. This is the most common type of shock absorbing gear used today. For simplicity, *fixed orifice* type of oleos are going to be used, see Figure 9.7 and 9.8.

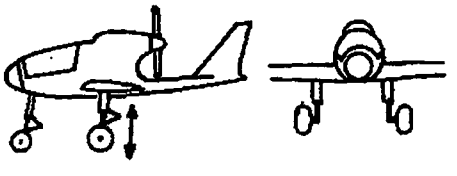

Figure 9. 7 Oleo type gear/shock absorber.

9.3.2 Stroke Determination

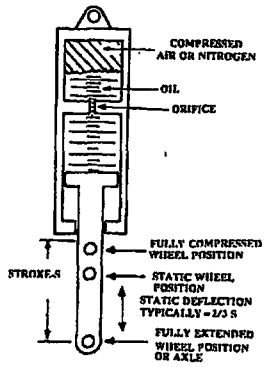

Figure 9. 8 Oleo shock absorber (most simple type). [1]

The required deflection of the shock absorbing system, the shock-absorber stroke is defined as,

$$S = \frac{V^2_{vertical}}{2g\eta.N_{gear}} - \frac{\eta_T}{\eta} S_T \qquad (9.2)$$

where, from Table 11.4 of Ref. [1] → $\eta_T \cong 0.47$ and $\eta \cong 0.70$

from Table 11.5 of Ref. [1] → $N_{gear} \cong 2.5$

The tire stroke of the main and the nose wheels will be evaluated as follows,

Main wheel :

$$S_T = \left(\frac{d}{2} - R_r\right) = \left(\frac{10}{2} - 3.25\right) = 1.75in. = 0.146ft$$

Nose wheel :

$$S_T = \left(\frac{d}{2} - R_r\right) = \left(\frac{8.0}{2} - 2.85\right) = 1.15in. = 0.096ft$$

For the case of the design VTOL UAV, a vertical velocity of 10 ft/s = 120 in/s will be assumed. Then, from Eqn. (9.2), the shock-absorber strokes of the main and nose landing gears become,

$$S)_{main} = \frac{(10)^2}{2(32.2)(0.70)(2.5/12)} - \frac{0.47}{0.70}(1.75/12) \cong 10.55in. = 0.879ft$$

$$S)_{nose} = \frac{(10)^2}{2(32.2)(0.70)(2.5/12)} - \frac{0.47}{0.70}(1.15/12) \cong 10.583in. = 0.882ft$$

The historical data give a 8 in of stroke is a minimum and at least a 10-12 in. of stroke is desirable. For the design UAV, these values are satisfactory, for the time being.

9.3.3 Oleo Sizing

The total length (h) of the oleo (stroke + fixed portion) is approximately 2.5 times the stroke.

$$h_{oleo_{main}} \cong 2.5(10.55) = 26.37in$$

$$h_{oleo_{nose}} \cong 2.5(10.58) = 26.46in$$

Oleo diameter is determined according to the load carried by the oleo. The main oleo number is selected to be two, as usual, then,

$$L_{oleo})_{main} = \frac{271.72}{2} = 135.86lb$$

$$L_{oleo})_{nose} = 53.28lb$$

$$D_{oleo})_{external} = 1.3\sqrt{\frac{4L_{oleo}}{P\pi}} \qquad (9.3)$$

where, P ≅ 1800 psi. Then, by use of Eqn. (9.3),

$$D_{oleo})_{main} = 1.3\sqrt{\frac{4(135.86)}{1800\pi}} = 0.403ft = 4.83in$$

$$D_{oleo})_{nose} = 1.3\sqrt{\frac{4(53.28)}{1800\pi}} = 0.252ft = 3.03in$$

9.4 Castoring Wheel Geometry

A nose wheel or main wheel must be capable of castoring (turning) for ground steering. The castoring can cause the problem of 'wheel shimmy' which is a rapid side-to-side motion of the wheel that can even tear the landing gear off the a/c

To prevent the problem of 'shimmy', a corresponding *'rake angle'* and *'trail'* should be selected, see Figure 9.9.

For this case, the rake angle will be selected as 7° positive and the trail will be selected as,

$$trail)_{main} = 0.20(r_T) = 0.20\left(\frac{10}{2}\right) = 1.0in$$

$$trail)_{nose} = 0.20(r_T) = 0.20\left(\frac{8.0}{2}\right) = 0.8in$$

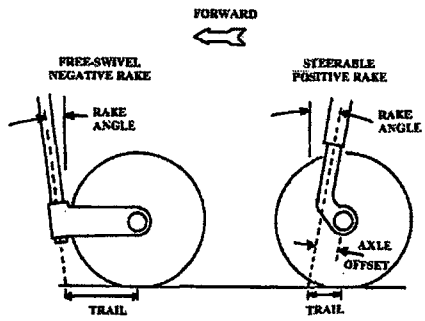

Figure 9. 9 Castoring Wheel Geometry. [1]

9.5 Subsystems

Aircraft subsystems generally include the hydraulic, electrical, pneumatic and auxiliary/emergency power systems. But, for the case of the design-automatically piloted UAV, the subsystems will happen to be quite simpified.

i. *Hydraulics* are used for a/c flight control as well as actuation of the flaps, landing gear, speed brakes and spoilers, etc. Most of these properties will not exist in the design VTOL UAV.

ii. A/c *electrical system* provides electrical power to the avionics, hydraulics, environmental control, etc. The electrical system consists of batteries, generators, TR's, cables, etc. For example, generators produce AC current and are located on or near by the engine.

On the average, avionics weight can be estimated from the a/c's empty weight, by assuming a density of about 30-45 lb/ft.cube. Selecting a convenient ratio from Table 11.6 of Ref. [1], i.e. for general aviation-single engine,

$$\frac{W_{avionics}}{W_{empty}} \cong 0.02$$

$$_{avionics} \cong (W_e)0.02 = (151.5)0.02 = 3.03lb$$

$$ol_{avionics} = \frac{W_{avionics}}{\rho_{avionics}} \cong \frac{3.03}{37.5} \cong 0.081ft^3 = 0.002m^3$$

9.6 Results of Chapter 9

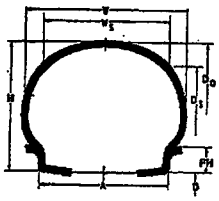

Table 9. 1 Table of results for Chapter 9.

Property	Main Gear	Nose Gear
Gear Type	Non-retractable, tricycle, oleo pneumatic shock absorber on each unit, carbon hydraulic disk brakes.	
Number of Tires	2	1
Accessories	Aerodynamic cab	Aerodynamic cab
Max. Static Load (lb)	271.72	50.76
Min. Static Load (lb)	-	26.83
Dynamic Braking Load (lb)	-	28.84
Load per wheel (lb)	135.86	-
Total Dynamic Nosewheel Load (lb)	-	53.28
Tire Type	TT- Type I	TT- Type I
W (in.)	4.09 - 3.19 (max - min)	3.00 - 2.88 (max – min)
D_o (in.)	10	8
Max. Loading (Lbs.)	450	650
Tread Patterns	Smooth	Smooth
Unloded. Infl. Pressure, (psi)	45	55
Rolling radius (in.)	3.25	2.85
Footprint Area (ft^2)	0.86	0.54
Shock Absorber Type	Oleopneumatic	Oleopneumatic
Tire Stroke (in.)	1.75	1.15
Stroke (in.)	10.55	10.58
Oleo Length (in.)	26.37	26.46
Oleo Diameter (in.)	4.83	3.03
Trail (in.)	1.00	0.80
Over Turn Angle (deg.)	53.35°	
Tip Back Angle (deg.)	34.8°	

Strut Travel Angle	7°
Rake Angle	7°
$W_{avionics}$ (lb)	3.03
$Vol_{avionics}$ (ft^3)	0.081

9.7 Conclusion

This chapter served to perform required calculations for the landing gear design of the Tilt-Duct VTOL UAV. Landing gears are selected to be of type tricycle and non-retractable. They are designed to satisfy all ground stability criteria, such as tip back, over turn and shimmy, considering the case of the a/c to land in forward mode. All the selections are done in order to satisfy the requirements, yet to minimize the structural complexity.

The ground clearance of the fuselage turned out to be 0.67 ft. which is prevents the propeller box to hit the ground even in forward flight mode. This will also enable the conventional takeoff and landing for the design UAV.

It is necessary to provide sufficient volume for the avionics for the initial layout. Hence, approximated estimations of the avionics weight and volume are performed in the subsystems section, 9.5.

The next chapter will illustrate the aerodynamics calculations for the design a/c.

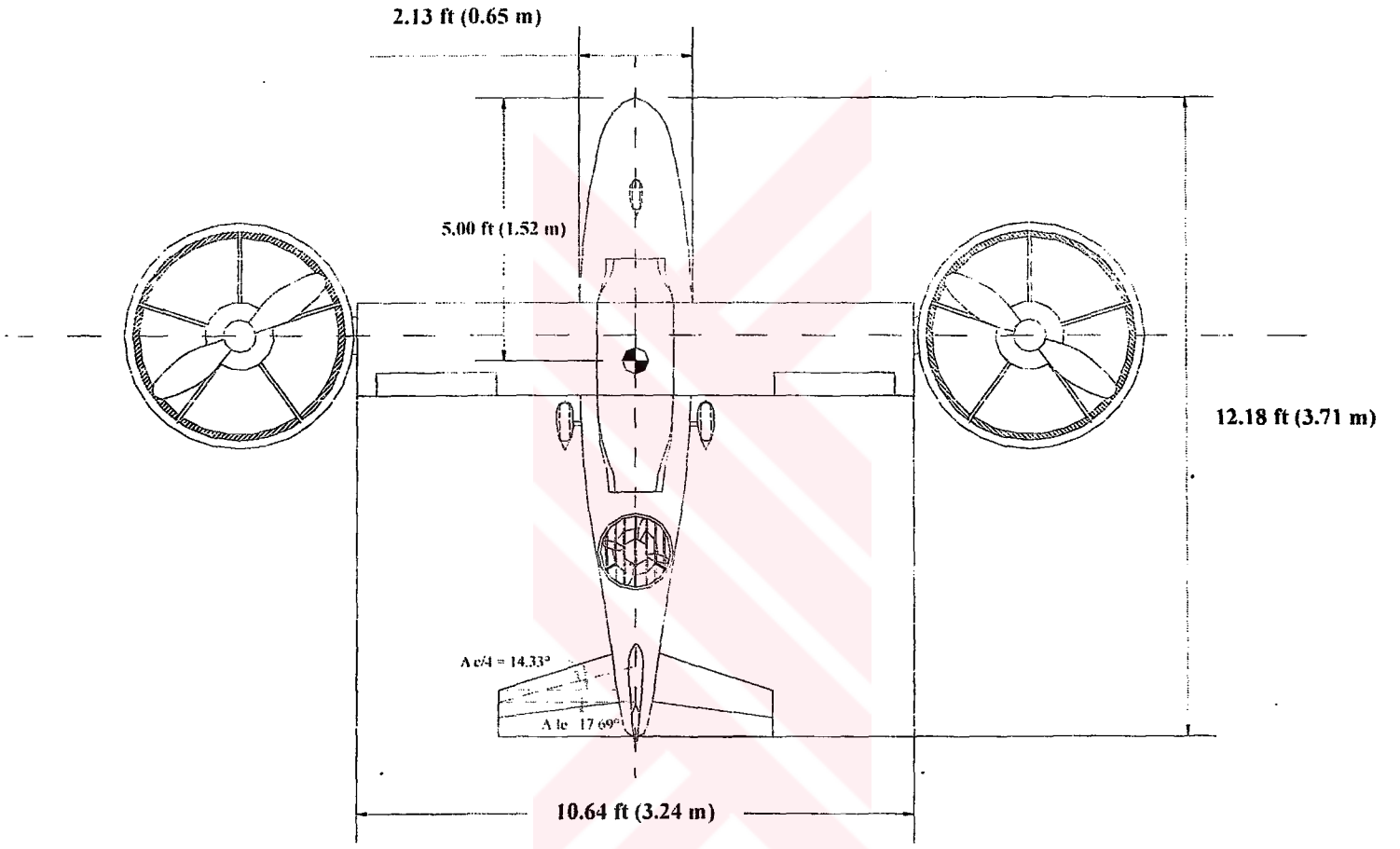

Figure 9. 10 Top view of Tilt-Duct VTOL UAV in hover mode.

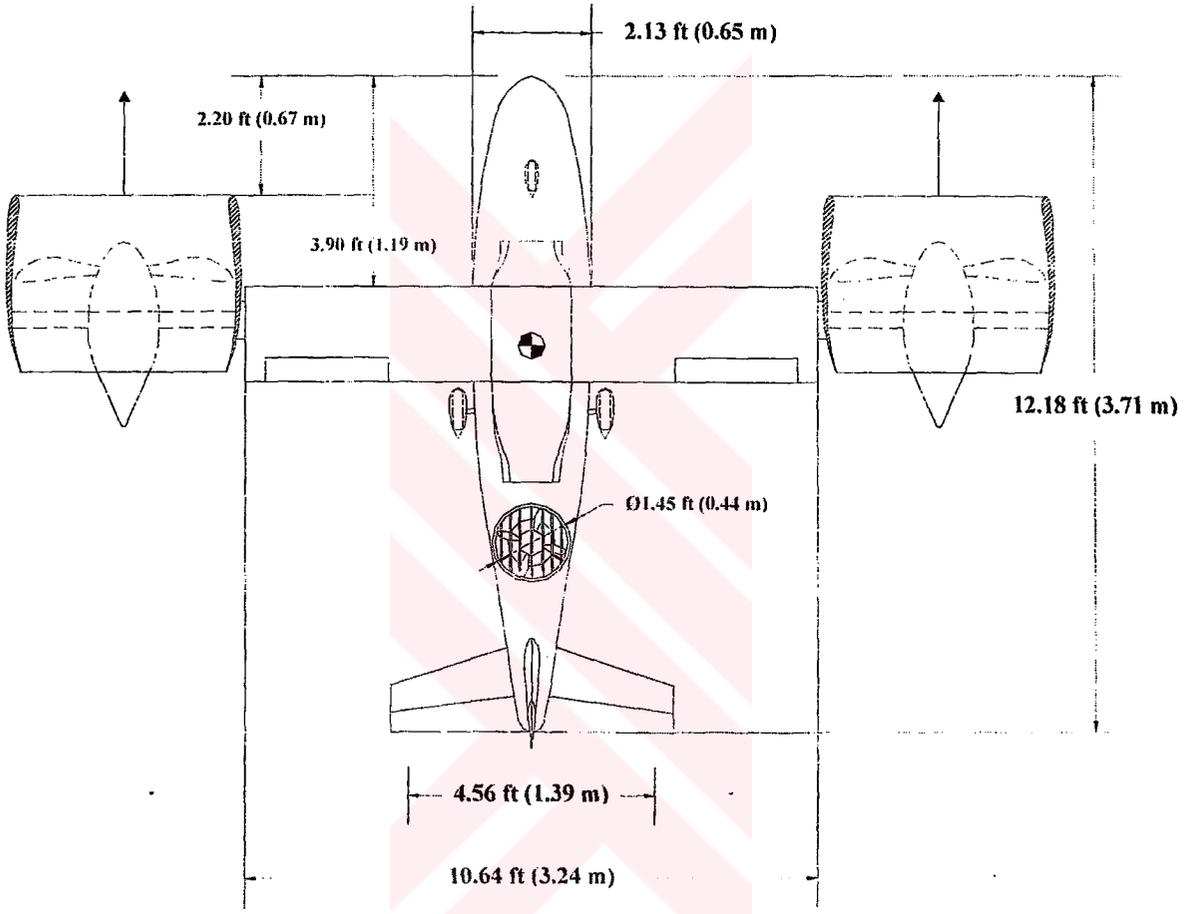

Figure 9. 11 Top view of Tilt-Duct VTOL UAV in forward flight mode.

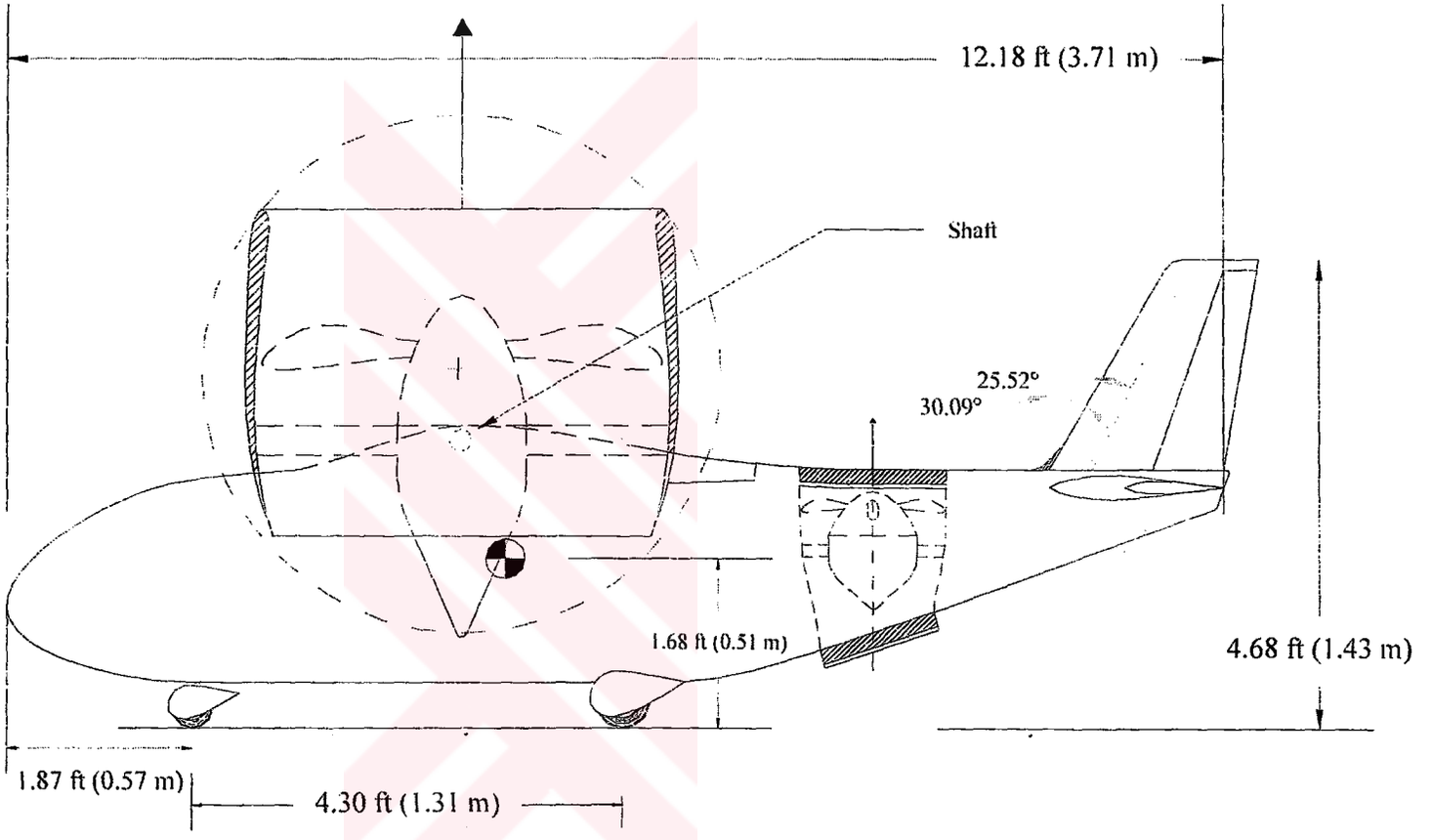

Figure 9. 12 Side view of Tilt-Duct VTOL UAV in hover mode.

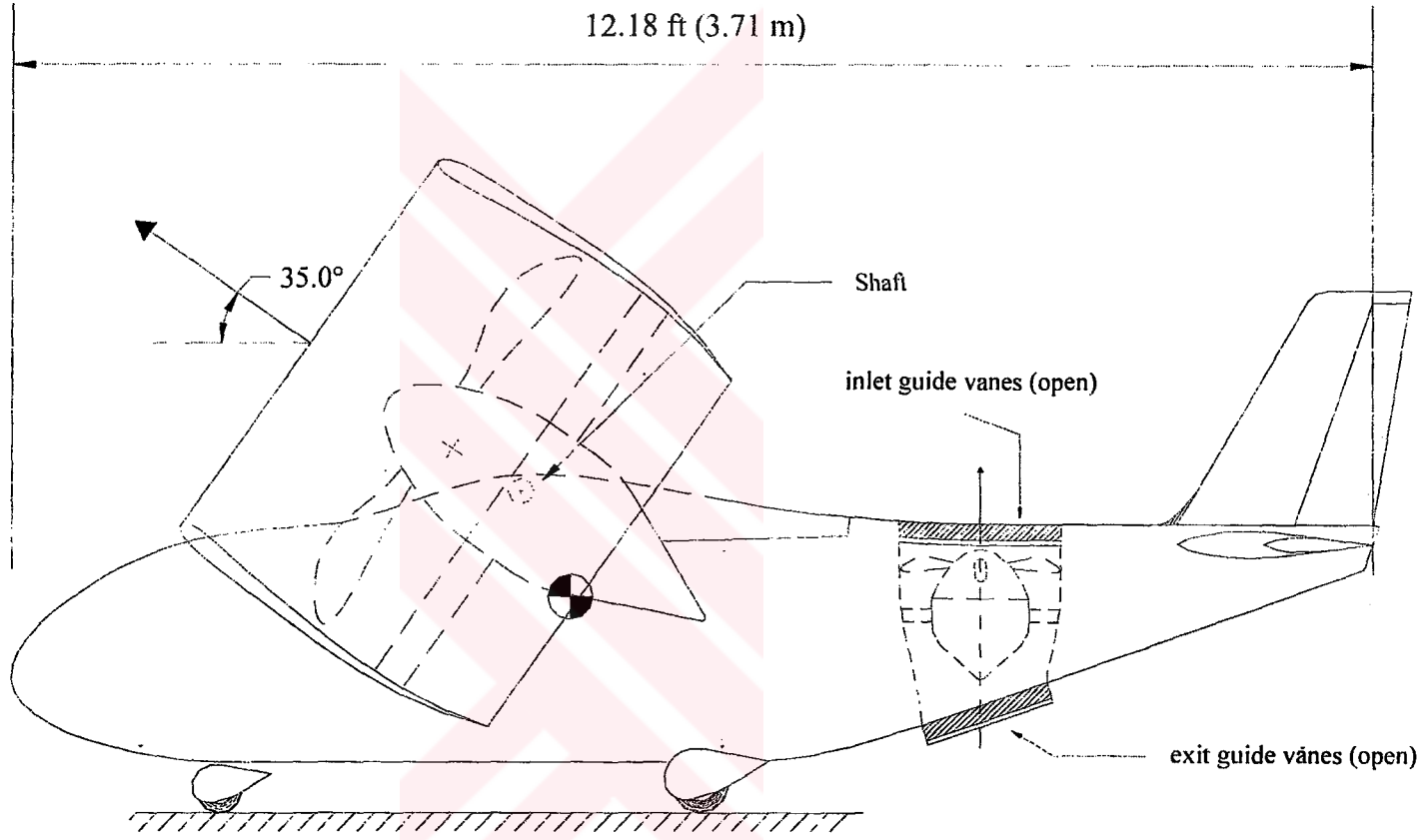

Figure 9. 13 Side view of Tilt-Duct VTOL UAV in transition mode, e.g. tilt angle = 35°.

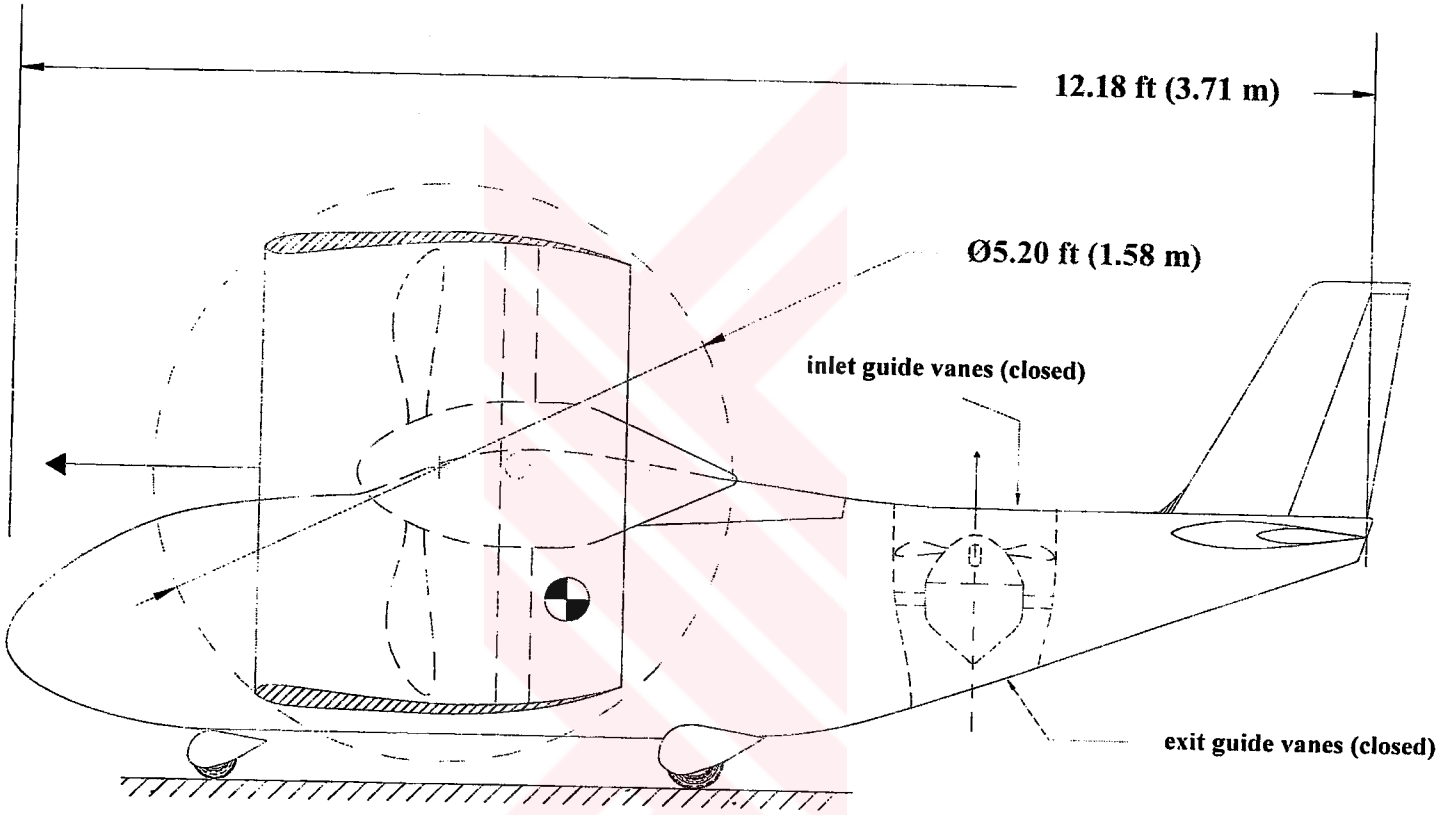

Figure 9. 14 Side view of Tilt-Duct VTOL UAV in forward flight mode.

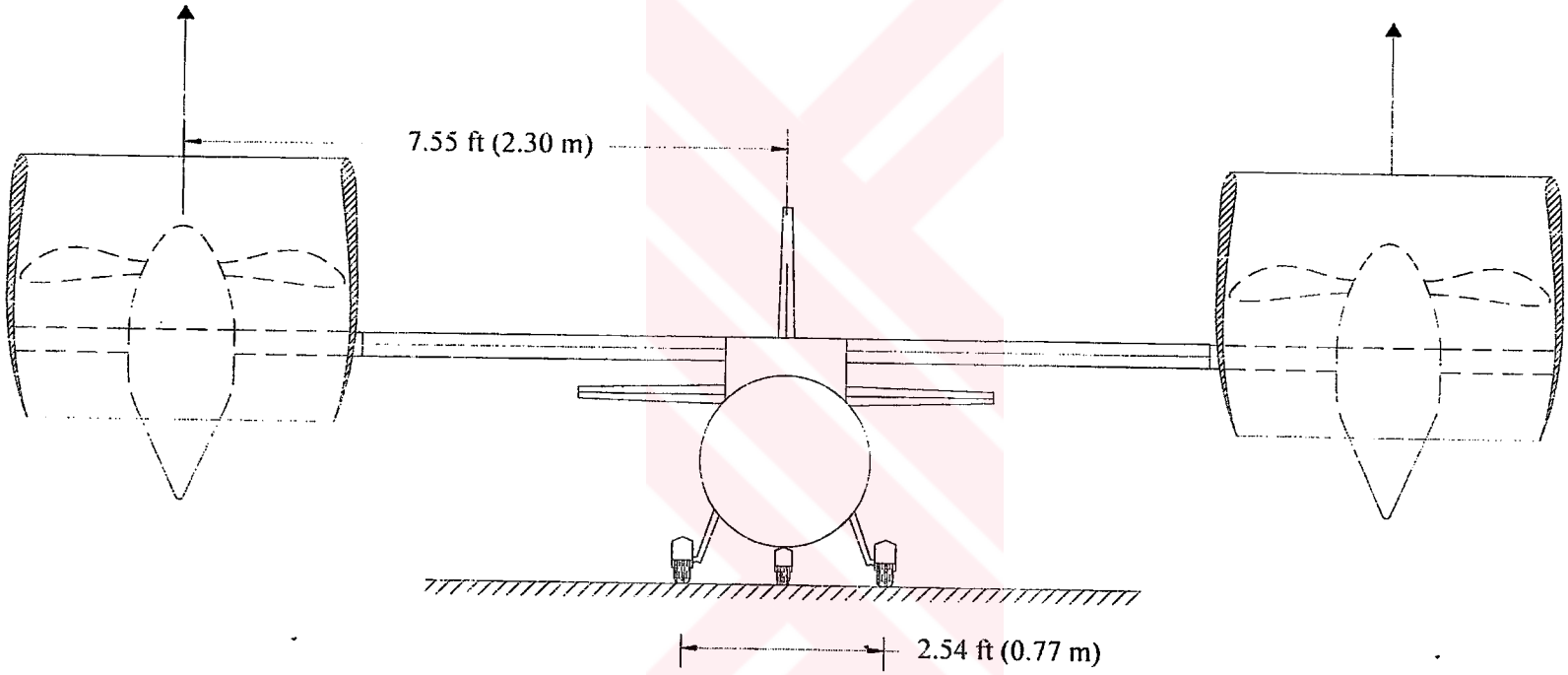

Figure 9. 15 Front view of Tilt-Duct VTOL UAV in hover mode.

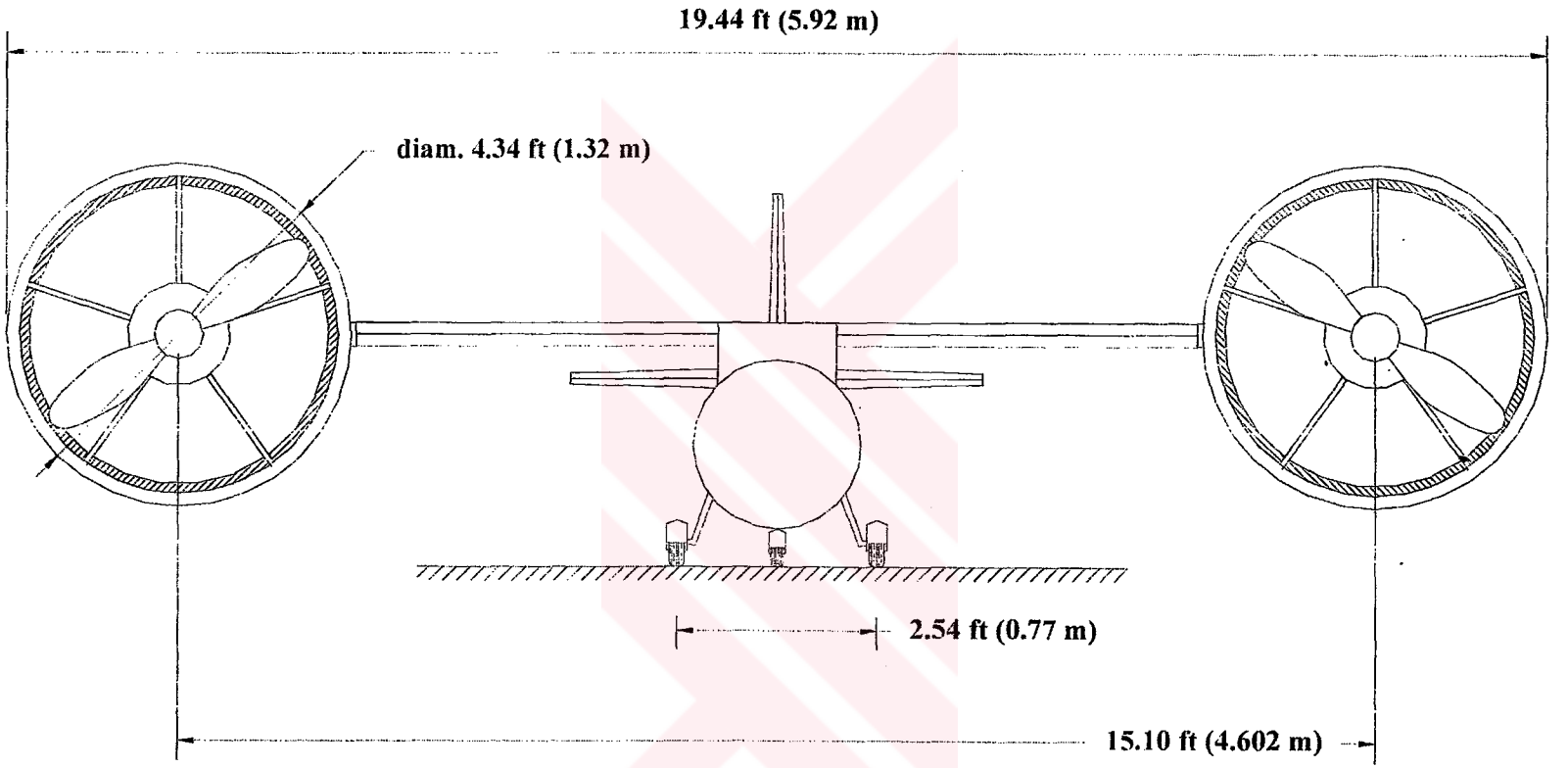

Figure 9. 16 Front view of Tilt-Duct VTOL UAV in forward flight mode.

CHAPTER 10

AERODYNAMICS

10.1 Introduction

In this chapter, the aircraft design will be analyzed "as-drawn" to see if it actually meets the mission requirements. Some of the aerodynamic coefficients, such as $C_{Do}, C_{Lmax}, C_D, \alpha_{CLmax}, \alpha_{OL}, C_{L\alpha}$ are calculated for clean, take-off and landing conditions. More precise estimations of oswald efficiency factor e and drag-due-to-lift factor K are also performed as a part of this chapter.

According to the results obtained, the corresponding C_L - α and C_L - C_D curves of the design UAV are plotted.

10.2 Lift

Lift is defined as the aerodynamic force produced by a surface in the direction normal to the velocity vector. In the case of an aircrafti it is basically produced by the airfoils by means of the pressure being higher on the lower surface than on the upper surface.

In this section, the aircraft lift related parameters will be evaluated as follows.

10.2.1 Lift Curve Slope

Equation (10.1) is a semi-emprical formula for the complete wing lift curve slope (per radian). This is accurate up to the drag-divergent Mach number, and reasonably accurate almost to Mach one for a swept wing.

$$C_{L_\alpha} = \frac{2\pi.A}{2+\sqrt{4+\frac{A^2\beta^2}{\eta^2}\left(1+\frac{\tan^2\Lambda_{\max t}}{\beta^2}\right)}}\left(\frac{S_{\exp}}{S_{ref}}\right)(F) \qquad (10.1)$$

where,

$$\beta^2 = 1 - M^2 \qquad (10.2)$$

$$\eta = \frac{C_{L\alpha}}{2\pi./\beta} \qquad (10.3)$$

$$F = 1.07\left(1-\frac{d}{b}\right)^2 \qquad (10.4)$$

Λ_{max} is the sweep of the wing at the chord location where the airfoil is thickest, F is the fuselage lift factor.

It should be noted that Eqn. (10.4) is modified than the original one taken from Ref. [1]. The modification is that the '+' sign is corrected to be the '-' sign where it should be. The original '+' sign gives illogical results. After the modiication all the results evaluated coincide with the results evaluated by use of the methods given in Ref. [2] and [3].

Then, the lift-curve-slopes for takeoff, cruise and landing will be evaluated as follows.

i. Take-off

Here, all the variables will be evaluated for takeoff.

$$M_{TO} = 1.1M_{STALL} = 1.1\left(\frac{84.45}{1104.9}\right)0.076$$

Then from Equations 10.2 and 10.3,

$$\beta^2 = 1 - 0.076^2 = 0.994$$

$$\eta \cong \frac{Cl_\alpha}{2\pi/\beta} = \frac{6.16}{2\pi/0.994} = 0.986$$

Since there is an endplate effect of the ducts at the tips of the wings, it will be taken into account as A_{eff} in the following.

A_{eff} =7.2

Since, there is no sweep and dihedral,

$\Lambda_{max\,t} = 0°$

$$\frac{S_{exp}}{S_{ref}} = \frac{1}{\cos(Diherdal)} = \frac{1}{\cos 0°} = 1$$

Then, from Equations 10.3 and 10.4,

$$F = 1.07\left(1 - \frac{2.13}{10.64}\right)^2 = 0.684$$

$$C_{L_\alpha} = \frac{2\pi(7.2)}{2 + \sqrt{4 + \frac{7.2^2(0.994)^2}{0.986^2}(1+0)}}(1)(0.684)$$

Then the takeoff lift-curve slope is evaluated to be,

➢ $$C_{L\alpha})_{TO} = 3.247(1/rad) = 0.057(1/\deg)$$

ii. **Cruise**

Here, all the variables will be evaluated for cruise.

$$M_{cruise} = \frac{150}{1091} = 0.137$$

Then from Equations 10.2 and 10.3,

$$\beta^2 = 1 - M^2 = 1 - (0.137)^2 = 0.981$$

$$\eta \cong \frac{Cl_\alpha}{2\pi/\beta} = \frac{6.16}{2\pi/0.981} = 0.962$$

Finally, from Equation 10.4,

$$C_{L_\alpha} = \frac{2\pi(7.2)}{2+\sqrt{4+\frac{7.2^2(0.981)^2}{0.962^2}(1+0)}}(1)(0.684)$$

➢ $$\boxed{C_{L\alpha})_{cruise} = 3.218(1/rad) = 0.056(1/\deg}$$

iii. Landing

Here, all the variables will be evaluated for landing. It will be assumed that the design UAV will have a landing velocity of 10 m/s. Then,

$$M_{Landing} \cong \frac{32.81}{1116.4} = 0.029$$

Similarly, from Equations 10.2 and 10.3,

$$\beta^2 = 1 - M^2 = 1 - (0.029)^2 = 0.999$$

$$\eta \cong \frac{Cl_\alpha}{2\pi/\beta} = \frac{6.16}{2\pi/0.999} = 0.979$$

$$C_{L_\alpha} = \frac{2\pi(7.2)}{2+\sqrt{4+\frac{7.2^2(0.999)^2}{0.979^2}(1+0)}}(1)(0.684)$$

➢ $$\boxed{C_{L\alpha})_{Landing} = 3.218(1/rad) = 0.056(1/\deg)}$$

10.2.2 Maximum Lift

In this section, the maximum lift coefficient of the design VTOL UAV will be predicted by use of methods given in Ref.s [1], [2] and [3].

The maximum lift coefficient of the wing usually determines the wing area. It in turn has a great influence upon the cruise drag. And this strongly affects the aircraft takeoff weight to perform the design mission.

Yet, it should be noted that, the estimation of maximum lift is probably the least reliable of all of the calculations used in aircraft conceptual design. Even refined wind-tunnel tests cannot predict maximum lift with great accuracy. Taking these notes into account, the following calculations are performed in order to estimate the approximate maximum lift coefficient of the design VTOL UAV.

The Eqn. (10.5) is valid for aspect ratio greater than 3. Since, the design UAV is in this category, this equation will be utilized in order to evaluate the maximum lift coefficient.

$$C_{L\max} = C_{l\max}\left(\frac{C_{L\max}}{C_{l\max}}\right) + \Delta C_{L\max} + \Delta C_{L\max}_{flapped} \qquad (10.5)$$

From Table 12.21 of Ref. [1], for NACA 4 Digit type of airfoil, which has a similar profile with the selected Eppler-E583 airfoil,

$\Delta Y = 26\,(t/c) = 26\,(0.165) = 4.29$

The ratio of $C_{L\max}/C_{\ell\max}$ will be evaluated from Eqn. (10.6),

$$C_{L\max} = 0.9 C_{l\max}\cos\Lambda_{c/4} \qquad (10.6)$$

Then,

$$\frac{C_{L\max}}{C_{l\max}} = 0.9$$

From Figure 12.19 of Ref. [1], taking into account that there is no flap for the case of the design UAV,

$$\frac{S_{flapped}}{S_{ref}} = 0$$

By use of Figure 4.3, the airfoil maximum lift coefficient of the Eppler-E 583 airfoil turns out to be,

$$C_{\ell \max} = 1.45$$

From Figure 12.9 of Ref. [1], for zero leading edge sweep, ΔC_{Lmax} is approximated as,

$$\Delta C_{L\max})_{clean} = 0$$

Then, Eqn. (10.5) gives a maximum lift coefficient as,

$$C_{L\max})_{clean} = (1.45)(0.9) = 1.305$$

➢ $\boxed{C_{L\max})_{clean} = 1.305}$

10.2.3 $\alpha_{L=0}$ and α_{CLmax}

The angle of attack for maximum lift is defined in Eqn. (10.7). In this equation, the first and second terms represent the angle of attack if the lift curve slope were linear all the way up to stall. The second term may be approximated by the airfoil zero-lift angle, which is negative for a cambered airfoil. The third term in Eqn. (10.7) is a correction for the nonlinear effects of vortex flow.

$$\alpha_{CL\max} = \frac{C_{L\max}}{C_{L\alpha}} + \alpha_{OL} + \Delta\alpha_{C_{L\max}} \qquad (10.7)$$

From, Figure 4.3, the performance plots of airfoil Eppler-E 583,

$$\alpha_{OL} \approx \alpha_{0l,\ airfoil} = -5^{\circ}$$

From Figure 12.10 of Ref. [1], for $\Lambda_{LE} = 0^{\circ}$ & $\Delta y > 4$,

$$\Delta\alpha_{Clmax} \approx 2.5^{\circ}$$

Then, Eqn. (10.7) becomes,

$$\alpha_{CL\max})_{clean} = \frac{1.305}{0.056} - 5° + 2.5° = 20.8°$$

10.3 Zero – Lift (Parasite) Drag

10.3.1 Equivalent Skin Friction Method

This method is based on the fact that a well designed a/c in subsonic cruise will have a parasite drag that is mostly skin friction drag plus a small separation drag.

Eqn. (10.8) will be used for an initial estimate of parasite drag. This will be somewhat a checking result for the more detailed method given in next sub-section. Here, C_{f_e}, "equivalent skin friction coefficient", includes both skin-friction and separation drag.

$$C_{D_o})_w = C_{fe}\frac{S_{wet}}{S_{ref}} \qquad (10.8)$$

Then, for wing, horizontal and vertical tails,

$$C_{D_o})_w = 0.0055\frac{39.945}{18.88} = 11.6\times10^{-3}$$

$$C_{D_o})_{HT} = C_{fe}\frac{S_{wet}}{S_{ref}} \cong 0.0055\frac{13.921}{18.88} = 4.05\times10^{-3}$$

$$C_{D_o})_{VT} = C_{fe}\frac{S_{wet}}{S_{ref}} \cong 0.0055\frac{5.631}{18.88} = 1.638\times10^{-3}$$

10.3.2 Parasite Drag From Aircraft Wetted Area

This is a more precise method than that of given in the previous sub-section. This is a method given in Ref. [2]. Here, the aircraft parasite drag will be estimated from the total wetted area of the aircraft. For this purpose, an average equivalent skin friction coefficient, C_{f_e}, is assumed for this UAV, i.e. 0.005 out of the range of 0.002-0.008 given in Ref. [2].

The following procedure was also given in section 5.4.5.

$$\log_{10} S_{wet_{a/c}} = c + d \log_{10} W_o \qquad (10.9)$$

$$\log_{10} f = a + b \log_{10} S_{wet_{a/c}} \qquad (10.10)$$

where, c, d are "Regression Coefficients" used to estimate Wetted Area of the aircraft from Take-off Weight and a, b are "Regression Coefficients" used to estimate Parasite Area from the Wetted Area of the aircraft.

$$C_{Do} = \frac{f}{S_{wing}} \qquad (10.11)$$

By use of equations (10.9-10.11),

$$\log_{10} S_{wet_{a/c}} = 0.8635 + (0.5632)\log_{10}(226.57) = 2.1899$$

$$\boxed{S_{wet_{a/c}} = 154.864\, ft^2}$$

$$\log_{10} f = -2.301 + \log_{10}(154.864) = -0.1111$$

$$\boxed{f = 0.7743}$$

$$\therefore\ C_{Do} = \frac{0.7743}{18.88} = 0.041$$

➢ $\boxed{C_{Do} = 0.041}$

10.3.3 Component Buildup Method

The component build-up method estimates the subsonic parasite drag of each component of the aircraft using a calculated flat-plate skin-friction drag coefficient, C_f, and a component form factor, FF, that estimates the pressure drag due to viscous

separation. Then the interference effects on the component drag are estimated as a factor, Q, and the total component drag is determined as the product of the wetted area, C_f, FF and Q.

The contributions of miscellaneous drags, $C_{D_{misc}}$, e.g. unretracted landing gear for this case, and the contributions of leakages and protuberances, $C_{D_{L\&P}}$, are added to the total amount. Eqn. (10.12) represents this subsonic parasite-drag buildup. The subscript "c" indicates that those values vary for each component.

$$\left(C_{D_O}\right)_{subsonic} = \frac{\sum\left(C_{f_c} FF_c Q_c S_{wet_c}\right)}{S_{ref}} + C_{Dmisc} + C_{D_{L\&P}} \qquad (10.12)$$

where,

$$C_f = \frac{0.455}{\left(\log_{10} R\right)^{2.58}\left(1+0.144M^2\right)^{0.65}} \qquad (10.13)$$

$$R = R_{cutoff} = 38.21\left(\ell / k\right)^{1.053} \qquad (10.14)$$

where,

ℓ : characteristic length, i.e., total length for the fuselage, mac for wing or tail.

From Table 12.4 of Ref. [1], for smooth molded composite, the skin roughness value is selected as,

$k = 0.17\times10^{-5}$ ft

Then, by using Equations (10.13) and (10.14), R_{cutoff}, and C_f values are tabulated in Table 10.1. The Mach number used is 0.137.

Table 10. 1 Table of ℓ, R_{cutoff}, C_f for different aircraft components at M=0.137.

Components	ℓ *(ft)*	$R_{cutoff} \times 10^6$	$C_f \times 10^{-3}$
Fuselage	12.18	631.976	1.665
Wing	1.77	82.914	2.171
Horizontal tail	1.738	81.336	2.177

Vertical Tail	1.745	81.681	2.175
Nacelle	3.29	159.265	1.982

10.3.3.a Component Form Factors (*FF*) and Interference Factors (*Q*)

Form factors for subsonic–drag estimation are presented in Eqn.s (10.15-10.17),

Wing, tail, strut :

$$FF = \left[1 + \frac{06}{(x/c)_m}(t/c) + 100(t/c)^4\right]\left[1.34M^{0.18}(\cos\Lambda_m)^{0.28}\right] \qquad (10.15)$$

Fuselage :

$$FF = 1 + \frac{60}{f^3} + \frac{f}{400} \qquad (10.16)$$

Nacelle :

$$FF = 1 + \left(\frac{0.35}{f}\right) \qquad (10.17)$$

where,

$$f = \frac{\ell}{d} = \frac{\ell}{\sqrt{(4/\pi)A_{max}}} \qquad (10.18)$$

i. Fuselage

From Eqn. (10.18),

$f = 12.18 / 2.13 = 5.718$

From Eqn. (10.16),

$$FF = 1 + \frac{60}{5.718^3} + \frac{5.718}{400} = 1.335$$

$Q_{fus} \cong 1.0$

ii. **Wing**

From Eqn. (10.15), where,

$(x/c)_m = 0.38$, $(t/c) = 0.165$, $\Lambda_m = 0°$ at $M = 0.137$

Here, "$(x/c)_m$" is the chordwise location of the airfoil maximum thickness point. Then,

$$FF = \left[1 + \frac{06}{(0.38)}(0.165) + 100(0.165)^4\right]\left[1.34(0.137)^{0.18}(\cos 0°)^{0.28}\right]$$

$FF = 1.25$

$Q_w \cong 1.0$

iii. **Horizontal Tail**

From Eqn. (10.15), where for the horizontal tail,

$(x/c)_m = 0.3$, $(t/c) = 0.1378$, $\Lambda_m = 13.31°$ at $M = 0.137$

Here, "Λ_m" refers to the sweep of the maximum-thickness line. Then,

$$FF = \left[1 + \frac{06}{(0.3)}(0.1378) + 100(0.1378)^4\right]\left[1.34(0.137)^{0.18}(\cos 13.31)^{0.28}\right]$$

$FF = 0.989$

Then for conventional tail, the interference factor can be taken as,

$Q_{HT} \cong 1.05$

iv. **Vertical Tail**

From Eqn. (10.15), where for the vertical tail,

$(x/c)_m = 0.3$, $(t/c) = 0.1378$, $\Lambda_m = 24.56°$ at $M = 0.137$

$$FF = \left[1 + \frac{06}{(0.3)}(0.1378) + 100(0.1378)^4\right]\left[1.34(0.137)^{0.18}(\cos 24.56)^{0.28}\right]$$

$FF = 0.970$

Then for conventional tail, the interference factor will be taken as,

$Q_{VT} \cong 1.05$

v. **Nacelle**

From Eqn. (10.18),

$$f = \frac{3.29}{4.34} = 0.758$$

Then, from Eqn. (10.17),

$$FF = 1 + \left(\frac{0.35}{0.758}\right) = 1.462$$

where, the interference factor for the nacelle is,

$Q_n \cong 1.0$

Now, the component parasite drag coefficients, $C_{Do})_c$, can be evaluated by use of Eqn. (10.19). The results of this calculation process are given in Table 10.2.

$$C_{Do})_c = \frac{\sum C_{fc} FF_c Q_c S_{wetc}}{S_{ref}} \qquad (10.19)$$

where,

$S_{ref} = 18.88 ft^2$

Table 10. 2 Table of component parasite drag coefficients at M = 0.137.

Components	$C_f \times 10^{-3}$	*Q*	*FF*	S_{wet} (ft^2)	S_{ref} (ft^2)	$C_{Do})_c \times 10^{-3}$
Fuselage	1.665	1.0	1.335	68.782	18.88	8.098
Wing	2.171	1.0	1.25	39.945	18.88	5.741
Horizontal T.	2.177	1.05	0.989	13.921	18.88	1.667
Vertical T.	2.175	1.05	0.970	5.631	18.88	0.661
Nacelle	1.982	1.0	1.462	44.857	18.88	6.885

Therefore, the total parasite component drag coefficients become,

$$\sum C_{Do})_c = (8.098 + 5.741 + 1.667 + 0.661 + 6.885) \times 10^{-3} = 0.0023$$

10.3.4 Miscellaneous Drags

The drag of miscellaneous items, e.g. unretractable landing gear, aft fuselage, canopy, etc., can be determined separately using a variety of empirical graphs and equations. The results then will be added to the parasite drag as given by Eqn. (10.12).

i. Drag due to upsweep of aft fuselage :

The extra drag that is created by the upsweep of the aft fuselage is a complicated function of the fuselage cross-sectional shape and the aircraft angle of attack. But it can be approximated using Eqn. (10.20). Here, "u" is the upsweep angle (in radians) of the fuselage *centerline* and A_{max} is the maximum cross-sectional area of the fuselage.

$$\frac{D}{q}\Big)_{upsweep} = 3.83u^{2.5}A_{\max} \qquad (10.20)$$

where, for the case of the design VTOL UAV,

$u = 10° = 0.1745\ rad$

Then, from Eqn. (10.20),

$$\frac{D}{q}\Big)_{upsweep} = 3.83(0.1745)^{2.5}(3.6) = 0.175$$

$$C_{Do})_{upsweep} = \frac{D/q}{S_{ref}} = \frac{0.175}{18.88} = 0.00927$$

ii. Base Drag :

The base area of an aircraft produces drag according to Eqn. (10.21) for the case of the *subsonic* aircraft. A_{base} includes any aft-facing flat surfaces see Figure 10.1.

$$\frac{D}{q} = \left[0.139 + 0.419(M - 0.161)^2\right] A_{base} \qquad (10.21)$$

where, A_{base} is estimated as,

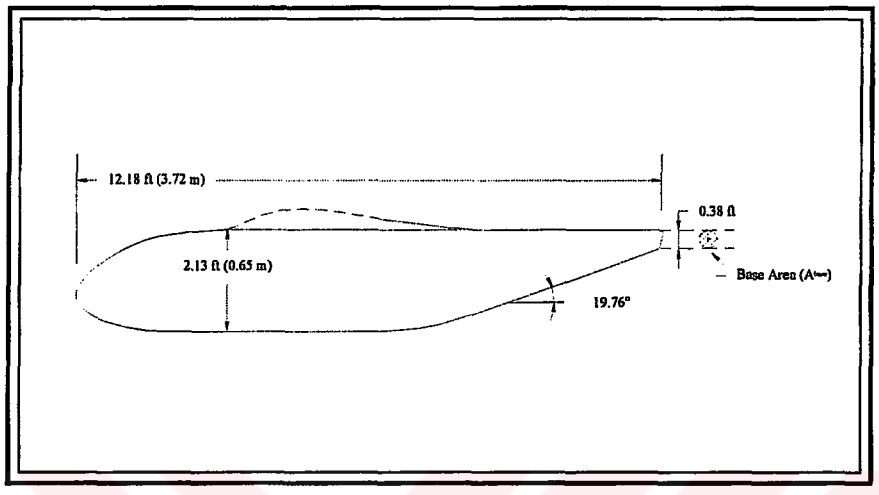

Figure 10. 1 The base area of theTilt-Duct VTOL UAV.

$$A_{base} \cong \frac{\pi(0.38)^2}{4} = 0.113 ft^2$$

$$\left.\frac{D}{q}\right)_{base} = \left[0.139 + 0.419(0.137 - 0.161)^2\right] \; 0.113 = 0.0157$$

$$C_{Do})_{base} = \frac{0.0157}{18.88} = 0.000833$$

The contributions of the other terms are relatively very small and can be ignored for the initial analysis. Then, the miscellaneous drag becomes,

$$C_{Dmisc} = 0.00927 + 0.000833 = 0.0101$$

Considering the contributions of other components (landing gears, canopy, etc.), C_{Dmisc} can be taken as ~ 0.02 for the sake of accuracy.

iii. Leakage and Protuberance Drag :

The effect of leakage and protuberance on C_{Do} is 5% of the total parasite drag,

$$C_{D_{L\&P}} = 0.05(0.0023 + 0.0101 + 0.02) = 0.00161$$

Then by use of Eqn. (10.12), the total parasite drag by component buildup method turns out to be,

$$C_{Do}\Big)_{\substack{clean \\ M=0.137}} = 0.0023 + 0.0101 + 0.02 + 0.000974 = 0.0334$$

➢ $$\boxed{C_{Do}\Big)_{\substack{clean \\ M=0.137}} = 0.0334}$$

10.4 Drag Due To Lift (Induced Drag)

The induced-drag coefficient at moderate angles of attack is proportional to the square of the lift coefficient by a ratio of a proportionality factor, K, which is called as "drag-due-to-lift factor", see Eqn.s (10.22-23). Since, the lift coefficient is a known parameter at the moment, the factor, K, will be evaluated.

$$C_D = C_{Do} + C_{Di} \qquad (10.22)$$

$$C_{Di} = KC_L^{\,2} \qquad (10.23)$$

Eqn. (10.24) will be utilized in order to evaluate K. This method depends on the oswald efficiency factor, e, which represents the extra drag due to the nonelliptical lift distribution and the flow separation. These effects in turn reduces the aspect ratio, producing the following equation for K.

$$K = \frac{1}{\pi . Ae} \qquad (10.24)$$

where, the oswald efficiency factor will be evaluated from Eqn. (10.25). This equation is valid for the straight-wing aircraft, i.e. no sweep.

$$e = 1.78\left(1 - 0.045A^{0.68}\right) - 0.64 \qquad (10.25)$$

Then

$$e = 1.78\left(1 - 0.045(7.2)^{0.68}\right) - 0.64 = 0.833$$

➢ $\boxed{e = 0.833}$

Then, from Eqn. (10.24), K, becomes,

$$K = \frac{1}{\pi.(7.2)0.833} = 0.0531$$

➢ $\boxed{C_{Di} = KC_L^2 = 0.0531C_L^2}$

10.5 Ground Effect

When a wing is near the ground, the drag-due-to-lift factor, K, can be reduced substantially. This is explained as a reduction in the induced downwash angle theoretically, but it can be visualized as a trapping of a "cushion of air" under the wing. This effect is accounted for by using a $K_{effective}$, defined by Eqn. (10.26).

$$K_{effective} = K\left(\frac{33(h/b)^{1.5}}{1+33(h/b)^{1.5}}\right) \qquad (10.26)$$

where h is the wing height above the ground. Then,

$$K_{effective} = (0.0531)\left(\frac{33(2.43/18.88)^{1.5}}{1+33(2.43/18.88)^{1.5}}\right) \cong 0.106$$

10.6 Results of Chapter 10

10.6.1 Tables

Table 10. 3 Some aerodynamic parameters calculated in Chapter 10.

Parameter	*Result*
$C_{L\alpha})_{TO}$ **(rad^{-1})**	3.247
$C_{L\alpha})_{clean}$ **(rad^{-1})**	3.218
$C_{L\alpha})_{Landing}$ **(rad^{-1})**	3.218
C_{Lmax}	1.305
α_{0L} **(deg.)**	-5
α_{CLmax} **(deg.)**	20.8
C_{Do} **(Ref. [1] method)**	0.033
C_{Do} **(Ref. [2] method)**	0.041
C_D **(clean)**	$0.041 + 0.0531 C_L^2$
C_D **(ground effect)**	$0.041 + 0.106\ C_L^2$

10.6.2 Figures

The C_L-α and drag polar curves are given in Figures 10.1 and 10.2.

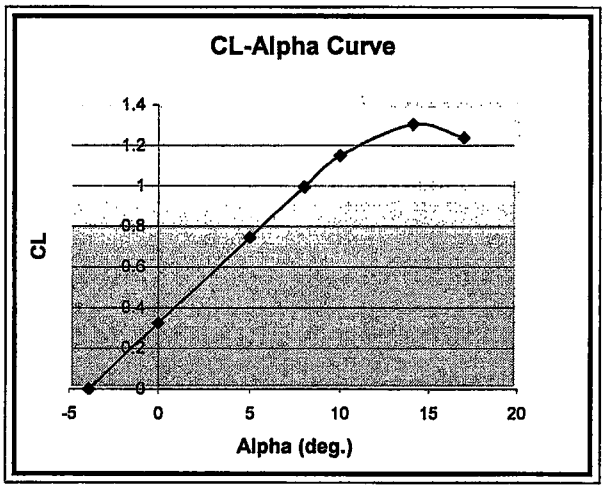

Figure 10. 2 C_L-α curve of the design UAV.

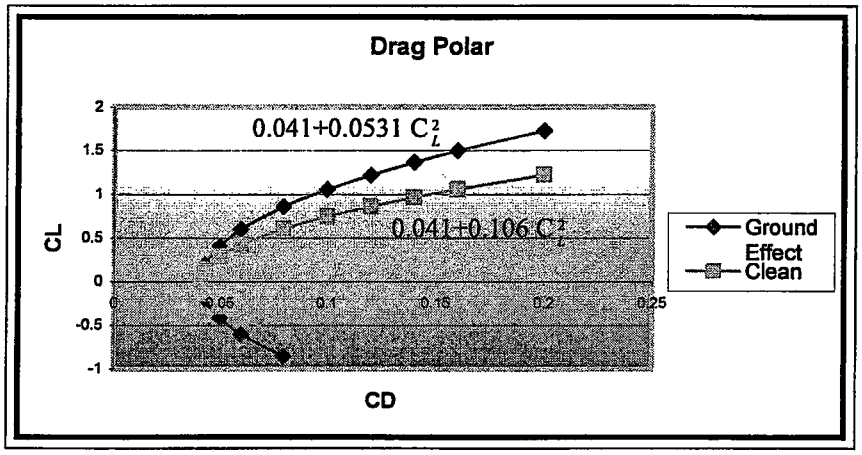

Figure 10. 3 Drag polar plot of the design UAV.

10.7 Conclusion

From the calculations, it is found that C_{Lmax} for landing is greater than C_{Lmax} for take-off. This is what is expected since for landing, to obtain maximum lift, the flaps are deployed over two times the take-off conditions. As a consequence, we should expect a total drag which is much greater than the total drag of take-off, as can be seen in the results. A smaller drag is desirable for take-off in terms of rapid acceleration and climb; while for landing, a larger drag will help the a/c to slow down faster.

A rough estimation of 'oswald span factor, "*e*", yielded a value of 0.833, where in the previous studies an assumed *e* of 0.8 was utilized. On the other hand, the calculations of C_{Do} yielded a value of 0.041 and 0.0334 according to two different methods taken from Ref. [1] and [2] respectively. In the previous calculations a C_{Do} value of 0.02 was assumed approximately. Recall that $C_D = C_{Do} + C_{Di}$, and induced drag C_{Di} is inversely proportional with '*e*'. since *e* increased, now a lower C_{Di} value is obtained than that was obtained before, by more approximate methods.

The next chapter illustrates the weights and balance calculations for the design UAV.

CHAPTER 11

WEIGHTS and BALANCE

11.1 Introduction

This chapter illustrates a roughly estimation of the a/c component weights and the c.g. location. Two approaches are available for this purpose: *Approximate Group Weights Method* and the *Statistical Group Weights Method*. The latter method is more refined than the first method based on approximations. The component weights, the location of the components and the corresponding moments with respect to the datum are tabulated at the end of each calculation procedure.

11.2 Approximate Group Weights Method

A statistical approach to the component weight estimations. It is based on historical values given in Table 15.2 of Ref. [1].

The components can be grouped under two types: *structural* and *propulsion* group.

11.2.1 Structural Group

For *General Aviation* type of a/c, which is the most closest type to the case of the design UAV than the other two choices available, i.e. fighters, transports and bombers.

i. Wing

$$_{w} \cong (2.5)S_{exposed} = (2.5)(18.88) = 47.42lb$$

$$X_{cg} / mac \cong 0.4$$

Note: Let's recall that $S_{exposed} = S_{ref} / cos(dihedral)$. In the case of the design UAV, dihedral is 0°.

ii. Horizontal Tail

$$_{HT} \cong (2.0)S_{exposed} = (2.0)\frac{S_{ref}}{\cos(Dihedral)} = (2.0)\frac{6.796}{\cos 0} = 13.592lb$$

$$X_{cg} / mac \cong 0.4$$

iii. Vertical Tail

$$_{VT} \cong (2.0)S_{exposed} = (2.0)\frac{S_{ref}}{\cos(Dihedral)} = (2.0)\frac{2.75}{\cos 0} = 5.5lb.$$

$$X_{cg} / mac \cong 0.4$$

iv. Fuselage

$$_{fuselage} \cong (1.4)S_{wet} = 1.4(68.782) = 96.3lb$$

$$X_{cg} = 0.45L_f$$

v. Landing Gear

$$_{nose} \cong (0.15)(0.057)W_O = (0.15)(0.057)(227) \cong 1.94lb$$

$$_{main} \cong (0.85)(0.057)W_O = (0.85)(0.057)(227) \cong 11lb$$

11.2.2 Propulsion Group

i. Installed Engine

$$_{ie} \cong 2(1.4)W_E = (2)1.4(16.54) = 46.3lb$$

ii. A/c "All-Else Empty" Weight

All-else empty weight refers to the weights of all the remaining items of the empty weight.

$$_{all-else,empty} \cong (0.1)W_O \cong (0.1)(227) \cong 22.7lb$$

$$X_{cg} \cong 0.45L_f$$

Then, the total aircraft weight will be a summation of these component weights. This will be a very rough approximation, since the historical data is valid for only three types of aircraft.

$$W_o = W_{wing} + W_{HT} + W_{VT} + W_{fuselage} + W_{nose} + W_{main} + W_{inst-eng} + W_{all-else,empty}$$

$$W_o = 47.2 + 13.592 + 5.5 + 96.3 + 1.94 + 11 + 46.3 + 22.7 = 175.93\ lb$$

As, indicated before this is a very rough estimation. As a comparison, the Initial Sizing method of Chapter 6 gave the takeoff weight of the design UAV as 227 lb.

11.3 Statistical Group Weights Method

This method yields a more refined estimate of the group weights. [1] Statistical equations based on sophisticated regression analysis are used for this purpose. Again, this method is valid for three types of aircraft, i.e. fighter, cargo/transport and general aviation. The relations given for the General Aviation type of aircraft will be used for the case of the design UAV. Hence, it is again obvious that, these results will not reflect the actual case, only a rough approximation it will be.

i. **Wing :**

$$_{w} = 0.036 S_{w}^{\ 0.758} W_{fw}^{\ 0.0035} \left(\frac{A}{\cos^2 \Lambda}\right)^{0.6} q^{0.006} \lambda^{0.04} \left(\frac{100t/c}{\cos\Lambda}\right)^{-0.3} \left(N_z W_{dg}\right)^{0.49} \qquad (10.11)$$

where, from Table 14.2 of Ref. [1], the limit load factors are given as follows for the General Aviation type of aircraft.

$n_{positive} = 3$

$n_{negaative} = -1.25$

Let, $W_{fw} = 10\ lb = Wing\ Fuel\ Weight$

$N_z = 1.5(3) = 4.5$

where, N_z is the "ultimate load factor", i.e. 1.5 times the limit load factor, n.

$\Lambda = 0°$

$\left(N_z W_{dg}\right) = 1021.5$

where, W_{dg} is the "Design Gross Weight" which is 227 *lb* for the design UAV.

The dynamic pressure at the cruising altitude,

$$q = \frac{1}{2}\rho V^2 = \frac{1}{2}(0.001953)(150)^2 = 21.97 sl/ft^3$$

Then, Eqn. (10.1) gives the following result,

$$_{wing} = 0.036(18.88)^{0.758}(10)^{0.0035}\left(\frac{6}{\cos^2 0°}\right)^{0.6}(21.97)^{0.006}(1)^{0.04}\left(\frac{100(0.165)}{\cos\Lambda}\right)^{-0.3}(1021.5)^{0.49}$$

➢ $\boxed{W_{wing} = 12.92 lb}$

ii. Horizontal Tail

For the horizontal tail the weight will be evaluated by use of Eqn. (11.2).

$$W_{HT} = 0.016(N_z W_{dg})^{0.414} q^{0.168} S_{ht}^{0.896} \left(\frac{100t/c}{\cos\Lambda_{ht}}\right)^{-0.12} \left(\frac{A}{\cos^2\Lambda_{ht}}\right)^{0.043} \lambda_{ht}^{-0.02} \qquad (11.2)$$

Then,

$$W_{HT} = 0.016(1021.5)^{0.414}(21.97)^{0.168}(6.796)^{0.896}\left(\frac{100(0.1378)}{\cos 17.69}\right)^{-0.12}\left(\frac{4}{\cos^2 17.69}\right)^{0.043}(0.5)^{-0.02}$$

➢ $W_{HT} = 2.068 lb$

iii. Vertical Tail

For the vertical tail the weight will be evaluated through Eqn. (11.3).

$$W_{VT} = 0.073\left(1+0.2\frac{H_t}{H_v}\right)(N_z W_{dg})^{0.376} q^{0.122} S_{vt}^{0.873} \left(\frac{100t/c}{\cos\Lambda_{vt}}\right)^{-0.49} \left(\frac{A}{\cos^2\Lambda_{vt}}\right)^{0.357} \lambda_{vt}^{0.039} \qquad (11.3)$$

Then,

$$W_{VT} = 0.073(1+0.2(0))(1021.5)^{0.376}(21.97)^{0.122}(2.75)^{0.873}$$
$$\times\left(\frac{100(0.1378)}{\cos 30}\right)^{-0.49}\left(\frac{1.6}{\cos^2 30}\right)^{0.357}(0.5)^{0.039}$$

➢ $W_{VT} = 1.146 lb$

iv. **Fuselage :**

The fuselage weight will be evaluated through Eqn. (11.4).

$$_{fuselage} = 0.052 S_f^{1.086} \left(N_z W_{dg}\right)^{0.177} L_t^{-0.051} \left(L/D\right)^{-0.072} q^{0.241} + W_{press} \qquad (11.4)$$

Then,

$$_{fuselage} = 0.052(68.782)^{1.086}(1021.5)^{0.177}(6.81)^{-0.051}(5.718)^{-0.072}(21.97)^{0.241}$$

➢ $\boxed{W_{fuselage} = 29.54 lb}$

v. **Main Landing Gear :**

The weight of the main landing gear will be evaluated through Eqn. (11.5).

$$_{\substack{main-landing \\ gear}} = 0.095(N_l W_l)^{0.768}(L_m/12)^{0.409} \qquad (11.5)$$

where, N_ℓ is the "Ultimate Load Factor, taken to be *5.70* from Ref. [3], $_\ell$ is the "Landing Design Gross Weight", *190 lb*, and L_m is the "Length of Main Landing Gear."

Then,

$$W_{\substack{main-landing \\ gear}} = 0.095(1083)^{0.768}(0.91(12)/12)^{0.409}$$

➢ $\boxed{W_{\substack{main-landing \\ gear}} = 19.5 lb}$

vi. **Nose landing gear**

The weight of the nose landing gear will be evaluated through Eqn. (11.6).

$$W_{\substack{nose-landing \\ gear}} = 0.125(N_l W_l)^{0.566}(L_n/12)^{0.845} \quad (11.6)$$

$$W_{\substack{nose-landing \\ gear}} = 0.125(1083)^{0.566}(0.68)^{0.845}$$

➢ $$\boxed{W_{\substack{nose-landing \\ gear}} = 4.71lb}$$

vii. **Installed Engine (Main) :**

The weight of the installed main engines will be evaluated through Eqn. (11.7).

$$W_{\substack{installed\ engine \\ (main)}} = 2.575W_{en}^{0.922}N_{en} \quad (11.7)$$

Then,

$$W_{\substack{installed\ engine \\ (main)}} = 2.575(16.54)^{0.922}(2)$$

This result gives the total weight of the two main engines, since it includes the number of engines as a factor in the equation.

➢ $$\boxed{W_{\substack{installed\ engine \\ (total,main)}} = 68.44lb}$$

viii. **Installed Engine (Aft) :**

The weight of the installed aft engine will be evaluated through Eqn. (11.7). Then,

$$W_{\substack{installed\ engine\\(aft)}} = 2.575(8.82)^{0.922}(1)$$

➢ $$\boxed{W_{\substack{installed\ engine\\(aft)}} = 19.16lb}$$

Then the total weight of the main and the aft engines become,

$$W_{\substack{installed\ engine\\(total)}} = 68.44 + 19.16 = 87.6lb$$

ix. Fuel System :

The approximate weight of the fuel system will be evaluated through Eqn. (11.8).

$$W_{\substack{fuel\\system}} = 2.49 W_t^{0.726}\left(\frac{1}{1+V_i/V_t}\right)^{0.363} N_t^{0.242} N_{en}^{0.157} \qquad (11.8)$$

Then,

$$W_{\substack{fuel\\system}} = 2.49(7.5)^{0.726}\left(\frac{1}{1+0}\right)^{0.363}(2)^{0.242}(2)^{0.157}$$

➢ $$\boxed{W_{\substack{fuel\\system}} = 14.2lb}$$

x. Flight Controls :

The approximate weight of the flight control system will be evaluated through Eqn. (11.9).

$$W_{\substack{flight\\controls}} = 0.053 L^{1.536} B_w^{0.371}\left(N_z W_{dg} \times 10^{-4}\right)^{0.80} \qquad (11.9)$$

Then,

$$W_{\substack{flight\\controls}} = 0.053(12.18)^{1.536}(10.64)^{0.371}\left(1021.5\times10^{-4}\right)^{0.80}$$

➢ $$\boxed{W_{\substack{flight\\controls}} = 0.955lb}$$

xi. **Hydraulics :**

The approximate weight of the hydraulics will be evaluated through Eqn. (11.10).

$$W_{hydraulics} = 0.001W_{dg} \qquad (11.10)$$

Then,

$$W_{hydraulics} = 0.001(227)$$

➢ $$\boxed{W_{hydraulics} = 0.227lb}$$

At this stage, the total aircraft empty weight can be calculated as the summation of the weights of each component evaluated above. Then,

$$W_{empty} = \sum W_i = 172.87lb. \quad \text{(for all metal aircraft)}$$

$$W_{empty} = \sum W_i = (0.85)(172.87) = 147lb \quad \text{(for composite-structured aircraft)}$$

This value, 172.87 *lb*, found of empty weight is multiplied by a "fudge factor" of 0.85 in order to have a better estimate for the design UAV in which composite structures will be widely used. This gives an empty weight of *147 lb* which is close to the value, 151.5 *lb*, estimated in Chapter 3.

11.4 C.G. Location

In this section, the aircraft center of gravity will be evaluated. For this purpose The corresponding c.g. locations will be calculated with respect to a/c nose, which is selected to be the datum.

In order to evaluate the location of the center of gravity, first, a chart is drawn out in order to locate the component center of gravities and weights, see Table 11.1 and Figure 11.1.

Table 11. 1 The component weights and cg locations of the design UAV.

Components	*Weight (lb)*	*Location (X_{cg}/mac)*
Wing	12.92	2.703
Horizontal Tail	2.068	6.144
Vertical Tail	1.146	6.587
Fuselage	29.54	3.253
Main Landing Gear	19.5	3.486
Nose Landing Gear	4.71	1.056
Main Engines	68.44	2.491
Aft Engine	19.16	4.83
Camera	17.64	0
Aircraft estimated cg location	227	2.78

This corresponds to distance of 4.93 ft from the nose which was taken as a datum in these calculations.

➢ $X_{cg} = 4.93$ ft

The component and the aircraft cg locations and corresponding weights are shown in Figure 11.1.

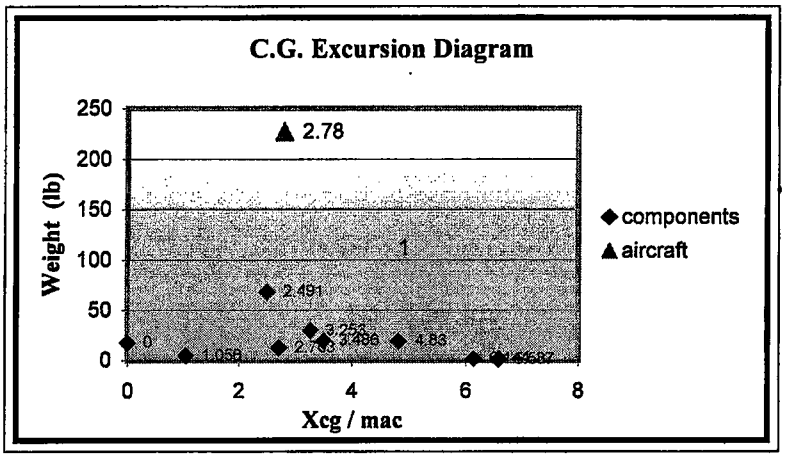

Figure 11. 1 C.G. Excursion Diagram of the design UAV.

11.5 Conclusion

In this chapter, first the component weights of the a/c are estimated through two methods from Ref. [1] which are *Approximate Group Weights Method* and *Statistical Group Weights Method*, respectively.

Also, the a/c empty weight found by the approximation method yields a value of approximately 176 *lb*, while the statistical method yields a value of 173 *lb*. These are very close values to each other, but still they are higher than the calculated value, 151.5 *lb*, in Chapter 3. This is something expected, since these calculations are done for a general aviation type of aircraft. It can be concluded that having a more simplified structure, the design UAV will end up with a smaller empty weight than the ones calculated by these approximate methods.

An approximation for the aircraft cg location is also performed in section 11.4. For this purpose, the structural component weights evaluated in this chapter are used. As a result, the cg location of the design UAV turned out to be around 4.93 ft. This result will be checked out in the proceeding chapter, i.e. Stability and Control.

CHAPTER 12

STABILITY and CONTROL

12.1 Introduction

Stability of an aircraft refers to the tendency of an aircraft under steady conditions to return to a trimmed condition when disturbed instead of undergoing any other motion after the disturbance. For this purpose, in this chapter, the forces and moments will be examined in order to determine if they are in the direction to force the design UAV back to its equilibrium flight conditions. If so, the aircraft will be statically stable.

As a part of this chapter, the longitudinal and lateral stability characteristics of the mission a/c are examined. The neutral point, static margin, the longitudinal and lateral moment coefficients are determined. These parameters will then lead to a conclusion if the design UAV is statically stable or not.

12.2 Coordinate Systems and Definitions

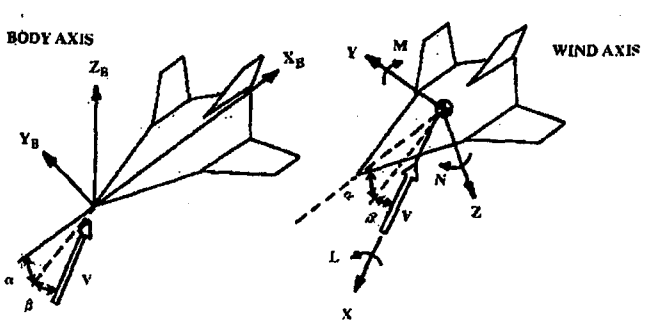

Figure 12. 1 Aircraft coordinate system. [1]

There are two axis systems commonly used in aircraft analysis, see Figure 12.1. The "body-axis system" is rigidly fixed to the aircraft, with the X-axis aligned with the fuselage and the Z-axis upward, and it moves with the aircraft. The origin is at an arbitrary location, usually the nose.

The "wind-axis system" orients the X-axis into the relative wind regardless of the aircraft's angle of attack, α, or sideslip, β. The aircraft is not fixed to the axis system, so the axis projections of various lengths, e.g. L_{HT}, L_{VT}, will vary for different angles of attack or sideslip.

The "stability axis system" commonly used in stability and control analysis, is somehow between these two. The X-axis is aligned at the aircraft angle of attack, as in the wind axis system, but is not offset to the yaw angle. Directions of X, Y and Z are as in the wind-axis system.

12.3 Longitudinal Stability And Control Analysis

An aircraft is in trim if all of the forces, aerodynamic and gravitational, and aerodynamic moments acting on the aircraft about the cg are in balance.

12.3.1 Estimation of Neutral Point

Neutral point is a location for aircraft cg about which the moment is constant, independent of the angle of attack. The location of the neutral point will be evaluated according to the method given in Ref. [1] as follows. The relation for the neutral point location is given in Eqn. (12.1).

$$\overline{X}_{np} = \frac{C_{L\alpha}\overline{X}_{acw} - C_{m\alpha_{fus}} + \eta_h \frac{S_h}{S_w} C_{L\alpha_h} \frac{\partial \alpha_h}{\partial \alpha} \overline{X}_{ach} + \frac{F_{p\alpha}}{qS_w} \frac{\partial \alpha_p}{\partial \alpha} \overline{X}_p}{C_{L\alpha} + \eta_h \frac{S_h}{S_w} C_{L\alpha_h} \frac{\partial \alpha_h}{\partial \alpha} + \frac{F_{p\alpha}}{qS_w}} \qquad (12.1)$$

where, the following parameters are taken from AAA (Advanced Aircraft Analysis) Program, Ref. [3], as a result of running the program for the characteristics of the design UAV, see Table 12.1.

Table 12. 1 Some AAA data for the design UAV, in order to solve Eqn. (12.1).

Parameter	***Value***
X_{ac_w}	4.36 ft
X_{ac_h}	11.32 ft
α_0	-3.9°
C_{L_w}	4.591
$C_{L_{wh}}$	3.5982

Now, the parameters in Eqn. (12.1), will be evaluated as follows,

i. $\overline{X}_{ac_w} = \dfrac{X_{ac_w}}{\bar{c}} = \dfrac{4.36ft}{1.77ft} = 2.463$

ii. By use of Eqn. (12.2), the second parameter, $C_{m\alpha_{fus}}$, in Eqn. (12.1) will be evaluated as follows,

$$C_{m\alpha_{fus}} = \frac{K_f W_f^2 L_f}{cS_w} \qquad (12.2)$$

where, K_f the empirical pitching moment factor is obtained from Figure 16.14 of Ref. [1] as, $K_f \cong 0.014$. The W_f is the maximum width of the fuselage, i.e. 2.13 *ft*, and L_f is the length of the fuselage, i.e. 12.18 *ft*. Then, Eqn. (12.2) becomes,

$$C_{m\alpha_{fus}} = \frac{0.014(2.13)^2(12.18)}{1.77(18.88)} = 0.02315 rad^{-1}$$

iii. $\eta_h = \dfrac{q_h}{q}$

where, q_h is the dynamic pressure of horizontal tail, and q is the freestream dynamic pressure. In Ref. [1], a range of (0.85-0.95) is given for η_h. An average value of 0.90 will be taken for this case.

iv. $\dfrac{S_h}{S_w} = \dfrac{6.796}{18.88} = 0.3602$

v. From, Figure 12.2,

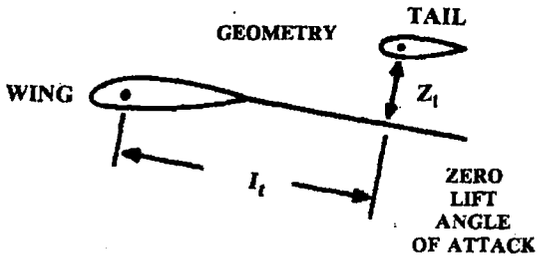

Figure 12. 2 Downwash estimation. [1]

$$\ell_t = \frac{6.9ft}{\cos 4.71°} = 6.923ft$$

$$z_t = 0.56 + 6.9\tan 4.71° = 1.128ft$$

Then, from Figure 16.12 of Ref. [1],

$$m = \frac{z_t}{b/2} = \frac{1.128}{10.64/2} = 0.212$$

$$r = \frac{\ell_t}{b/2} = \frac{6.923}{10.64/2} = 1.301$$

Then, corresponding to these values of m and r, from the same figure,

$$\frac{\partial \varepsilon}{\partial \alpha} \cong 0.3$$

Then,

$$\frac{\partial \alpha_h}{\partial \alpha} = 1 - \frac{\partial \varepsilon}{\partial \alpha} = 1 - 0.3 = 0.7$$

vi. $$\overline{X}_{ac_h} = \frac{X_{ac_h}}{\bar{c}} = \frac{11.32ft}{1.77ft} = 6.395$$

vii. It is common to neglect the F_p term in Eqn. (12.1). This term is generally used to determine the power–off stability. Here, this term will be neglected.

Then, Eqn. (12.1) becomes,

$$\overline{X}_{np} = \frac{4.591(2.463) - 0.02315 + (0.9)(0.3602)(3.5982)(0.7)(6.395)}{4.591 + (0.9)(0.3602)(3.5982)(0.7)} = 3.052$$

$$X_{np} = \overline{X}_{np}\,\bar{c} = (3.052)(1.77) = 5.403\,ft$$

$\boxed{X_{np} = 5.403\ ft}$ (Ref. [1])

As mentioned before, this result is obtained by use of the methods of Ref. [1]. On the other hand, Ref. [3] is also used to obtain the location of the neutral point. It gives a result as,

$\boxed{X_{np} = 5.37\ ft}$ (Ref. [3])

These results will be tabulated at the end of this chapter, under the section heading of "Results of Chapter 12."

12.3.2 Estimation of aircraft Most Forward CG Location

In this section, the cg location of the design UAV will be evaluated according to the "takeoff rotation criteria." For this purpose the pitch moment coefficient is derived with respect to the main landing gear, see Eqn. (12.3)

$$C_{mlg} = C_L\left(\overline{X}_{mlg} - \overline{X}_{acw}\right) + C_{mw} + C_{m_{fus}} + \eta_h \frac{S_h}{S_w} C_{Lh}\left(\overline{X}_{ach} - \overline{X}_{mlg}\right)$$

$$- \frac{T}{qS_w}\overline{Z}_t - \frac{W_{TO}}{qS_w}\left(\overline{X}_{mlg} - \overline{X}_{cg}\right) \qquad (12.3)$$

where, the following parameters are taken from AAA (Advanced Aircraft Analysis) Program, Ref. [3], for the characteristics of the design UAV, see Table 12.2. The common variables that are being used in both Eqn. (12.1) and Eqn. (12.3) exists in Table 12.1. hence will not be repeated here, in Table 12.2.

Table 12. 2 Some AAA data for the design UAV, for the solution of Eqn. (12.3).

Parameter	***Value***
X_{mlg}	6.17 ft
Z_t	2.52 ft
$C_{L_{\delta e}}$	0.9744
$\partial\varepsilon_h/\partial\alpha$	0.3431

Now, the parameters in Eqn. (12.3), will be evaluated as follows,

i. Aircraft lift coefficient, C_L, will be represented in terms of aircraft angle of attack, α, by use of Eqn. (12.4).

$$C_L = C_{L\alpha}(\alpha + i_w - \alpha_{0L}) \qquad (12.4)$$

where,

$\alpha_{0L} = -3.9° = -0.0681 rad$

$i_w = 0.0$

Then, by use of Table 12.2, for the rest of unknowns, Eqn. (12.4) becomes,

$$\boxed{C_L = 4.591\alpha + 0.3126}$$

ii. The next term that will be evaluated is C_{m_w}. By use of the method defined in Ref. [1], it will be evaluated by use of Eqn. (12.5).

$$C_{mw} = C_{mo_{airfoil}}\left(\frac{A\cos^2\Lambda}{A + 2\cos\Lambda}\right) \qquad (12.5)$$

From the performance graphs of the Eppler E-583 airfoil, see Figure 4.3,

$$C_{mo_{airfoil}} = -0.115$$

Then, Eqn. (12.5) becomes,

$$C_{m_w} = -0.115\left(\frac{6}{6+2}\right) = -0.0862$$

iii. $C_{m_{fus}}$ will be evaluated at this step. This is the third term in Eqn. (12.3). For this purpose the following relation from Ref. [1], given by Eqn. (12.6), will be used.

$$C_{m_{fus}} \cong C_{m\alpha_{fus}}\alpha \qquad (12.6)$$

Since, $C_{m\alpha_{fus}}$ was evaluated in section 12.3.1.*ii*, Eqn. (12.6) becomes,

$$\boxed{C_{m_{fus}} = 0.02315\alpha}$$

iv. C_{L_h} will be evaluated at this step. The methods given in Ref. [1] will be utilized for this purpose, see Eqn.s (12.7-8),.

$$C_{L_h} = C_{L_{\alpha h}}(\alpha + i_w)\left[1 - \frac{\partial\varepsilon_h}{\partial\alpha} + (i_h - i_w) - \alpha_{oL_h}\right] \qquad (12.7)$$

$$\Delta\alpha_{oL_h} = -\frac{1}{C_{L_{\alpha h}}}\frac{\partial C_L}{\partial\delta_e}\delta_e \qquad (12.8)$$

where, i_w and i_h are zero for the design UAV. Then, by use of Table 12.2 and Eqn. (12.8),

$$\Delta\alpha_{oL_h} = -\frac{1}{3.5982}(0.9744)\delta_e = -0.271\delta_e$$

Then, Eqn. (12.7) becomes,

$$C_{L_h} = 3.5982\alpha(1 - 0.3431 + 0.271\delta_e)$$

$$C_{L_h} = (2.3636 + 0.975\delta_e)\alpha$$

v. The dynamic pressure ratio, will be evaluated as follows,

$$q = \frac{1}{2}\rho V^2 = \frac{1}{2}(0.001953)(150)^2 = 21.971 lb/ft^2$$

Now, Eqn. (12.3) will be evaluated by use of Table 12.1, 12.2 and the parameters evaluated above.

$$C_{m_{mlg}} = (4.591\alpha + 0.3126)\left(\frac{6.17+4.36}{1.77}\right) - 0.0862 + 0.02315\alpha$$

$$+ (0.9)\left(\frac{6.796}{18.88}\right)(2.3636 + 0.975\delta_e)\alpha\left(\frac{11.32-6.17}{1.77}\right) - \frac{(141.6\times 2)}{27.91(18.88)}\left(\frac{2.52}{1.77}\right)$$

$$- \frac{226}{27.91(18.88)}\left(\frac{6.17 - X_{cg}}{1.77}\right)$$

$$\boxed{C_{m_{mlg}} = (6.9458 + 0.9192\delta_e)\alpha + (0.2418)X_{cg} - 2.022} \qquad (12.9)$$

Eqn. (12.9) gives a most forward cg location of 4.35 ft for $\alpha = 8°$ and $\delta_e = 0°$. This is our cruise condition. The actual position of aircraft cg is given by AAA program as 5.00 ft. This value is also close to the value, i.e. 4.93 *ft*, of cg location which was calculated in section 11.4.

$\boxed{X_{cg} = 5.00 ft}$ (by methods of Ref. [3])

12.3.3 Static Margin

The distance between the cg and neutral point locations in percentage of mean aerodynamic chord is called as the "static margin." It will be denoted as *SM*.

$$SM = \overline{X}_{np} - \overline{X}_{cg} = \left(\frac{5.37-5.00}{1.77}\right) = 0.209 = 20.9\%$$

$\boxed{SM = 20.9\%}$ (Ref. [1])

$\boxed{SM = 20.8\%}$ (Ref. [3])

A positive static margin yields a negative pitching-moment derivative, see Eqn. (12.10) which means that the aircraft is stable.

$$C_{m_\alpha} = -C_{L_\alpha}\left(\overline{X}_{np} - \overline{X}_{cg}\right) \qquad (12.10)$$

Then, by use of Table 12.1 and Eqn. (12.10) C_{m_α} will be evaluated as follows,

$$C_{m_\alpha} = -4.591(0.209) = -0.959 rad^{-1}$$

$$\boxed{C_{m_\alpha} = -0.959 rad^{-1}} \qquad \text{(Ref. [1])}$$

$$\boxed{C_{m_\alpha} = -0.954 rad^{-1}} \qquad \text{(Ref. [3])}$$

These close results indicate that the design UAV is stable during the forward flight mode.

12.4 Lateral-Directional Stability and Control Analysis

Lateral directional analysis resembles to the longitudinal analysis in many ways. The only difference comes from that lateral-directional analysis is based on two closely-coupled analyses: the yaw (directional) and the roll (lateral).

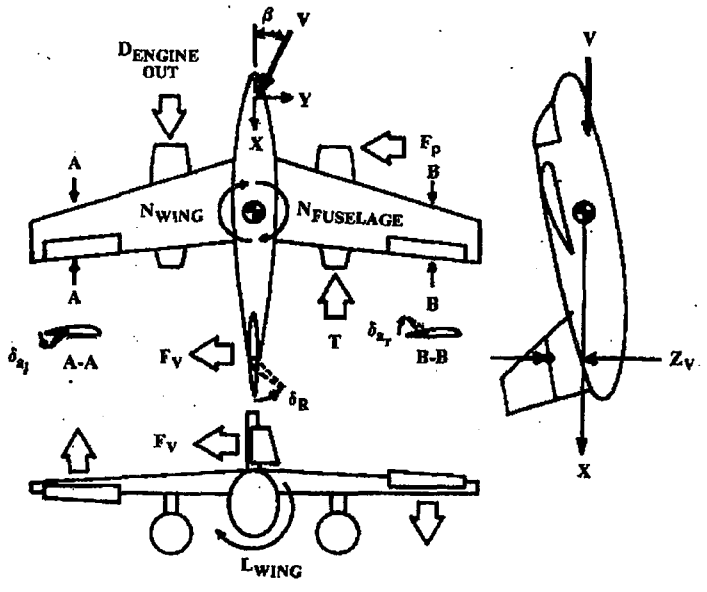

Figure 12. 3 Lateral geometry. [1]

The geometry for lateral analysis is illustrated in Figure 12.3. In this figure, the major contributions to the yawing moment, N, and rolling moment L are shown. By definition, yaw and roll are positive to the right. In longitudinal stability a negative moment derivative was required. In this case, a positive value of yawing moment derivative with respect to β is stabilizing. This is because, the yawing moment is opposite in direction to the angle β.

$$C_{n_\beta} > 0 \qquad (12.11)$$

On the other hand, a negative value of the rolling moment derivative with respect to β is stabilizing (dihedral effect).

$$C_{\ell_\beta} < 0 \qquad (12.12)$$

12.4.1 Static Directional Stability Analysis

The yawing moment derivative with respect to sideslip is provided in Eqn. (12.13). The power-off C_{n_β} is simply the sum of the wing, fuselage and vertical tail contributions.

$$C_{n_\beta} = C_{n_{\beta_W}} + C_{n_{\beta\,fus}} + C_{n_{\beta_v}} - \frac{F_{p_\beta}}{qS_w}\frac{\partial \beta_p}{\partial \beta}\left(\overline{X}_{cg} - \overline{X}_p\right) \qquad (12.13)$$

The terms in Eqn. (12.13) will be evaluated as follows.

12.4.1.a Wing Directional Derivative

An empirical formulation for the wing yawing moment coefficient due to sideslip is provided in Eqn. (12.14).

$$C_{n_{\beta_W}} = C_L^2\left\{\frac{1}{4\pi A} - \left[\frac{\tan\Lambda}{\pi A(A+4\cos\Lambda)}\right]\left[\cos\Lambda - \frac{A}{2} - \frac{A^2}{8\cos\Lambda} + \frac{6\left(\overline{X}_{acw} - \overline{X}_{cg}\right)\sin\Lambda}{A}\right]\right\} \qquad (12.14)$$

In Eqn. (12.14), since, the wing has no sweep, $tan\Lambda$ term turns out to be zero. This makes the whole terms in cornered brackets as zero. Then, Eqn. (12.14) becomes,

$$C_{n_{\beta_w}} = 1.305\left\{\frac{1}{4\pi 7.2} - 0\right\} = 0.0144 rad^{-1}$$

12.4.1.b Fuselage Directional Derivative

The yawing moment due to sideslip is expressed in Eqn. (12.15) as a function of the fuselage volume, depth, and width.

$$C_{n_{\beta_{fus}}} = -1.3\frac{Vol}{S_w b}\left(\frac{D_f}{W_f}\right) \qquad (12.15)$$

The contribution of fuselage to roll is generally negligible except its influence upon the wing effective dihedral. Then, Eqn. (12.15) becomes,

$$C_{n_{\beta_{fus}}} = -1.3\frac{28.50}{18.88(10.64)}\left(\frac{2.13}{2.13}\right) = -0.1844 rad^{-1}$$

12.4.1.c Vertical Tail Directional Derivative

Some empirical formulations for the vertical tail yawing moment coefficient due to sideslip are provided in Eqn.s (12.16-17).

$$C_{n_{\beta_v}} = C_{F_{\beta_v}}\frac{\partial\beta_v}{\partial\beta}\eta_v\frac{S_v}{S_w}\left(\overline{X}_{acv} - \overline{X}_{cg}\right) \qquad (12.16)$$

where,

$$\left(\frac{\partial\beta_v}{\partial\beta}\eta_v\right) = 0.724 + \frac{3.06\frac{S'_{vs}}{S_w}}{1+\cos\Lambda} - 0.4\frac{Z_{wf}}{D_f} + 0.009A_w \qquad (12.17)$$

where, S'_{vs} is the area of the vertical tail extended to the fuselage centerline, Z_{wf} is the vertical height of the wing above the fuselage centerline, D_f an W_f are the depth and width of the fuselage. Then, Eqn. (12.17) and (12.16) will be solved as follows, respectively.

$$\left(\frac{\partial\beta_v}{\partial\beta}\eta_v\right)=0.724+\frac{3.06\frac{3.40}{18.88}}{1+1}-0.4\frac{2.43}{2.13}+0.009(7.2)=0.608$$

Then,

$$C_{n_{\beta_v}}=(2.8245)(0.608)\left(\frac{2.75}{18.88}\right)\left(\frac{11.32-5.00}{1.77}\right)=0.892\,rad^{-1}$$

Now, Eqn. (12.13) can be used in order to evaluate C_{n_β},

$$C_{n_\beta}=0.0144-0.1844+0.892=0.722\,rad^{-1}$$

$$\boxed{C_{n_\beta}=0.722\,rad^{-1}}$$

Recall that, the criterion for the directional static stability, given by Eqn. (12.11), requires a positive value of the yawing moment derivative with respect to β. Hence, the calculated value, 0.722 rad^{1}, of C_{n_β} the design UAV satisfies the directional static stability requirement.

12.4.2 Static Lateral Stability Analysis

The rolling moment derivative with respect to sideslip is provided in Eqn. (12.18). The power-off C_{ℓ_β} is simply the sum of the wing, and vertical tail contributions.

$$C_{\ell_\beta}=C_{\ell_{\beta_W}}+C_{\ell_{\beta_v}} \qquad (12.18)$$

The terms in Eqn. (12.18) will be evaluated as follows.

12.4.2.a Wing Lateral Derivative

An empirical formulation for the wing rolling moment coefficient due to sideslip is provided in Eqn. (12.19).

$$C_{\ell_{\beta_w}} = \left(\frac{C_{\ell_{\beta_w}}}{C_L}\right) C_L + \left(C_{\ell_\beta}\right)_\Gamma + C_{\ell_{\beta_{wf}}} \qquad (12.19)$$

where,

$$C_{\ell_{\beta_{wf}}} = -1.2\frac{\sqrt{A}Z_{wf}(D_f + W_f)}{b^2} \qquad (12.20)$$

where, Z_{wf} is the vertical height of the wing above the fuselage centerline, D_f an W_f are the depth and width of the fuselage. Since, the term $\left(C_{\ell_\beta}\right)_\Gamma$ represents the dihedral effect, it turns out to be zero since there is no dihedral for the design UAV. Then, Eqn. (12.20) becomes,

$$C_{\ell_{\beta_{wf}}} = -1.2\frac{\sqrt{7.2}(2.43)(2.13+2.13)}{10.64^2} = -0.1233 rad^{-1}$$

From Figure 16.21 of Ref. [1], for $A = 7.2$, $\lambda = 1.0$, $\Lambda_{c/4} = 0°$,

$$\left(\frac{C_{\ell_{\beta_w}}}{C_L}\right) \cong -0.03$$

Then, Eqn. (12.19) becomes,

$$C_{\ell_{\beta_w}} = (-0.03)1.305 + 0 - 0.1473 = -0.1864$$

12.4.2.b Vertical Tail Lateral Derivative

The vertical tail rolling moment coefficient due to sideslip is provided in Eqn. (12.21).

$$C_{\ell_{\beta_v}} = -C_{F_{\beta_v}} \frac{\partial \beta_v}{\partial \beta} \eta_v \frac{S_v}{S_w} \overline{Z}_v \qquad (12.21)$$

where, the ratio of $\partial \beta_v / \partial \beta$ was defined by Eqn. (12.17) and evaluated as 0.608. Then,

$$C_{\ell_{\beta_v}} = -(2.8245)(0.608)\left(\frac{2.75}{18.88}\right)\left(\frac{1.59}{1.77}\right) = -0.2247 rad^{-1}$$

Now, Eqn. (12.18) can be used in order to evaluate C_{ℓ_β},

$$C_{\ell_\beta} = -0.2247 - 0.1864 = -0.411 rad^{-1}$$

$$\boxed{C_{\ell_\beta} = -0.411 rad^{-1}}$$

This result, -0.411 rad^{-1}, of C_{ℓ_β} indicates that the design UAV satisfies the lateral static stability criterion. Recall that, for the lateral static stability a negative rolling moment derivative with respect to β is required, see Eqn. (12.12).

12.4.3 Crosswind-Landing Analysis

Another trim condition which should be checked is the crosswind-landing case. The aircraft must be able to operate in crosswinds equal to 20% of takeoff speed, which is eqivalent to holding an 11.50° sideslip at takeoff speed. The vertical tail should provide sufficient force to produce zero yawing moment in Eqn. (12.22) for this case. The requirement is such that, no more than 20° of rudder should be used.

$$C_n = C_{n_{\beta_w}}\beta + C_{n_{\delta_a}}\delta_a + C_{n_{\beta_{fus}}}\beta + C_{n_{\beta_v}}\beta - \frac{T}{qS_w}\overline{Y}_p - \frac{D}{qS_w}\overline{Y}_p - \frac{F_p}{qS_w}\left(\overline{X}_{cg} - \overline{X}_p\right) \qquad (12.22)$$

The terms in Eqn. (12.21) will be evaluated as follows.

i. Drag (*D*)

The drag force created by the crosswind at a speed of 20% of takeoff speed is given by Eqn. (12.23).

$$D = \frac{1}{2}\rho V_{cw}^2 S_w \left(C_{D_0} + \frac{1}{\pi A e}C_L^2\right) \qquad (12.23)$$

The takeoff speed will be assumed as about 10 m/s, which corresponds to 32.81 ft/s. Then the crosswind speed becomes,

$$V_{cw} = (0.2)V_{TO} = 0.2(32.81) = 6.562 ft/s$$

Then, Eqn. (12.23) gives a drag value as the followings,

$$D = \frac{1}{2}(0.00238)(6.562)^2(18.88)\left(0.041 + \frac{1}{\pi(7.2)(0.833)}(1.305)^2\right) = 0.127 lb$$

ii. Yawing Moment Due to Aileron Deflection, $C_{n_{\delta_a}}$

Yawing moment due to aileron deflection can be approximated by Eqn. (12.24). It depends upon the spanwise distribution of induced drag with the aileron deflected. This varies with the wing-lift coefficient as well as the aileron deflection.

$$C_{n_{\delta_a}} = -0.2 C_L C_{l_{\delta_a}} \qquad (12.24)$$

where,

$$C_{l_{\delta_a}} = \frac{2\sum K_f \left(\frac{\partial C_L}{\partial \delta_f}\right) Y_i S_i \cos\Lambda_{H.L.}}{S_w . b} \qquad (12.25)$$

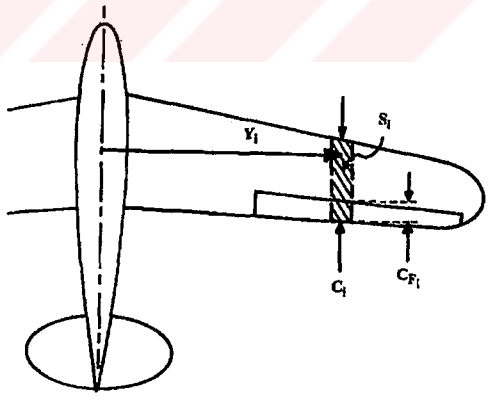

Figure 12. 4 Aileron strip geometry. [1]

In Eqn. (12.25) a strip method is used in order to approximate the aileron control power. The portion of the wing having the aileron is broken into strips as shown in Figure 12.4. Here, the lift increment due to aileron deflection is estimated as a flap effect using the method presented in Eqn. (12.26).

$$\frac{\partial C_L}{\partial \delta_a} = (0.9) K_f \left(\frac{\partial C_l}{\partial \delta_a} \right) \frac{S_a}{S_{ref}} \cos \Lambda_{H.L.} \qquad (12.26)$$

This lift increment is then multiplied by the strip's moment arm from the aircraft centerline, Y_b, as given in Eqn. (12.25), where K_f and the lift derivative with aileron deflection come from Figs. 16.6 and 16.7 of Ref. [1]. Then, for $c_f / c = 0.25$,

$$\left(\frac{\partial C_l}{\partial \delta_a} \right) \cong 4.3 \quad \text{and} \quad K_f \cong 1.0$$

Then, Eqn. (12.26) becomes,

$$\frac{\partial C_L}{\partial \delta_a} = (0.9)(4.3) \frac{8.089}{18.88} \cos 0° = 1.658 \ rad^{-1}$$

Then, from Eqn. (12.25),

$$C_{l_{\delta_a}} = \frac{2(1.658)(3.80)(8.089)\cos 0°}{(18.88)(10.64)} = 0.5074 \ rad^{-1}$$

The yawing derivative due to aileron deflection is evaluated from Eqn. (12.24) as,

$$C_{n_{\delta_a}} = -0.2(1.305)(0.5074) = -0.1324 rad^{-1}$$

Now, Eqn. (12.22) will be used to evaluate C_n. Let's recall that, $C_{n_{\beta_w}}$, $C_{n_{\beta_{fus}}}$ and $C_{n_{\beta_v}}$ were evaluated in sections 12.4.1.a, b and c, respectively. Then,

$$C_n = (0.0144)\beta - (0.1324)\delta_a - (0.1844)\beta + (0.892)\beta - \frac{0.127}{(0.0512)18.88}\left(\frac{7.55}{10.64} \right)$$

Then,

$$\boxed{C_n = 0.722\beta - 0.1324\delta_a - 0.0932} \qquad (12.27)$$

In order to check if sufficient force is obtained to produce zero yawing moment, Eqn. (12.27) will be set to zero and the necessary requirement will be found by this way.

Recalling that the 'crosswind' case corresponds to a sideslip of 11.5°, Eqn. (12.27) becomes,

$$\boxed{0 = 0.722(11.5)(\pi/180) - 0.1324\delta_a - 0.0932}$$

Then, the required amount of aileron deflection turns out to be 22.38°.

$$\boxed{\delta_a = 22.38°}$$

From Ref. [3], the change in airplane sideslip angle due to rudder deflection, β_{δ_r}, is calculated as,

$$\beta_{\delta_r} = \frac{\partial \beta}{\partial \delta_r} = -0.7562$$

Integrating and assuming that the integrating constant is approximately zero, then the sideslip angle can be related to the rudder deflection as follows,

$$\beta \equiv -0.7562\delta_r \qquad (12.28)$$

Then, in order to suppress the crosswind effect, i.e. a sideslip angle of 11.5°, an amount of −11.5° of sideslip angle should be produced. This will, in turn neutralize the crosswind effect. Hence, the required rudder deflection to produce that much of negative sideslip will be evaluated from Eqn. (12.28) as follows,

$$-11.5 = -0.7562\delta_r$$

Then, the required rudder deflection turns out to be,

$$\boxed{\delta_r = 15.2°}$$

Since, this result is a quite moderate amount, it can be concluded that the vertical tail is powerful enough in order to satisfy the crosswind criteria.

12.5 Results of Chapter 12

As mentioned before, in this chapter, both the methods of Ref. [1] and Ref. [3] are utilized. Ref. [3] is basically an analysis program. Hence, only the results will be given here. In the following tables, all the stability derivatives will be presented, which are calculated by these methods.

Table 12. 3 Derivatives related with longitudinal stability.

Parameter	*Value*
e	0.8405
X_{ac_h}	11.32 ft
X_{ac_w}	4.36 ft
$X_{ac_{wf}}$	4.02 ft
X_{cg}	5.00 ft
X_{np}	5.37 ft

Steady State Coefficients

C_{L_1}	1.0381
$C_{m_{T_1}}$	-0.1730

Speed Related Derivatives

C_{L_u}	0.02
C_{m_u}	0.0084

Rate of AOA Derivatives

$C_{D_{\dot{\alpha}}}$	0.00 rad^{-1}
$C_{L_{\dot{\alpha}}}$	3.1662 rad^{-1}
$C_{m_{\dot{\alpha}}}$	-11.278 rad^{-1}

Pitch Rate Related Derivatives

C_{D_q}	0.00 rad^{-1}
C_{L_q}	8.356 rad^{-1}

Parameter	*Value*
	Angle of Attack Related Derivatives
C_{D_α}	0.6016 rad^{-1}
C_{L_α}	4.591 rad^{-1}
$C_{l_{\alpha_{h@M=0}}}$	6.36 rad^{-1}
$C_{L_{\alpha_h}}$	3.5982 rad^{-1}
$C_{L_{\alpha_v}}$	2.8245 rad^{-1}
$C_{l_{\alpha_{w@M=0}}}$	6.16 rad^{-1}
$C_{L_{\alpha_w}}$	3.7590 rad^{-1}
$C_{L_{\alpha_{wf}}}$	3.7402 rad^{-1}
C_{m_α}	-0.9545 rad^{-1}
$\partial\varepsilon_h/\partial\alpha$	0.3431
SM	20.79 %

Pitch Rate Related Derivatives

$C_{L_{q_h}}$	9.2271 rad^{-1}
$C_{L_{q_w}}$	-0.8713 rad^{-1}
C_{m_q}	-33.6682 rad^{-1}
$C_{m_{q_h}}$	-32.8672 rad^{-1}
$C_{m_{q_w}}$	-0.8010 rad^{-1}

Table 12. 4 Derivatives related with lateral-directional stability.

Parameter	*Value*	*Parameter*	*Value*
Sideslip Related Derivatives		***Rate of Sideslip Related Derivatives***	
C_{ℓ_β}	-0.411 rad^{-1}	$C_{\ell_{\dot\beta}}$	0.006 rad^{-1}
$C_{\ell_{\beta_v}}$	-0.2247 rad^{-1}	$C_{n_{\dot\beta}}$	-0.0896 rad^{-1}
$C_{\ell_{\beta_{wf}}}$	-0.1233 rad^{-1}	$C_{y_{\dot\beta}}$	-0.1369 rad^{-1}
C_{n_β}	0.722 rad^{-1}	$(d\alpha/d\beta)_w$	-0.2543
$C_{n_{\beta_{fus}}}$	-0.1844 rad^{-1}	***Roll Rate Related Derivatives***	
$C_{n_{\beta_v}}$	0.892 rad^{-1}	C_{n_p}	-0.1303 rad^{-1}
$C_{n_{\beta_w}}$	0.0144 rad^{-1}	C_{y_p}	0.0524 rad^{-1}
C_{y_β}	-0.6305 rad^{-1}	***Yaw Rate Related Derivatives***	
$C_{y_{\beta_{fus}}}$	-0.3528 rad^{-1}	C_{ℓ_r}	0.2762 rad^{-1}
$C_{y_{\beta_v}}$	-0.2777 rad^{-1}	C_{y_r}	0.3344 rad^{-1}
$C_{y_{\beta_w}}$	0.000 rad^{-1}		
$(d\alpha/d\beta)_v$	0.1861		

Table 12. 5 Derivatives related with longitudinal control.

Parameter	*Value*	*Parameter*	*Value*
Horizontal Tail Incidence Related Derivatives		***Elevator Related Derivatives***	
$C_{D_{ih}}$	0.1697 rad^{-1}	$C_{D_{\delta_e}}$	0.1277 rad^{-1}
$C_{L_{ih}}$	1.2952 rad^{-1}	$C_{L_{\delta_e}}$	0.9744 rad^{-1}
$C_{m_{ih}}$	-4.6135 rad^{-1}	$C_{m_{\delta_e}}$	-3.4708 rad^{-1}
		α_{δ_e}	-0.7523

Table 12. 6 Derivatives related with lateral-directional control.

Parameter	*Value*	*Parameter*	*Value*
Aileron Related Derivatives		***Rudder Related Derivatives***	
$C_{l_{\delta_a}}$	0.3217 rad^{-1}	$C_{l_{\delta_r}}$	0.0013 rad^{-1}
$C_{l_{\delta_{a_r}}}$	0.1608 rad^{-1}	$C_{n_{\delta_r}}$	-0.2006 rad^{-1}
$C_{l_{\delta_{a_l}}}$	0.1608 rad^{-1}	$C_{y_{\delta_r}}$	0.3111 rad^{-1}
$C_{y_{\delta_a}}$	0.00 rad^{-1}	β_{δ_r}	-0.7562

Table 12. 7 Airplane coefficients at zero angle of attack.

Parameter	*Value*	*Parameter*	*Value*
Coefficients at Zero Angle of Attack			
C_{L_0}	0.3164 rad^{-1}	$C_{m_{0_h}}$	0.1520 rad^{-1}
$C_{L_{0_h}}$	-0.0427 rad^{-1}	$C_{m_{0_{wf}}}$	0.4615 rad^{-1}
$C_{L_{0_{wf}}}$	0.3590 rad^{-1}	α_{0_h}	-5.5°
C_{m_0}	0.6134 rad^{-1}	ε_{0_h}	1.9°

12.6 Conclusion

In this chapter, the required lateral and longitudinal stability characteristics of the design UAV are analyzed. For this purpose the methods given in Refs. [1], [2] and [3] are utilized. Correspondingly, some parameters are calculated, such as the location of the aircraft neutral point, static margin, etc. Besides, the longitudinal and lateral-directional stability analyses are performed.

In the analysis of longitudinal stability, C_{m_α} is found to be –0.954 rad^{-1}, which indicates that the design VTOL UAV is longitudinally stable. For the case of lateral stability, C_{ℓ_β} is calculated to be –0.411 rad^{-1}, which also indicates that the design VTOL UAV is laterally stable. And, for directional stability, C_{n_β} is calculated to be 0.722 rad^{-1}, which indicates that the design VTOL UAV is directionally stable. As a result, it is observed that, the aircraft satisfies these stability requirements.

All the results evaluated as a part of this chapter are tabulated in section 12.5.

The next chapter will illustrate the calculations performed, for the performance and flight mechanics analyses of the design UAV.

CHAPTER 13

PERFORMANCE AND FLIGHT MECHANICS

13.1 Introduction

This chapter introduces the performance and flight mechanics analyses of the design UAV. Since some dimensions and aerodynamic parameters have changed in the recent studies, some performance parameters will be recalculated in this chapter.

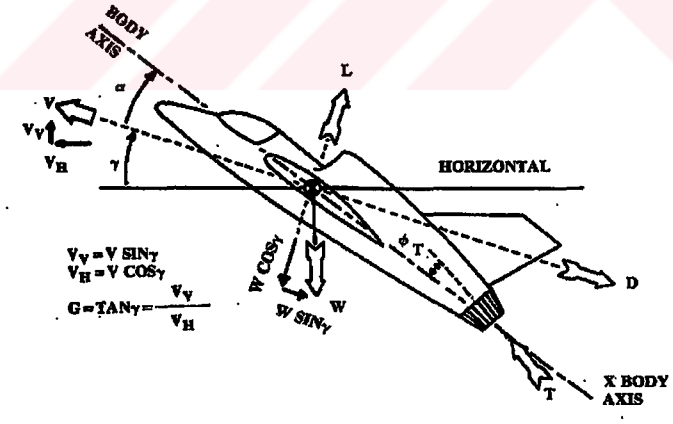

Figure 13. 1 Geometry for performance calculation. [1]

Figure 13.1 shows the geometry for flight mechanics and geometry calculation. Here, γ is the climb angle which is between horizontal and the wind (stability) X-axis. The climb gradient, G, the tangent of the climb angle, represents the vertical velocity divided by the horizontal velocity.

Taking into account Figure 13.1, the following calculations are performed as a part of this chapter.

13.2 Steady Level Flight

If the aircraft is flying in unaccelerated level flight, then the climb angle, γ, equals to zero, and the sum of the forces must equal to zero. Therefore, in level flight, thrust equals drag, and lift equals weight.

The following calculations will be performed for the condition of steady level flight.

13.2.1 Minimum Thrust Required for Level Flight

Eqn. (13.1) tells that for minimum thrust for a given weight, L/D should be maximized. In order to find the velocity at which thrust is minimum and L/D is maximum, the derivative with respect to velocity of Eqn. (13.1) is set to zero. The resulting relation is given by Eqn. (13.3).

$$\frac{T}{W}=\frac{1}{L/D}=\frac{qC_{Do}}{(W/S)}+\left(\frac{W}{S}\right)\frac{K}{q} \qquad (13.1)$$

$$\frac{\partial(T/W)}{\partial V}=\frac{qVC_{Do}}{(W/S)}-\left(\frac{W}{S}\right)\frac{2K}{1/2\rho V^3}=0 \qquad (13.2)$$

$$\underset{\substack{\min \ thrust \\ or\ drag}}{} = \sqrt{\frac{2W}{\rho S}}\sqrt{\frac{K}{C_{Do}}} \qquad (13.3)$$

This velocity yields a lift coefficient for minimum drag in level flight as given in Eqn. (13.4). At any given weight, the aircraft can be flown at this optimal lift coefficient for minimum drag by varying velocity or air density (altitude).

$$C_{L_{\substack{\min \ thrust \\ or\ drag}}} = \sqrt{\frac{C_{Do}}{K}} \qquad (13.4)$$

Then,

$$\underset{\substack{\min \ thrust \\ or\ drag}}{} = \sqrt{\frac{2(10.72)}{0.001953}}\sqrt{\frac{0.0531}{0.041}} = 111.76 ft/s$$

$$C_{L_{\substack{\min \text{ thrust} \\ \text{or drag}}}} = \sqrt{\frac{0.041}{0.0531}} = 0.879$$

13.2.2 Minimum Power Required for Level Flight

The conditions for minimum thrust and minimum power are not the same. Power is force times velocity. In the case of the steady flight, it corresponds to the drag times the velocity. It yields Eqn. (13.5). By setting the derivative of Eqn. (13.5) with respect to velocity to zero, the relation for the velocity for flight on minimum power is found. This relation is given in Eqn. (13.7).

$$P = \frac{1}{2}\rho V^3 S C_{Do} + \frac{KW}{1/2\,\rho V S} \qquad (13.5)$$

$$\frac{\partial P}{\partial V} = \frac{3}{2}\rho V^2 S C_{Do} - \frac{KW^2}{1/2\,\rho V^2 S} = 0 \qquad (13.6)$$

$$_{\substack{\min \\ power}} = \sqrt{\frac{2W}{\rho S}\sqrt{\frac{K}{3C_{Do}}}} \qquad (13.7)$$

This velocity yields the lift coefficient and drag for minimum power in level flight as given in Eqns. (13.8-9).

$$C_{L_{\substack{\min \\ power}}} = \sqrt{\frac{3C_{Do}}{K}} \qquad (13.8)$$

$$D_{\substack{\min \\ power}} = qS\left(C_{Do} + C_{Do}\right) \qquad (13.9)$$

Then,

$$_{\substack{\min \\ power}} = \sqrt{\frac{2(10.72)}{0.01953}\sqrt{\frac{0.0531}{3(0.041)}}} = 84.93 ft/s$$

$$C_{L_{\substack{\min \\ power}}} = \sqrt{\frac{3(0.041)}{0.0531}} = 2.316$$

$$D_{\substack{\min \\ power}} = \frac{1}{2}(0.001953)(84.93)^2(18.88)(0.041 + 0041) = 10.90lb$$

13.2.3 Range Optimization

The Breguet's range equation is given again in Eqn. (13.10). Here, there is no velocity term. Since, all other terms are constant with respect to velocity, it follows that propeller aircraft range will maximize by flying at the speed and lift coefficient for maximum L/D. This corresponds to the case, given by Eqns. (13.3) and (13.4).

$$R = \frac{550\eta_p}{C_{bhp}} \frac{L}{D} \ell n\left(\frac{W_i}{W_f}\right) \qquad (13.10)$$

$$_{b.r.} = \sqrt{\frac{2W}{\rho S}} \sqrt{\frac{K}{C_{Do}}} \qquad (13.11)$$

$$C_{L_{b.r.}} = \sqrt{\frac{C_{Do}}{K}} \qquad (13.12)$$

Then,

$$_{b.r.} = \sqrt{\frac{2(10.72)}{0.001953}} \sqrt{\frac{0.0531}{0.041}} = 111.76ft/s$$

$$C_{L_{b.r.}} = \sqrt{\frac{0.041}{0.0531}} = 0.879$$

13.2.4 Loiter Optimization

The endurance equation will be repeated in Eqn. (13.13). There is a velocity term in this loiter endurance equation, so the condition for best prop loiter will not be simply the maximum L/D.

$$E = \left(\frac{L}{D}\right)\left(\frac{550\eta_p}{C_{bhp}V}\right)\ell n\left(\frac{W_i}{W_f}\right) \qquad (13.13)$$

The derivative of Eqn. (13.13) with respect to velocity yields, the following relation for best loiter for prop.

$$V_{b.e.} = \sqrt{\frac{2W}{\rho S}}\sqrt{\frac{K}{3C_{Do}}} \qquad (13.14)$$

Eqn. (13.14) is identical to Eqn. (13.7), the velocity condition for minimum power. Hence, the lift coefficient and drag for maximum prop endurance will be identical to the case for minimum power given by Eqns. (13.8) and (13.9).

$$C_{L_{b.e.}} = \sqrt{\frac{3C_{Do}}{K}} \qquad (13.15)$$

$$D_{b.e.} = qS\left(C_{Do} + C_{Do}\right) \qquad (13.16)$$

Then,

$$_{b.e.} = \sqrt{\frac{2(10.72)}{0.01953}}\sqrt{\frac{0.0531}{3(0.041)}} = 84.93ft/s$$

$$C_{L_{b.e.}} = \sqrt{\frac{3(0.041)}{0.0531}} = 2.316$$

$$D_{b.e.} = \frac{1}{2}(0.001953)(84.93)^2(18.88)(0.041 + 0.041) = 10.90lb$$

13.3 Steady Climbing and Descending Flight

For the case of steady climbing and descending flight, the thrust-to-weight ratio is no longer the inverse of lift-to-drag ratio as in the case for the level flight. Hence, a new relation should be defined at this step. Eqn. (13.17) defines the thrust-to-weight ratio required for a steady climb at an angle of γ.

$$\frac{T}{W}=\frac{\cos\gamma}{L/D}+\sin\gamma\cong\frac{1}{L/D}+\sin\gamma \qquad (13.17)$$

The velocity for steady climbing is defined through Eqn. (13.18).

$$V=\sqrt{\frac{2}{\rho C_L}\left(\frac{W}{S}\right)\cos\gamma} \qquad (13.18)$$

The climb angle and rate of climb are given in Eqns. (13.19) and (13.20), respectively. The rate of climb, or vertical velocity, is the velocity times the sine of the climb angle.

$$\gamma=\sin^{-1}\left(\frac{T-D}{W}\right)=\sin^{-1}\left(\frac{T}{W}-\frac{\cos\gamma}{L/D}\right)\cong\sin^{-1}\left(\frac{T}{W}-\frac{1}{L/D}\right) \qquad (13.19)$$

$$_{v}=V\sin\gamma=V\left(\frac{T-D}{W}\right)\cong V\left(\frac{T}{W}-\frac{1}{L/D}\right) \qquad (13.20)$$

It should be noted that these calculations are valid for the conventional type of landing. Since, for the case of the design VTOL UAV the propellers will be tilted up or at an angle, in order to achieve a climb. Hence, for this case, the calculations will be based on the assumption that the UAV will use the 70% of its thrust for this conventional steady climbing action. It will also be assumed that, the UAV has completed the conventional/vertical takeoff flight segment, before entering to the steady climb. Then, from Eqn. (13.19),

$$\gamma\cong\sin^{-1}\left((1.25)(0.7)-\frac{1}{10.3}\right)=51.07^{\circ}$$

From Eqn. (13.18),

$$V=\sqrt{\frac{2}{(0.001953)(1.305)}(11.52)\cos(51.07^{\circ})}=75.37\,ft/s$$

From Eqn. (13.20),

$$V_v = (75.37)\sin(51.07°) = 58.63\,ft/s = 3517.8\,ft/\min$$

13.3.1 Time to Climb and Fuel to Climb

The time to climb to a given altitude is obtained by dividing the altitude to the rate of climb (vertical velocity). This is given in Eqn. (13.21).

$$t = \frac{h}{V_v} \qquad (13.21)$$

Then,

$$t = \frac{6562}{3517.8} = 1.865\min = 111.9\sec$$

The amount of the fuel burned can be calculated by having the product of the thrust, specific fuel consumption, and time to climb. This is given in Eqn. (13.22).

$$\Delta W_f = (-CT)_{average}(\Delta t) \qquad (13.22)$$

Then,

$$\Delta W_f = \left(-\frac{0.5}{3600}(141.6)(0.7)\right)_{average}(111.9) = 1.54lb$$

Hence, it can be concluded that the design VTOL UAV can climb to the cruising altitude, i.e. 6562 *ft*, at 70% thrust at a rate of 3517.8 *ft/s*. It takes approximately, 1.9 *min* and consumes 1.54 *lb* of fuel.

13.4 Level Turning Flight

In level turning flight, the lift of the wing is canted so that the horizontal component of the lift creates the centripetal force required to turn.

$$\dot{\Psi} = \frac{g\sqrt{n^2 - 1}}{V} \qquad (13.23)$$

where, n is the load factor. Turn rate ($d\Psi/dt$) equals to the radial acceleration divided by the velocity, as shown in Eqn. (13.23). This equation yields the result in radians per second. Since, turn rate is usually expressed in degrees per second, it needs a conversion.

The following calculations will be performed for the case of level turning flight.

13.4.1 Instantaneous Turn Rate

In the case of the instantaneous turn, the aircraft is allowed to slow down during the turn. Therefore, the load factor n will be limited only by the maximum lift coefficient or structural strength of the aircraft.

$$\left.\frac{W}{S}\right)_{cruise} = 10.72 lb/ft^2$$

$$n = \frac{qC_L}{W/S} = \frac{21.97(1.305)}{10.72} = 2.67$$

Then, from Eqn. (13.23),

$$\dot{\Psi} = \frac{32.2\sqrt{2.67^2 - 1}}{150} = 0.531 rad/s = 30.45 \text{deg}/s$$

13.4.2 Sustained Turn Rate

In the case of a sustained turn, the aircraft is not allowed to slow down or lose altitude during the turn. In a sustained turn, the thrust must equal to the drag and the lift must equal to the weight times the load factor n.

$$n = \frac{q\sqrt{C_{Do}/K}}{W/S} = \frac{32.2\sqrt{0.041/0.0531}}{10.72} = 2.64$$

$$\dot{\Psi} = \frac{32.2\sqrt{2.64^2 - 1}}{150} = 0.524 rad/s = 30.0 \text{deg}/s$$

13.5 Results of Chapter 13

Table 13. 1 List of parameters calculated in Chapter 13.

Parameter	*Value*	*Parameter*	*Value*
Steady Level Flight		***Steady Climbing Flight***	
$_{b.r.}$	111.76 ft/s	γ	51.07°
$C_{L_{b.r.}}$	0.879	V	75.37 ft/s
$_{b.e.}$	84.93 ft/s	V_v	3517.8 ft/s
$C_{L_{b.e.}}$	2.316	t	111.9 sec
$D_{b.e.}$	10.90 lb	ΔW_f	1.54 lb
		Level Turning Flight	
		Instantaneous Turn :	
		$\dot{\Psi}$	30.5 °
		Sustained Turn :	
		$\dot{\Psi}$	30.05 °

Table 13.2 The list of performance parameters evaluated in previous chapters.

Quantity	**Results**
$hp/W)_{TO}$	0.212 hp/lb
$W/S)_{TO}$	12 lb/ft^2
V_{stall} @ 3281 ft	50 knots (84.45 ft/s)
V_{cruise} @ 6562 ft	124.2 ft/s
M_{cruise}	0.113
$L/D)_{max}$	10.72
C_{Do}	0.041
e (Oswald Efficiency Factor)	0.833
$hp)_{cruise} / hp)_{TO}$	0.3
Takeoff Ground Roll	250 ft (76.2 m)
Takeoff Distance to clear 50 ft obstacle	500 ft (152.4 m)
Landing Field Length	965.5 ft (294 m)
Endurance	8.8 hr ($W_f = 45$ lb, $W_p = 30$ lb)
V_{loiter}	50.2 knots (84.76 ft/s)
C_{Lmax}	1.305
Instantaneous Turn Rate	0.398 rad/s
Rate of Climb (at the beginning of Climb)	3989 ft/sec
Rate of Climb (at the end of Climb)	1146 ft/sec
Max. Ceiling	38,871 ft (11,847 m)

13.6 Conclusion

This chapter illustrated the performance and flight mechanics analyses for the design VTOL UAV. For this purpose, the methods given in Ref. [1] are used. The calculations are performed as long as the methods were applicable for the case of the design UAV. The results are tabulated in section 13.5.

CHAPTER 14

COST ANALYSIS

14.1 Introduction

In this chapter, the cost analysis of the design UAV will be performed by use of modified DAPCA IV cost model, which is described in Ref. [1]. This model uses 1986 prices in terms of US $, therefore they need to be updated by considering the inflation rate in USA.

All the cost estimations in this chapter are performed, by assuming that 10 UAVs will be produced at the first step.

14.2 Modified Dapca IV Cost Model

Dapca IV model is a set of "cost estimating relationships" (CERs) which is developed by the RAND Corporation. This is the latest version of the Development and Procurement Costs of Aircraft (DAPCA) model.

DAPCA estimates the hours required for RDT&E (Research, Development, Test and Evaluation) and production by the engineering, tooling, manufacturing, and quality control groups. These are multiplied by the appropriate hourly rates to yield costs. Development, support, flight test, and manufacturing material costs are directly estimated by DAPCA.

It can't be said that DAPCA is the best set of CERs, but it is notable in providing reasonable results for several aircraft including fighters, bombers and transports. Here, it

will be applied for the case of design UAV, hence it should be noted that the results may not be accurate in this sense.

The cost estimating method will be applied for the design UAV by the following steps,

i. Average Wrap Rates

As mentioned before, the hours estimated with this model are multiplied by the appropriate hourly rates to calculate the labor costs. These hourly rates are called "wrap rates" because they include the direct salaries paid to employees as well as the employee benefits, and administrative costs. Average 1986 wrap rates are given in Ref. [1] as follows:

Engineering : \$ 59.10 = R_E

Tooling : \$60.70 = R_T

Quality Control : \$55.40 = R_Q

Manufacturing : \$50.10 = R_M

Predicted costs are then ratioed by some inflation factor to the selected year's constant dollar. Here, it should be noted that all he aircraft costs do not allow the same inflation factor. For example, the salaries of the engineers may increase at a slower rate than the raw-material cost for aluminum.

Now, cost estimations will be done as follows,

ii. Engineering Cost

The engineering cost will be evaluated as follows. Eqn. (14.1) will be used to calculate the engineering hours, H_E. Then, by multiplying this amount by the corresponding hourly rate, the cost will be evaluated.

$$H_E = 4.86 W_e^{0.777} V^{0.894} Q^{0.163} \qquad (14.1)$$

$$H_E = 4.86(151.5)^{0.777}(88.81)^{0.894}(10)^{0.163} = 19{,}308 hrs$$

Then,

$$Engineering\ Cost = H_E R_E = (19{,}308)(59.10) = 1.141 \times 10^6 \$$$

iii. Tooling Cost

The tooling cost will be evaluated as follows. Eqn. (14.2) will be used to calculate the tooling hours, H_T. Then, by multiplying this amount by the corresponding hourly rate, the cost will be evaluated.

$$H_T = 5.99 W_e^{0.777} V^{0.696} Q^{0.263} \qquad (14.2)$$

$$H_T = 5.99(151.5)^{0.777}(88.81)^{0.696}(10)^{0.263} = 12{,}323 hrs$$

Then,

$$Tooling\ Cost = H_T R_T = (12{,}323)(60.70) = 0.748 \times 10^6 \$$$

iv. Manufacturing Cost

The manufacturing cost will be evaluated as follows. Eqn. (14.3) will be used to calculate the manufacturing hours, H_M. Then, by multiplying this amount by the corresponding hourly rate, the cost will be evaluated.

$$H_M = 7.37 W_e^{0.82} V^{0.484} Q^{0.641} \qquad (14.3)$$

$$H_M = 7.37(151.5)^{0.82}(88.81)^{0.484}(10)^{0.641} = 17{,}356 hrs$$

Then,

$$Manufacturing\ Cost: H_M R_M = (17{,}356)(50.10) = 0.869 \times 10^6 \$$$

v. Quality Control Cost

The quality control cost will be evaluated by selecting the H_Q first from Ref. [1].

$H_Q = 0.133 \times$ (mfg hours)

$H_Q = 0.076(17{,}356) = 1319 hrs$

Then,

Quality Control Cost $= H_Q R_Q = (1319)(55.4) = 73{,}075\$$

vi. Development Support Cost

The development support cost, C_D, will be directly evaluated by use of Eqn. (14.4), as follows,

$$C_D = 45.52 W_e^{0.63} V^{1.3} \qquad (14.4)$$

then,

$C_D = 45.52(151.5)^{0.63}(88.81)^{1.3} = 0.367 \times 10^6\$$

vii. Flight Test Cost

The flight test cost, C_F, will be directly evaluated by use of Eqn. (14.5), as follows,

$$C_F = 1243.03 W_e^{0.325} V^{0.822} FTA^{1.21} \qquad (14.5)$$

then,

$C_F = 1243.03(151.5)^{0.325}(88.8)^{0.822}(2)^{1.21} = 0.587 \times 10^6\$$

viii. Manufacturing Materials Cost

The manufacturing materials cost, C_M, will be directly evaluated by use of Eqn. (14.6), as follows,

$$C_M = 11 W_e^{0.921} V^{0.621} Q^{0.799} \qquad (14.6)$$

then,

$$C_M = 11(151.5)^{0.921}(88.81)^{0.621}(10)^{0.799} = 0.114 \times 10^6 \$$$

ix. Engine Production Cost

The engine production cost, C_{eng}, will be directly evaluated by use of Eqn. (14.7), as follows,

$$C_{eng} = 1548[0.043 T_{max} + 243.25 M_{max} + 0.969 T_{turb-inlet} - 2228] \qquad (14.7)$$

then,

$$EPC = 1548[0.043(141) + 243.25(0.266) + 0.969(2642) - 2228] = 0.623 \times 10^6 \$$$

x. Avionics Cost

The avionics cost, $C_{avionics}$, will be directly evaluated by use of Eqn. (14.8), as follows,

$$C_{avionics} = W_{avionics}(2000) \qquad (14.8)$$

$$_{avionics}(2000) = (3.03)(2000) = 6{,}060\$$$

TOTAL A/C COST in 1986 : 4.528 M$

COST PER A/C in 1986: 3.899 M $ / 10 = 0.453 M$

This a/c cost should be updated for the year of 2001. Then, assuming a 5% inflation rate per year in USA,

A/C COST IN 2001 = $(1.05)^{14}(0.453 M\$) = 0.897 M\$$

A/C COST IN 2001 ≅ 0.897 *M*$

14.3 Conclusion

This chapter illustrated the cost analysis carried out for the design UAV by use of the DAPCA method defined in Ref. [1]. It should be noted that this does not give the exact cost of the design UAV. This is just an estimation, and gives the result for an industrial-produced aircraft. In the case of the Tilt-Duct VTOL UAV, considering that the first prototype will be built in a university type environment which makes the engineering cost almost zero, the cost evaluated as a part of this chapter will be substantially reduced.

On the other hand, an aircraft's cost may change due to many factors. For example, the cost will reduce as more aircraft are produced, i.e. the more aircraft produced, the more the manufacturer learns and the cheaper the next aircraft can be produced.

Another point is that, the DAPCA method used uses the rates of 1986. Hence, the results of the cost analysis are adopted to today, by considering an appropriate inflation rate in the US for the passed years.

CHAPTER 15

A TRADE STUDY : ASPECT RATIO OPTIMIZATION

15.1 Abstract

The objective of this design optimization process is to maximize the *Range* of a proposed aircraft without changing the amount of fuel. For this purpose a *user-friendly, web-interactive* computer program is developed by use of Visual Basic 5.0 programming language. The program predicts the best *Aspect Ratio* selection in order to achieve the maximum amount of Range for a proposed type of aircraft. During this procedure, aircraft fuel weight and empty weight are kept constant.

At the beginning, this optimization program was developed only for this newly developed *Tilt-Duct VTOL UAV.* Later on, the program is enabled so that the user could optimize the range of an aircraft of variable types by performing appropriate selections and utilizing various helpful tables and data in the user-friendly environment of the visual program.

'*Visual Basic 5.0 – Enterprise Edition*' is the programming language that is used during the development procedure. Besides, '*Microsoft Front Page Express 98*' and '*Netscape 4.61 – Composer*' are used for the web-page development. The computer program is web-interactive and this is achieved by use of "ActiveX control" within the structure of the program.

The program requires certain inputs from the user before starting the calculation process; i.e., *Wing Loading* (Wo/S), *Horsepower-to-Weight Ratio* (hp/Wo), *Wing Area* (Swing), *Maximum Cruise Velocity* (Vmax), *Payload Weight* (Wp), *Fuel Weight* (Wf), *Number of Crew Members* and *Sweep Angle*. This data input procedure is programmed such that, in the related 'key' forms, the user can find every little detail of information related with these variables, sometimes enriched with useful drawings.

As mentioned before, the aim of this program is the range optimization with respect to one main parameter: *Aspect Ratio*. The 'objective function' is arranged such that it is only a function of this parameter.

The program uses a 2-D maximization procedure, *Kaftanoglu Algorithm*, and finds out the best Aspect Ratio which provides the best Range at minimum Wo (takeoff weight) for the specific type of aircraft selected by the user.

15.2 Introduction

Today, CAD Design Optimization techniques are quite common in the aerospace industry in order to minimize the losses and obtain the maximum efficiency out of a design. Since, aerospace business is quite expensive to deal with, any small increment in efficiency of an aircraft saves millions of dollars to the manufacturer and the user firms.

In this case, this program is developed as a trade study. On the other hand, the results of this design optimization procedure can be applied to an aircraft and relevant modifications can be performed according to the optimum aspect ratio predicted. By this way, optimum range will be achieved.

15.3 About Visual Basic 5.0™

Visual Basic 5.0 is one of the most preferred compilers today. Because of its powerful components and easily learnable language, it is preferred. By using this computer language, a user can develop object oriented programmes. The advantages of object oriented programming are as follows; the produced parts can be updated very

easily and the speed of the programmes are very fast with respect to the ones developed by the conventional compilers. In addition to these factors, there exists very good documentations about Visual Basic 5.0 which helps the programmer in developing a programme when compared with the other compilers. Figure 15.1 illustrates a standard window when a user starts VB and opens a new VB project.

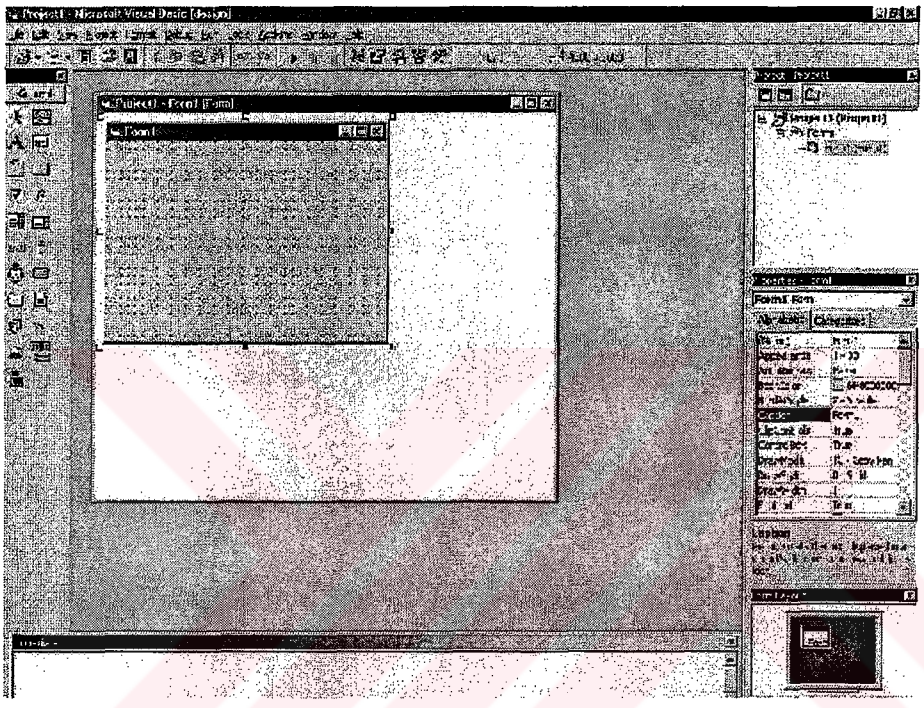

Figure 15. 1 The standard window of VB 5.0, when a new project is opened.

A programming language today, such as Visual Basic, differs greatly from programming languages of just a few years ago. The visual nature of the Windows operating system requires more advanced tools than were available a few years ago. Before windowed environments, a programming language was a simple text-based tool with which a programmer wrote programs. Today, languages such as VB 5.0 are developed as a graphical development tool that can work inside the Windows system and create applications that take advantage of all the graphical, multimedia, online, and multiprocessed activities that Windows offers.

In Visual Basic environment, describing simply, there are forms that the users can see when the program is run. The forms are visual platforms, that the pogrammer can put command buttons, frames, text boxes, etc., any control proposed by VB. The trick that

makes the buttons response to the user click, or the check box does its duty, depends on the program code that the programmer writes in the code window of these forms. These code windows can only be seen in the design mode of VB. When running the program, the user will just see the forms and any controls on it, responding to the user the way the programmer programmed them so. In Figure 15.2, a form from the Aspect Ratio Optimization program, developed as a part of this thesis, and its code behind are shown.

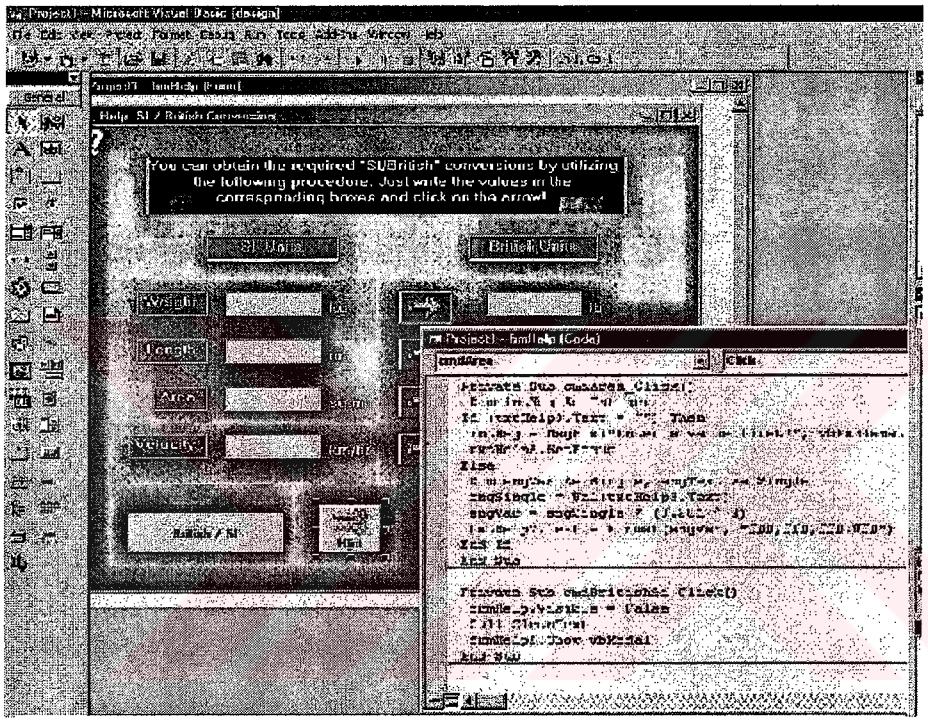

Figure 15. 2 A 'design' window of VB 5.0, i.e. the form of 'conversion table' and a part of its code (Aspect Ratio Optimization Program).

15.3.1 Standard Controls of Visual Basic 5.0™

In object oriented languages like Visual Basic 5.0 or Borland Delphi 3.0, standard controls provide user to perform particular events or specify different variables by a few mouse clicks or keystrokes. Standard controls can be listed as: text boxes, label, picture box, image, command button, check box, option button, frame, list box, combo box, horizontal and vertical scroll bar, timer, drive list box, directory list box and file list box.

These controls will be briefly introduced as the followings.

15.3.1.a Text Boxes

In general, the text box control is used for editable text. Setting its 'Locked' property to 'True', it can be made just read-only. This property is used in developing the Aspect Ratio Optimization Program whenever it is not wished that the user to edit the written value/text in the relevant text box. Figure 15.3 shows the use of text box, as an example, that is used in the developed optimization program.

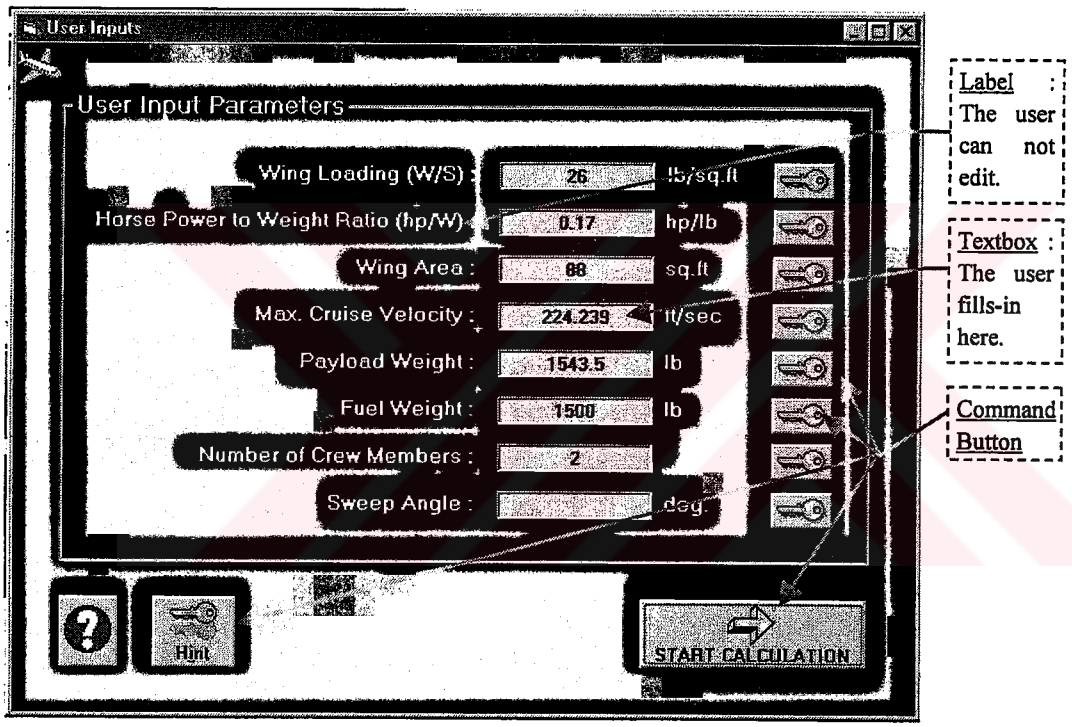

Figure 15. 3 Typical uses of the 'text box', 'label' and 'command button' controls in the optimization program.

15.3.1.b Label

Label controls are used to display text and cannot be edited by the user. They are used to identify objects on a form and to provide a description of what a certain control will do if clicked. During the run time, they can display the required information in response to an event or process in the application. Figure 15.3 shows the use of label, as an example, that is used in the developed optimization program.

15.3.1.c Picture Box

The picture box control is used to display graphics, to act as a container for other controls and to display output from graphics methods or text using the Print method. The picture box control is similar to the image control since both of them can be used to display graphics in the applications and to support the same graphic formats. The picture box control, however, contains functionality, the ability to act as a container for other controls and support for graphics methods, which is not a property of the image control.

15.3.1.d Image

The image control is used to display graphics. It can display graphics as bitmap, icon, metafile, enhanced metafile, or as JPEG or GIF files. This control is often preferred over the picture control whenever possible.

15.3.1.e Command Button

The command button control is used to begin, to interrupt, or to end a process. When clicked, it invokes a command that has been written into its Click event procedure, i.e. in the code window. Most of the Visual Basic applications have command buttons that

allow the user to simply click them to perform actions. When the clicks on the button, it carries out not only the appropriate action, it also looks as if it's being pushed in and released and is therefore sometimes referred to as a push button. See Figure 15.3, for a typical use of command button control.

15.3.1.f Check Boxes

The check box control displays a check mark when it is selected. It is commonly used to offer a Yes / No or True / False selection to the user. A programmer can use check box controls in groups to display multiple choices from which the user can select one or more.

15.3.1.g Option Button

Option button controls are used to display options, usually in the form of option button groups, from which the user can choose one. The only difference between the option button and the check box is that only one option button in a group can be selected at a time. With the check box control, one may select any desired number of check boxes. Figure 15.4 shows a typical use of the option buttons in the Aspect Ratio Optimization Program.

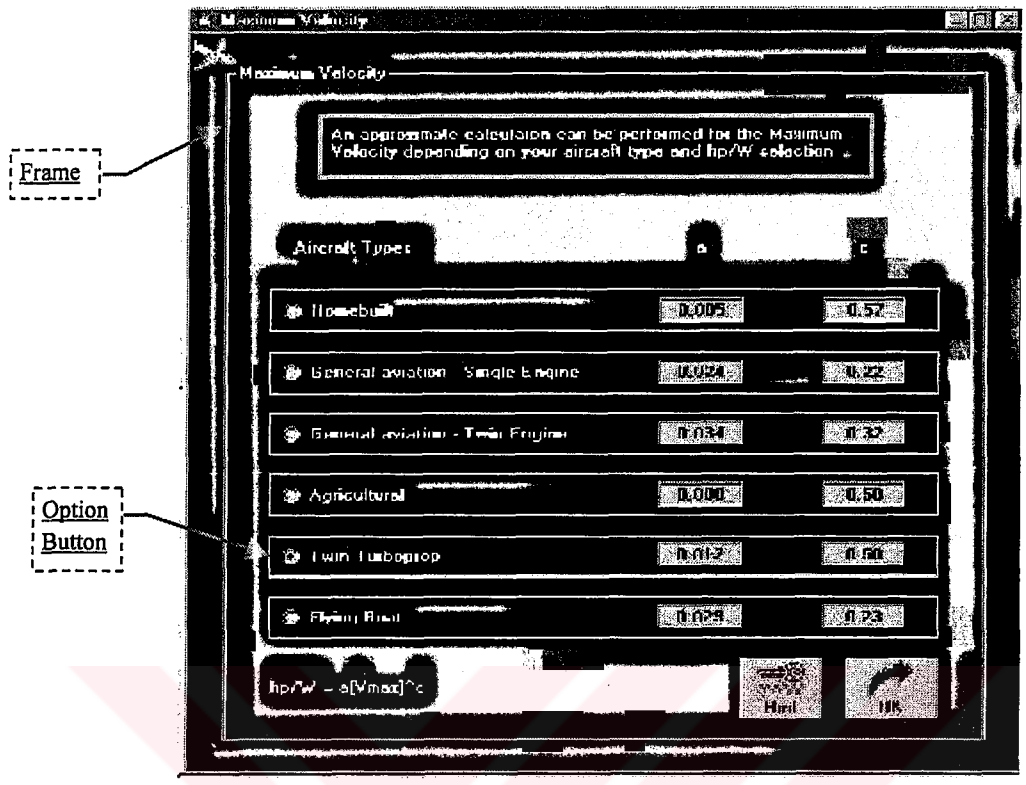

Figure 15. 4 Typical uses of the 'option button' and 'frame' controls in the developed program.

15.3.1.h Frame

Frame controls are used to provide an identifiable grouping for other controls. For example, a programmer can use frame controls to subdivide a form functionally into separate groups of option button controls. Figure 15.4 shows a typical use of frame in the Aspect Ratio Optimization Program.

15.3.1.i List Box

A list box control displays a list of items from which the user can select one or more. List boxes present a list of choices to the user. By default, the choices are displayed vertically in a single column, although they can be set up in multiple columns as well. If the number of items exceeds the number that can be displayed in the list box, scroll bars

automatically appear on the control. The user can then scroll up and down, or left to right through the list.

15.3.1.j Combo Boxes

A combo box control combines the features of a text box and a list box. This control allows the user to select an item either by typing text into the combo box or by selecting it from the list. Combo boxes present a list of choices to the user. If the number of items exceeds what can be displayed in the combo box, scroll bars automatically appear. The user can then scroll up and down or left to right through the list. A combo box contains an edit field, and the choices not on the list can be typed in this field. In addition, combo boxes save space on a form. Since the full list is not displayed until the user clicks the down arrow, a combo box can easily fit in a small space where a list box would not.

15.3.1.k Horizontal & Vertical Scroll Bars

Scroll bars provide easy navigation through a long list of items or a large amount of information by scrolling either horizontally or vertically within an application or control. Scroll bars are also a common element of the Windows 95 and Windows NT interface. The horizontal and vertical scroll bar controls are not the same as the built-in scroll bars found in Windows or those that are attached to text boxes, list boxes, combo boxes or MDI (Multiple Document Interface) forms within Visual Basic. Those scroll bars appear automatically whenever the given application or control contains more information than that could be displayed in the current window size.

15.3.2 Active X

ActiveX is a set of technologies from the Microsoft Company that enables interactive content for the World Wide Web. By use of ActiveX, Web sites become alive using multimedia effects, interactive objects and sophisticated applications that create a user experience comparable to that of high-quality cd-rom titles.

ActiveX Controls are the interactive objects in a Web page that provide interactive and user-controllable functions and hence animate the experience of a Web site. ActiveX Documents enable users to view non-HTML documents, such as Microsoft Excel or Word files, through a Web browser. Active Scripting controls the integrated behavior of several ActiveX controls and/or Java Applets from the browser or server. Java Virtual Machine is the code that enables any ActiveX-supported browser such as Internet Explorer 3.0 to run Java applets and to integrate Java applets with ActiveX controls.

As a part of the Aspect ratio Optimization program, ActiveX control is used in order to achieve the www-interaction of the computer program developed; that is the program can be run via internet through an internet browser such as Internet Explorer 3.0 and up.

i. About the Internet Download Setup

Visual Basic allows to create ActiveX controls, ActiveX DLLs, ActiveX EXEs, and ActiveX documents that can be used within an Internet browser, such as Internet Explorer 3.0. For example, a control can be created that prompts a user for a certain type of information and then processes that information in some manner. To use this control in Internet Explorer, the programmer should refer to it in the underlying HTML code, perhaps using VBScript. In other words, the control created is hosted on a Web page.

The Web page, along with the control created and any other dependent files, resides at a specific location on the World Wide Web. When the user accesses this Web page, the control created is activated. That is, it is downloaded (in the form of a compressed ".cab" file) along with the Web page to the user's computer. The control is then verified

for safety, decompressed, registered in the Windows registry, installed, and *then* activated.

All of this occurs in the background and is controlled by the Internet browser application. Since this form of distribution differs from the more common method of application distribution via disks or compact discs, there are new issues to be considered. Most important of these is safety, both for the user and for the programmer's source code.

The purpose of the "Setup Wizard"- that the programmer can reach from the "start" menu of his computer, under the Microsoft Visual Basic 5.0- in all this is to package the ActiveX component. Setup Wizard determines which files the project needs at run time, gathers those files, compresses them into a ".cab" file, and generates the sample HTML code that points to the programmer's control.

The Setup Wizard creates a ".cab" file that contains the component, an ".inf" file, and space for digital signing. It also creates a sample ".htm" file which the programmer can use to refer to his/her component from the Web page.

In an Internet download package for an ActiveX document, the following files are created, given in Table 15.1.

Table 15. 1 The files created in an Internet Download Setup for a project named *Project1*.

File	***Property***
Project1.cab	The ".cab" file which contains: the ActiveX document (.dll) and the ".inf" file.
Project1.htm	An HTML file containing sample HTML code.
UserControl.vbd	The state file for the UserControl object in the ActiveX document.

The programmer distribute the ".cab" and ".vbd" files along with the Web page on the Web site. The ".htm" file contains sample HTML code which points the browser to

the ActiveX document objects. The programmer can cut and paste sections of the sample code into the underlying HTML code of the Web page to instantiate either of the ActiveX document components.

The Setup Wizard also creates a subdirectory called "Support" which contains all of the files that were compressed into the ".cab" file. The following files would be found in the Support directory, given in Table 15.2.

Table 15. 2 The files created in the Support directory for an ActiveX component named UserControl.

File	*Property*
UserControl.dll	The compiled ActiveX document.
UserControl.ddf	The ".ddf" file is used by the compression program.
UserControl.inf	The ".inf" file which contains all dependency, version, setup, and safety information for the component.

ii. The Procedure to Create an Internet Download Setup

In order to create an Internet Download Setup, the programmer should have used an ActiveX control in his/her Visual Basic™ project. If this is done, the procedure is as follows :

- Open your project in the design mode of Visual Basic 5.0. From File-Menu, select "Make Project1.ocx..." Here, *Project1* is an arbitrary project name. It will appear with the name of your project, as you browse through the File-Menu.

  Warning : If you fail to find an option in your File-Menu as "Make Project1.ocx..." This most probably means that you have failed in creating the ActiveX control in a proper way. In this case, it may be helpful to go through the "Books Online" and study through creating an ActiveX control. You can

access to "Books Online" from the start-menu of your computer, under the prompt of Microsoft Visual Basic.

- Go through the "Windows Explorer" and create a folder that the Internet Download Setup files will be located in.

- Click the "start-menu" of your computer, browse through Programs, Microsoft Visual Basic 5.0, and then select "Application Setup Wizard."

- In the "Select Project and Options" window of Application Setup Wizard, use the browse button and input the location of your ".vbd" project fro which the Internet Download Setup will be created. Then, from the options, select "Create an Internet Download Setup." Click Next.

- In the "Internet Distribution Location" window, browse through the location of the folder that you have created in Step 2. This will be taken as the "destination" for the Internet Download Setup files. Click Next.

- In the "Internet Package" window, there are options for the download of separate runtime cabinet files. The author of this thesis preferred them to be downloaded from the Microsoft web site. Before leaving this window, click the "safety" button. Your ActiveX control should automatically occur in the component window (if not, this means that there is a problem with your control!). Select "Safe for Initialization" and "Safe for Scripting." Click OK. Click Next.

- In the "ActiveX Server Components" window, click Next.

- In the "Confirm Dependencies" window, click Next.

- In the "File Summary" window, click Next.

- Click Finish.

As mentioned before, this procedure will create a ".htm" file, a ".cab" file and a "Support" folder in the destination folder that you have selected in Step 5. In order to see how the program works through internet, open the created ".htm" file through Internet

Explorer. Be sure that your security level is set to "low." It somehow affects the ActiveX controls.

15.4 Theory

This design optimization procedure will serve to maximize the *Range* for a proposed aircraft type. The main objective is to find the best *AR* (Aspect Ratio) of the aircraft which gives the maximum Range for a given amount of fuel.

All the equations used in the calculation procedures of the computer program are just identical to the ones used in the previous chapters of this thesis. Basically, the methods presented in Ref. [1], [2] and [3] are utilized. These methods will be briefly reminded as the followings.

i. **Range :**

For this purpose, the Breguet's Range Equation is used, which is given again in Eqn. (15.1).

$$\left(\frac{W_i}{W_{i-1}}\right) = \exp\left(\frac{-RC}{V(L/D)}\right) \qquad (15.1)$$

where :

$\left(\frac{W_i}{W_{i-1}}\right)$: Segment Weight Fractions

R : Range in *ft.*

C : Specific Fuel Consumption in *1/sec.*

V : Cruise Velocity in *ft/sec.*

(L/D) : Lift to Drag ratio.

ii. Specific Fuel Consumption

For this purpose Eqn. (15.2) is utilized, which is a relation defined in Ref. [1].

$$C = C_{bhp} \frac{V}{550\eta_p} \qquad (15.2)$$

where,

C_{bhp} : Propeller specific fuel consumption = constant.

η_p : Propeller efficiency = constant.

iii. Maximum Lift-to-Drag Ratio :

For this purpose Eqn. (15.3) is utilized, which is a relation defined in Ref. [1].

$$\left(\frac{L}{D}\right)_{max} = \frac{1}{2}\sqrt{\frac{\pi Ae}{C_{Do}}} \qquad (15.3)$$

where,

A : Wing Aspect Ratio (in the program it is referred as : AR).

e : Oswald efficiency factor.

C_{Do} : Zero lift drag coefficient.

iv. Aspect Ratio :

This is one of the most important parameters in the design of an aircraft. The developed computer program also aims to evaluate an optimum value of the aspect ratio which gives the maximum Range out of the same amount of fuel. Eqn. (15.4) gives the definition of the aircraft aspect ratio.

$$AR = \frac{b^2}{S} = \frac{b}{\bar{c}} \qquad (15.4)$$

where,

b : Wing span in ft.

$\bar{c}$: Wing mean aerodynamic chord in ft.

S : Wing area in ft.

v. Parasite Drag Coefficient :

The parasite drag coefficient is calculated according to the method given in Ref. [2], which evaluates the C_{Do}, depending on the aircraft wetted area. The equations used are given in Eqn.s (15.5) to (15.8).

$$C_{Do} = \frac{f}{S_{wing}} \qquad (15.5)$$

where,

$$\log_{10} f = a + b \log_{10} S_{wet_{a/c}} \qquad (15.6)$$

$$\log_{10} S_{wt_{a/c}} = c + d \log_{10} W_{TO} \qquad (15.7)$$

c, d are "Regression Coefficients" used to estimate Wetted Area of the aircraft from the Take-off Weight and a, b are "Regression Coefficients" used to estimate aircraft Parasite Area from the Wetted Area of the aircraft.

As the parameters are installed in Eqn. (15.5) and simplified, the C_{Do} is obtained as a function of wing area and aircraft takeoff weight as given in Eqn. (15.8). The program uses this relation.

$$C_{Do} = \frac{10^{(-2.301+c)} W_o^{\,d}}{S_{wing}} \qquad (15.8)$$

vi. Oswald Efficiency Factor :

Oswald efficiency factor is calculated via Eqn. (15.9). This is a method defined in Ref. [1] and valid for the unswept aircraft.

$$e = 1.78\left(1 - 0.045AR^{0.68}\right) - 0.64 \qquad (15.9)$$

vii. Fuel Weight :

Fuel weight is given by Eqn. (15.10). This is a method defined in Ref. [1].

$$W_F = 1.06\left(1 - \frac{W_x}{W_0}\right) \qquad (15.10)$$

where,

$$\frac{W_x}{W_0} = \frac{W_7}{W_0} = \frac{W_7}{W_6}\frac{W_6}{W_5}\frac{W_5}{W_4}\frac{W_4}{W_3}\frac{W_3}{W_2}\frac{W_2}{W_1}\frac{W_1}{W_0}$$

$\frac{W_2}{W_0}$: Vertical Take-off + Transition = 0.96

$\frac{W_3}{W_2}$: Climb= 0.99

$\left(\frac{W_4}{W_3}\right) = \exp\left(\frac{-RC}{V(L/D)}\right)$: Cruise

$\frac{W_5}{W_4}$: Descend= 0.99

$\frac{W_7}{W_5}$: Vertical Landing+ Transition = 0.97

viii. Empty Weight :

Empty weight is calculated according to the relation given in Eqn. (15.11). This is a method defined in Ref. [1]. The optimization program evaluates the aircraft empty weight by proposing the user several aircraft types, that he can select out of one via the option buttons. This form comes into view with the caption 'Empty Weight' through the run of the program. This form is illustrated in Figure 15.5.

$$\frac{W_e}{W_o} = a + bW_o^{C_1} A^{C_2} \left(\frac{hp}{W_o}\right)^{C_3} \left(\frac{W_o}{S}\right)^{C_4} V_{\max}^{C_5} \qquad (15.11)$$

where,

$\left(\frac{hp}{W_o}\right)$: Horsepower-to-weight ratio in *hp/lb*.

$\left(\frac{W_o}{S}\right)$: Wing loading in lb/ft^2.

V_{max} : Cruise speed in *miles/hr*.

$A, b, C_1, C_2, C_3, C_4, C_5$ are coefficients depending on the aircraft type.

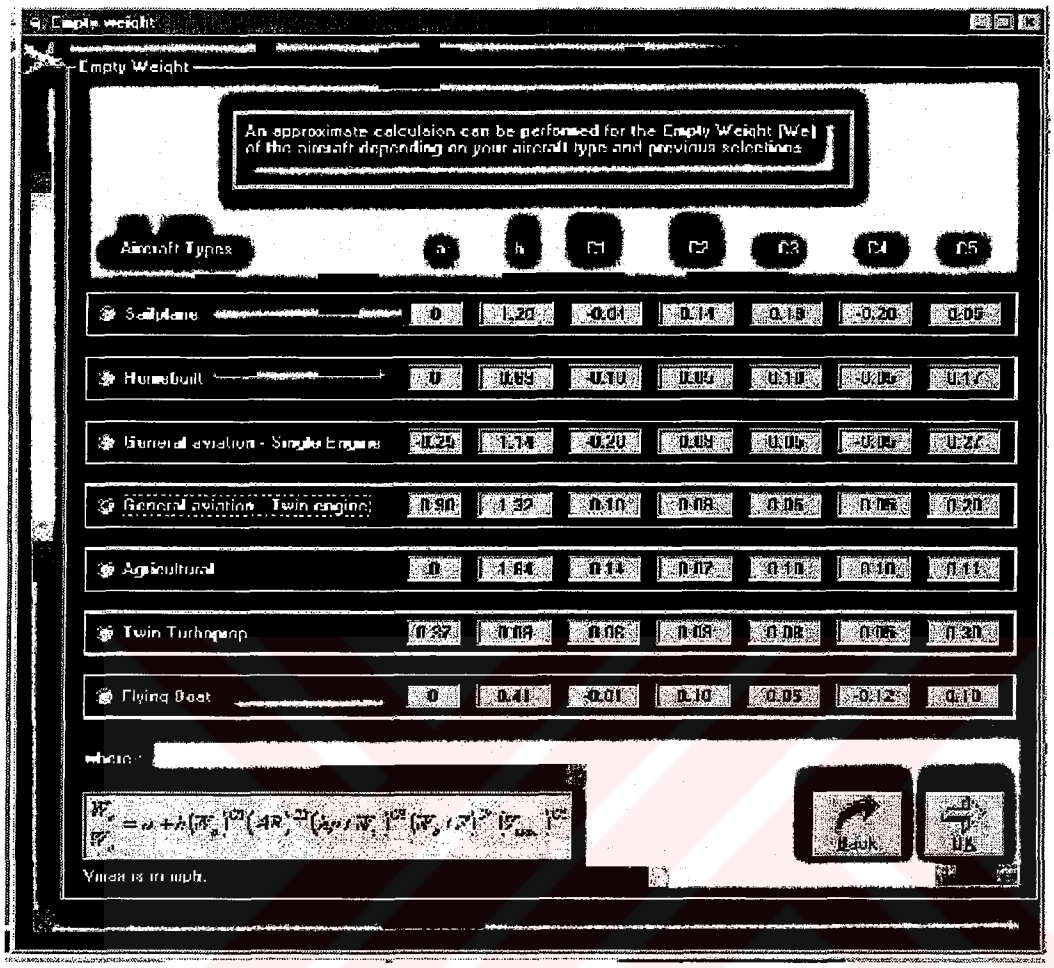

Figure 15. 5 The 'Empty Weight' form that a user uses in the Optimization program.

As the parameters are installed in Eqn. (15.11) and simplified, the empty weight of the design UAV is obtained as a function of takeoff weight only, as given in Eqn. (15.12). The program uses this relation in the case of that the user selects the VTOL UAV type.

$$\frac{W_e}{W_o} = 0 + 0.59(W_o)^{-0.1}(7.2)^{0.05}(0.212)^{0.1}(12)^{-0.05}(84.87)^{0.17}$$

$$W_e = 1.05(W_o)^{0.9} \qquad (15.12)$$

ix. Takeoff Weight :

For the case of the design VTOL UAV, since there is no crew, Eqn. (15.13-14) is utilized. For the case of the conventional type of aircraft, Eqn. (15.15-16) is valid and used by the program.

$$W_o = \frac{W_p}{1 - W_f/W_o - W_e/W_o} \qquad (15.13)$$

or

$$W_o = W_{empty} + W_{fuel} + W_{payload} \qquad (15.14)$$

$$W_o = \frac{W_p + W_{crew}}{1 - W_f/W_o - W_e/W_o} \qquad (15.15)$$

or

$$W_o = W_{empty} + W_{fuel} + W_{payload} + W_{crew} \qquad (15.16)$$

x. Optimization : *The Kaftanoğlu Algorithm*

The *Kaftanoğlu Algorithm* is a method developed by Prof. Kaftanoğlu, Bilgin, currently a faculty member of the Department of Mechanical Engineering, Middle East Technical University. [24]

The method finds out the maximum or minimum of a function and the value of the argument at which this occurs. For example let the function to be $y = f(x)$, and let be the three initial points are given/known as x_o, x_1, x_2 and y_o, y_1, y_2.

The algorithm determines, the point where the signs of $\frac{y_2 - y_1}{x_2 - x_1}$ and $\frac{y_1 - y_0}{x_1 - x_0}$ become different. Let's call the first fraction as A, and the second fraction as B. If the

signs of the fractions A and B are different, this means that the required maximum or minimum is between x_2 and x_o. For the case of a minimum, the corresponding signs of A and B should be (-) and (+) respectively. And vice versa, for the case of a maximum, the corresponding signs of A and B should be (+) and (-) respectively. For this purpose, in a case of a minimum, if all the values of y are negated, it will turn out to be a problem of finding the maximum.

Assuming that such a point is reached and the minimum is bound by x_2 and x_o. Figures 15.6 and 15.7, approaching in an increasing and decreasing sequence are illustrated respectively.

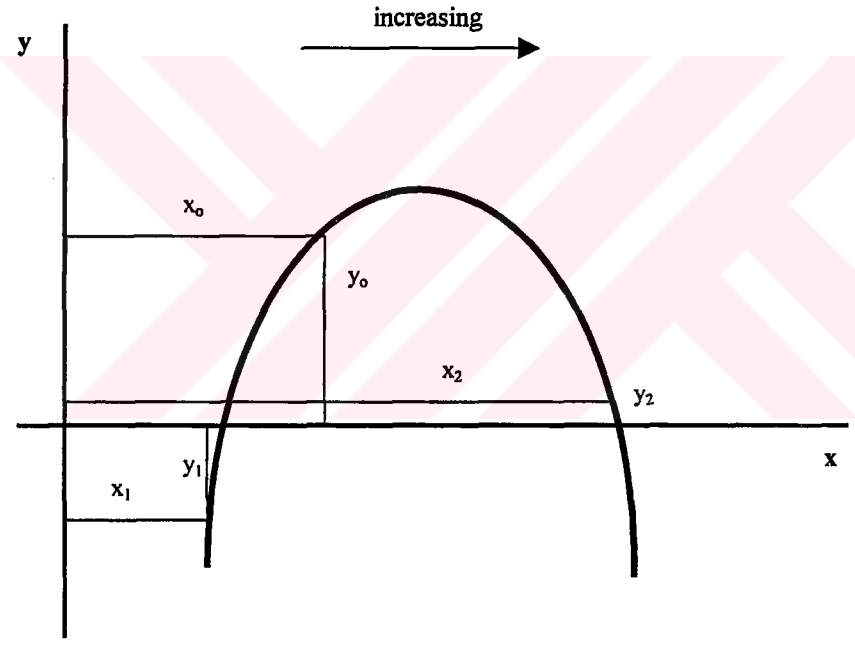

Figure 15. 6 Sequence of points in minimization, increasing. [24]

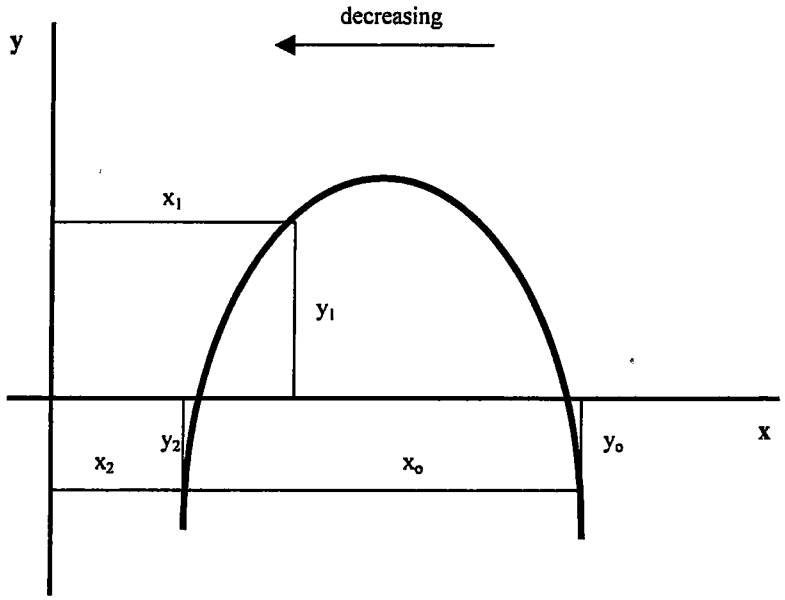

Figure 15. 7 Sequence of points in minimization, decreasing. [24]

Such a function can be approximately represented by a Lagrange polynomial, for this case a second degree one. Differentiation of this equation and equating it to zero yields Eqn. (15.18).

$$\frac{dy}{dx}=\frac{2x-x_2-x_1}{(x_0-x_1)(x_0-x_2)}y_0+\frac{2x-x_2-x_0}{(x_1-x_0)(x_1-x_2)}y_1+\frac{2x-x_1-x_0}{(x_2-x_0)(x_2-x_1)}y_2=0 \qquad (15.18)$$

Solving for the unknown x, after some algebraic manipulation, gives the following relation defined in Eqn. (15.19).

$$x=\frac{(x_1^2-x_2^2)y_0+(x_2^2-x_0^2)y_1+(x_0^2-x_1^2)y_2}{2[(x_1-x_2)y_0+(x_2-x_0)y_1+(x_0-x_1)y_2]} \qquad (15.19)$$

where, for the case of the developed Optimization program,

$x = AR$

$y = -Range$

Here (-) sign comes in order to convert the Eqn. (15.19) to a problem of a *maximization* process, since it was originally defined for a minimization process.

In the program, the Kaftanoğlu Algorithm, is utilized as follows in order to obtain the maximum *Range* (= y) and the corresponding *AR* (= x). First, since at 64 points by an interval of 0.2, the ARs and their corresponding Ranges are evaluated before in the program, three arbitrary points are selected as x_o, x_1, x_2 and y_o, y_1, y_2. Then by use of Eqn. (15.19), the first approximation for x and y is obtained. The next step is that, to replace one of the initial points, e.g. x_o, y_o , with the newly evaluated couple of x, y. This iteration process goes on until the values of either x or y does not differ more than a specified amount, i.e. defined as '*ErrX*' in the program.

The Kaftanoğlu Algorithm, used to find the maximum Range of the aircraft for a given amount of fuel, is given as a flow-chart in the following :

The Flowchart of Kaftanoğlu Optimization Algorithm

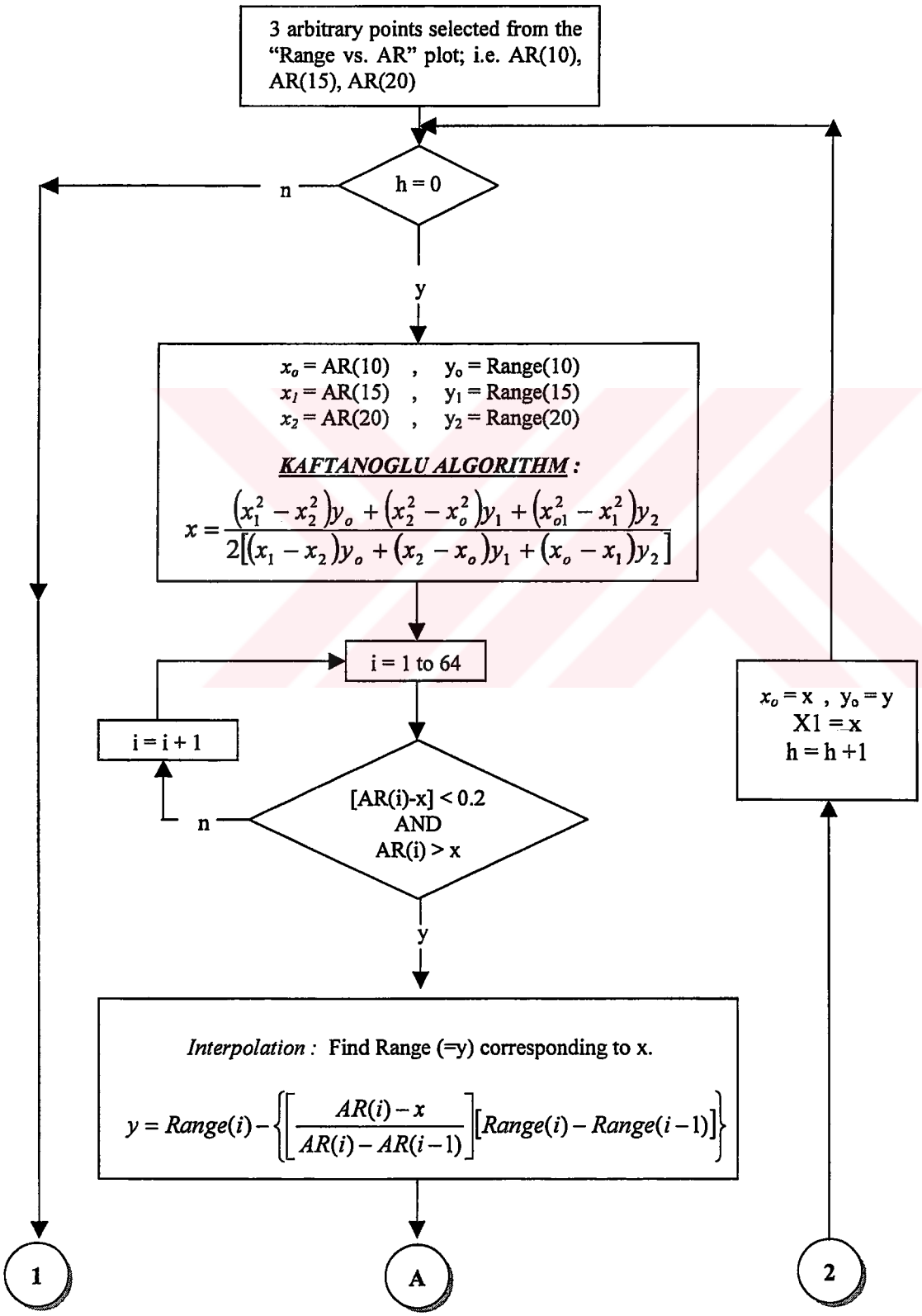

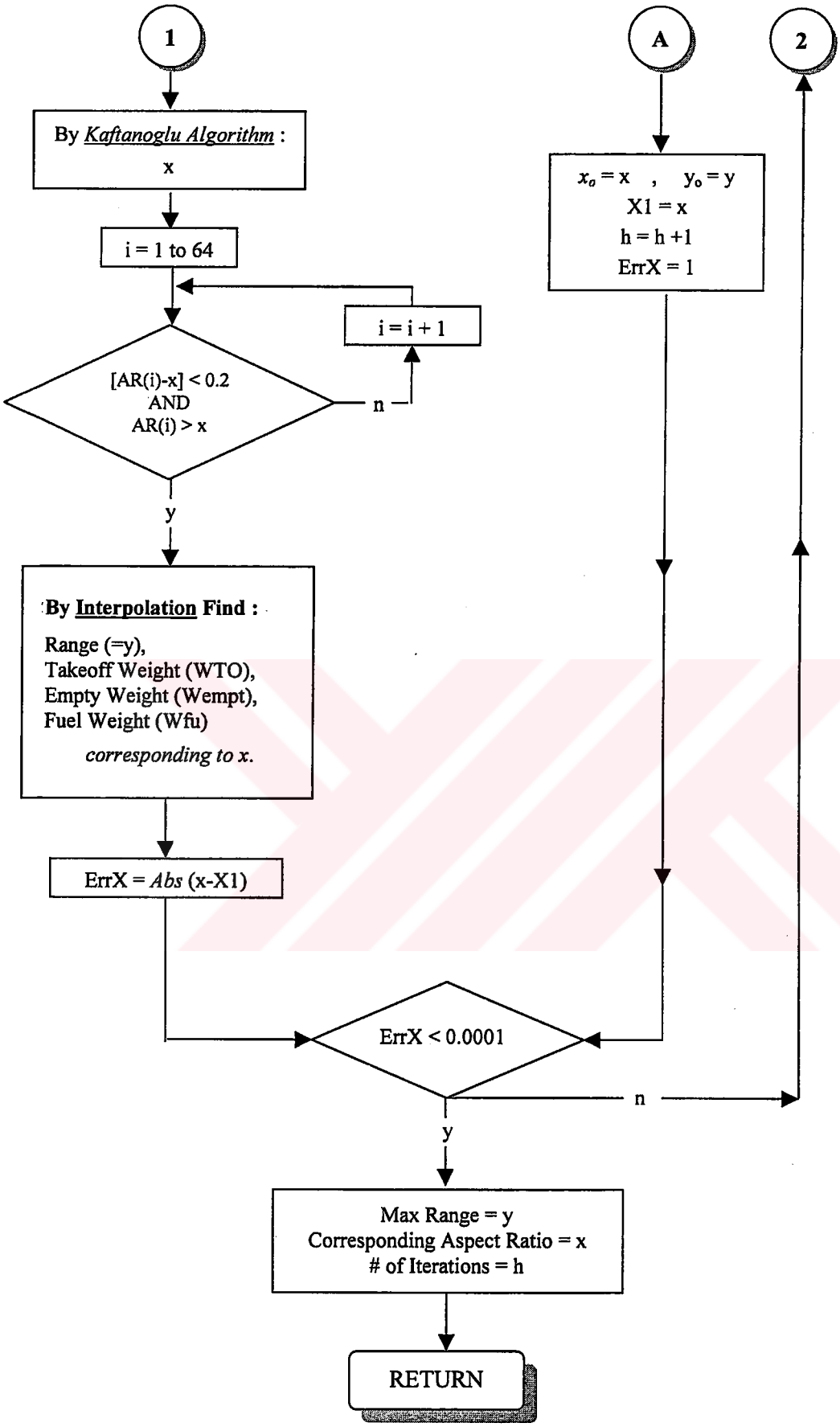
1
By Kaftanoglu Algorithm :
x
i = 1 to 64
i = i + 1
[AR(i)-x] < 0.2
AND
AR(i) > x
n
y
By Interpolation Find :
Range (=y),
Takeoff Weight (WTO),
Empty Weight (Wempt),
Fuel Weight (Wfu)
corresponding to x.
ErrX = Abs (x-X1)
A
x_o = x , y_o = y
X1 = x
h = h +1
ErrX = 1
2
ErrX < 0.0001
n
y
Max Range = y
Corresponding Aspect Ratio = x
# of Iterations = h
RETURN

15.4.1 Mission Profile (Tilt-Duct VTOL UAV)

The development procedure of the program requires the definition of the mission profile before starting the calculations. The mission profile for the Tilt-duct VTOL UAV is illustrated in Figure 15.8.

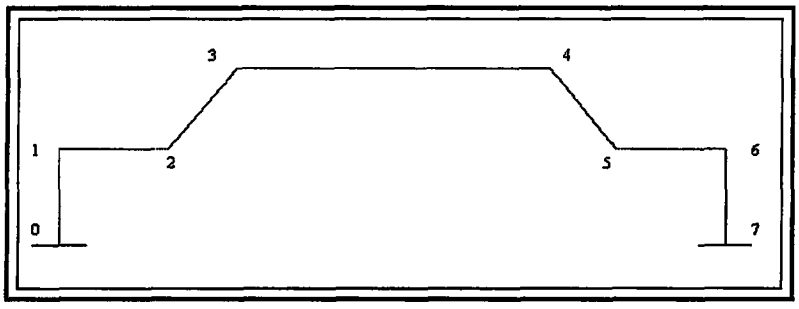

Figure 15. 8 The mission profile for the Tilt-Duct VTOL UAV.

where, the corresponding flight segments in Figure 15.8 are defined as follows:

(0-1) : Vertical Take-off
(1-2) : Transition
(2-3) : Climb
(3-4) : Cruise
(4-5) : Descend
(5-6) : Transition
(6-7) : Vertical Landing

15.4.2 Mission Profile (Other Conventional Types of Aircraft)

A typical mission profile for the other conventional types of aircraft is given in Figure 15.9. This mission profile is selected in order to reduce the complexity of the computer program.

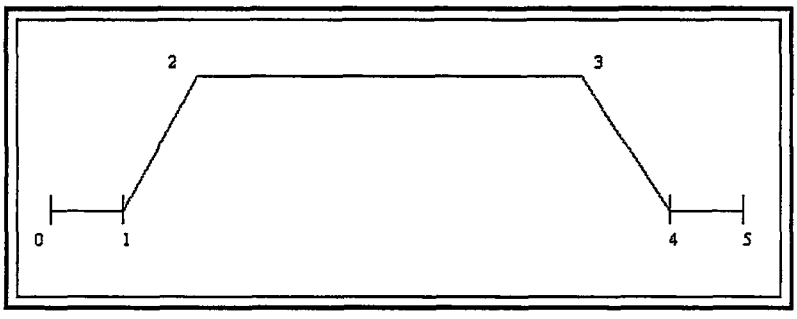

Figure 15. 9 The mission profile for the conventional type of aircraft.

where, the corresponding flight segments in Figure 15.9 are defined as follows:

(0-1) : Conventional Take-off
(1-2) : Climb
(2-3) : Cruise
(3-4) : Descend
(4-5) : Conventional Landing

15.5 About the Optimization Program

As mentioned before, 'Visual Basic 5.0 – Enterprise Edition' is the programming language used in developing the program. Mainly used VB controls are : command buttons, text boxes, option buttons, frames, labels. In addition to these controls, some different components are used such as 'progress bar' to represent the status of the data evaluation process and 'MS Chart Control' to represent the evaluated data in the form of 2D and 3D charts.

The program is developed as "web-interactive" by use of ActiveX controls. In order to run the program in www environment, the user should have an Internet Explorer 3.0 at least or a higher version. ActiveX plug-in is required to run this program by use of Netscape.

The program requires 8 inputs from the user in order to recognize the aircraft and use the input data in the evaluation process. At every step of this data input process, the program supports many source of help by means of "key" buttons, "tool-tip texts" and "?" buttons.

Another remark about the program is that it is designed to be very self-protecting against illogical inputs. The program interrupts such a process by deploying warning/caution messages that never disappears until the user changes the illogical data to a logical one. In Figure 15.10, such a case is illustrated. Here the user tries to proceed without filling-in one of the required data, i.e. in this the wing area. If this were be let by the program, it would most probably enter a run-time error or so.

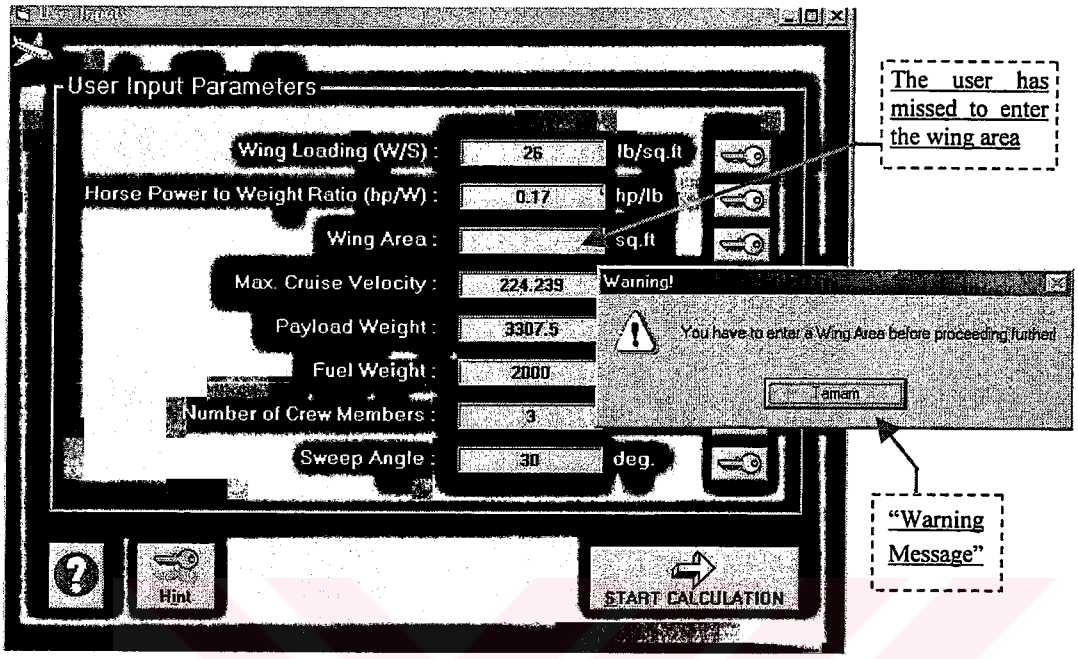

Figure 15. 10 A warning message in the optimization program, in case of incomplete data.

The basic requirements to operate this program are: Pentium 133 MHz or higher Central Processing Unit, 32 MB or higher Random Access Memory and 50 MB or higher free swap space.

The theory and the structure of the computer program are introduced in the preceding chapters, in detail. Now, in order to achieve a better understanding the program flowchart is presented as the followings:

THE FLOWCHART OF THE ASPECT RATIO OPTIMIZATION PROGRAM

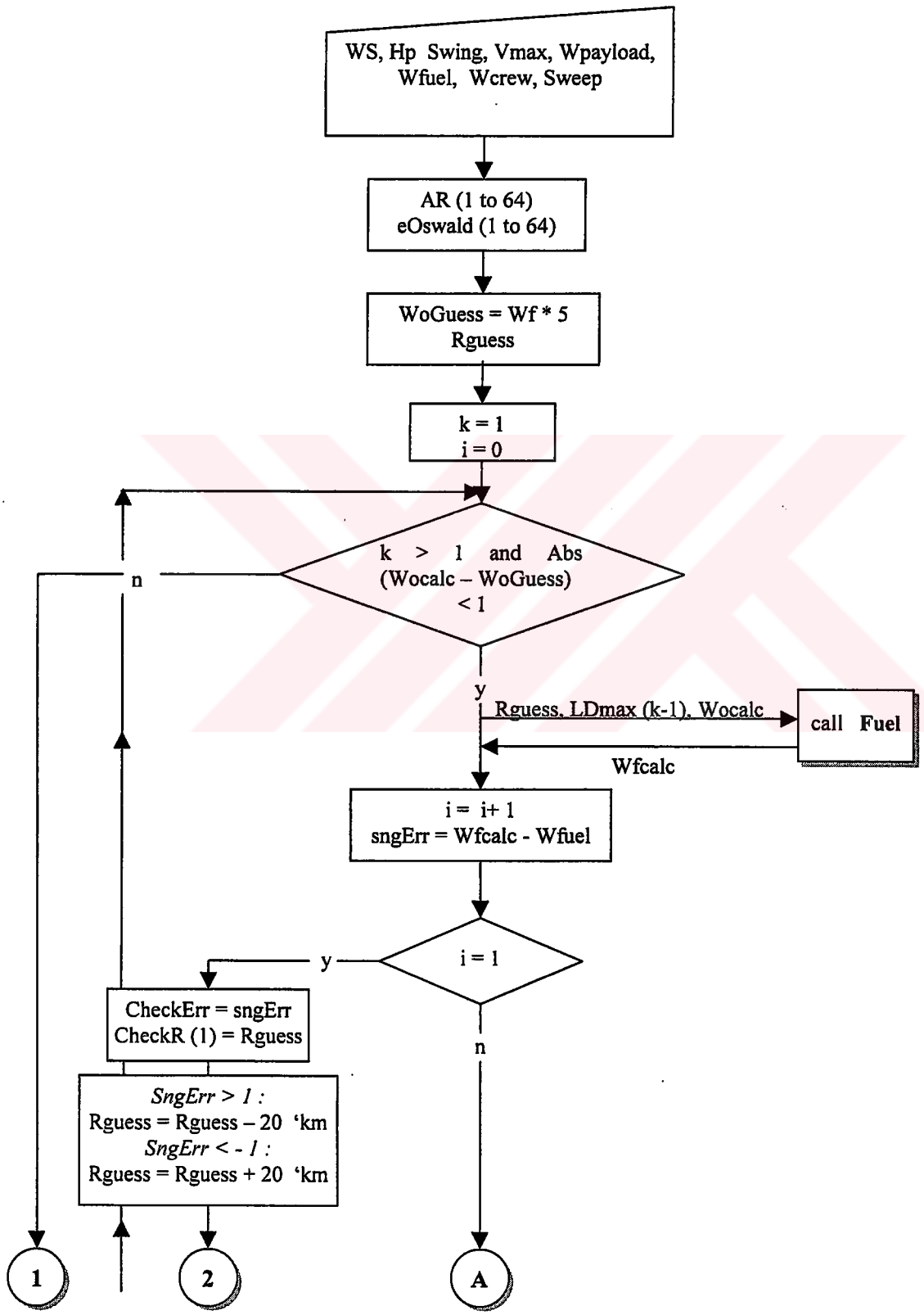

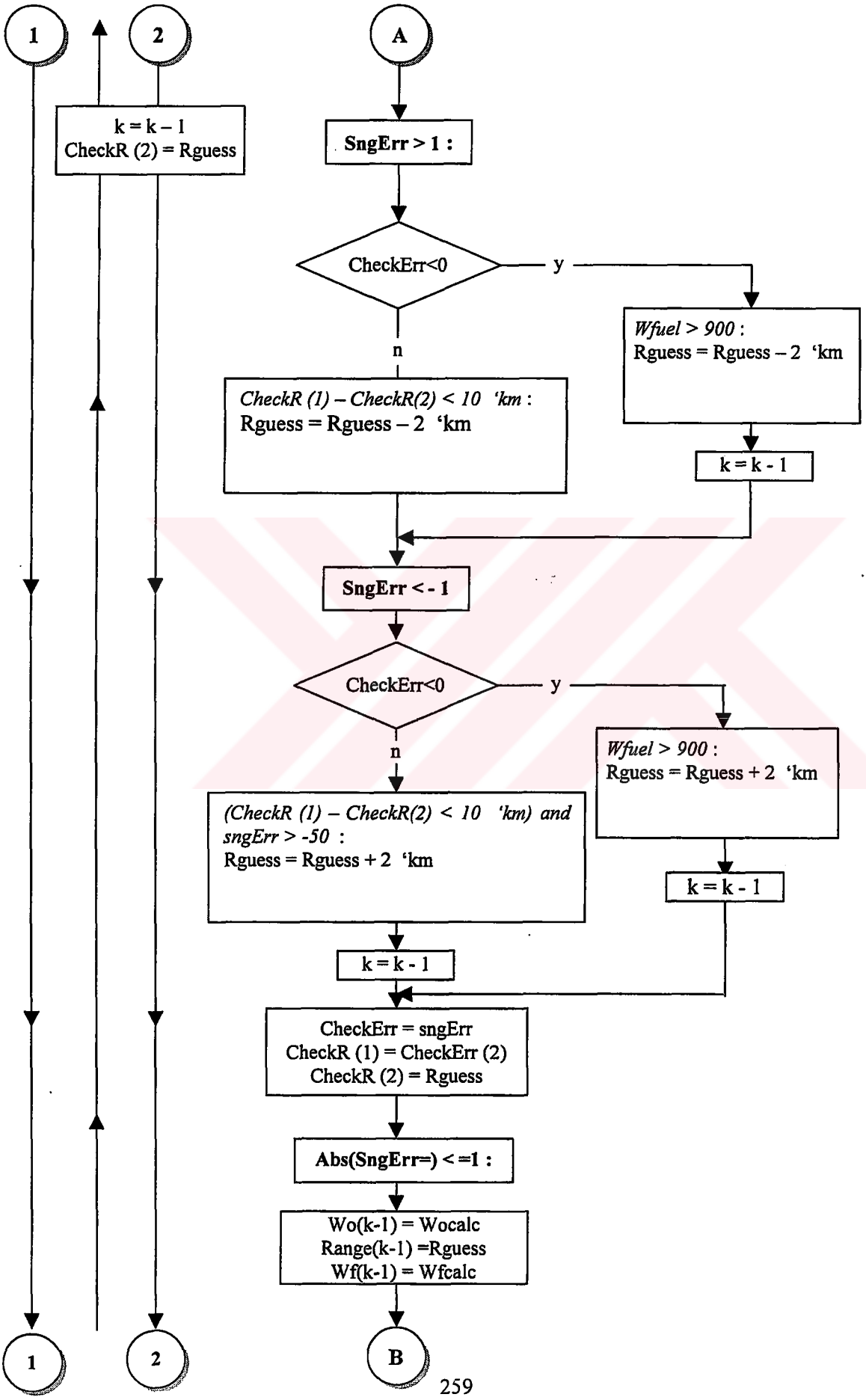
1
2
A
k = k – 1
CheckR (2) = Rguess
SngErr > 1 :
CheckErr<0
y
n
Wfuel > 900 :
Rguess = Rguess – 2 'km
CheckR (1) – CheckR(2) < 10 'km :
Rguess = Rguess – 2 'km
k = k - 1
SngErr < - 1
CheckErr<0
y
n
Wfuel > 900 :
Rguess = Rguess + 2 'km
(CheckR (1) – CheckR(2) < 10 'km) and sngErr > -50 :
Rguess = Rguess + 2 'km
k = k - 1
k = k - 1
CheckErr = sngErr
CheckR (1) = CheckErr (2)
CheckR (2) = Rguess
Abs(SngErr=) < =1 :
Wo(k-1) = Wocalc
Range(k-1) =Rguess
Wf(k-1) = Wfcalc
1
2
B

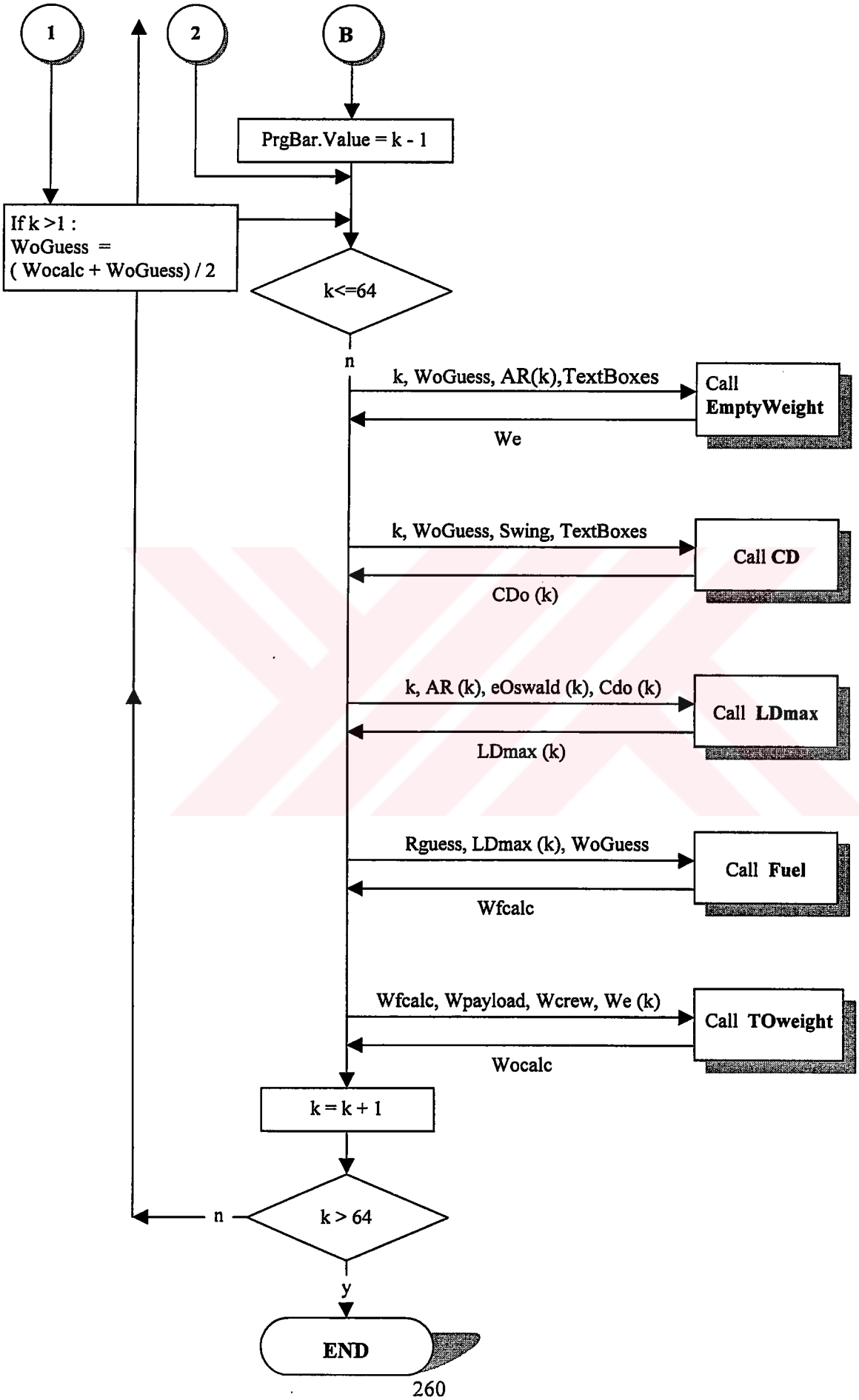
1
2
B
PrgBar.Value = k - 1
If k >1 :
WoGuess =
(Wocalc + WoGuess) / 2
k<=64
n
k, WoGuess, AR(k),TextBoxes
Call
EmptyWeight
We
k, WoGuess, Swing, TextBoxes
Call CD
CDo (k)
k, AR (k), eOswald (k), Cdo (k)
Call LDmax
LDmax (k)
Rguess, LDmax (k), WoGuess
Call Fuel
Wfcalc
Wfcalc, Wpayload, Wcrew, We (k)
Call TOweight
Wocalc
k = k + 1
n
k > 64
y
END

15.6 Conclusion And Discussion

The results show that as Aspect Ratio increases Range curve shows two basic reactions: 1. It draws a clear maximum peak and then bends down; 2. It increases parabolically and then stabilizes at a certain Range value. These are quite logical and as expected. The different behaviors of Range vs. AR curves depend on the Wing Sweep Angle. In order to illustrate this effect, two of the sample outputs include the results for an aircraft that the only data modified is the Sweep Angle. The differences can be observed by use of the charts supplied; or the user himself can input these data and observe the results in the active environment of the computer program.

Another point of the computer program is the accuracy of the results. The evaluation process of this program is quite iterative. Hundreds sometimes thousands of iterations are being made. It is observed that as the takeoff weight increases, i.e. aircraft size increases, any small increments in Range cause large fluctuations in the fuel weight evaluation process. For this purpose, the increment/decrement amounts between the iterations are kept as small as possible; but this time it is observed that, time collapsed for evaluation process increased tremendously. It is especially observed in the Visual Basic™ environment. For this purpose, the error amount in the fuel weight kept at a level of approximately 0.005%.

The results are quite satisfactory in the aeronautical engineering point of view. The author would like to indicate that it was a quite challenging but that much enjoyable experience to develop a "web-interactive" computer program in the Visual Basic 5.0™ programming environment.

CHAPTER 16

CONCLUSION and DISCUSSION

This thesis illustrated the conceptual design process of the Tilt-Duct VTOL UAV. This study is a part of a research activity being carried out in the research group, with members from the Department of Aeronautical Engineering and the Department of Electrical and Electronics Engineering, Middle East Technical University. The core of the team consists of three faculty members and two research assistants, see section 1.4. The project had started in 1998.

The design VTOL UAV combines the vertical flight capability of a helicopter and the superior forward flight performance of an airplane. It achieves the vertical take off capability by tilting the propeller-ducts mechanisms, which are located at the tips of the wing, on each side of the fuselage. It is basically designed for civil purposes, such as aerial surveys for agriculture, traffic monitoring and pollution control; meteorological data collection; pipeline survey; early forest fire detection; etc.

The thesis presents the conceptual design process of the design Tilt-Duct VTOL UAV in the first fourteen chapters. The process is sub-divided and examined under certain titles as the followings: First Guess Sizing, Airfoil and Geometry selection, Horsepower-to-Weight Ratio Selection, Initial Sizing, Configuration Layout, Propulsion and Fuel System Integration, Landing Gear and Subsystems, Aerodynamics, Weights and Balance, Stability and Control, Performance and Flight Mechanics and Cost Analysis. As a last chapter, a trade study that contains an optimization program, which is developed by use of Visiual Basic 5.0™ programming language, in order to evaluate the optimum aircraft aspect ratio which gives the maximum Range without changing the fuel capacity of the aircraft.

In this chapter, the achievements, the possible problems and the recommendations to obtain a better design will be presented and discussed.

i. The Comparison of Fixed-Wing Aircraft and Helicopter

As mentioned before, the design VTOL UAV aims to combine the vertical flight capability of a helicopter and the superior forward flight performance of an airplane. This is a quite useful achievement that enhances the aircraft's performance. At this stage, let's discuss what are the advantages and disadvantages of fixed wing aircraft and helicopters, and what can be achieved when the characteristics of these two are combined in a VTOL aircraft.

Fixed wing aircraft are efficient in the cruise configuration, when the propulsion and aerodynamic configurations are operating somewhere near to optimum conditions. The disadvantage of fixed wing aircraft is that they are far from optimum, during the low speed takeoff and landing phases when special provisions such as, flaps, slats and other similar high lift devices are required to reduce the aircraft speed to acceptable levels during these critical stages of flight.

Helicopters suffer from the reverse problem. Helicopters are extremely effective for low or zero speed vertical landing and takeoff, but are very limited for high speed cruise due to rotor-tip stall and other features of the rotary wing. Helicopters and other types of VTOL aircraft, e.g. tilt-duct, tilt-rotor, tilt-wing, require a very high ratio of thrust-to-weight ratio, generally greater and equal to 1.25 : 1 for an effective vertical takeoff and landing. It therefore, follows that a vehicle capable of combining the characteristics of both VTOL and conventional flight would a lot of advantages to offer, even though it might not compete with the optimum vehicle designed for either two of the regimes.

ii. About the Transition Mode of VTOL Aircraft

One of the major problems faced by all VTOL configurations is that two entirely different modes of flight, i.e. hover and forward flight modes, must be achieved and meshed. The points where they are meshed, that is, the times during which the aircraft changes from vertical to horizontal flight and back again, i.e. the transition mode is the most challenging stage that such a VTOL aircraft experiences.

The transition can be divided into two modes: accelerating transition (takeoff and climb) and decelerating transition (descent). These pose entirely different problems for the aircraft.

Accelerating transition : In this mode, the aircraft goes from hover to forward flight, transferring lift from the propeller to the wing, or it makes a run and takes off using wing and propeller forces to provide required lift. In both of these cases, the propellers operate at high thrusts and produce large slipstream velocities over the wings or in the ducts. For the tilt-wing and tilt-duct (i.e. for the design UAV) systems, this is beneficial because it allows large angles of attack to be used at low speeds, resulting in high lift coefficients. It should be indicated that, the propeller slipstream acts to suppress wing stall. In the case of these two aircraft, there is a substantial increase in lift with speed and, correspondingly, the wing or duct tilt angle can be lowered rapidly with speed. In a tilt-wing type of aircraft, this angle reduction is pronounced especially passing rapidly from a propeller supported condition to operation as the slipstream is deflected over the aircraft. For the case of a tilt-propeller aircraft, the aircraft maintains high shaft angles up to substantial speeds. For example the Curtiss-Wright X-19 tilt-propeller VTOL aircraft experienced a 60 degrees of shaft angle at 80 knots after which the angle was reducing rapidly. This was a consequence of the design approach followed, that is the use of non-tilting wings and high wing loadings. While X-19 successfully negotiated with the accelerating transition, the use of propellers instead of wings to produce lift at the lower speeds did not result in efficient flight. Such a case, not only impacts on the STOL capability of the machine, but its ability to perform special flight operations. Accordingly, the operational flexibility is reduced which is an important and desirable characteristics of V/STOL aircraft. [9]

Another harmful effect of high shaft angle is the increase in fatigue loading of the blades. This loading is a function of the shaft angle and flight speed (called the Aq factor). However, this same effect produces the radial lift force which is desirable. In conventional aircraft, propeller shaft angles are trying to be kept low at higher speeds, to reduce blade fatigue bending loads. In the case of the example aircraft, X-19, since the blades exploited the propeller radial force, they were designed to handle the fatigue loads. This was one reason for the large chord near the blade root.

Decelerating transition : This poses a quite different problem for the V/STOL aircraft, particularly during descent, since this must be done with the power reduced. For tilt-wing aircraft, the reduction in propeller slipstream velocity has highly harmful effects on descent velocity. The tilting duct system is also affected adversely by power reduction during descent, but it may still have phenomenal capabilities under full control, e.g. 1600 fpm descent capability of X-22A. Generally, the descent limits are expressed in terms of rate of descent vs. airspeed and are defined by buffet onset.

For this purpose, in the case of the design UAV, it is recommended to perform detailed wind-tunnel and flight tests, in order to better understanding the UAV's characteristics and responses in such a transition mode. It will also be useful in terms of comparing the aircraft responses in two modes, i.e. vertical and horizontal, and in the transition mode.

iii. About the Use of Tilting Duct Configuration of the Design UAV

Another point is the behavior of the propeller slipstream in an aircraft. One would expect that the slipstream of a conventional propeller to spread out as it moves backward. The fact is that, it just does the opposite. Indeed, it tapers down to about half of its original area. This is a change that reduces significantly the effective thrust of the propeller. The part *A* of Figure 16.1 illustrates this event.

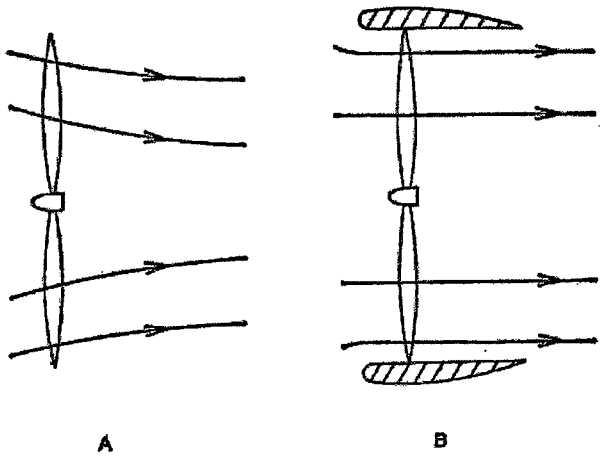

Figure 16. 1 Ducts around propeller prevents slipstream from narrowing down as it moves backward. [7]

One way to prevent this from happening is to surround the propeller with a duct (as in the case of the Tilt-Duct VTOL UAV) , or ring, to change the shape of the slipstream, as shown in part *B* of Figure 16.1. Use of ducts prevents the tapering, so that a given thrust can be produced by a smaller propeller. [7]

Ducting provides other advantages as well. It provides protection for the prop as well as for the objects and for the people who may approach too close to the spinning object. And, under certain circumstances, it also provides a certain amount of extra lifting surface in horizontal flight.

However, all these advantages bring a penalty which is the increased structural weight and complexity.

iv. About Disc Loading

Disc loading is a key characteristics of propellers. While it is commonly thought that VTOL propellers must have very high disc loadings compared with helicopter rotors, e.g. 30 to 50 lb / ft^2 against 4 to 10 lb / ft^2, this, in fact, is not correct, no longer. The recent and continuing development works on propeller-rotor aircraft and the effort on large-diameter propellers, clearly show that propellers can be built for practically any disc loading, e.g. 10 to 15 lb / ft^2. For the case of the Tilt-Duct VTOL UAV, the disc loading appears to be 9.46 lb / ft^2. In this respect, it should be mentioned that the present aerodynamic, dynamic and structural technologies eliminates the previous limits on size. [9]

v. About the Static Thrust Performance

fails below the expectations. This design deficiency requires a number of tests on the design UAV in order to improve the propeller performance.

In order to illustrate an example, the problems experienced with the Ling-Temco-Vought X-142A, a tilt-wing VTOL aircraft, on propeller performance will be examined. This problem existed with the XC-142A. The measured performance of the original propeller blade 2FE16A3-4A was approximately 10% less than the predicted value. A program was undertaken to recover the loss, resulting in a new blade, designated 2FF16A1-4A. The basic design differences between these two propellers were that the 2FF propeller had a round tip and a substantial increase in blade activity factor (from 86 to 105). It also had a higher integrated lift coefficient with the peak camber lift distribution located further outboard. With the new propeller design, the performance was reasonably augmented. Most of the original thrust deficiency was recovered for the typical operating conditions. However, the maximum figure of merit still was not reached.

vi. About The Thrust Losses

In the design of a V/STOL aircraft, some additional thrust losses unique to these types of aircraft have to be taken into account. These losses come from such items as wing download and tail rotor power used. Such an aircraft may use 7-10% of its power to drive its tail rotor. In the case of Tilt-Duct VTOL UAV there is no tail rotor used that will consume some amount of the aircraft power.

An additional loss that have to be considered during the design of these type of aircraft is associated with the wing interference with the propeller slipstream. This is a case that the tilt-rotor and tilt-propeller type of VTOL aircraft generally experience. It is commonly expected that, such a propeller/rotor slipstream on the wing will produce negative angle of attack and large downloads on the wings especially during transition.

During hover, e.g. in the case of the Bell/Boeing V-22 Osprey (see Chapter 2 for details), the flaps are let full down in order to reduce the wing interference with the strong rotor slipstream. An other example comes from the Curtiss-Wright X-19, a tilt-rotor VTOL aircraft (see Chapter 2 for details). In the case of this aircraft, this problem caused a 6.5% thrust loss on the front wing and a 9.5% loss on the rear wing. In the case of Tilt-Duct VTOL UAV, the interference of wing with the propeller slipstream is eliminated by ducting the propellers and locating them at the wing tips.

vii. About the Ground Effect

A common problem that is experienced by the VTOL aircraft is the ground effect comes into view especially during hovering. These are mostly due to the propeller/rotor slipstream or jet being deflected from the ground and generating forces and moments on fuselage, wing, and tail. Most of this can probably be avoided by proper positioning and aiming of the slipstream or jet. With a little extra control the remaining effects can also be tolerated.

As an example, the Bell X-22A and Ling-Temco-Vought XC-142A VTOL aircraft were experiencing positive ground effect. In the case of X-22A, ground effect produced random accelerations about all axes. But, the ground effect experienced was small compared with that of a helicopter.

In the case of XC-142A, it was determined that a positive ground effect was evident up to 30 ft wheel height. This positive ground effect, up to approximately two propellers diameters, was thought to be the "fountain" effect on the fuselage, however, the greatest effect was found to be at approximately 0 to 7 feet. It was also observed that hovering at a 7 ft wheel height, resulted in approximately 3.4% less power than was required for out-of-ground effect. While there were no serious instabilities for the XC-142A in the hover configuration, a divergent lateral-directional oscillation was encountered in ground effect during STOL operation. This region of instability was identifies as between the wing conversion angles of 80 to 35 degrees, below 25 ft. The aircraft was able to be used effectively avoiding this region.

In this respect, there is another defect that should be avoided. This is the negative ground effect, causing to negative vertical stability, which makes precision vertical control very difficult. This problem can be caused by the central location of the very high velocity slipstream. Absence of vertical damping can also be expected in this case, which in turn will contribute to the difficulties of accurate height control.

For the case of the Tilt-Duct VTOL UAV, the author of this thesis suggests that investigation of the particular design is necessary. Adverse ground effect can be detected by model tests. This will lead to define the regions of instability and let the design of the aircraft to be modified such that the instabilities are either eliminated or made controllable. One way to avoid these instabilities may be the proper location and orientation of the ducted propellers.

viii. About the Noise Problem

For the case of this problem, the tilt-rotor type of VTOL aircraft will be investigated as an example. the noise from a tilt rotor during approach to a landing is potentially a significant barrier to widespread acceptance of these aircraft. This approach noise is primarily caused by Blade Vortex Interactions (BVI), which are created when the blade passes near or through the vortex trailed by preceding blades. The XV-15 Aeroacoustic test will measure the noise from a tilt rotor during descent conditions and demonstrate several possible techniques to reduce the noise.

Several techniques are studied in an attempt to reduce the highest measured BVI noise conditions. The first of these techniques is to use sub-wings mounted on the blade tips. These sub-wings are expected to alter the size, strength, and location of the tip vortex, therefore changing the BVI acoustics of the rotor. The sub-wings are approximately 20% of the blade chord and increase the rotor radius by about 3 percent. Four different sub-wing configurations are be tested for this purpose, including square tipped sub-wings with different angles of incidence.

The ability of active controls to reduce BVI acoustics is another thing that will also be assessed in this respect. For this purpose, in Ref. [23] it is implied that the dynamic control system of the RTA will be used to implement open- and closed-loop active control techniques, including individual blade control. Open-loop testing will be conducted using a personal computer based, automated, real-time data acquisition system. This system features combined automated output of open loop control signals and automated data acquisition of the resulting test data.

A final technique to alter the noise of the rotor will involve changing the number of blades from three to four. A four-bladed rotor hub has been fabricated on which the XV-15 blades will be mounted. While the solidity of the rotor will increase, much useful information can be gained by examining the changes in the thrust and RPM with four blades.

The abbreviation of RTA stands for The Rotor Test Apparatus which is a special-purpose drive and support system for operating helicopter rotors in the 40-by 80- and 80- by 120-Foot Wind Tunnels.

REFERENCES

[1] Raymer, D.P., *Aircraft Design: A Conceptual Approach*, 2nd Edition, AIAA Education Series, 1992.

[2] Roskam, J., *Airplane Design*, 2nd Printing, Roskam Aviation and Engineering Corp., Parts I-VIII, KS, 1990.

[3] *Advanced Airplane Analysis (AAA) Program*, Version 2.2, DAR Corporation, 1999.

[4] Armutcuoğlu, Ö., Kavsaoğlu, M. Ş., Tekinalp, O., Okan, A., Tulunay, E., "*Conceptual Design of a Tilt-Duct VTOL UAV*", Proceedings of UAVs-15th Bristol International Conference, pp. 28.1-28.11, 2000.

[5] McCormick, Barnes W. Lean, *Aerodynamics, Aeronautics and Flight Mechanics*, Second Edition, John Wiley and Sons, 1995.

[6] Moir, Ian and Seabridge, Allan G., *Aircraft Systems*, First Edition, Longman Scientific & Technical, 1992.

[7] Hellman, Hal, *Helicopters and Other VTOLs*, First Edition, Doubleday & Company, 1970.

[8] This web-site includes many photos and descriptions about numerous types of US Airforce Aircraft.

http://usmilitary.about.com/

[9] Lindenbaum, Bernard and Fraga, Daniel E., "A Review of the US Tri-Service V/STOL Programs", AGARD-CP-126, Oct. 1972, Belgium.

[10] The web-site of NASA. The following web-address includes a wide photo gallery of numerous aircraft. Here, the information on XV-15 is utilized.

http://trc.dfrc.nasa.gov/gallery/photo/XV-15/HTML/EC80-13848.html

[11] Carlson, Eric Bernard, *Optimal Tiltrotor Aircraft Operations During Power Failure*, PhD thesis, Department of Aerospace Engineering, University of Minnesota, July, 1999.

[12] The web-site of NASA. The following web-address includes a wide movie gallery of numerous aircraft. Here, the information on XV-15 is utilized.

http://trc.dfrc.nasa.gov/gallery/movie/XV-15/HTML/EM-0040-01.html

[13] The web-site of *The Boeing Company*. The following web-address includes various information about V-22 Osprey.

http://www.boeing.com/rotorcraft/military/v22

[14] Mark, Dr H., "*Aircraft Without Airports, The Tilt-Rotor Concept and VTOL Aviation*", 75th Wilbur and Orville Wright Lecture, Royal Aeronautical Society, December, 1986.

[15] The web-site of *The Bell/Textron Company*. The products pages are utilized as a reference.

http://www.bellhelicopter.textron.com/products/

[16] E. Seckel, "Stability and Control of Airplanes and Helicopters", Academic Press, 1964.

[17] Eppler, Richard, *Airfoil Design and Data*, Springer-Verlag, Heidelberg, 1990.

[18] Limbach Flugmotoren, Installation Manual for L 275 E, 1999.

[19] Limbach Flugmotoren, Installation Manual for L 90 E, 1993.

[20] Okan, A., Tekinalp, O., Kavsaoğlu M. Ş., Armutcuoğlu, Ö. and Tulunay, E., "*Flight Mechanics Analysis of a Tilt Rotor UAV*", proceeding paper 99-4255, AIAA Atmospheric Flight Mechanics Conference and Exhibit, 9-11 August 1999.

[21] The web-site of *The Scaled Composites Company* which is an aerospace and specialty composites development company located in Mojave, California, USA.

http://www.scaled.com/projects/eagleeye/eagleeye.htm

[22] The web-site of *The Adroit Systems Inc.* which provides scientific an research and development for the US Government. It is headquartered in Alexandria, Virginia, USA.

http://www.adroitnet.com/uavforum/

[23] The web-site of *The Aeromechanics Branch of the Army/NASA Rotorcraft Division* which is responsible for aeromechanics research activities that directly support the Department of Defense and the U.S. rotorcraft industry.

http://halfdome.arc.nasa.gov/research/xv15.html

[24] Kaftanoğlu, Bilgin, "An Investigation of Stretch Forming in Relation to Deep-Drawing and Testing Sheet Metal", Ph.D. Thesis, University of London, 1966.